Investigating geomorphic and structural change at historic wreck sites using CFD and difference modelling

By

JAN MAJCHER

M.Sc., Oceanography, University of Gdańsk

Supervisors:

DR RORY QUINN

DR RUTH PLETS

DR CHRIS MCGONIGLE

Advisors:

DR FABIO SACCHETTI

DR THOMAS SMYTH

Thesis submitted for the degree of Doctor of Philosophy

School of Geography and Environmental Sciences

Faculty of Life and Health Sciences

ULSTER UNIVERSITY

February 2022

I confirm that the word count of this thesis is less than 100,000

Contents

Acknowledgements

I came to explore the wreck.

The words are purposes.

The words are maps.

I came to see the damage that was done

and the treasures that prevail.

I stroke the beam of my lamp

slowly along the flank

of something more permanent

than fish or weed

the thing I came for:

the wreck and not the story of the wreck

the thing itself and not the myth

the drowned face always staring

toward the sun

the evidence of damage

worn by salt and sway into this threadbare beauty

the ribs of the disaster

curving their assertion

among the tentative haunters.

-Adrienne Rich, *Diving into the wreck*, 1973, lines 52-70

Abstract

Shipwrecks not only provide unique opportunities to investigate relatively unaltered archaeological deposits, but they are also linked to environmental, heritage management and marine spatial planning issues. Physical processes, comprising linked hydro- and sediment-dynamics, can determine the pathways of evolution of shipwreck sites. For example, water flowing around a submerged wreck may cause scour, and together with changes in local geomorphology, can greatly influence the preservation state of the wreck. This geomorphic change can be exacerbated further by anthropogenic activities. This complex interplay between hydro-dynamics, geomorphic change, anthropopressure and structural deterioration remains poorly understood. Consequently, monitoring and management strategies capable of conserving this vast and finite submerged resource remain inefficient.

This thesis aims to extend our knowledge of the influence of combined sediment- and hydro-dynamic processes on the *in-situ* preservation of fully submerged, historic wreck sites. This study uses multibeam echosounder (MBES) data of exceptional, centimetric resolution collected over ten metal-hulled shipwrecks standing proud on the seabed in the Irish Sea between water depths of 26 and 84 m. Additional seabed and sub-seabed geological and hydrodynamic data are derived from sediment grabs, shallow-seismics and an oceanographic model. This unique combination of datasets is used in three complementary studies corresponding to the research objectives set out in the thesis.

Residual relief modelling (RRM) is tested for the objective mapping and delineation of wreck-related scour features, enabling their quantitative description. RRM relies on high-pass filtering of digital elevation model (DEM) data and is enhanced with breakpoint classification, with final separation of the features of interest supported by DEM visualisation enhancement techniques. The results indicate that the semi-automated workflow is time-efficient and quantifies the products of scour with improved objectivity when compared to manual digitisation. Development of the method has important implications for site formation studies and decision-making in *in-situ* preservation planning.

The temporal and spatial scales at which sediment erosion and deposition occur around wrecks remain largely unknown. Analysis of timelapse MBES survey data successfully captures true site extents and allows for the investigation of weekly, annual, multi-annual and decadal seabed changes, significantly expanding the number of case-studies reported for shipwreck site scour. Results of difference modelling show major changes at all time intervals for sites located in sand-dominated environments, whereas the seabed around wrecks settled in multimodal sediments shows virtually no geomorphic change outside of vertical measurement uncertainty (±30 cm). Quantification of local environmental processes and factors, including bed shear stress, sediment supply, and spatial barriers to scour explains variability in geomorphic change and aids predictions of future site dynamics. The study demonstrates that individual wrecks in similar shelf sea regions can be in very different equilibrium states with their environment, which has critical implications for their *in-situ* management.

Computational fluid dynamics (CFD) is used in conjunction with high-resolution MBES data-derived 3D wreck models to simulate tidal flows at two contrasting sites. Intricate patterns of wake and horseshoe vortices are observed, and modelled wall shear stresses successfully explain geomorphic change recorded in 4-year and one-week interval difference models. Moreover, substantial damage is detected on the wreck structures, correlated with areas of elevated wall shear stress and pressure in CFD simulations. The combined approach aids site management and provides analogies for offshore engineering.

It is anticipated that new knowledge realised in this study on the multi-method characterization of physical site formation processes at shipwreck sites will aid decision making in underwater heritage management and marine spatial planning.

Common abbreviations

CFD – Computational Fluid Dynamics

DEM – Digital Elevation Model

DoD – DEM of Difference/difference model

EMODnet – European Marine Observation and Data Network

FV – Fishing Vessel

GIS – Geographic Information System

HMS – His or Her Majesty's Ship

IHO – International Hydrographic Organization

INFOMAR – Integrated Mapping for the Sustainable Development of Ireland's Marine Resource

LES – Large Eddy Simulation

MBES – Multibeam Echosounder

UCH – Underwater Cultural Heritage

RANS – Reynolds-Averaged Navier Stokes Equations

ROMS – Regional Ocean Modelling System

RMS – Royal Mail Ship

RRM – Residual Relief Modelling

RV – Research Vessel

SS – Steam Ship

Notes on access to contents

I hereby declare that with effect from the date on which the thesis is deposited in the Research Office of the University of Ulster, I permit:

- The librarian of the university to allow the thesis to be copied in whole or in part without reference to me on the understanding that such authority applies to the provision of single copies made for study purposes or for inclusion within the stock of another library.
- The thesis to be made available through the Ulster Institutional Repository and/or EThOS under the terms of the Ulster eTheses Deposit Agreement which I have signed.

Cover page image: Simulated flow streamlines visualized for the HMS *Vanguard* site using high-resolution bathymetric data obtained from the *World War I shipwrecks in the Irish Sea: commemoration, visualization and heritage management* project, Ulster University and Marine Institute Ireland.

1. Introduction

1.1. Conceptual framework

One of the most iconic elements in maritime archaeology, underwater cultural heritage and even general marine science is the shipwreck. Shipwrecks are widely regarded as time capsules providing insights into the past for archaeologists and historians. Many of the most notable underwater archaeological discoveries have been made on ancient and medieval wrecks of wooden sailing vessels (Weinberg *et al.* 1965; Sténuit 1973; Moore 1997; Ballard *et al.* 2001, 2018; Cederlund 2006; Ballard 2007; Eriksson and Rönnby 2017). From the mid-nineteenth century onwards, the ship-building industry started using metals as the primary construction material to replace wood. The wrecks of metal-hulled ships are important, as they exhibit technological solutions and capture progress and life on board at the time of sinking (e.g. Elkin *et al.* 2020), and reflect the nature and course of sinking events (e.g. Church 2014), similar to their wooden counterparts (e.g. Secci *et al.* 2021). Many of these vessels are associated with tragic loss of life and direct connections to relatives and communities. As such, they also have continued commemorative significance (Firth 2018).

In addition to their historical and commemorative significance, submerged shipwrecks are environmentally significant. As many wrecks are highly complex structures, they provide habitats for fish and also enhance local diversity and biomass (Perkol-Finkel *et al.* 2006; Walker *et al.* 2007; Zintzen *et al.* 2008; Balazy *et al.* 2019). There have been multiple cases where decommissioned metal ships have been specially prepared and deliberately sunk in order to create artificial reefs. Shipwrecks therefore can act as natural laboratories, allowing, for example, the investigation of succession of individual communities, their composition and diversity (e.g. Walker *et al.* 2007). Additionally, the biological abundance and historical significance of these objects also attracts recreational wreck divers. The diving tourism industry is expanding rapidly and the amount of revenue-generating diving days each year has been estimated to be £4.5 million in the UK (Firth 2018), many of which are related to wreck diving.

The biological abundance of shipwreck sites is also well known among the fishing community, who focus their activities on locations where fish aggregate. Consequently, many wrecks and individual artefacts have been discovered due to fishers' reports. On the other hand, bottom trawling irreversibly damages and reorganises underwater sites, often resulting in the loss of archaeological material and its contexts (e.g. Brennan *et al.* 2016). Additionally, fishing nearby wrecks frequently results in equipment entanglement, snagging of nets and their abandonment, leaving behind so-called 'ghost nets', posing threats to marine fauna and recreational divers, and acting as a source of microplastics (Andrady 2011).

Metal wrecks may contain hazardous substances like fuels, unexploded ordnance and other toxic agents. This poses the risk of either slow, continuous leaks of pollutants or sudden, catastrophic

collapse and discharge; wrecks are therefore sometimes referred to as 'ticking time bombs' (Bełdowski *et al.* 2020; Carter *et al.* 2021). Prioritising wrecks which pose the highest environmental risk is a complex problem and oil spill prevention or unexploded ordnance retrieval activities require costly technologies. Determining which party should be responsible for financing such operations adds further complexity. Management of potentially polluting wrecks is complicated and therefore has been subject to extensive research (Basta *et al.* 2013; Landquist *et al.* 2013; Ndungu *et al.* 2017; Hac and Sarna 2021).

Furthermore, upstanding structures of shipwrecks located in shallower parts of the continental shelf are dangerous for marine navigation. Wrecks tend to be concentrated in busy shipping lanes and geomorphic changes can cause temporary exposure or burial. In shallow areas, this necessitates close monitoring for navigational safety. For example, the Dutch Ministry of Infrastructure and Water Management conducts shipwreck monitoring in the Dutch part of the North Sea every year in order to guarantee nautical depths (Bos and Frederiks 2019).

The concept of wrecks acting as natural laboratories can also be expanded to marine engineering. Shipwrecks are complex manmade structures, often unintentionally positioned on the seabed. They are therefore affected by similar processes which compromise the stability of engineering structures such as wind turbine monopiles and tidal turbine arrays. Hence, examining the deterioration processes of shipwrecks may inform the design of offshore renewables. This idea is not new: local geomorphological changes due to seabed scour around wrecks have been determined to act as excellent proxies for oceanographic and geotechnical parameters and processes like bed scour, net sediment transport, current direction and magnitude (Caston 1979).

Increasing coverage of high-quality, open-source bathymetric data delivered by international (e.g. EMODNet: EMODnet Bathymetry Consortium 2018) and national (e.g. INFOMAR: Guinan *et al.* 2020) seabed mapping programmes creates a vast resource for conducting quantitative research on broad- and fine- scale seabed geomorphology (Coughlan *et al.* 2020; Peters *et al.* 2020) and shipwrecks (Davis *et al.* 2020). Maximising the applications of these data is becoming more important than ever, as nations shift towards renewable energy sources. Marine and coastal engineering will assume the central role in this shift for many countries. The use of available bathymetric and backscatter datasets can be expanded with analyses of how shipwrecks interact with the seabed, providing an additional layer of information for the future developments.

Unfortunately, shipwrecks are often associated with treasure hunting. Today, modern technology allows precise salvage operations at a full range of depths (Davies 2011; Pringle 2013) and therefore wrecks containing valuables continue to be targeted for profit, either legally through ownership claims or illegally through unauthorised salvage.

Nevertheless, the sheer amount of shipwrecks in our oceans and seas, approximating 3 million, (Croome 1999; UNESCO 2017) creates perplexing management challenges, compounded by the

forementioned variegated interests of many parties (Fig. 1.1) (Firth 2018; Papageorgiou 2018). It is clear, that in order to manage shipwreck sites properly, they need to be understood at many levels, assuming various perspectives. Perhaps one link, important to all the interested parties, is a shipwreck's structural integrity which is related to its *in-situ* preservation state. International conventions aimed at protecting the archaeological resource (the Valletta Treaty (European Convention on the Protection of the Archaeological Heritage 1992), the ICOMOS charter (ICOMOS 2007) and the UNESCO-2001 Convention on the Protection of the Underwater Cultural Heritage (UNESCO 2002)) emphasise *in-situ* preservation strategies where applicable. One of the main reasons for this is the extent of the resource, which is still growing while new sites are discovered every year using efficient prospecting technologies.
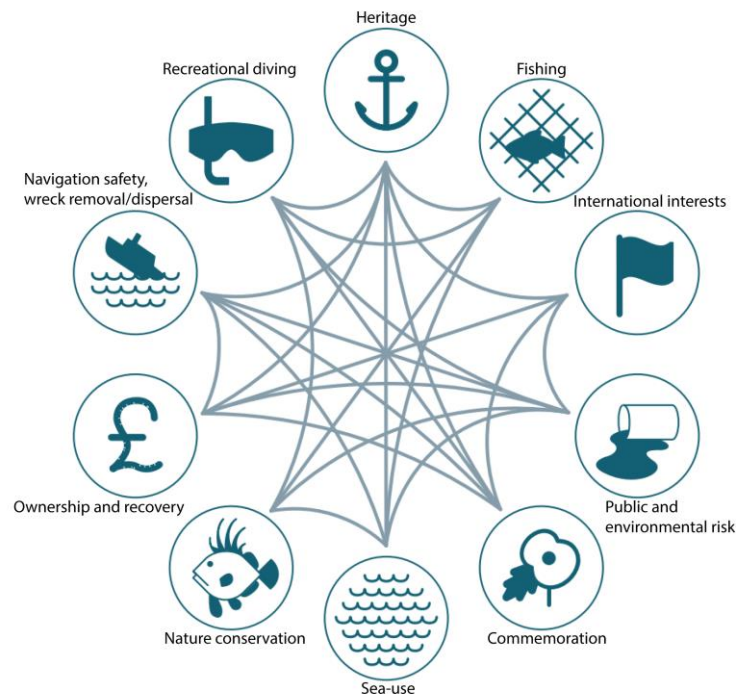
Figure 1.1. Chord diagram illustrating interrelations between multiple interests affecting the management of shipwrecks (adapted from Firth 2018).

Multiple research initiatives have emerged after the establishment of the conventions (notably the UNESCO-2001 convention), focusing on developing coherent workflows enabling informed management of underwater cultural heritage, putting cost-efficient *in-situ* preservation at the forefront. Among them there are ongoing international projects, for example: CHERISH (http://www.cherishproject.eu/en/) and the North Sea wreck project (https://northsearegion.eu/nsw) and past projects, for example: MACHU (Manders *et al.* 2009), Wreck Protect (Al-Hamdani *et al.* 2011), MERMAID (Pournou 2013), and SASMAP (Gregory and Manders 2015a, b).

The SASMAP project's *Guidelines to the process of underwater archaeological research* (Gregory and Manders 2015a) provide direct reasoning as to why the *in-situ* preservation option should be considered for most of the sites. Firstly, excavating, curating and conserving underwater finds is expensive and becomes financially prohibitive to perform at a large scale. A shipwreck can cost anywhere from 0.5 to 4 million EUR to conserve and this does not include additional storage, exhibition and other maintenance costs. Secondly, underwater cultural heritage preserved *in-situ* can be considered as being kept in safe underwater storage until new, cost-efficient excavation and conservation methods are developed. Nonetheless, the *in-situ* preservation strategy requires site monitoring in order to determine whether a site is being successfully preserved (Gregory and Manders 2015a).

Site monitoring not only helps to determine the significance of sites after initial archaeological prospection, but it is also necessary to understand a set of physical (mechanical, hydro- and sediment-dynamic action), biological (e.g., encrustation), chemical (e.g., corrosion) and anthropogenic influences contributing to the destruction or preservation of a site. These influences, referred to as site formation processes (Schiffer 1996) are often site-specific and operate at various temporal and spatial scales (e.g. Astley 2016). Appropriately designed site monitoring strategies allow us to assess site formation and make decisions, firstly, whether a site can be preserved within its environment and, if so, whether to leave it as is or to implement active *in-situ* preservation measures (e.g. polypropylene nets, sandbags or geotextiles) (Gregory and Manders 2015b; Pournou 2017). Monitoring is also paramount in conducting risk assessments and safe management of potentially polluting metal shipwrecks (Goodsir *et al.* 2019) and unexploded ordnance (e.g. chemical weapons in the Baltic Sea: Vanninen *et al.* 2020).

With regard to metal shipwrecks, although individual artefacts or structural elements can be salvaged for curation and conservation purposes, the *in-situ* preservation pathway is the only realistic option for the majority of them. Significantly, their site formation processes and long-term stability on the seabed are still not well understood (Keith 2016). In order to establish efficient monitoring strategies of metal-hulled shipwrecks and be able to identify vulnerable sites, we need to understand which factors affect their stability.

Stability is strongly influenced by the combined hydro- and sediment-dynamic action, or in other words physical site formation processes (Quinn 2006). Apart from exerting mechanical loads, these processes frequently result in seabed scour (erosion), which is controlled by a set of geotechnical and oceanographic parameters including the presence and strength of currents/waves, seabed substrate composition, size and orientation of an object (e.g., a wreck) and others (Soulsby 1997; Whitehouse 1998; Quinn 2006; Melling 2015; Astley 2016). Scour seems to affect wrecks especially at the initial phases of site formation, but it may (or may not) be exacerbated by internal factors e.g., a part of a wreck's structure collapsing and creating new

scour nuclei (Quinn 2006) and external factors e.g., migration of sediment waves (researched for wind farm scour: Couldrey *et al.* 2020), storm events (e.g. Fernández-Montblanc *et al.* 2018) and anthropogenic influences (e.g. dredging: Quinn and Boland 2010).

Metal-hulled shipwrecks in particular present substantial and highly complex obstacles to flow. Therefore, their scour signatures tend to be complex, with erosional and depositional features (referred to as 'wreck marks') often extending hundreds of metres parallel to peak flows, and reaching depths/elevations of tens of metres (e.g. in Caston 1979; Garlan *et al.* 2015). In order to understand how these physical processes affect wrecks in the long-term, their temporal development needs to be understood, and monitoring should be performed at multiple time scales. Monitoring needs be conducted over large spatial scales, and at high-resolution, to allow the complexity and full extents of scour signatures and archaeological structures/features to be captured.

Hydrographic surveying using acoustic remote sensing devices such as multibeam echosounder (MBES) has proven highly effective in delivering data complying with these monitoring requirements. A modern MBES can deliver bathymetric measurements with centimetric accuracy when used with high-grade positioning systems. MBES systems can also acquire backscatter data for substrate mapping and can be accompanied by shallow-seismic surveys to assess the sub-seabed structure. In parallel, sediment samples can be collected with grabs or cores to obtain physical samples of substrates. Surveys can be repeated at various time intervals, using a time-lapse approach (Quinn and Boland 2010; Bates *et al.* 2011; Stieglitz and Waterson 2013; Astley 2016; Brennan *et al.* 2016; Fernández-Montblanc *et al.* 2016). In archaeology and heritage science, the time-lapse strategy has been employed predominantly for wooden wrecks (Manders 2009; Quinn and Boland 2010; Astley 2016; Brennan *et al.* 2016). As noted by Astley (2016), who researched stability of three upstanding metal-hulled wrecks, there is a need to expand the number of case studies in order to have better understanding of wreck site formation pathways.

Processing of MBES data can result in digital elevation models (DEM) and backscatter mosaics, which can be used in various ways in site formation studies. GIS software allows their efficient handling and integration and development of new workflows (Gregory and Manders 2015a). In recent years, MBES data has been successfully integrated with hydrodynamic and geological data in computational fluid dynamic (CFD) simulations of shipwreck sites (De Hauteclocque *et al.* 2007; Smyth and Quinn 2014; Fernández-Montblanc *et al.* 2018b; Quinn and Smyth 2018). As CFD modelling provides detailed understanding of flow regimes, is desk-based and can be conducted using open-source software (Quinn and Smyth 2018), it can contribute positively to effective *in-situ* preservation and site management.

Nevertheless, more research is necessary to determine how flows at different geographic locations and related current/wave regimes affect the long-term stability of underwater sites. Only then can

comparisons between sites be performed in order to evaluate analogies and allow extrapolating and applying knowledge to other sites affected by similar environmental contexts, without the need to conduct extensive surveys for each site separately. For example, such analogies between sites have already been established for the development of wreck marks under various flow regimes (Caston 1979; Quinn 2006). A CFD investigation (Quinn and Smyth 2018) provided an explanation for these analogies through a comprehensive study of how flows are modified by a wreck according to its orientation.

To date, no CFD investigation of flows around upstanding, metal-hulled wrecks has been published. As mentioned earlier, these shipwrecks often pose substantial obstacles to flow and depending on the local oceanographic and geological conditions, their stability may be influenced by geomorphic changes. CFD simulations could potentially be used in conjunction with repeat MBES data for metal-hulled wrecks in order to record and explain geomorphic change, its interrelations with site stability and inform site management.

1.2. Aim and objectives

The overarching aim of this PhD project is to extend the knowledge of shipwreck site formation processes by integrating and maximising the use of very high-resolution hydrographic and geophysical, geological and oceanographic data collected over a range of metal-hulled shipwrecks in the Irish Sea. The main focus is on coupled hydro- and sediment-dynamics (i.e., physical processes) and understanding how these processes affect *in-situ* preservation of shipwreck sites.

The aim is met through the following objectives:

- To objectively map geomorphological features at shipwreck sites and delineate erosional and depositional signatures (wreck marks) on high-definition DEMs derived from the multibeam echosounder data.
- To characterise the evolution of the sites through the investigation of geological and oceanographic contexts, and observations of geomorphic change at both local and regional spatial scales and four temporal scales: short-term (1 week), annual, inter-annual (4-5 years) and decadal (10 years).
- To advance CFD modelling of flow regimes around complex shipwreck structures and validate the simulations with time-lapse MBES data.

1.3. Significance of the investigated shipwreck sites and their historical context

This PhD project is linked to a Marine Institute ship-time application (2014): *World War I shipwrecks in the Irish Sea: commemoration, visualization and heritage management*, which resulted in two scientific cruises on the state research vessel *Celtic Voyager*: CV15021 in 2015 and CV16031 in 2016. During these cruises very high-resolution repeat MBES coverage and geoscientific data were acquired over a range of World War I (WW1) shipwrecks in the Irish Sea

to facilitate research into site formation processes, 3D visualization and cultural heritage management. The ship-time proposals addressed both the UNESCO-2001 convention that aims to protect cultural heritage which has been submerged for at least 100 years and WW1 centenary commemorations.

To date, 68 countries have ratified the UNESCO-2001 convention (see section 1.4 below), but the Republic of Ireland and the United Kingdom are yet to do so (Kirwan 2010; Roberts 2018). Nevertheless, both countries have established heritage protection legislation applicable to shipwrecks. In the UK, there is the Protection of Wrecks Act (PWA) 1973; the Ancient Monuments and Archaeological Areas Act (AMAA) 1979; and the Historic Monuments and Archaeological Objects (Northern Ireland) Order 1995. In the Republic of Ireland, there is a blanket protection for all shipwrecks over 100 years old, as implemented under the National Monuments Acts 1986 and 1994. In the UK, the Protection of Wrecks Act (1973) grants protection only to specific wrecks and individual artefacts designated based on their significance. Considering both the aim of the UNESCO-2001 convention and the compliance with the national legislations, it is paramount to develop efficient techniques for monitoring of the underwater cultural heritage and garner information about its long-term stability.

As this project has concentrated on wrecks located in the Irish Sea, it is worthwhile exploring the Irish setting in more detail. More than 18000 wrecking incidents are recorded for the island of Ireland, with at least 1800 ships lost during WWI (Brady *et al.* 2012; Cotswold Archaeology 2015). Long-term stability and formation processes of these shipwrecks are largely unknown and before the 2014 Marine Institute grant proposal, little had been done on these sites.

During the 2015 and 2016 *Celtic Voyager* cruises, surveys were completed over ten historic metal-hulled shipwrecks, nine of which date back to WWI and one to 1875. The wreck sites were chosen to represent a range of environmental conditions, characterized by varied tidal settings and different geological substrates. However, all wrecks are more than 100 years old and according to the UNESCO-2001 convention should be treated as underwater cultural heritage. Additionally, each of these wrecks is associated with some elements of the matrix of interests, described earlier (Fig. 1.1).

All the WWI wrecks investigated in this PhD were lost due to submarine action, either torpedoed, sunken by gunnery or hit by mines. The unrestricted submarine warfare resumed by Germany in early 1917 is recognized as a key narrative of the period (Wessex Archaeology 2011) and highlighted in an archival assessment of WWI wrecks in the Northern Irish Waters by Cotswold Archaeology (2015). The wrecks are of relevance for understanding the historic and military contexts of WWI in the region. Additionally, three of the them: RMS *Leinster*, SS *W.M. Barkley* and SS *Hare*, are associated with loss of life. They therefore present commemorative value and are monuments for those who lost their lives at sea in the tragic circumstances of naval warfare.

Moreover, the Irish Sea, including the areas immediately surrounding the investigated shipwrecks, is exploited through commercial fishing, including bottom trawling for *Nephrops Norvegicus* (Hensley 1996) and extensive existing and planned offshore renewable developments (Coughlan *et al.* 2020; Guinan *et al.* 2020). Some of the wrecks, namely SS *Chirripo*, RMS *Leinster* and HMS *Vanguard* are also popular dive sites, regularly visited by recreational divers. The other shipwrecks, although seemingly visited less frequently, are also within the limits of sport diving: either recreational or more advanced decompression (technical) diving.

Among other interests, the deterioration of these metal-hulled wrecks on the seafloor means they are potential pollution risks. The shipwreck of *SS Santa Maria* off the north coast is of the highest concern from an environmental perspective, as it may pose an oil leakage threat. Although investigation of this potential environmental risk is not within the scope of this PhD project and would require different methods (Landquist *et al.* 2013), the problem adds an additional layer of importance for physical site formation research.

A brief historical background of the vessels is provided below, and their locations are shown in Fig. 1.2. Additional information about the wrecks' history can be obtained from previously published history- and archaeology-oriented resources, for example, Brady *et al.* (2012) and Cotswold Archaeology (2015).
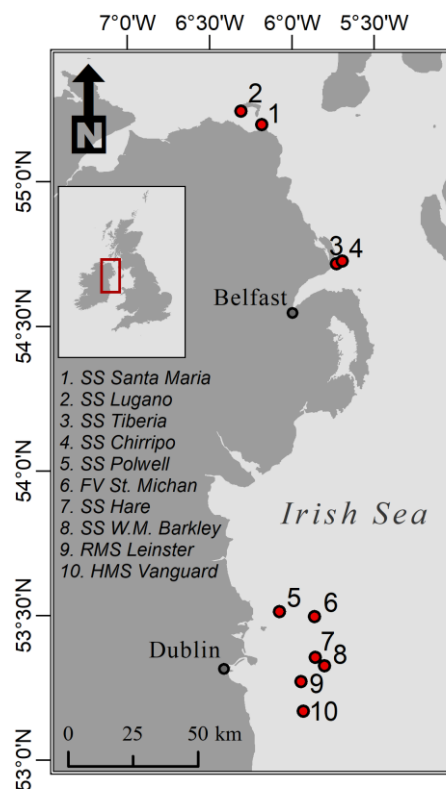
Figure 1.2. Locations of the shipwreck sites.

1.3.1. SS *Santa Maria*

SS *Santa Maria* was built in 1901 by the *American Shipbuilding Company.* (Cleveland, Ohio) and initially named *Minnetonka*. She was propelled by a triple-expansion engine and at the time of sinking was owned by the *Sun Company* of Philadelphia. In 1906, the ship was renamed *Santa Maria* and converted from a bulk to a tank vessel capable of carrying 55,000 barrels of oil. Importantly, some modifications were made enabling the vessel to use oil as a fuel instead of coal. This conversion represents a relatively early example of the technology (Cotswold Archaeology 2015). During a convoyed cruise from Philadelphia to Glasgow with a cargo of fuel oil (6597 tons), she was separated from the convoy and was torpedoed by *U-19* (on 25.02.1918). There were no casualties. The same U-boat attacked and sank SS *Tiberia* off Belfast Lough the next day, a site that is also included in this PhD project and described below.

The presence and state of the oil which *Santa Maria* is thought to have been carrying is unknown (Cotswold Archaeology 2015). Further prospection and site-focused risk assessment could shed more light on the potential environmental threat. This is especially important considering that the parts of the coast closest to the wreck (Antrim coast and Glens), together with Rathlin Island are defined as one of the 46 UK Areas of Outstanding Natural Beauty (designated exceptional landscapes in the UK). Any discharge and dispersal of oil from the wreck could have serious consequences for the adjacent coastlines. The potential threat is magnified by very strong tidal currents in the area (up to 3m/s), which is also under consideration for tidal turbine development (Lewis *et al.* 2015; Pérez-Ortiz *et al.* 2017).

1.3.2. SS *Lugano*

Built by the *Irvine's Shipbuilding & Dry-dock Company.* (West Hartlepool) in 1917 as a British cargo-carrying steamship, SS *Lugano* was propelled by a triple-expansion engine (Cotswold Archaeology 2015). She was owned by the *Gulf Line Ltd.* and was part of a convoy escorted by HMS *Drake* and HMS *Brisk*, going from Newport News (Virginia, USA) to Liverpool. The convoy needed to split up and *Lugano* sailed towards Rathlin Island. On 24.10.1917, she was hit by a mine laid by *U-79*, which at the time also torpedoed HMS *Drake* and HMS *Brisk.* While there were no lives claimed during the wrecking of *SS Lugano*, 18 people died on HMS *Drake*, when it collided with the merchant cargo vessel, *Mendip Range,* due to the damages sustained by the torpedo attack and 32 people died on HMS *Brisk*.

1.3.3. SS *Chirripo*

SS *Chirripo* was a triple-expansion engine steamship built in 1906 by *Workman, Clark and Company.* of Belfast. She was owned by *Elders & Fyffes, Ltd.*, Liverpool and had two masts and schooner rigging (Cotswold Archaeology 2015). She was used as a cargo ship and conducted transatlantic voyages between the West Indies, South America and Britain, also carrying

passengers. *Elders & Fyffes, Ltd* was mainly involved in banana trade between Jamaica and Britain. *Chirripo* was sunk on 27.12.1917 after hitting a mine laid by the U-boat *UC-75* and her propeller was salvaged in 1970.

1.3.4. SS *Tiberia*

SS *Tiberia* was built as a cargo ship in 1913 by the *Northumberland Shipbuilding Company*, Howdon-on-Tyne. Formerly known as *Frimley*, she was owned by the *Anchor Line*, Scotland at the time of sinking (Cotswold Archaeology 2015). She had a single triple-compound engine and was a schooner with two masts. On her last cruise she participated in a mercantile convoy which had an escort of 6 destroyers and 4 sweepers sailing from Glasgow to New York with a general cargo. After the convoy was ordered to seek shelter in Belfast due to bad weather, she was torpedoed on 26.02.1918 by *U-19*, which sank SS *Santa Maria* a day earlier (desribed above). There were no casualties.

1.3.5. SS *Polwell*

Initially named *Northumbria*, SS *Polwell* was built in 1888 by *J.L. Thompson & Son in Sunderland*. She was powered by a triple-expansion engine and changed owners and name many times in her history. In 1914, being registered in Hamburg under the name *Syra*, she was captured sailing nearby Gibraltar by the British Admiralty. From 1917 to 1918, after gaining the name *Polwell*, the vessel was used as an armed collier, managed by the *Clyde Shipping Co. Ltd.* based in Glasgow. She was sunk on 4.06.1918 by *U-96* during a cruise from Scotland to France, with a cargo of coal onboard, intended to support allied forces. Before sinking, a warning shot was fired by the hostile submarine and the whole crew managed to escape the vessel safely (Brady *et al.* 2012).

1.3.6. FV *St. Michan*

St. Michan was a motor fishing trawler built in 1912 by Michael Tyrell of Arklow, operated by Joseph Harford and Christopher Shines, Dublin. On 30.03.1918 she was sunk by gunnery of *U-96* (Helgason), with no loss of life.

1.3.7. RMS *Leinster*

RMS *Leinster* was a twin-screw steel steamer, propelled by two independent triple-expansion engines and built in Liverpool in 1896 by *Lairds*. The vessel was owned by the City of Dublin *Steam Packet Company* and delivered mail between Ireland and Britain. On 10.10.1918, just a few weeks before the Armistice in November, *Leinster* was torpedoed without notice by a German *UB-123*. She was on the way from Carlisle to Holyhead with a general cargo and sacks of mail. With 501 casualties from 771 passengers (over 400 of which were soldiers), it is one of the worst

maritime tragedies in Irish waters (Brady *et al.* 2012). *Leinster*'s anchor was raised from the seabed in 1996 and is displayed in a coastal town of Dún Laoghaire as a memorial.

1.3.8. SS *W.M. Barkley*

SS *W.M. Barkley* was built in June 1891 by the *Ailsa Shipbuilding Company* (Troon, Scotland) as a cargo ship. Powered by a compression engine, she was the first steamship employed by the producers of *Guinness* stout; *Arthur Guinness and Sons Ltd*. During the war, the *Guinness* fleet was taken by the British Admiralty, but in 1917 *W.M. Barkley* was deemed too expensive to maintain by the navy. On 12.10.1917 she was torpedoed without any notice by *UC-75* U-boat while sailing from Dublin to Liverpool, delivering a cargo of stout. There were 4 casualties, as most of the crew managed to escape. The collapsing vessel contained a cargo of barrels and maintained buoyancy long enough for the crew to deploy a life boat (Brady *et al.* 2012). A model of the vessel is on display in the *Guinness Storehouse* in Dublin.

1.3.9. SS *Hare*

SS *Hare*, powered by triple-expansion engines, was built in 1886 by *Barclay Curle &Co.*, Glasgow and was owned by *George Lowen & Co.*, Manchester. The ship is well known in Irish history for for the support it offered to workers and their families in Dublin during the 1913 Lockout dispute. She delivered significant amounts of food for the starving protesters, who were fighting against low-wages and bad living conditions. On 14.12.1917, carrying 470-tons of cargo, *Hare* was torpedoed without notice by *U-62* and her captain managed to deploy a lifeboat and escape with 5 other crew members. However, tragically, the sinking claimed 10-12 lives (Brady *et al.* 2012).

1.3.10. HMS *Vanguard*

HMS *Vanguard* is the only shipwreck investigated in this PhD project which was not lost during WWI. Powered by a steam engine and sails, the Audacious-class ironclad battleship was able to achieve a speed of 14 knots. She was built in Birkenhead (England) in 1870 by *Cammel Laird & Co.* and started service as a guardship at Kingstown. On 1.09.1875 she was accidentally sunk by her sister ship HMS *Iron Duke* during manoeuvres in low-visibility, foggy conditions with no loss of life (Brady *et al.* 2012).

1.4. Methodological approach in the context of the UNESCO-2001 convention

The methodological framework is inspired by the UNESCO-2001 convention. It is therefore important to summarize its main components. This section provides the general description and identifies parts of the convention which guided the choice and developments of techniques utilised in the PhD project. Comprehensive descriptions of the methods are contained in chapters 3, 4 and 5.

Among other points, the UNESCO-2001 (UNESCO 2002) convention:

(1) Defines underwater cultural heritage (UCH) as 'all traces of human existence having a cultural, historical or archaeological character which have been partially or totally under water, periodically or continuously, for at least 100 years' (Article 1, definition 1a)

(2) Encourages *in-situ* preservation of UCH as the first option (Article 2, point 5; Annex: Rule 1)

(3) Promotes the idea that the 'responsible non-intrusive access to observe or document *in-situ* underwater cultural heritage shall be encouraged to create public awareness, appreciation, and protection of the heritage except where such access is incompatible with its protection and management' (Article 2, point 10)

(4) Promotes the use of non-destructive techniques and survey methods (Annex: Rule 3, 4, 16).

(5) Provides strict guidelines on the design of projects directed at UCH (Annex: Section II) including the so-called 'preliminary work'.

(6) The preliminary work 'shall include an assessment that evaluates the significance and vulnerability of the underwater cultural heritage and the surrounding natural environment to damage by the proposed project' (Annex: Rule 14).

(7) Additionally, 'the assessment shall include background studies of […] environmental characteristics of the site, and the consequences of any potential intrusion for the long-term stability of the underwater cultural heritage affected by the activities' (Annex: Rule 15).

(8) Furthermore, with regards to site management and conservation: "The site management programme shall provide for the protection and management *in-situ* of underwater cultural heritage […]. The programme shall include public information, reasonable provision for site stabilization, monitoring, and protection against interference" (Annex: Rule 25).

As the shipwrecks investigated in the project are all more than 100 years old, they are defined as UCH, according to definition (1). The PhD focuses on the assessment of, and improving knowledge of, physical site formation processes, which are paramount for understanding *in-situ* preservation issues, highlighted in point (2). Furthermore, the main methodological focus is on collecting and analysing field data using high-resolution marine, acoustic remote sensing techniques, namely multibeam echosounders and sub-bottom profilers, complying with points (3) and (4). The only potentially invasive component is introduced through sediment sampling, however, all the samples are taken at reasonable, safe distances from the shipwrecks.

The combination and developments of methods presented in chapters 3, 4 and 5 support the 'preliminary work' before undertaking actions targeting UCH referred to by the points (5), (6)

and (7), by assessing long-term stability and vulnerability of the sites to external environmental and anthropogenic factors. This research is expected to be ultimately beneficial for site management of Underwater Cultural Heritage (8).

1.5. Outline of the thesis

Following this introduction, chapter 2 provides a detailed review of methods and research aimed at physical site formation processes at shipwreck sites. It identifies knowledge gaps and presents further justification both for the selection of the objectives and the methods for this project.

Chapter 3 contains a published research paper addressing the first objective. In the study, a residual relief modelling method is presented for the semi-automated extraction of depositional and erosional signatures (wreck marks). The GIS method is developed and successfully tested for three shipwreck sites: SS *Hare*, SS *Polwell* and SS *Tiberia* using the high-resolution bathymetric DEMs obtained for the project. In the end of the chapter, methodological considerations and archaeological implications for the presented workflow are discussed in detail.

Chapter 4 presents a published research paper addressing the second objective. Sediment budget change and its hydrodynamic triggers are investigated for all the sites described in the introduction. This is conducted through a GIS integration of time-lapse multibeam echosounder, geophysical, geological and modelled oceanographic data. The time-lapse bathymetry datasets allowed investigating evolution of the sites in multiple temporal (weekly, annual, multiannual and decadal) scales and at a spatial resolution previously unrealised in underwater physical site formaton assessments. The quantified sediment budget change is discussed from geotechnical and archaeological perspectives. While the former perspective explores factors controlling the variability in recorded geomorphic change between individual sites, the latter discusses the sites based on their equilibrium states (static and dynamic), yielding different *in-situ* preservation estimates.

Chapter 5 contains a detailed investigation of hydro- and sediment-dynamic settings at the sites of SS *W.M. Barkley* and HMS *Vanguard*. Hence, it addresses the third objective of the thesis. The study combines the use of advanced CFD simulations involving 3D models of the complex wreck sites and is validated with difference modelling performed using the time-lapse multibeam echosounder data. Results show intricate patterns of flow developed around the wreck structures and demonstrate that CFD simulations can explain and predict which areas at shipwreck sites are prone to erosion. The discussion of the findings highlights their implications spanning across marine science, engineering and spatial planning and cultural heritage management.

The discussion of the thesis is presented in Chapter 6. The chapters corresponding to the research objectives are discussed individually, and additional remarks are made regarding the methodologies developed in the thesis. The summary and recommendations sections

subsequently present a narrative linking all the chapters together to form a multi-method approach for the characterization of shipwreck sites, and then identify future research prospects based on the newly acquired knowledge.

2. Physical formation processes of shipwreck sites: A review

2.1. Introduction

The rapid development of marine survey technologies in recent decades has led to the discovery and identification of a great number of shipwrecks (Croome 1999; Ballard 2007; Brady *et al.* 2012). These sites have become part of our common underwater landscape and are of interest to many parties (Firth 2018). Historic wrecks act as time capsules, reflecting technology and life on board at their time of loss (Elkin *et al.* 2020; Geraga *et al.* 2020). Many of these vessels were lost in dramatic circumstances of naval warfare and are commemorated as mass graves. Shipwrecks are also islands of hard substrata on the seabed, resulting in thriving marine communities on and around them (Zintzen *et al.* 2008; Balazy *et al.* 2019; Johnson *et al.* 2020). Accordingly, wrecks are often visited by sport divers, fishers and sea anglers.

On the other hand, wrecks are sometimes negatively perceived; as threats to navigation and to the environment, often containing unused fuels, heavy elements and unexploded ordnance (Landquist *et al.* 2013; Ndungu *et al.* 2017; Vanninen *et al.* 2020). All these factors make shipwrecks a very important hidden resource, often neglected by authorities and presenting multiple challenges with respect to site management and marine spatial planning (Firth 2018; Papageorgiou 2018). These two activities can only be implemented effectively when shipwrecks are understood in their local environmental context. This context determines whether a given shipwreck needs immediate attention, due to risk of accelerated degradation, or can be left as it is. One way to better understand shipwrecks and their surroundings, through assessing their environmental context and conservation status, is the study of site formation processes.

2.2. Definition of site formation processes

In archaeology, site formation processes are defined as the factors which create the archaeological and historic records (Schiffer 1996). In shipwreck research, site formation comprises singular and/or continuous events and processes that contribute to the condition of a wreck site at a given time (Oxley and Keith 2016). Site formation is influenced by cultural factors (C-Transforms), where the driver is human behaviour, and natural factors (N-Transforms), driven by the natural environment (Oxley and Keith 2016).

One of the pioneers of shipwreck site formation research was Keith Muckelroy, who proposed a model representing the evolution of submerged shipwrecks as a function of N- and C-Transforms (Fig. 2.1a) (Muckelroy 1976). In a simple but organized manner it categorizes processes and events which change a site over time. He identified processes that lead to the loss of material from

a wreck site: the wrecking incident, salvage operations and the disintegration of perishables and termed these 'extracting filters'. After a shipwreck lands on the seabed, so-called scrambling devices start to act. The archaeological material is rearranged (scrambled) due to a variety of natural and anthropogenic processes, including seabed movement, authorised archaeological excavation, unauthorised salvage activities and others (Muckelroy 1978).

Even though Muckelroy's (1978) study described the evolutionary route of shipwrecks, the sequences contained within it show only products, rather than the events and processes influencing and causing them. Hence, Muckelroy's model is more descriptive, than predictive, as noted by Ward *et al.* (1999) who further developed the disintegration model by introducing the key N-Transforms affecting shipwrecks (Fig. 2.1b). These natural processes can be grouped into physical, biological and chemical deterioration (Ward *et al.* 1999) and are described in the following sections. As the biological and chemical formation processes are not the focus of this review, they are only briefly introduced to reveal their interrelation with physical site formation processes.
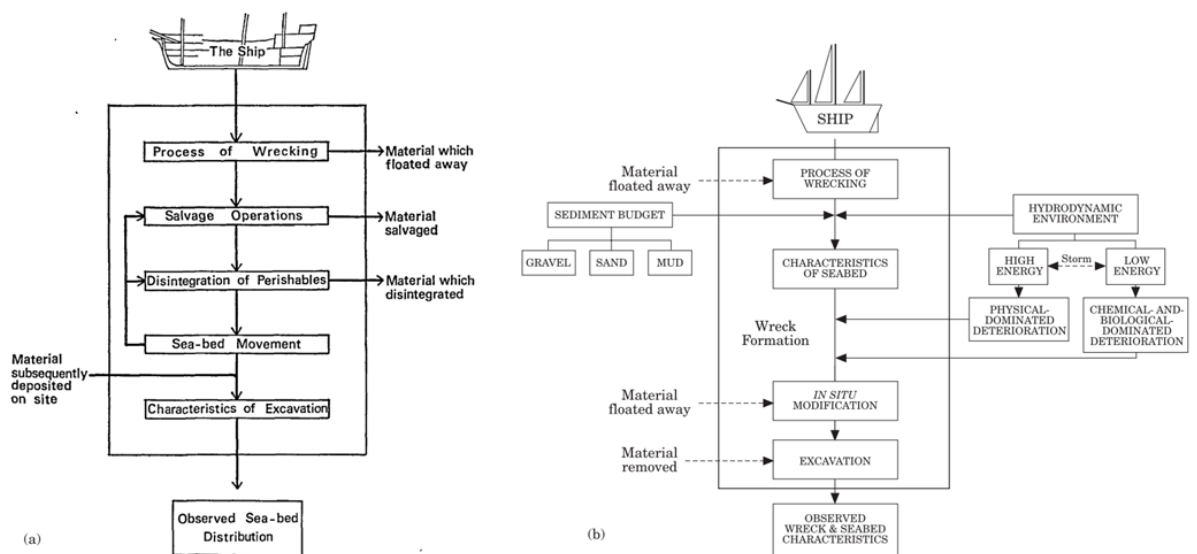
Figure 2.1. (a) Flow diagram with the evolution of a ship after an event of wrecking (from Muckelroy 1978), (b) modified version highlighting the key processes which affect wreck disintegration (from Ward *et al.* 1999).

2.2.1. Physical site formation processes

In this review, physical site formation processes are understood as linked hydro- and sediment-dynamic processes controlling seabed movement, sediment erosion and deposition and hydraulic forcing applied directly to the wreck by currents and waves (Ward *et al.* 1999). The influence of waves can be related to the ambient wave climate or punctuated events like storms and hurricanes, while the current regime can be unidirectional (e.g. wind-driven) and multidirectional (e.g. tidal).

2.2.2. Biological site formation processes

Wooden materials placed on the seabed are colonized by various marine organisms (Gregory 2016). Water masses in the pelagic zone usually contain higher levels of dissolved oxygen, which supports wood boring organisms capable of causing substantial deterioration in a relatively short period of time (Eriksen and Gregory 2016; Gregory 2016; Pournou 2017). Therefore, wooden parts of shipwrecks tend to be well-preserved only when exposed on the seabed to water with low oxygen content (e.g. Eriksson and Rönnby 2012) or when buried in dysoxic and anoxic sediments. Buried wooden parts of shipwrecks are protected from wood boring organisms due to the limited dissolved oxygen supply preventing their respiration, therefore these parts are affected mostly by microbiological processes (Gregory 2016, 2020).

Steel wrecks can be attacked by microbial organisms creating rusticles (Cullimore and Johnston 2008). Under specific conditions (e.g. the RMS *Titanic* wreck site) iron oxidising bacteria can mobilize iron from a ship's structure at rates causing rapid deterioration (Salazar and Little 2017).

In some cases, biological encrustation can contribute positively to the conservation of shipwreck materials. Barnacles, polychaetes, coralline algae, bryozoans, molluscs and serpulids produce calcareous deposits, acting as protective layers against corrosion (MacLeod 2016; Bethencourt *et al.* 2018; González-Duarte *et al.* 2018).

2.2.3. Chemical site formation processes

Corrosion of metal materials can be regarded as a process which reverses the processes used to create them (MacLeod 2016). The build-up of corrosion products is complex and the chemical formation processes which cause it are usually unique to a site, which can make them difficult to assess and compare (MacLeod 2016).

Dependent on oxygen availability, corrosion can be divided into two types: aerobic and anaerobic. In oxygenated marine and freshwater environments, where the main oxidizing agent is O_2, corrosion is aerobic. Shipwrecks and artefacts which are open to aerobic processes are usually exposed to the water column, although objects buried in the first 20 to 50 cm of sediment are also influenced by aerobic conditions (MacLeod 2016). Below this depth, anaerobic control takes over under dysoxic and anoxic conditions. Anaerobic corrosion is influenced by microbiological activity i.e. metabolic processes of certain species of bacteria. This type of biochemical deterioration can be intensive, as seen for example at the RMS *Titanic* wreck site (Cullimore and Johnston 2008).

2.2.4. Anthropogenic site formation processes

C-transforms, also referred to as cultural or anthropogenic processes, are associated with the impact of humans. There are numerous possible sources of human activity, which can influence underwater sites, including the construction of underwater pipelines, development of renewables, oil and gas infrastructure, port structures, cable laying, dredging, illegal salvage, disposal of material, bottom trawling and sport diving, occasionally ending up in looting (Stewart 1999; Gibbs 2006; Quinn and Boland 2010; Brennan *et al.* 2013, 2016). Excavations and invasive research conducted at shipwreck sites also change the site permanently, and are therefore also classified as formation processes (Muckelroy 1978).

2.3. The importance of physical site formation research

Changes in sediment budget may directly lead to complete or partial burial/exposure of a shipwreck (Ward *et al.* 1999; Quinn 2006; Quinn *et al.* 2007). Whether the shipwreck structure is buried or exposed to the water column determines oxygen availability, which in turn limits the accessibility of marine organisms and controls corrosion. Therefore, physical site formation processes strongly influence biological and chemical processes, especially in the early stages, when changes in sediment budget due to scour are the most dynamic (Quinn 2006). Although the temporal scales of geomorphic seabed changes are not fully understood at shipwreck sites, some of them undergo reorganization multiple times during their residence on the seafloor (Quinn and Boland 2010; Pascoe 2012; Astley 2016). Hence, physical site formation is a decisive consideration for *in-situ* preservation.

In ocean engineering, geomorphic change of the seabed and scour processes are considered detrimental to submerged offshore structures (Whitehouse *et al.* 2011). Offshore development plans require extensive environmental assessments and suitability studies and constructions like windfarm monopiles require scour mitigation measures (Melling 2015). Scour can potentially cause partial or complete collapse of manmade structures, including wrecks (Quinn 2006).

Conversely, the signatures developed by scour processes (i.e. wreck marks) and continuous geomorphic change (or its absence) are useful indicators of the local hydro- and sediment-dynamic environment. By assessing the seabed geomorphology in detail, it is possible to derive information about the direction of net sediment transport (Caston 1979). Therefore, wreck sites can potentially act as proxies and studying them allows us to characterise geotechnical and oceanographic processes operating in the local environment.

In summary, we require a better understanding and quantification of physical site formation processes at wreck sites. This review therefore assesses recent developments in the field and identifies gaps in knowledge which contribute to developing the research questions addressed in this project.

2.4. Physical site formation: methods of research

Due to the rapid development of marine survey technologies in recent decades, physical site formation research has gradually progressed from constructing conceptual models based on the pioneering, primarily diver-led assessments (Frost 1961; Muckelroy 1976, 1978) to advanced, digital data-informed and very detailed site formation case studies using sophisticated tools. Noteworthy, comprehensive guidelines describing novel methods for underwater prospection, site formation assessment, monitoring and aiding excavation have been developed in the SASMAP project (Gregory and Manders 2015b). Additionally, McCarthy *et al.* (2019) provide an exhaustive description of 3D recording methods in maritime archaeology. This section highlights the recent methodological advancements in the field of physical site formation research in order to identify methods suitable for the investigation conducted within the framework of the PhD project.

2.4.1. Hydrographic survey

Currently, acoustic remote sensing of the seabed can be performed with centimetric accuracy in a time-effective way (Westley *et al.* 2019). The most common hydrographic devices used in seabed mapping and underwater archaeological prospection are side scan sonars (SSS) and multibeam echosounders (MBES).

Survey-grade side-scan sonars (SSS) are usually towed behind a research vessel on a towfish or mounted to an underwater vehicle (e.g. to an AUV), operating a few metres above the seabed (typically 10-20 m) to reduce the distance between sensors and targets and to enhance data quality. Similar to other hydrographic devices, the position of the sensor needs to be determined precisely and for an SSS this can be accomplished using acoustic positioning systems like ultra-short baseline (USBL) or estimated through manual layback. SSS data are mostly used for object detection, however as they provide an image of the seabed (frequently referred to as a sonogram) based on the intensity of acoustic reflection and scattering, they are also used to differentiate seafloor substrates in a similar was to MBES-derived backscatter data (Collier and Brown 2005; McLarty *et al.* 2020). SSS devices are used widely in archaeological prospection and can provide detailed images of archaeological material (Quinn *et al.* 2005) and shipwrecks, allowing for detailed assessments of their *in-situ* preservation (Geraga *et al.* 2020; Grządziel 2020a).

Multibeam echosounders are usually hull-mounted or pole-mounted on a research vessel, however they can also be attached to unmanned underwater vehicles (UUVs) like autonomous underwater vehicles (AUVs) and remotely operated vehicles (ROVs). In order to achieve the highest accuracy, MBES sensors need to be coupled with high-performance positioning systems involving Global Navigation Satellite System (GNSS) data and compensating for vessel movements such as pitch, roll and heave. In order to maximise data quality and sharing, surveys

should adhere to the evolving standards of the International Hydrographic Organization (IHO 2020).

MBES can deliver three kinds of data: bathymetric measurements, backscatter intensity values of the seabed and water column information. In shallow to moderate water depths, hull-mounted MBES sensors can map shipwrecks with centimetric accuracy (Westley *et al.* 2019) (Fig. 2.2). MBES-derived bathymetric measurements are invaluable for shipwreck research, as they allow us not only to detect and describe new sites (Plets *et al.* 2011; Westley *et al.* 2011), but also to evaluate geomorphic changes around shipwrecks through repeat or time-lapse surveys (Quinn and Boland 2010; Bates *et al.* 2011; Stieglitz and Waterson 2013; Astley 2016; Brennan *et al.* 2016). In practice, repeat high-resolution bathymetric data add the fourth dimension to an investigation of physical formation processes at shipwreck sites: time. Essentially, this approach allows us to capture information about site evolution.

Backscatter intensity images or mosaics result in information about the seabed's surface composition, as different substrates produce echoes of various strengths (Lamarche and Lurton 2018). These types of data are widely used in spatial ecology and benthic habitat mapping (McGonigle and Collier 2014; Calvert *et al.* 2015; Lamarche and Lurton 2018), and can provide valuable information for archaeological assessments (Masetti and Calder 2012), where knowledge about substrates is of vital importance (Astley 2016). Backscatter data are conventionally validated using classified sediment samples (i.e. ground-truthing data).

Lastly, MBES water column data provide observations of water column scattering and reflection and has been increasingly used in many disciplines of marine science, including mapping of shipwrecks (Colbo *et al.* 2014). Essentially, incorporation of the water column data in MBES-derived point clouds allows improved detection of upstanding parts of shipwrecks like masts (van der Werf 2010). Altogether, given their versatility, MBES systems provide an excellent solution for assessing physical shipwreck site formation processes in a time-efficient and non-invasive way (Astley 2016).
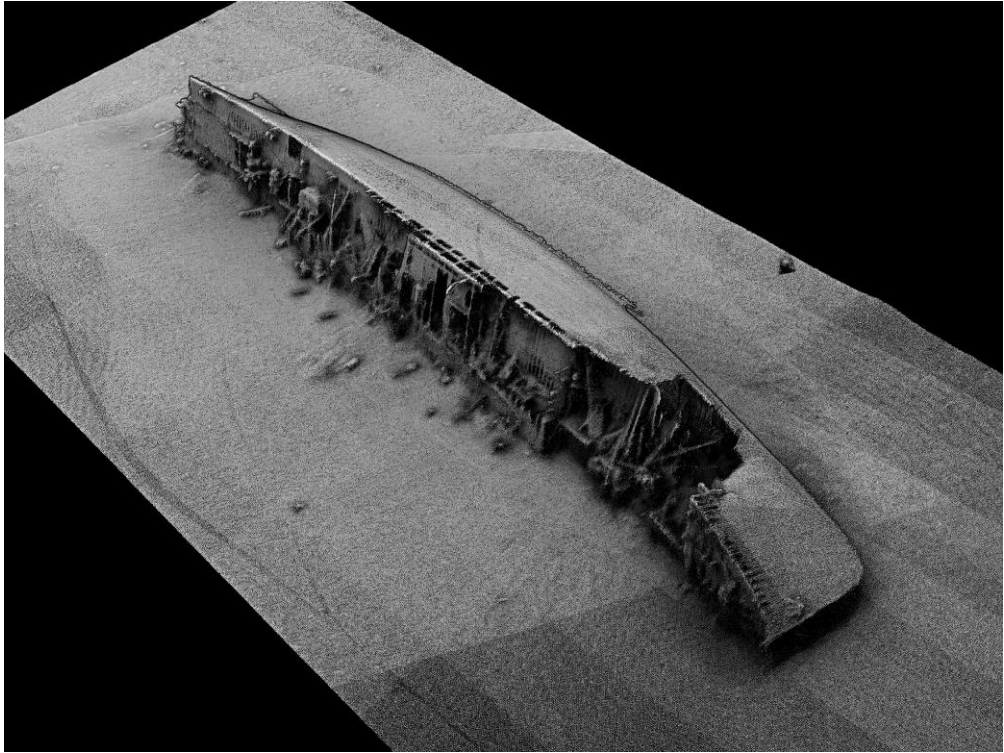
Figure 2.2. High density, MBES-derived point cloud of SS *Chirripo*, lost in 1917 off Northern Ireland, Belfast Lough (20–25 m water depth). The high definition representation was created using data from multiple passes over the wreck during the hydrographic survey (from Westley *et al.* 2019).

2.4.2. Seismic survey and sediment sampling

Seismic methods allow sub-seabed imaging, which enables access to a record of past site formation. Different seismic devices operate at different frequency bands, allowing for their equivalent depth of penetration and vertical resolution. In underwater archaeology, sub-bottom profilers have proven useful in accessing records of site formation (Fig. 2.3), assessing geological environments around shipwrecks (Quinn *et al.* 1997; Gregory and Manders 2015b; Geraga *et al.* 2020) allowing to construct geoarchaeological models of sites (Gregory and Manders 2015b), detection and characterization of the preservation state of buried wooden shipwrecks (Plets *et al.* 2008; Cvikel *et al.* 2017) and detailed mapping of buried sites (Plets *et al.* 2009; Winton 2019; Boldreel *et al.* 2021).
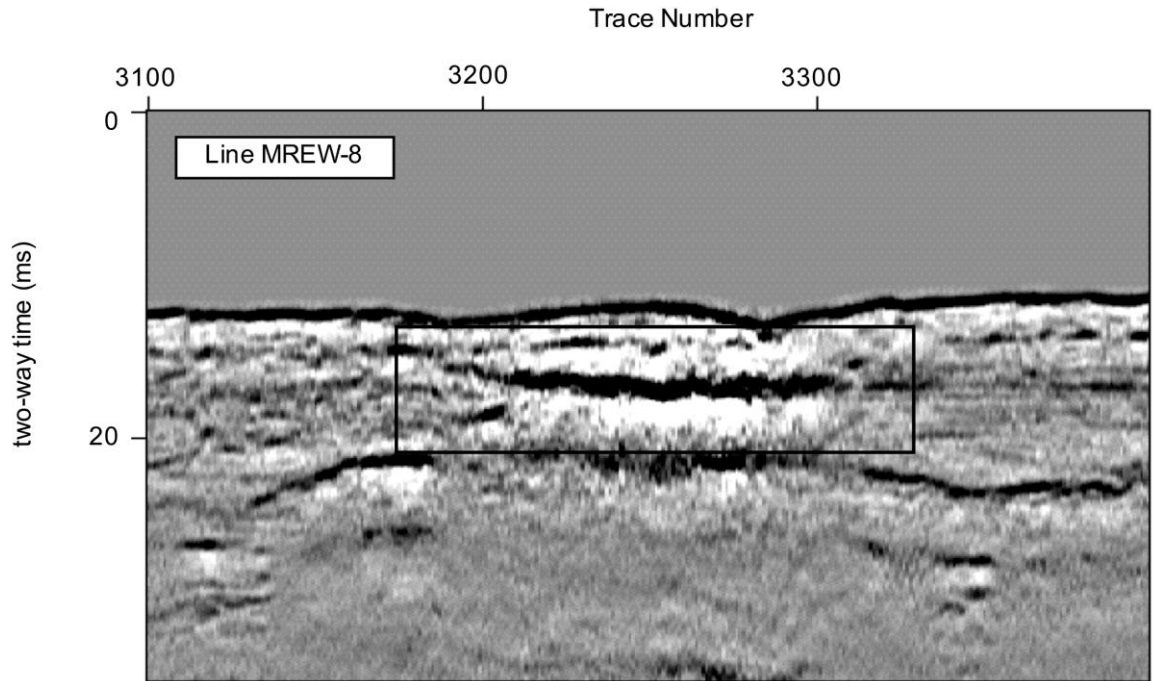
Figure 2.3. Processed seismic sub-bottom profile, displaying an anomaly (highlighted by the black box) at the shipwreck site of *Mary Rose* (lost in 1545 in the Solent, southern England). The anomaly, characterized by a discrete high amplitude reflector, was determined to be one of the wreck-related, buried 'palaeo-scour marks' (from Quinn *et al.* 1997).

When assessing physical site formation processes, sediment sampling at underwater shipwreck sites is performed to understand geological controls, sedimentary history, susceptibility of sediments to mobilization due to hydro-dynamic forces (McNinch *et al.* 2006; Astley 2016) and to ground-truth remote sensing datasets (Brown *et al.* 2011). The sampling can also deliver information about biota around a shipwreck (Balazy *et al.* 2019), oxygen availability and other chemical properties (Gregory 2020) and provide information about contamination resulting from the introduction of toxic compounds to the environment (Vanninen *et al.* 2020). Depending on the objective of the sampling, various devices can be used to collect sediment samples, including Van Veen, Day or Shipek grabs and box, piston, gravity and vibro corers.

2.4.3. Photogrammetric survey

Multi-image photogrammetry or structure-from-motion is currently among the most widely used techniques for recording archaeological sites both on land (Discamps *et al.* 2016) and underwater (McCarthy *et al.* 2019). This method involves combining multiple photographs of an object into a 3D model. Photogrammetry provides mosaics and 3D models with the greatest detail among the methods listed in this chapter (together with laser scanning, described later) and results in some spectacular representations of underwater sites (e.g. Fig. 2.4; Eriksson and Rönnby 2017). It is,

however, time-consuming and has some limitations, especially in low-visibility environments (Van Damme 2015; Pacheco-Ruiz *et al.* 2018).

Figure 2.4. Photogrammetry of a portside of the Swedish warship *Mars* (lost in 1564) resting in total darkness at a depth of 75 m in the Baltic Sea, off the island of Öland (adapted from Eriksson and Rönnby 2017).

Photogrammetry usually requires multiple dives of an experienced diver or an ROV. Underwater sites may pose risks to both divers and ROVs, depending on their depth, presence of strong currents, ghost nets and other impediments. Substantial, well-preserved and upstanding (often metal-hulled) shipwrecks naturally require more time and resources to obtain full-scale photogrammetric models (Nornes *et al.* 2015). Although photogrammetry has been successfully used in shipwreck site formation assessments (Demesticha *et al.* 2014; Secci *et al.* 2021), it focuses primarily on the shipwrecks and not on the seabed around them. Therefore, it can best serve to evaluate the state of a shipwreck's preservation, but is ineffective when it comes to assessing the regional context of the site, which requires capturing information on wide areas of the seabed around the wreck (Astley 2016).

2.4.4. Hydro-dynamic modelling

Hydro-dynamic forces acting at shipwreck sites result from a combination of sea surface waves, currents and storm surges. These can be modelled using various integrated numerical modelling software packages such as the commercial package MIKE 3 (DHI 2021) or open-source software Delft3D-FLOW (Lesser *et al.* 2004). Additionally, computational fluid dynamics (CFD) available in commercial software with graphical user interface like Ansys Fluent (Ansys 2021) or as open-source software packages like OpenFOAM (OpenCFD 2021) can be used for more detailed simulations of water flows. While broad-scale hydro- dynamic models can serve to assess shelf scale, coarse-resolution seabed dynamics (Dix *et al.* 2009a; Robakiewicz 2009; Fernández-

Montblanc *et al.* 2016), CFD simulations provide site-focused, detailed evaluation of the acting hydro-dynamic patterns and forces (e.g. Smyth and Quinn 2014; Quinn and Smyth 2018) (Fig. 2.5).
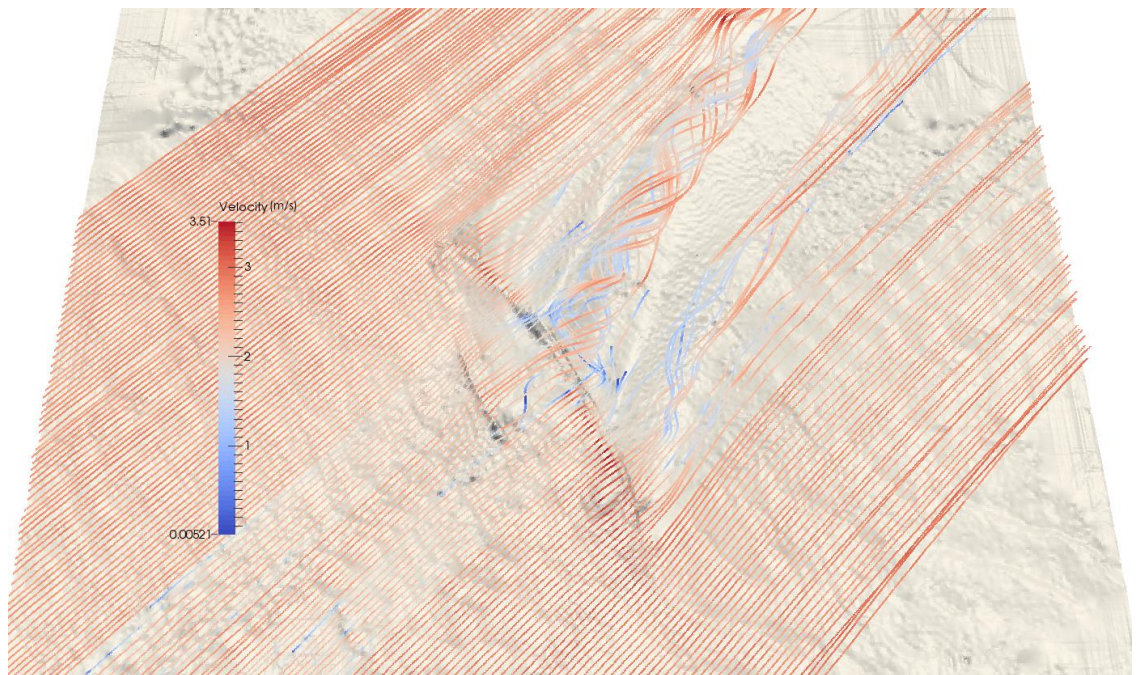
Figure 2.5. 3D streamline patterns coloured according to flow velocity, obtained with CFD simulations over a MBES data-derived 3D surface of a shallow-water (16 m depth) shipwreck site located at Arklow Bank in the Irish Sea (east coast of Ireland) (from Smyth and Quinn 2014).

CFD can be defined as the analysis of problems involving fluid flow using computer simulations. CFD uses Navier-Stokes equations to describe fluid motion and characterise various fluid dynamic quantities. The most commonly used numerical solution technique of the governing equation is the finite volume method. This algorithm initially integrates the governing equations over control volumes of a domain or mesh. Then the resulting integral equations are converted to a system of algebraic equations, which are iteratively solved (Versteeg and Malalasekera 2007).

Solving the Navier-Stokes equations directly is currently computationally prohibitive for turbulent flows with high Reynolds numbers (the ratio of inertial to viscous forces). Therefore, approximated solutions of the governing equations are applied that either average the turbulence (Reynolds-Averaged Navier Stokes Equations, RANS) or filter and model fine scales of turbulence, while directly simulating larger scales (large eddy simulations, LES). A combined RANS/LES approach is also used, referred to as a detached eddy simulation (DES). To date, only the RANS approach has been used to model turbulent flows over shipwreck sites. It is a common method across many disciplines including environmental (e.g. Smyth 2016) and industrial applications (marine engineering, aerodynamics and others) of CFD. Computationally expensive simulations using the LES model are recommended when very accurate results are required.

In RANS modelling, the Navier-Stokes equations are time-averaged and extra terms appear due to the interactions between turbulent fluctuations (Versteeg and Malalasekera 2007). The extra terms are modelled using turbulence closure schemes, among which the most popular are k–ε and k-ω models. To date, renormalised group (RNG) k–ε models (Yakhot *et al.* 1992) and k-ω shear-stress transport models (SST) (Menter 1992) have been the most commonly employed turbulence models for the investigations of flow patterns at shipwreck sites (De Hauteclocque *et al.* 2007; Smyth and Quinn 2014; Fernández-Montblanc *et al.* 2018b; Quinn and Smyth 2018).

The RNG k–ε model was developed to renormalise the Navier-Stokes equations, in an attempt to account for the effects of smaller scales of motion, as the standard k- ε model determines the eddy viscosity from a single turbulence length scale (Yakhot *et al.* 1992). Smyth and Quinn (2014) and Quinn and Smyth (2018) demonstrated that this model accurately describes transient flow patterns at shipwreck sites. The k-ω SST model combines the use of the k–ε model in the free-stream zone and the k–ω model in the inner region of the boundary layer (i.e. the layer of fluid in vicinity of a bounding surface, where viscosity effects are significant), using so-called blending functions. This combined turbulent closure approach has been shown to predict vortices, flow reattachment, turbulent kinetic energy and wall shear stress at a shipwreck site with a good accuracy while requiring significantly lower computational costs compared to the LES modelling (De Hauteclocque *et al.* 2007).

CFD modelling has been used for a variety of purposes in both underwater and terrestrial heritage science (Grau-Bové *et al.* 2019), including air and water flow visualizations (Hussein and El-Shishiny 2009; Smyth and Quinn 2014; Mikayama *et al.* 2015; Quinn and Smyth 2018), aiding preventive conservation (D'Agostino and Congedo 2014) and providing historical evidence for exploring past contexts (Castro-García *et al.* 2015). It is applicable to solving multiple problems involving any fluid flow, which are otherwise impossible to solve (i.e. manually, without computers) (Grau-Bové *et al.* 2019).

However, Grau-Bové *et al.* (2019) highlight some caveats/considerations in the application of CFD simulations in heritage science. They can be grouped into the following criteria (Grau-Bové *et al.* 2019), and are equally applicable to CFD modelling at shipwreck sites: (1) models should be experimentally validated in the environment of interest or laboratory settings, using spatially resolved data, (2) particular care should be taken when implementing boundary conditions, choosing turbulence models, parameters and functions simulating flows near surfaces, (3) time-scales of any problems investigated should be considered and stated, and (4) analysis and discussion of results should include a usefulness assessment.

When it comes to using CFD for physical shipwreck site formation assessments, simulations require knowledge of fluid dynamics and computational software implementation, in addition to knowledge of oceanography, marine physics and seabed morphodynamics. Only when these

parameters are defined can appropriate boundary conditions be established for a computational domain. Additionally, although performing CFD simulations can be entirely desk based with use of open-source software, applying it in order to investigate site formation processes requires a 3D model of a site (Fig. 2.5) (Smyth and Quinn 2014). Such 3D models can be obtained using a variety of techniques described in previous sections of this chapter and other papers/guidelines listing such methods (e.g. Gregory and Manders 2015a; McCarthy *et al.* 2019). Lastly, both inputs and outputs of shipwreck site CFD simulations need to be validated. For example, input velocity profiles in the water-column could be obtained over a shipwreck using a deployed or ship-mounted acoustic doppler current profiler (ADCP) or acquired from a broad scale models like the regional ocean modelling system (ROMS) (Shchepetkin and McWilliams 2005). Outputs of a simulation can be compared with other ADCP profiles, but also against bedforms and other geomorphological forms, whose directions and morphology can be correlated with the outputs (Quinn and Smyth 2018), or results of physical modelling in a flume channel.

Physical modelling is another hydro-dynamic modelling method which can be employed to understand physical site formation processes at shipwreck sites. It is conducted through laboratory experiments using specially designed flume channels and scaled shipwreck models (Dix *et al.* 2009b). Such modelling can be used to validate broad- and fine-scale numerical models (e.g. CFD), predict sediment transportation patterns in laboratory settings and compare results against spatially referenced *in-situ* measurements conducted at shipwreck sites.

2.4.5. Other methods

2.4.5.1. Methods used in assessments of hazardous shipwrecks

Many modern shipwrecks, especially dating back to World War II, are considered as environmental threats, as they often contain fuels and unexploded ordnance. They have been referred to as potentially polluting wrecks (Landquist *et al.* 2013). One study identified 8569 such shipwrecks around the world (Michel *et al.* 2005), each having the potential to cause an environmental disaster. Identifying sites which are susceptible to oil leaks becomes more important with time, as the vessels gradually disintegrate. Such identification may be performed through desk-based assessments (Landquist *et al.* 2013), using probabilistic models, which by definition should include acting physical processes to be reliable. For example, Ventikos *et al.* (2016) list oil discharge as a result of a wreck's positional change due to external factors (e.g. seismic activity) and hull breaching due to wave and current action as factors in their stochastic simulation. The authors use an example where the change of position occurred due to seismic activity, causing migration of the shipwreck on the seabed.

Hac and Sarna (2021) proposed a general methodology for oil removal on shipwrecks in the Baltic Sea region. They enumerate multiple methods aimed at gathering information about a wreck site and its present state on the seabed, including a desk-based review using archival documentation,

in-situ geophysical surveys, sediment sampling and others. They adopt a previously established list of criteria for assessing the probability of oil release (Basta *et al.* 2013; Goodsir *et al.* 2019), which includes seabed type and stability (Goodsir *et al.* 2019; Hac and Sarna 2021) and physical processes occurring in the area of a wreckage (hydro-dynamics and sedimentology) (Basta *et al.* 2013).

2.4.5.2.   Other remote sensing techniques

Technological developments in marine robotics, acoustic sensors and navigation systems, have caused an increased accessibility to novel technologies, including for example autonomous underwater vehicles (AUVs) with a mounted synthetic aperture sonar (SAS), capable of very high-resolution imaging of shipwrecks in deep waters. For example, Ødegård *et al.* (2018) used an AUV-mounted SAS to detect and investigate deep water sites (567-655 m), delivering images with a centimetric spatial resolution. This enables us to assess physical processes operating at depth without the typical constraints associated with hull-mounted sonars.

Another high-definition survey technique recently adopted in underwater archaeology is laser-line scanning. Johnson *et al.* (2020) coupled laser surveys with video recording to investigate deep-water wrecks (500 m), providing information on the physical integrity of shipwrecks, while also obtaining ecological metrics of local fish populations.

Among other remote sensing methods which have proven effective in detecting shipwrecks and have provided insights into physical site formation, are airborne bathymetric LiDAR surveys (Shih *et al.* 2014) and satellite imaging techniques (Baeye *et al.* 2016). The former method has been used to detect shipwrecks in shallow waters, where traditional hydrographic surveys are challenging due to navigational hazards. LiDAR surveys are not only capable of detecting shipwrecks, but can also provide information about the surrounding seabed geomorphology (Shih *et al.* 2014). High-resolution ocean colour satellite imagery has been used to detect shipwrecks in tidally-dominated coastal waters (Baeye *et al.* 2016). Using this method, wreck locations can be detected when they generate plumes of suspended particular matter (SPM) before maximum ebb and flood currents (Baeye *et al.* 2016). The study demonstrated that under some circumstances, this methodology not only allows nearshore shallow-water shipwrecks to be detected in environments where water-borne and airborne-lidar surveys are challenging, but also provides understanding of local sediment dynamics through the mapping of the SPM plumes.

2.4.5.3.   Other desk-based assessment methods

Another novel approach to understanding site formation processes was demonstrated by Fernández-Montblanc *et al.* (2018a) at the *Fougueux* (1805) site, where they coupled documentary research using archival materials with numerical modelling involving a Lagrangian dispersion model for a shipwreck site. The model, fed by archival information on meteorological

and oceanographic conditions at the time of wrecking, successfully predicted the spatial distribution of artefacts (Fernández-Montblanc *et al.* 2018a).

Another case study attempting to understand physical aspects of site formation and the distribution of sites was conducted by Church in 2014, analysing deep-water (534 – 1490 m) World War II shipwreck sites. The author combined archival documentation with a mathematical formula termed the 'Equation of Site Distribution', considering some basic parameters related to a sinking of a vessel like its heading, speed, time of deceleration, water currents and water depth. This method captured not only the distribution of wreck sites on the seabed, but also the wrecking process itself (Church 2014).

Another example of a project where a desk-based study was successfully applied, is the application of finite element modelling (FEM) to investigate structural degradation of the shallow-water (12 m) USS *Arizona* wreck, which contains large volumes of oil (Foecke *et al.* 2010). This engineering model successfully predicts theoretical stresses, forces and structural changes based on estimated corrosion rates, survey data, sediment compaction data and examination of concretion that covers the wreck's hull (Foecke *et al.* 2010).

Finally, information regarding physical site formation can be obtained through public engagement, by involving various groups which may have witnessed ongoing processes: sport divers, fishers and others (Firth 2018). It is important to note that a desk-based, documentary investigation exhausting available materials and archives should always be considered before making decisions about any additional or new surveys plans (Gregory and Manders 2015a).

2.5. Physical site formation: processes and patterns

Depending on the regional geological context, shipwrecks may rest on a seabed characterized by variable dynamics. The seabed may be covered with bedforms like lineations, furrows, grooves, ridges, sediment waves and others (Stow *et al.* 2009; Van Landeghem *et al.* 2009b). Some of the bedforms can be actively progressing, while others remain dormant. The active component of the seabed inevitably influences shipwreck site formation, resulting in burial or exposure of the archaeological material and its physical abrasion (Ward *et al.* 1999).

Sediment-dynamics and related seabed movement at shipwreck sites is exacerbated by seabed scour. Scour occurs at the seabed when sediment is eroded from an area due to forcing by waves and/or currents (Whitehouse *et al.* 2011). It can be initiated by a change in morphology and/or migration of bedforms (Soulsby 1997; Hay and Speller 2005; Ginsberg and Aliotta 2019) or by the intentional (e.g. seabed engineering; Whitehouse *et al.* 2011, unexploded ordnance, mines; Jenkins *et al.* 2007) or accidental (e.g. shipwreck; Quinn 2006) introduction of an object to the seabed.

Shipwrecks usually act as substantial obstacles to flow, hence seabed scouring around them is often extensive (Fig. 2.6), frequently creating deep erosional signatures, occasionally extending to great distances (Quinn 2006; Garlan *et al.* 2015). Scour signatures are typically accompanied by mounds of re-deposited sediments, and together the erosional and depositional features are referred to as wreck marks (Caston 1979). Depending on the depth of a shipwreck, the seabed scour can be caused by waves, currents or combined waves and currents (Soulsby 1997).
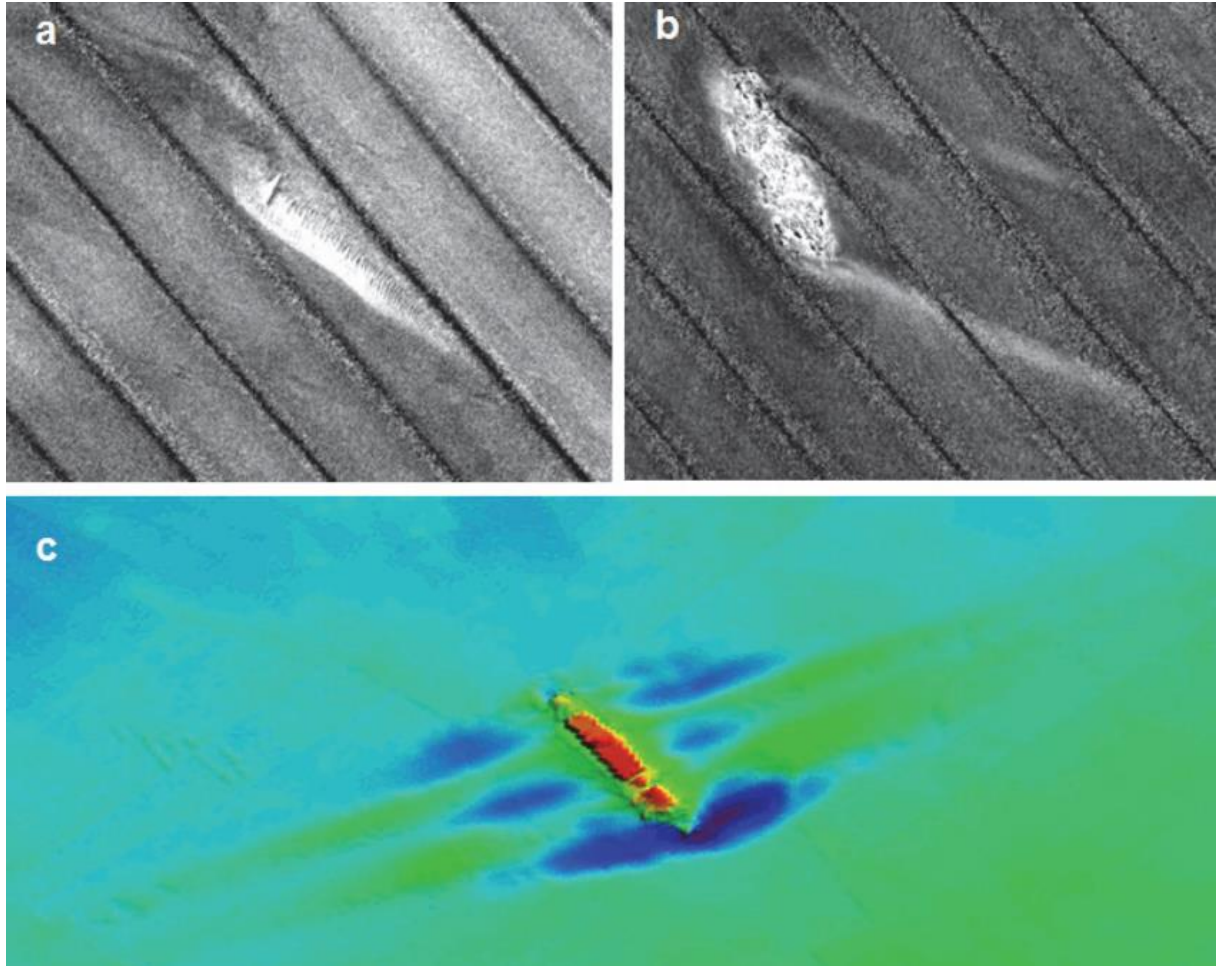
Figure 2.6. MBES backscatter (a,b) and (c) bathymetric plots showing examples of unidirectional singular (a) and twin (b), and bidirectional triplet (c) scour/depositional features around shipwrecks in the macrotidal regime off the coast of France (from Garlan *et al.* 2015).

As physical formation processes comprise a variety of oceanographic, geological and geotechnical phenomena, their objective assessment is challenging. One way to measure them is by evaluating changes in sediment budgets, defined as net sediment gain and loss in the wreck area (Ward *et al.* 1999). As the hydro-dynamic regime and the geomorphic changes (resulting in the sediment budget changes) are inextricably linked, this approach enables us to discuss physical site formation in a quantitative way, allowing comparisons between and across case studies.

2.5.1. Geomorphic change at shipwreck sites

When a structure like a shipwreck, monopile or any other obstacle is introduced at the seabed, it leads to an increase both in the speed of the water's flow in the object's vicinity and in the turbulent intensity due to the generation of vortices around the structure (Whitehouse 1998). This results in an amplification of bed shear stress levels, which enhances seabed scour around the structure.

Perhaps the first work which reported and analysed scour processes around shipwrecks in detail is that of Caston (1979). The author described scour marks visible around numerous wreck sites north of Dover Strait (outer Thames Estuary), an area characterized by strong tidal currents. For this purpose, images of seabed and bathymetric soundings were obtained with a side scan sonar and a single-beam echosounder, respectively. The paper provided a thorough description of the main characteristics of the recorded wreck marks where possible, including their dimensions, depths, and composition with respect to substrates. Additionally, the author noted that the orientation of individual wrecks relative to peak flow controls the patterns of associated wreck marks. The main conclusion of the study was that wreck marks can serve as proxies for net sediment transport, as they form parallel to the dominant tidal currents (Caston 1979). Although the study did not investigate the archaeological implications of wreck marks, it set a precedent for the future investigation of physical site formation processes.

The first paper which noticed an archaeological significance of wreck marks (Quinn *et al.* 1997), focused on the shipwreck of *Mary Rose*, King Henry VIII's flag-ship, lost in 1545 in the Solent (southern England, off Southampton). The authors used a chirp sub-bottom profiler to investigate the site, after remains of the shipwreck's hull had been lifted from the seabed to be displayed at the Portsmouth Historic Dockyard. Densely acquired 2D seismic profiles allowed the detection of four anomalies in proximity to the site and their morphology resembled that of wreck marks described by Caston (1979). Hence, they were described by the authors as paleo-scour marks, buried within sediments (Quinn *et al.* 1997). They were developed around the wreck after its deposition on the seabed. As the wreck gradually disintegrated, it presented less of an obstruction to tidal flow and the scour pits were been subsequently filled (Quinn *et al.* 1997). This detection of the palaeo-scour marks entailed some profound implications for maritime archaeological research (Quinn *et al.* 1997). Firstly, they act as sinks for archaeological material from a disintegrating shipwreck. Therefore, they should be considered when planning excavations, as they may contain trapped artefacts preserved within infilling sediments. Secondly, information about their morphology allows to draw conclusions about the nature and chronology of wreck's disintegration within its dynamic environment (i.e. site formation). Lastly, as in many cases wooden shipwrecks disintegrate and undergo burial quickly, extensive paleo-scour marks generating echoes in shallow seismic data may help to detect a site, where there is absence of a

ship's superstructure and archaeological material is scattered. The seismic method has since proven effective in archaeological investigations, both in terms of shipwreck detection (Plets *et al.* 2009; Grøn *et al.* 2015) and in the investigation of wreck site formation (Plets *et al.* 2008, 2009; Ferentinos *et al.* 2020; Geraga *et al.* 2020).

Changes in sediment budget due to scour and other sedimentary processes occurring at underwater sites have been directly linked to other physical, biological and chemical processes by Ward *et al.* (1999). The authors explain how the net removal and supply of sediment to wreck sites cause its subsequent burial or exposure, which in turn enhances or hinders the action of corrosion, biological encrustation and other site formation processes. The work resulted in expanding the site formation diagram presented in Fig. 2.1a, by integrating the main physical site formation processes affecting underwater sites (Fig. 2.1b).

In inshore waters and marine engineering, local erosion of the seabed due to scour is traditionally divided into two cases: clear-water and live-bed scour (Whitehouse 1998). They are defined in terms of the bed shear stress, τ_0 , which is the frictional force exerted by the flow on the bed per unit area of bed (Nm^{-2} or Pa in SI units), and the corresponding critical shear stress value, which represents a threshold for sediment motion (τ_{cr}) (Whitehouse 1998). When the upstream flow-induced bed shear stress τ_0 is less than the critical bed shear stress τ_{cr} in the ambient seabed, but exceeds it where it is amplified near the structure, clear-water scour occurs (Whitehouse 1998). In this case, the seabed is static across the site and sediment is washed away from around the structure only. An equilibrium scour depth is reached at some time after the structure is introduced to the seabed, when the forces exerted by the flow are balanced by the resistive force of the particles (Whitehouse 1998). On the other hand, when the τ_{cr} is exceeded everywhere across the site, live-bed scour occurs. An equilibrium scour depth is also obtained despite the fact that critical shear stress is exceeded (Whitehouse 1998). Although this description and classification of scour by Whitehouse (1998) has been established for engineering applications, the distinction between live-bed and clear-water scour can also be applied to describe physical formation processes affecting shipwreck sites (Astley 2016). Examining whether the seabed around a shipwreck is at the live-bed or clear-water scenario, may help to understand the dynamics and the nature of equilibrium of a wreck site within its environmental setting (Quinn 2006; Astley 2016).

A detailed description of scour processes at shipwreck sites in the context of site formation was provided by Quinn (2006), building on previous work discussing scour at shipwreck sites (Caston 1979; Quinn *et al.* 1997; Ward *et al.* 1999) and other underwater objects (e.g. Soulsby 1997; Whitehouse 1998). Quinn (2006) described patterns of flow around a fully submerged shipwreck site using a conceptual model (Fig. 2.7), which is further described in the following section. Understanding the main patterns of the current flow and bringing together case studies and the author's observations resulted in a description of the main factors affecting the development of

scour at shipwreck sites and their archaeological implications. Among the main factors controlling the morphology of scour signsatures are the orientation of the wreck structure in relation to the prevailing hydro-dynamic regime, shape and size of the wreck and other site components, the hydro-dynamic regime, local bathymetry and the geological composition of the seabed (Quinn 2006; Garlan *et al.* 2015; Astley 2016; Quinn and Smyth 2018). Additionally, Quinn (2006) noticed that individual artefacts may act as nuclei to promote scour at a local scale, which has important implications for scattered sites (Manders 2009; Fernández-Montblanc *et al.* 2018a). Perhaps one of the most important conclusions from the work of Quinn (2006) is that the impact of scour processes on site formation is concentrated towards its beginning, when physical processes dominate wreck disintegration after its deposition on the seabed. After scour reaches its maximum depth, the site reaches a quasi-equilibrium state. This, however, can still be disrupted by external environmental (for example live-bed conditions) or anthropogenic forcing (for example dredging) (Quinn 2006). This conclusion added momentum for further research, exploring sites as process-response systems, interacting with their ambient environment (Quinn and Boland 2010; Astley 2016).

The scour processes and related dynamism of a site can be investigated through so-called time-lapse bathymetric surveys (Quinn and Boland 2010; Bates *et al.* 2011). The term time-lapse refers to performing hydrographic surveys (commonly with multibeam echosounders) at least two times over the same area. This strategy has a significant advantage over a one-off survey, as it captures changes at a site. Time-lapse surveys can be performed at various intervals, capturing change at different temporal scales. Although this approach has been gaining attention in shipwreck site formation research (Quinn and Boland 2010; Bates *et al.* 2011; Raineault *et al.* 2013; Stieglitz and Waterson 2013; Astley 2016; Brennan *et al.* 2016; Fernández-Montblanc *et al.* 2016), the number of case studies using this technique remains small, taking into consideration the total number of shipwrecks in seas and oceans around the world (Croome 1999; Astley 2016).

Time-lapse case studies have confirmed that the spectrum of possibilities regarding stability and instability at shipwreck sites is vast. Quinn and Boland (2010) described changes at two sites, probably impacted by anthropogenic forces, using time-lapse surveys conducted with relatively short intervals (5 to 13 days). One of them, the *Drogheda Boat* dating back to the 16th century, and located in 2 m of water in the River Boyne (Co. Louth, Ireland), experienced significant geomorphic changes after extensive dredging operations. As the time-lapse survey indicated that the site was undergoing material loss, a preventive intervention by the dredging company was necessary (Quinn and Boland 2010). The second site investigated an unidentified wooden shipwreck resting at 16 m water depth on the Arklow Bank (Irish Sea) which was also affected by significant geomorphic change, probably associated with a cable-lying operation, but stabilized shortly after (Quinn and Boland 2010). Hydro-dynamic patterns of tidal currents at the Arklow Bank site were later investigated using CFD (Smyth and Quinn 2014) and elevated

turbulent kinetic energy and shear stress were observed in an area downstream of the wreck, approximately where the geomorphic change had been previously recorded (Quinn and Boland 2010). Nevertheless, the time-lapse investigation (Quinn and Boland 2010) concluded that some wreck sites are in an equilibrium state, and resilient enough to absorb an external forcing like the Arklow Bank site, while others, like *Drogheda Boat*, are not. The latter type of site evolves to a new state after experiencing external forcing.

Another example of intense anthropogenic forcing detected with time-lapse multibeam data gathered at 11 months interval was presented by Brennan *et al.* (2016), who quantified bottom trawling damage to ancient shipwreck sites. Trawling not only damages and scatters artefactual material, but also removes sediments, exposing artefacts, and smooths out natural morphological features of the seabed (Brennan *et al.* 2016).

Bates *et al.* (2011) investigated the site of *HMS Stirling Castle*, a ship-of-the-line lost on the Goodwin Sands in 1703, using similar time-lapse methods. The shipwreck, located in a highly dynamic, tidally- and wave- influenced environment, has been reported to periodically disappear under sediments, since its discovery in 1979 (Pascoe 2012). The time-lapse investigation of the *Stirling Castle* site involved MBES data collected between 2002 and 2006, allowing for the assessment of geomorphic changes at the site over various time-scales: within a few months, one year and four years (Bates *et al.* 2011). The investigation determined that coarser-grained sediments are present in areas around the wreck, where erosion has occurred, while depositional areas are characterized by a finer-grained substrate. The geomorphic changes were attributed to a local perturbation of the tidal flow by the wreck, migration of sand dunes around the site and a large scale, regional migration of the entire sandbank, on which the wreck is located (Bates *et al.* 2011). The authors, similar to Quinn and Boland (2010), highlighted the complexity of factors affecting sedimentary conditions at sites located in dynamic environments, and the necessity to continuously conduct time-lapse surveys, to allow site formation assessments at multiple temporal scales.

A scenario of perhaps one of the most extreme possible hydro-dynamic forcing occurring at a wreck site in the marine environment was recorded and described by Stieglitz and Waterson (2013). The authors investigated how Cyclone *Yasi* affected the shipwreck of SS *Yongala,* a luxury passenger steamer lost in 1911 off north Queensland, Australia, now resting in 30 m of water. They reported substantial damage to the hull structure, recorded in multibeam datasets acquired before and after the cyclone had passed through the site. They noted that damage may be further exacerbated by scour processes activated by extreme weather events like cyclone *Yasa*.

Raineault *et al.* (2013) investigated scour development at tidally- and storm-influenced artificial reef structures (i.e. subway cars) located at the continental shelf off Delaware Bay (United States) at a mean water depth of 28 m in an area where the seabed is composed of multimodal sediments.

The authors acquired time-lapse data using phase measuring bathymetric and side scan sonars and determined that, while scour processes have settled around individual subway cars after 6-7 years since their deployment, the erosion is generally more intense and still ongoing around larger clusters of objects. Additionally, the analysis of sediment samples revealed that sediments increase in gravel content (coarser material) and decrease in silt and clay (finer materials) content in proximity to the reef structures (Raineault *et al.* 2013), a conclusion similar to that reported by Bates *et al.* (2011).

In her 2016 PhD thesis, Astley examined geomorphic change at five wreck sites using repeat MBES surveys at intra-annual, annual and multi-annual time-scales coupled with metocean, geological and geomorphological data. The wreck sites represented a range of environments, from the storm-dominated HMS *Scylla* (20 m depth, lost in 2004), through the tidally-dominated sites of SS *Richard Montgomery* (8 m depth, lost in 1944, containing a large amount of unexploded ordnance), *Burgzand Noord* (also investigated by Manders 2009) (7 m depth, lost in 1650) and HMS *Stirling Castle* (15 m depth, lost in 1703) (also investigated by Bates *et al.* 2011; Pascoe 2012) to the more sheltered site of SS *Algerian* (21 m, lost in 1916). Analyses of the time-lapse data demonstrated that some sites were exposed to dynamic environmental forces, while others remained nearly static. Dynamic changes were associated with a storm event (HMS *Scylla*), implementation of physical protection (sandbags and polypropylene nets at *Burgzand Noord*; Manders 2009) and large-scale sandbank migration (HMS *Stirling Castle*). SS *Richard Montgomery* and SS *Algerian* experienced little geomorphic change at the timescales investigated (Astley 2016). In the study, Astley (2016) also highlighted the problem of accurately defining zones of scour and deposition in bathymetric data. She concluded that these can be delineated manually, however the process is time-consuming and highly subjective. The same conclusion was noted in another PhD thesis, which investigated scour around windfarm monopiles (Melling 2015). Both authors tried various approaches to objectively delineate scour signatures and none of the methods they trialled was optimal. Nevertheless, Astley (2016) assembled numerous datasets for the site formation research and developed, tested and applied techniques for time-lapse data processing and analysis at wreck sites, significantly expanding the number of overall time-lapse case studies and contributing to the knowledge of scour development at shipwreck sites.

In 2016, Fernández-Montblanc *et al.* integrated numerical modelling with time-lapse bathymetric surveys to assess formation processes of the shallow (5-10 m), wave-dominated wreck site of *Fougueux* (1805), a French ship-of-the-line, resting in the Gulf of Cadiz (south-east of Spain). The sand-dominated site located close to a rocky shoal, comprises the remains of the wooden hull, cannons and a large anchor . Time-lapse data were gathered using a single-beam echosounder, allowing for intra- (May to September 2013) and inter-annual (November 2011 to May 2013) investigations of geomorphic change at the site at a coarse spatial resolution (10 m). Analysis

indicated that the geomorphic change recorded exhibited strong correlation with seasonal wave patterns at the site. The seabed across the *Fougueux* site experienced net erosion during low-energy conditions, and net deposition during high-energy conditions. The authors attributed this to an enhanced sediment transport from coastal dunes and beaches towards the offshore direction during stormy periods, resulting in the net deposition at the site. On the other hand, the low-energy, swell wave conditions carry sediments in the opposite, inshore direction, stripping sediment off the site (Fernández-Montblanc *et al.* 2016). However, around the hull structure, the inverse situation was observed, with net erosion during the high energy period and net accretion during the low energy period. In the paper, the authors also conducted hydro- dynamic modelling, and the flow patterns were further investigated in another study utilising CFD (Fernández-Montblanc *et al.* 2018b), both described in the next section.

Geraga *et al.* (2020) examined 11 shipwrecks located in the inner Ionian Sea, resting at moderate depths (27-62 m), of which one is ancient (1st century BC/1st century AD), while others were lost in the 20th century. The study includes a holistic assessment of the shipwrecks in the Ionian Sea, describing their history, environmental contexts, and site formation processes, using digital elevation models and acoustic data from side-scan sonar, multibeam echosounder and sub-bottom profiler surveys. Ground-truthing was provided by an ROV equipped with a camera. Data analysis indicated that some of the sites are heavily affected by fishing activities, being covered with ghost-nets. Scour depressions were reported around some of the investigated wrecks. The survey also recorded crater-like features around one of the wrecks, at an average distance of 20 m from the centre of the vessel. The authors proposed that their distribution suggests that these seabed depressions were formed due to the loading of the wreck on the soft seabed, causing interstitial fluids to escape and form the craters (Geraga *et al.* 2020). The paper concludes that that there is a need to establish a local shipwreck protection framework, as the physical integrity of the shipwrecks is fragile and susceptible to anthropogenic forcing.

In 2021, a novel approach to assessing past site formation was presented by Secci *et al.* who used photogrammetric techniques at an ancient shipwreck located off Mazotos village (Cyprus). The authors investigated site formation processes using combined photogrammetric models of the whole shipwreck site with models of excavated and raised amphorae, bearing sediment and biogenic horizon marks on their walls. The horizons, created by redox reactions induced by a decomposition of organic material, correspond to current and past seabed levels. Hence, they served as proxies, and their separation from the photogrammetric models allowed the researchers to digitally reconstruct surfaces representing the seabed levels (Secci *et al.* 2021). This knowledge allowed the authors to draw conclusions about sedimentary processes involving the wreck's burial and exposure, artefact dislocation (scrambling devices; Muckelroy 1978) and to better understand the archaeological record, while at the same time digitally preserving the wreck, by creating the very detailed photogrammetric models.

In summary, research on geomorphic change at shipwreck sites has progressed significantly during recent decades. However, some limitations persist. Firstly, no robust objective method for delineating scour and depositional signatures has been developed. The associated erosional and depositional signatures are often developed at multiple spatial scales, from near-field scour pits to depositional and erosional wreck marks extending up to kilometres from a shipwreck, and the problem is exacerbated as these features are frequently embedded in other regional geomorphological features. In order to understand these complex local zones of erosion and deposition, they first need to be accurately and objectively delineated.

Survey methodologies for shipwreck site monitoring are well-established at this stage, and currently allow us to characterize sites and evaluate geomorphic change at very high resolution, at various spatial and temporal scales. Although the number of published case studies is increasing all the time, the time-lapse survey approach is still under-utilised (possibly due to prohibitive costs and lack of expertise in archaeological research teams), despite the great number of shipwrecks estimated in seas and oceans (3 million according to Croome 1999). Therefore, we need to expand time-lapse case studies in order to improve the resolution and sophistication of site formation models.

Geomorphic change at shipwreck sites needs to be understood at multiple time-scales, ranging from very-short (e.g. daily changes related to storms), intermediate (weekly, monthly changes related to tidal cycles), long (intra-annual, seasonal changes) and very long (inter-annual, decadal changes) periods. Such data can enhance site management and allow us to construct accurate site formation models. Site formation models with the added time-variability component would allow archaeologists, site managers and other parties to prioritise shipwreck interventions. For example, an emergency excavation or physical protection might be required on one site, while others could be left as they are for the time being. Additionally, understanding geomorphic change and the related physical processes is critical to construct relevant decision trees for managing potentially polluting shipwrecks (Landquist *et al.* 2013).

The idea of Caston (1979) to use shipwrecks as indicators of net sediment transport can potentially be expanded further. If enough case studies are conducted at sites with varying environmental factors, models can be constructed, deriving current magnitude and direction from scour signatures (data about local sediment substrates, wreck morphology and local geomorphology would still be necessary for such models to be accurate). Similar models exist for deriving current magnitudes and directions by observing natural bedforms: for example, the bedform velocity matrix proposed by Stow *et al.* (2009). As shipwrecks are distributed in many seas and oceans, especially in places with intense marine traffic, this indirectly derived information about currents could be used, for example, to validate large-scale hydro-dynamic models, which are often

constructed for the shipping lane operators and multiple other industrial and scientific purposes related to ocean science.

2.5.2. The hydro-dynamic environment at shipwreck sites

Patterns of flow have been investigated extensively for several types of submerged objects including cylinders (Whitehouse 1998; Voropayev *et al.* 2003), piers (Ramos *et al.* 2014; Zaid *et al.* 2019) and shipwrecks (Quinn 2006; De Hauteclocque *et al.* 2007; Smyth and Quinn 2014; Fernández-Montblanc *et al.* 2018b; Quinn and Smyth 2018). Although analogies are observed between flow modifications caused by these objects, the patterns of flow around individual shipwrecks may be very different due to the complexity of the structures. Among the most important contributing factors to these patterns are the type of flow investigated (oscillatory flow by waves or steady flow by currents), its magnitude and turbulence, orientation of the shipwreck on the seabed, its shape, size and height, local geomorphology, sediment type and water depth (Quinn 2006). The main methods used to investigate flows at shipwreck sites include *in-situ* measurements and physical and numerical modelling. Numerical modelling can be broad-scale or site-focused. While the former approach usually utilises simplified models to reduce computational costs (Dix *et al.* 2009a; Fernández-Montblanc *et al.* 2016), the latter is performed on smaller areas, frequently using advanced computational fluid dynamics (De Hauteclocque *et al.* 2007; Smyth and Quinn 2014; Fernández-Montblanc *et al.* 2018b; Quinn and Smyth 2018). This section highlights recent advances in understanding the flow patterns around shipwrecks, brought by the advanced numerical modelling efforts.

The study of Quinn (2006), which focused on describing how scour processes affect shipwreck sites, proposed a conceptual model of idealised flow patterns and vortex development around a fully submerged wreck site (Fig. 2.7). The model is based upon data and discussions presented in previous investigations of flow around submerged objects (Quinn 2006). The author describes the horseshoe and lee wake vortices as the two basic flow structures around wreck sites. The former is induced by the rotation of the incoming flow, due to the development of an adverse pressure gradient caused by the structure, a separation of the boundary layer, which then rolls up and forms a vortex, enveloping the wreck and terminating in its downstream zone. The latter are formed behind the wreck structure, due the rotation induced over it, and reattached at some distance from the structure (Quinn 2006). Morphologies of both the horseshoe and lee wake vortices depend on many factors including the geometry of the wreck and the flow regime. Additionally, two counter-rotating vortices frequently form in the near-field downstream zone of the structure. This conceptual model (Fig. 2.7) of Quinn (2006) has been a frame of reference for many subsequent studies, involving numerical modelling of hydro-dynamic patterns at shipwreck sites (summarized in Table 2.1).
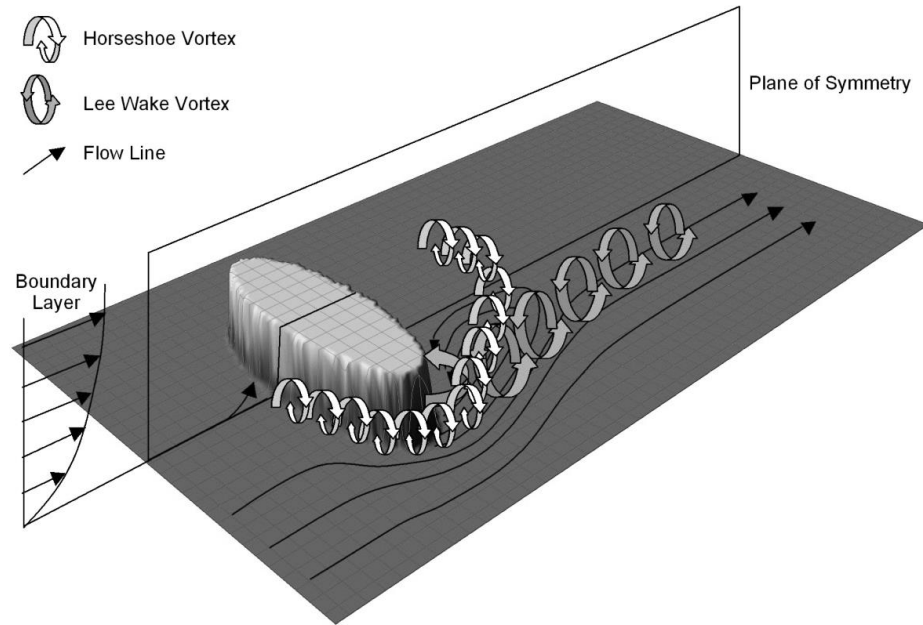
Figure 2.7. A conceptual model of flow patterns and vortices operating on a fully submerged wreck site (from Quinn 2006).

The first publicly available CFD study conducted to investigate flow at a shipwreck site was that of De Hauteclocque *et al.* (2007). This study was divided into four phases. In the first phase, flow was modelled around a surface mounted cube and results of steady-state, unsteady RANS (URANS) and LES simulations were compared; this includedvarious turbulence models for the RANS simulations, including k-ω SST, k-ω and k-ε. Secondly, simulations were performed around a cuboid, oriented at various angles in relation to the upstream flow's direction using k-ω SST and k-ε models and compared against physical modelling results. In the third phase, flow around a modelled shipwreck was simulated and again validated with a physical modelling study. In the fourth phase, flow was modelled on a DEM of an unknown shipwreck site located off the south coast of England and the results were compared against acoustic Doppler current profiler (ADCP) data and observed scour signatures. One of the objectives of the last two phases was to estimate scour and deposition patterns around the shipwreck geometries, by examining wall shear stress and turbulent kinetic energy exerted by the flow. Additionally, the influence of a roughness length parameter on the flow properties was investigated.

The results of the first phase indicated that although LES provides the most accurate results compared to physical modelling, the simulations require very fine meshes, for which computation times are prohibitive. RANS k-ω SST was deemed an optimal model, yielding good accuracy in reproducing flow patterns, while retaining reasonable computation times (De Hauteclocque *et al.* 2007). The second phase of the modelling indicated that unsteadiness of simulation generally decreases, when a cuboid is at an oblique angle in relation to the upstream flow. Both the k-ε and k-ω SST models provided acceptable results when compared to the results of physical modelling.

The last two phases involved modelling of flow around shipwreck geometries. The influence of a roughness length parameter was deemed insignificant, with only 3% relative difference in wall shear stress calculated for a smooth surface and a surface with the roughness length of a medium sand (d_{50} = 0.47mm). The simulation conducted on the modelled wreck and on the real wreck DEM both concluded that the turbulent kinetic energy distribution provides a better estimation of scour patterns than the wall shear stress pattern (De Hauteclocque *et al.* 2007).

Table 2.1. Summary of studies investigating hydro-dynamic patterns at shipwreck sites using numerical methods.

	Site	*Type of flow investigated*	*Region*	*Regime at the site*	*Method*	*Solver*	*Turbulence model*	*Validation*
De Hauteclocque et al. (2007)	*Unknown shipwreck* and a scaled wreck model	Averaged velocity/direction for an early/middle/late flood tide	South England coast, North Sea	Tidally-dominated	CFD, Ansys CFX v. 11	Steady-state and transient RANS	Compared various. k-ω SST deemed optimal	Yes, ADCP *in-situ* and physical modelling
Dix, Cazenave, et al. (2009)	Multiple, shelf-scale model	Tidal currents and combined tidal and wave influence	English Channel/southern North Sea, Goodwin Sands	Tides and waves	MIKE 21 2D	Decoupled, shelf-scale hydro-dynamic/sediment transport model	-	*In-situ* data
Smyth and Quinn (2014)	*Arklow Bank shipwreck* (19th century)	Peak, steady-current condition simulated	Arklow Bank, Irish Sea	Tidally-dominated	CFD, OpenFOAM	Transient RANS, PIMPLE solver	RNG k-ε	Yes, cross-validated with the observed bathymetry and time-lapse data
Fernández-Montblanc et al. (2016)	*Fougueux* (1805)	High and low wave energy, and storm conditions	Gulf of Cadiz, Atlantic Ocean	Wave-dominated, currents present	Coupled Delft3D-FLOW and SWAN	Broad-scale hydro-dynamic model	-	ADCP, current meter, time-lapse, Oluca-SP model and wave buoy data
Fernández-Montblanc et al. (2018b)	*Fougueux* (1805)	Simulations for low and high energy periods: Mean and fading storm, swell wave, wave breaking and offshore wave breaking	Gulf of Cadiz, Atlantic Ocean	Wave-dominated, currents present	CFD, OpenFOAM, IHFoam	RANS, InterFoam solver	k-ω SST	Time-lapse bathy and cross-validation with Fernández-Montblanc *et al.* (2016)
Quinn and Smyth (2018)	Modelled hull of the ship *Jylland* (1860)	Investigated different attack angles of steady currents	Modelled flat seabed	Steady-current	CFD, OpenFOAM	Transient RANS, PIMPLE solver	RNG k-ε	Yes, cross-validated with the observed seabed topography

Dix *et al.* (2009) took a broad-scale modelling approach to simulate sediment erosion/accumulation off the southern North Sea. The authors used MIKE 21 2D software to construct a shelf-scale model, which was calibrated using multiple offshore stations delivering *in-situ* data on tidal elevation, current speed and direction. The model was divided into sub-domains, of which the Goodwin Sands subdomain was a priority concern, as it is recognized as a final resting place to many historical ships, hence the area is commonly referred to as the ship swallower (Pascoe 2012). The results of the broad-scale modelling demonstrated which sites are affected by storms and whether they are exposed to depositional or erosional conditions. The

study concluded that that the outputs of the regional, shelf-scale modelling can be used as input for more detailed, nested, site-focused models.

The first peer-reviewed study to examine flow patterns at a historic shipwreck site using CFD was published by Smyth and Quinn (2014). The authors used OpenFOAM software, with a large time-step, transient solver for incompressible flow named PIMPLE and the RNG k-ε turbulence model. The 3D model of the *Arklow Bank* shipwreck site (previously investigated in the time-lapse MBES study; Quinn and Boland 2010) and its surrounding seabed was obtained using interpolated MBES data. The simulation successfully captured flow separation, lee wake vortices, vortex shedding and an amplification of turbulent kinetic energy and wall shear stress by a factor of 3-4 downstream of the wreck site (Smyth and Quinn 2014). The authors highlighted that the outputs of the CFD simulations including distribution of turbulent kinetic energy, wall shear stress and pressure can be used to estimate areas of increased mechanical stress at archaeological sites. Hence, CFD modelling aids *in-situ* management of shipwreck sites, by delivering direct data about physical site formation (Smyth and Quinn 2014).

In their next study, Quinn and Smyth (2018) again used OpenFOAM with the PIMPLE solver and the RNG k-ε turbulence model, but this time to evaluate how different incidence angles affect the patterns of flow around a fully submerged, upstanding shipwreck. They used a model of the hull of one of the largest wooden warships in history: *Jylland* (1860), as the obstacle to the flow. The results indicated a strong dependence of flow patterns on the flow incidence angle (Fig. 2.8). The authors compared the results of the CFD to bathymetric data with shipwreck sites, where depositional and erosional wreck marks are present. They noted a good agreement between the outputs of CFD (wall shear stress and turbulent kinetic energy) and the observed scour/depositional features in the natural environment. Specifically, the spatial correlation between zones of elevated turbulent kinetic energy and erosional signatures is most notable, which compliments the findings of De Hauteclocque *et al.* (2007). The simulations predicted flow contraction and separation, formation of a horseshoe vortex and lee wake vortices. The authors also suggest that the horseshoe vortex is responsible for the erosion of sediment on the upstream side of a shipwreck, while the lee wake vortices control scour and deposition on the downstream side. The study significantly extended knowledge about hydro-dynamic patterns at shipwreck sites, confirming the previously established theoretical models (Quinn 2006).
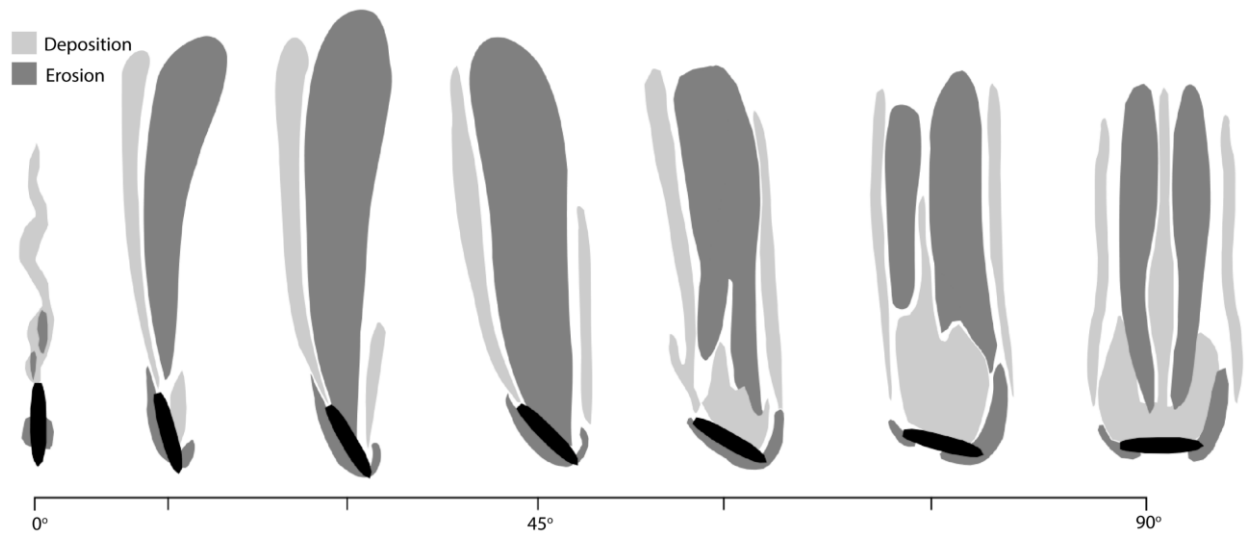
Figure 2.8. Patterns of wreck associated erosional and depositional signatures corresponding to the incidence angle of flow inferred from the output of CFD simulations (from Quinn and Smyth 2018).

In two complimentary studies, Fernández-Montblanc *et al.* (2016; 2018b) examined the hydro-dynamic patterns at the *Fougueux* site (Gulf of Cadiz, Spain). Fernández-Montblanc *et al.* (2016) focused on broad-scale modelling using the Delft3D-FLOW model, combined with SWAN and Oluca-SP model, which propagated a historical wave hindcast to the shipwreck area. The main findings of the paper indicated that the wave-dominated site is influenced by steady flow induced by the waves. Wave height and current velocity are amplified by the shoaling wreck's hull, which in turn cause amplification of turbulence, near-bed orbital velocity and bed shear stress. Hence, sediment transport and scour are exacerbated at the site. Additionally, there is a strong seasonal variability in sediment dynamics at the site, corresponding to low and high energy periods and storms.

The subsequent 2018 study utilised a more advanced approach to hydro-dynamic modelling, for the first time using CFD to simulate the wave environment at a historic wreck (*Fougueux;* Fernández-Montblanc *et al.* 2018b). The authors used OpenFOAM with its multiphase InterFoam solver, solving RANS equations for two incompressible phases: seawater and air, and applied the k-ω SST model for turbulence modelling. Meshes used for the simulations were constructed on time-lapse bathymetric profiles obtained in summer (low energy period) and winter (high energy period). During the low energy period, friction velocity due to oscillatory flow and flow velocity amplification are the dominant physical processes and a large coherent structure formed at the toe of the wreck initiates scour. During the high energy period, turbulent shear and the large coherent structure have more influence, as the flow is generally increased at the wreck site. Additionally, steady streaming and undertow are magnified in this period, resulting in modification of vortex shedding trajectories, thus increasing sediment transport. The study further demonstrated that CFD allows deeper understanding of site formation processes, when combined with time-lapse bathymetric datasets.

50

Taken together, the three archaeology-oriented papers (Smyth and Quinn 2014; Fernández-Montblanc *et al.* 2018b; Quinn and Smyth 2018) put CFD modelling in the spot-light as a cost-effective (with open-source software), desk-based method of assessment of hydro-dynamic patterns at shipwreck sites, providing tools for their management and evaluation of the *in-situ* preservation potential.

Nevertheless, shipwreck sites are located in varying environments and can be dominated by currents, or waves, or by a complex combination of both. In turn, local, site-specific geomorphology influences flow and *vice-versa,* in that local flow strongly influences geomorphic change at a site. As highlighted by the review of time-lapse survey studies in the previous section, some wrecks lie on an almost static seafloor (e.g. with clear-water scour), while others are exposed to dynamic changes which persevere continuously after the wrecking incident (e.g. with live-bed conditions or extensive trawling). These dynamic changes reorganise sediment at sites, acting as scrambling devices (Muckelroy 1978) and affecting near-seabed hydro-dynamic patterns.

Indeed, feedback loops exist between geomorphic change and patterns of flow at shipwreck sites (Fernández-Montblanc *et al.* 2018b) and the number of case studies need to be expanded in order to understand this relationship. Moreover, although the relations between bed shear stress, turbulent kinetic energy, seabed scour and sediment deposition have been noted and discussed by all the works reviewed here, there is a need to quantitively evaluate at which spatial and temporal scales these outputs may be used to predict changes at shipwreck sites. Such assessments do exist for the natural world, for example airflow modelling over dune fields (Smyth *et al.* 2019), and could therefore be performed for shipwreck sites by statistically comparing CFD outputs and geomorphic changes registered with time-lapse surveying. Only then, will successful coupled hydro- and sediment-dynamic models be realised for shipwreck sites.

Finally, although the studies cited in this review do highlight the potential for CFD in predicting mechanical stresses on shipwreck structures (Smyth and Quinn 2014), to date no attempt has been made to directly correlate these simulated loads with actual physical damage on shipwrecks. Such observations would require either detailed and frequent monitoring of a selected site, where CFD indicated heavy loads on a shipwreck structure, or further expansion of the combined time-lapse survey/CFD studies, which would allow quantitative evaluation of CFD to predict site evolution.

2.6. Conclusions

The following knowledge gaps have been identified from the literature review and form the basis for the research questions explored in this thesis:

- No method has been established for the accurate and objective delineation of local geomorphology at shipwreck sites. Instead, researchers use various *ad-hoc* methods for defining, separating, and describing scour and depositional signatures: from manual GIS vectorization to using custom GIS tools. There is a need to develop an automated or semi-automated, objective method, which will standardize wreck mark separation and enhance quantification of sediment-dynamic processes at shipwreck sites.

- Time-lapse, repeat bathymetric survey investigations at shipwreck sites should be expanded. More case studies should be conducted at different temporal scales in order to understand the short- and long-term evolution of sites. Case studies should be expanded and compared between varying marine environments.

- The influence of seabed geomorphic change on the integrity of shipwreck structures should be understood. It is clear that scour has detrimental effects on the stability of engineering structures such as bridges (Sumer 2007) and windfarms (Whitehouse *et al.* 2011). However, the scale of potential damage induced by the erosive scour processes at shipwreck sites remains unclear.

- CFD research at shipwreck sites should attempt to quantitatively assess whether, and at which temporal scales, CFD outputs (including wall shear stress and turbulent kinetic energy) can be used to predict site evolution. This could be achieved by statistical comparison between difference models from time-lapse bathymetric surveys and outputs from CFD simulations (Smyth 2016).

- The applicability of CFD for predicting loads exerted on shipwreck structures should be investigated.

Addressing these knowledge gaps would allow us to construct coupled hydro- and sediment-dynamic models, aimed at creating predictive site formation models at various temporal scales.

3. Residual relief modelling: digital elevation enhancement for shipwreck site characterisation

3.1. Introduction

The UNESCO Convention on the Protection of the Underwater Cultural Heritage states that *in-situ* preservation of sites should be the first option (UNESCO 2002). In response, recent research has concentrated on better understanding and quantifying natural and anthropogenic forces affecting preservation and degradation of submerged sites commonly referred to as site formation processes (Quinn *et al.* 2007; Ruuskanen *et al.* 2015; Fernández-Montblanc *et al.* 2016, 2018b, a; Bethencourt *et al.* 2018). Among them, linked hydrodynamic and sediment-dynamic processes are understood to control other natural formation processes such as biological encrustation and chemical corrosion (Ward *et al.* 1999).

One of the key morphodynamic processes that dominate wreck site formation is seabed scour, which occurs when a shipwreck placed on the seabed perturbs the local hydrodynamic regime (Quinn 2006), resulting in complex erosional and depositional patterns commonly described as scour or wreck marks. These features act as indicators of local net sediment transport and provide valuable information about the magnitude and direction of ocean currents (Caston 1979; Quinn 2006; Garlan *et al.* 2015). In seabed engineering, scour development around submerged bridge and windfarm piles is recognised as highly detrimental to structural stability and often requires special mitigastion measures (Sumer 2007). Similarly, scour processes at shipwreck sites can lead to burial and/or exposure, accelerating wreck disintegration, and in extreme cases, it can cause the complete collapse and loss of structures (Quinn 2006). Furthermore, the pace of a shipwreck's physical degradation close to scour pits may be enhanced by hydro-abrasive action, as these areas are subject to increased water turbulence and shear stress (Smyth and Quinn 2014; Quinn and Smyth 2018). Erosional scour pits may also be filled with archaeological artefacts from a disintegrating wreck (Quinn *et al.* 1997), thus acting as depositional zones for archaeological material. Therefore, in order to fully assess the preservation state of wreck sites, and to inform *in-situ* preservation, it is essential to map and quantify scour marks.

Previous studies investigated how shipwreck-related scour signatures develop and progress, based on difference modelling of time-lapse bathymetric surveys (Quinn and Boland 2010; Bates *et al.* 2011; Astley 2016) and computational fluid dynamic (CFD) simulations (Smyth and Quinn 2014; Fernández-Montblanc *et al.* 2018b; Quinn and Smyth 2018). Nevertheless, no objective method has been developed for the detection and extraction of scour marks at wreck sites. In order to delineate these features, they need to be separated from the background geomorphology, enabling

objective quantification of scour area, depth, shape, volume and other morphometric characteristics (Garlan *et al.* 2015; Melling 2015).

An ideal way to identify scour signatures around wrecks would be to compare two bathymetric datasets: one collected before the wrecking incident (over an undisturbed seabed) and one after it (with scour fully developed). However, as no original high-resolution bathymetric datasets are available for historic wreck sites, a proxy for the pre-disturbed seabed can be reconstructed to a very limited extent using GIS methods (Garlan *et al.* 2015; Astley 2016). Nevertheless, such reconstructions do not provide accurate solutions for the delineation of wreck marks, which exhibit complex patterns of erosion and deposition on the seabed (Caston 1979). Currently, the only available method for mapping a shipwreck site's geomorphology is the visual interpretation of bathymetric data accompanied by labour-intensive vectorisation. This traditional approach to the problem is highly subjective and time-consuming.

Digital elevation models (DEMs) derived from remotely sensed data portray geomorphological features at different length-scales. Fine-scale features or forms are usually superimposed onto broad-scale forms. Therefore, the problem of the separation and classification of local features characterised by various length-scales is present in multiple applications of DEM data, and numerous mapping solutions have been proposed to solve this issue. Guisan *et al.* (1999) and Weiss (2001) proposed the Topographic Position Index (TPI), which employs methods of classifying landform types for ecological predictions. The TPI method was subsequently adjusted for seabed applications and evolved into the Bathymetric Position Index (BPI) (Walbridge *et al.* 2018) which is mainly used for the classification of benthic environments. An alternative approach is to use high-pass filtering techniques to remove regional landscape features from DEMs, leaving local, fine-scale morphology termed 'residual relief' (Wessel 1998, 2016; Hiller and Smith 2008). Hesse (2010) proposed an analogous 'local relief' technique for terrestrial archaeological prospection. Smith and Clark (2005) investigated the application of DEM visualisation methods for the mapping of local landform features. However, none of the aforementioned methods has been tested or adapted to map scour-related wreck marks.

In this paper, we present a new method to objectively extract and classify erosional and depositional features from high-definition DEMs derived from multibeam echosounder (MBES) surveys using a combination of fine-scale feature delineation methods. A residual relief modelling (RRM) technique comprising high-pass filtering, a conditional classification tool and DEM visualisation techniques is used to isolate scour signatures from regional geomorphology. The methodology is tested on three World War 1 shipwreck sites, and manual vectorisation is used to compare the results. This method will significantly improve *in-situ* preservation planning of shipwreck sites with respect to dominant physical site formation processes. This issue of local morphological feature extraction is not only relevant in underwater archaeology but also has

important applications in offshore engineering (Melling 2015). We believe that this study will add to the existing knowledge on the use of high-resolution MBES data for such applications and presents a step towards automated seabed morphology extraction and characterisation.

3.2. Materials and methods

3.2.1. Study area

The three World War 1 shipwrecks used in this study are located in the Irish Sea; two off Dublin and one off Belfast (Fig. 3.1). The steam collier SS *Polwell* was sunk by the German submarine *U-96* on 5 June 1918 (Brady *et al.* 2012). The 93-m long wreck is located at a depth of 30 to 36 m, 20 km northeast of Dublin. On 14 December 1917, SS *Hare* was torpedoed by the German *U-62* (Brady *et al.* 2012) 22 km east of Dublin. The 54-m passenger/cargo ship now rests in 53 to 60 m of water. The merchant vessel SS *Tiberia* was torpedoed on 26 February 1918, probably by the German *U-19* (Wilson 1979). The 125-m long wreck is located in 48 to 63 m of water at the northern entrance to Belfast Lough.
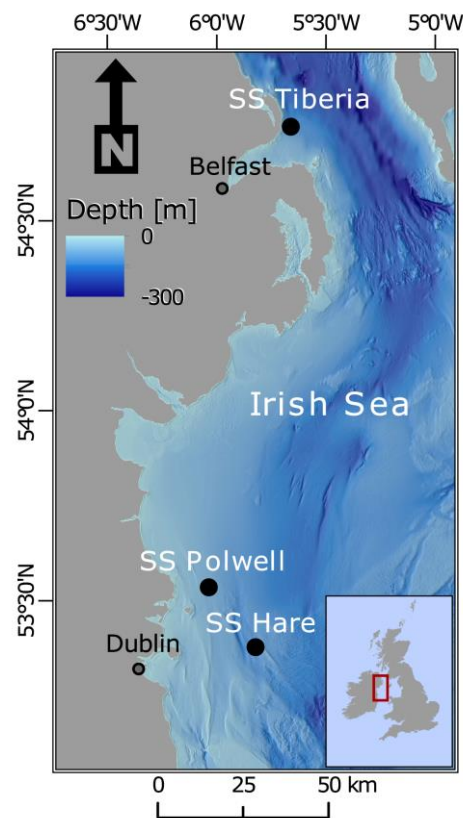
Figure 3.1. Locations of the sites chosen for the study in the Irish Sea (backdrop bathymetry obtained from (EMODnet Bathymetry Consortium 2018).

All three wrecks lie on non-cohesive sandy sediments (Brady *et al.* 2012; Bond 2014). Considering the depths of the shipwrecks and their location in the western part of the semi-enclosed Irish Sea, the wave influence at the sites is minimal, and processes acting on the sites are dominated by bi-directional tidal currents. Around SS *Tiberia*, depth-averaged tidal currents

reach up to 0.5 m/s during spring tides (Atkins 1997). In the more open Irish Sea, SS *Polwell* and SS *Hare* are influenced by stronger currents, with velocities up to 1.0 m/s (Howarth 2001).

3.2.2. Bathymetric data from shipwreck sites

MBES surveys over the three shipwreck sites were conducted between 4 and 10 September 2016 onboard RV *Celtic Voyager* using a Kongsberg dual-head EM2040 operating at 400 kHz. Position fixing was provided by an Integrated GNSS/L-Band receiver CNAV 3050 (horizontal/vertical accuracies of ± 5 cm/10 cm). Motion referencing, secondary positioning, and accurate timing were provided by a Seatex Seapath 330+. Water column sound velocity control used a Valeport Midas SVP and a real-time AML surface sound velocity sensor. Data were logged onboard using the Kongsberg's Seafloor Information System (SIS) v. 3.8.3 acquisition software. Raw and processed data are currently archived at the Marine Institute of Ireland under the Integrated Mapping for the Sustainable Development of Ireland's Marine Resource (INFOMAR) programme. DEMs of the wreck sites were derived from tidally corrected and cleaned MBES data at 0.5-m resolution using Caris HIPS and SIPS v. 8.1.

3.2.3. Objective separation of erosional and depositional wreck marks

The RRM method employed for the objective separation of scour marks was designed and performed using ESRI ArcMap v. 10.6.1 and consists of three steps (Fig. 3.2): (1) application of a high-pass filter on the DEM data, (2) preliminary classification of a local, residual morphology on the resulting layer and (3) a final separation of scour-related wreck marks with the support of DEM visualisation techniques. A detailed, step-by-step GIS workflow is given in the supplementary material. To compare and test the method, the wreck marks were also separated manually.
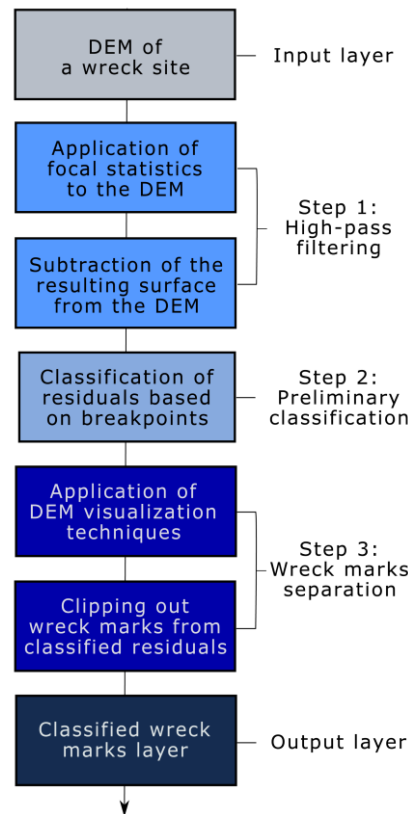
Figure 3.2. Schematic representation of the workflow for the proposed RRM method.

3.2.3.1. High-pass filtering of the DEM

Focal statistics were calculated for each DEM, with the resultant raster values representing a function of the input cell within a specified neighbourhood around it. In this study, a moving mean function was used, calculated for a circular kernel or window for all the DEMs. The radius of the kernel was based on a visual estimation of the length-scales (i.e. widths) of the scour marks. The general rule is that the moving kernel needs to be wide enough to capture more cells from the outside of a scour mark than from the inside. The radii defined in this study were 50 m for SS *Tiberia,* 100 m for SS *Polwell* and 200 m for SS *Hare*.

Application of the focal function can be termed as low-pass filtering, as it smooths local morphology, leaving only regional characteristics (Wessel 1998). A high- pass filter, on the other hand, extracts local, residual morphology, with positive and negative cells respectively representing areas which are higher or lower than the average (regional) height of the surrounding seabed. The high-pass filtered layer (HP) was obtained by a subtraction of the focal mean raster (low-pass filtered data, LP) from the original DEM (3.1), hence measuring the difference between a central cell and the mean elevation in the kernel (Wilson and Gallant 2000):

$$HP = DEM - LP \tag{3.1}$$

High-pass–filtered data is scale-dependant, i.e. when the kernel size increases, so does the range of values. Therefore, to establish a robust classification tool for residual reliefs, which can be

applied for sites with various geomorphological settings, the resulting HP layers need to be normalised. This standardisation was performed by the subtraction of the layer's global mean and dividing it by its standard deviation (std) (3.2).

$$HP_{stdd} = (HP - mean)/std \qquad\qquad (3.2)$$

By standardising the layer, the resulting raster's standard deviation has a value approximating 1 and a mean value of 0. This process should be performed only if the original HP layer's global mean is also reasonably close to zero. This standardisation is an inherent step for methodologies dealing with datasets containing multiple variables such as for principal component analysis (PCA) or neural networks. It is also used in the TPI (Weiss 2001) and BPI (Walbridge *et al.* 2018) workflows, where different kernel sizes are used to separate both broad-scale and fine-scale morphology. However, in the latter two methods, the values are converted to integers. In the case of the detection of wreck marks with submetric variations in sizes, centimetric accuracy is required. Therefore, in the RRM technique proposed here, the numbers are always stored as floating-point type, thus preserving decimals. After the standardisation of values representing residual reliefs, their classification using breakpoint values was performed.

3.2.3.2.   Preliminary classification of residuals

The standard score values derived from the HP layer were classified into three groups of residuals: positive (class 1), negative (class 2) and highly positive (class 3). Positive and negative classes consisted of cell values which were higher or lower than +0.5 and −0.5 standard deviations respectively and were designed to store values corresponding to depositional and erosional wreck marks. A highly positive class (more than 5 standard deviations) separates the actual wreck structure from the DEM. The remaining values (between −0.5 std and +0.5 std) are defined as a featureless seabed (class 0). At this stage, the residuals were classified in such a way that significant deviations in local bathymetry were captured into classes. In the final step, the wreck marks were separated from classified residuals which were more likely to represent natural morphological features.

3.2.3.3.   Separating wreck marks with support of DEM visualisation techniques

The preliminary classification of residuals separated the local morphology from its regional background. An additional step involving the application of visualisation techniques on the original bathymetric DEMs was designed to distinguish wreck marks from other local geomorphic features. The traditional shaded relief technique tends to introduce directional bias (Smith and Clark 2005). Therefore, in this study, a multidirectional hillshade function was applied to the original DEM using multiple illumination angles. With transparency set to 50%, it was used as an occluding layer for the original DEM with an increased contrast. As scour features are

associated with flow regimes affected by the presence of a wreck, they often exhibit directional characteristics, especially in the far-field. Closer to a wreck (i.e. in the near-field), scour marks are usually associated with steep slopes (Quinn 2006). Such characteristics can be exposed by calculating bathymetric derivatives like aspect and slope to distinguish the scour marks from other residuals. Here, the aspect function was used to show the direction of slope, which was also calculated with a 3×3 pixel rectangular window to differentiate areas with steep slopes. Additionally, Sobel horizontal and vertical edge detection filters were applied on the DEMs to emphasise edges in both horizontal and vertical directions. Finally, a focal standard deviation filter was applied as another measure to expose areas with significant changes in values. With the given resolution of the DEMs, the filtering window for focal standard deviations was circular with a 2-m radius to expose local variations in relief (Wilson and Gallant 2000).

All these techniques support the final classification step. Areas assigned as either positive or negative residuals, which were not related to the presence of a shipwreck but were assigned by a breakpoint classifier, were manually clipped. The filters were designed to increase objectivity of this step, by visually exposing morphological characteristics of the seabed surrounding a shipwreck. The wreck marks were assumed to possess at least one of the following essential attributes during the final separation (Quinn 2006):

- Continuity from the area in proximity to the wreck structure
- Steep slopes in proximity to the wreck structure
- Distribution along some predominant direction associated with the bottom current regime
- Heights/depths decreasing with distance from the shipwreck

Residuals extending away from a wreck were separated up to the point where the amplitude difference with the surrounding seabed was less than 10 cm, as this was within the vertical positioning error of the survey platform.

3.2.3.4.   Manual vectorisation of wreck marks as a validation method

In an attempt to validate the RRM, the extent of the wreck marks on the DEMs were picked manually and vectorised as polygons by visual examination and 3D bathymetric profiling. The assumptions guiding the fully manual separation were the same as those used for the final extraction using DEM visualisation techniques in the RRM method. The vectorised polygons were divided into two classes corresponding to positive (depositional) and negative (erosional) wreck marks. Areas and extents of the wreck marks picked by the RRM and manual vectorisation methods were then compared. The effectiveness of the residual relief method was examined, focusing on areas where wreck marks were classified by their presence or absence.

3.3. Results

3.3.1. Digital elevation models

DEMs of the three wreck sites are presented in Fig. 3.3. These were chosen because they each have a different background geomorphology, allowing the methodology to be tested on different regional settings. On the SS *Polwell* site, a pipeline to the north of the shipwreck (Fig. 3.3a) intersects the extensive longitudinal erosional and depositional wreck marks. Ridge-shaped features of a similar length-scale as the scour marks are present to the south of the wreck structure. SS *Tiberia* (Fig. 3.3b) rests on a sloping seabed, which deepens to the east. Two distinct scour pits are imaged around the wreck, with more subtle far-field depositional and erosional marks to the north and south. SS *Hare* lies semi-buried within a deep and extensive scour pit, with dunes developed across the entire site (Fig. 3.3c). The regional bathymetry deepens to the south, with the trend being disrupted by the scour pit.
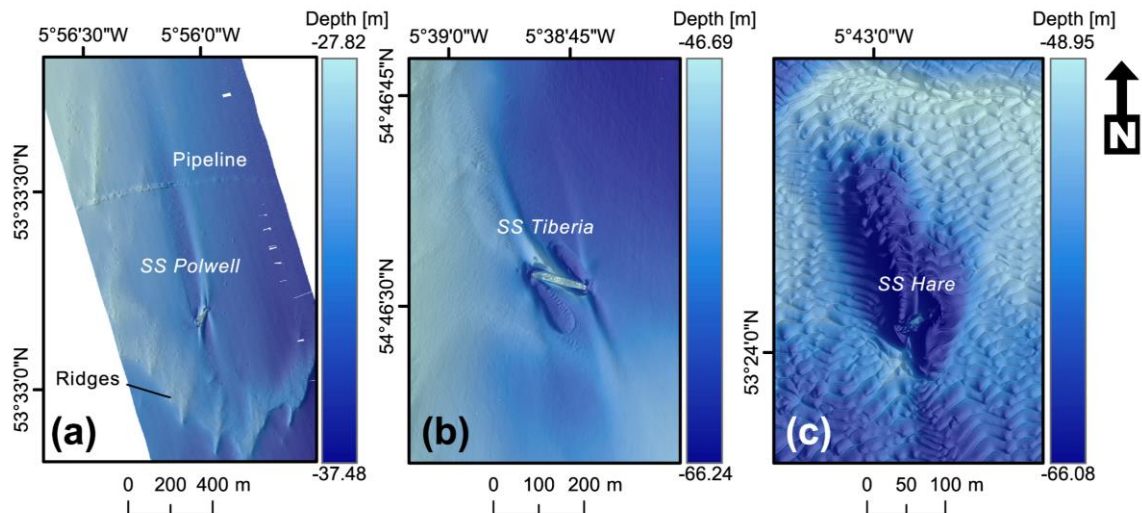
Figure 3.3. DEMs representing (a) SS *Polwell*, (b) SS *Tiberia* and (c) SS *Hare* sites. The rasters were occluded with a hillshade layer set to 70% transparency.

3.3.2. Residual relief modelling

The results of the residual relief modelling are shown in Fig. 3.4. On the SS *Polwell* site, the relief modelling distinguishes extensive, longitudinal positive and negative relief features clearly related to the presence of the wreck (Fig. 3.4c). On a preliminarily classified layer (Fig. 3.4b), the amount of positive and negative residuals is significantly higher than on the final output layer obtained after the final separation (Fig. 3.4c), as many of the local morphological features are of the same scale as the wreck marks and needed to be removed during the third step. This operation was supported by visual examination of the enhanced contrast DEM, occluded with the multidirectional hillshade and the Sobel vertical functions (Fig. 3.5a, d). Both visualisation techniques allowed for the clear distinction of the longitudinal far-field scour mark boundaries,

which were less clear on the original DEM. The wreck marks extend beyond the pipeline to the north of the site (Fig. 3.3a), which in turn gives rise to its own depositional marks (Fig. 3.4c). The high-pass filtering step identified negative reliefs near the pipeline, which were removed during the final separation, after being interpreted as natural bathymetric variation rather than effects of the seabed scour (Fig. 3.4b, c). The scour marks caused by the shipwreck extend 1200 m north/north-west of the wreck and 300–400 m to the south, with areas of 64,392 m^2 for the depositional marks and 12,4681 m^2 for the erosional marks (Table 3.1).

Table 3.1. Areas of depositional and erosional wreck marks extracted by the manual vectorisation and the RRM method.

Wreck	Manual vectorization		Residual relief modelling			
	Deposition [m^2]	Erosion [m^2]	Deposition [m^2]	Δ%	Erosion [m^2]	Δ%
SS *Polwell*	67193	98197	64392	-4.16	124681	+26.97
SS *Tiberia*	17292	17208	29115	+68.37	27094	+57.45
SS *Hare*	-	35482	-		32535	-8.31
Total area [m^2]	235373		277818			+18.03

On the SS *Tiberia* site (Fig. 3.4d), the more homogenous local morphology surrounding the wreck results in fewer residuals unrelated to scouring (Fig. 3.4e). During the third step of the relief modelling, the aspect function was used to support the final separation based on the variable directivity of the steepest sides of the scour marks (Fig. 3.5c). Additionally, the focal standard deviation function, highlighting local variations in values, exposed the boundaries of the main near-field pits and the marks extending to the far-field (Fig. 3.5f). The separated wreck marks on the RRM output layer (Fig. 3.4f) show nice symmetry, reaching lengths of 250 m to the south-east and 270 m to the north-west of the wreck. The depositional and erosional marks have similar areas of 29,115 m^2 and 27,094 m^2 respectively (Table 3.1).

Only negative residuals were picked by the relief modelling on the SS *Hare* site, delineating the scour pit observable on the high-pass filtered layer (Fig. 3.4g). A positive relief surrounding the pit was initially captured with the breakpoint classification (Fig. 3.4h); however, it was clipped out during the last step of the modelling, as this is clearly not associated with scouring. Slope function exposed the extent of the pit, which has steep sides, especially in proximity to the shipwreck (Fig. 3.5b). Sobel horizontal filtering significantly enhanced the visibility of the dunes imaged on the site (Fig. 3.5e). The separated erosional residual encompassing the pit (Fig. 3.4i) has an area of 32,535 m^2 (Table 3.1). The highly positive residuals were classified successfully as shipwrecks on the SS *Polwell* (Fig. 3.4c) and SS *Tiberia* (Fig. 3.4f) sites. The wreck structure of SS *Hare* was not separated successfully, as it was masked by the length-scale of the extensive scour pit. Only a small part of the wreck structure was initially classified as a positive residual after the high-pass filtering (Fig. 3.4h).
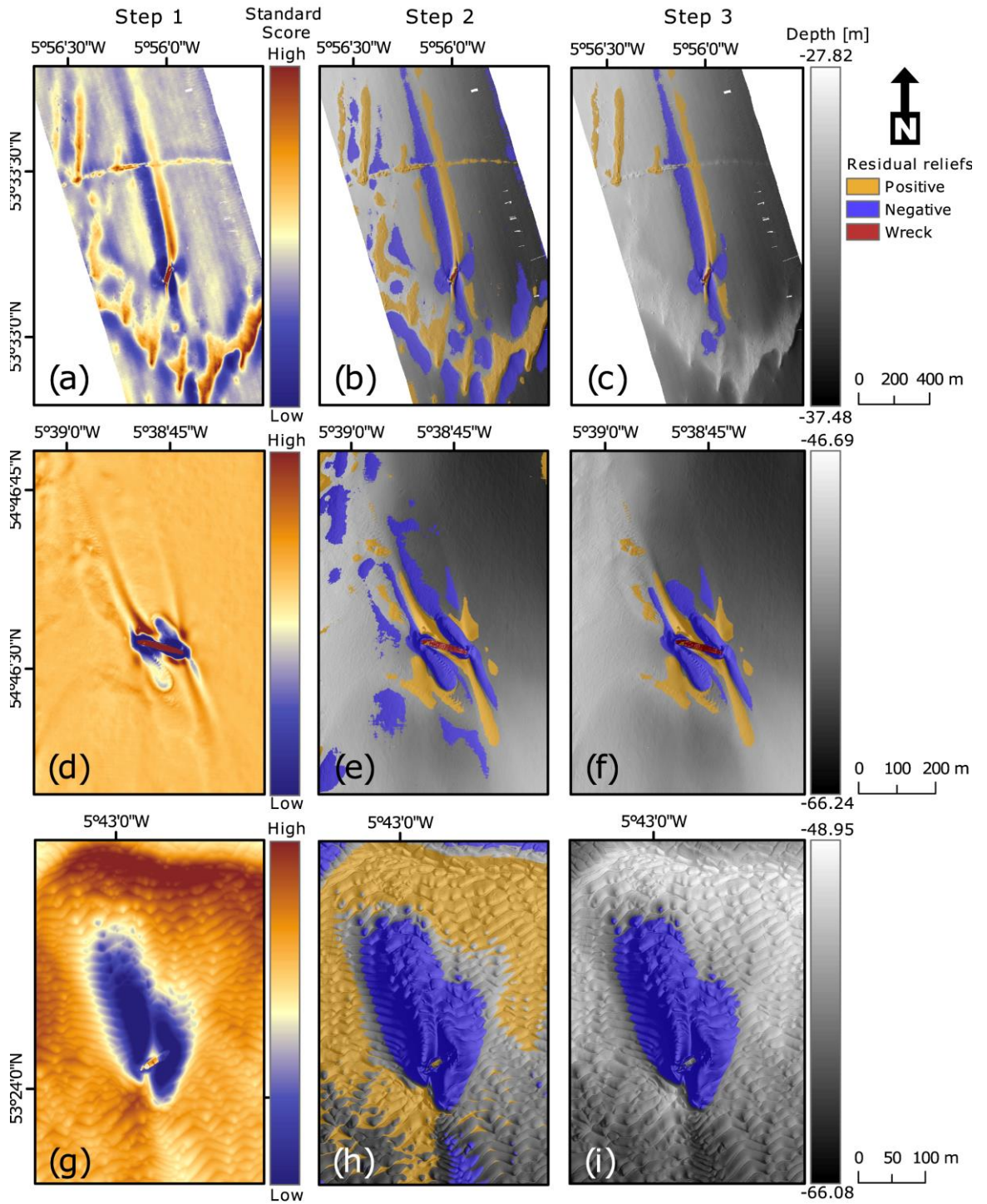
Figure 3.4. RRM's step 1 (high-pass filtering), step 2 (preliminary classification) and step 3 (separation ofwreck marks) are shown respectively in the first column (left), second column (middle) and third column (right). SS *Polwell* is shown in (a), (b), (c); SS *Tiberia* in (d), (e), (f) and SS *Hare* in (g), (h), (i).
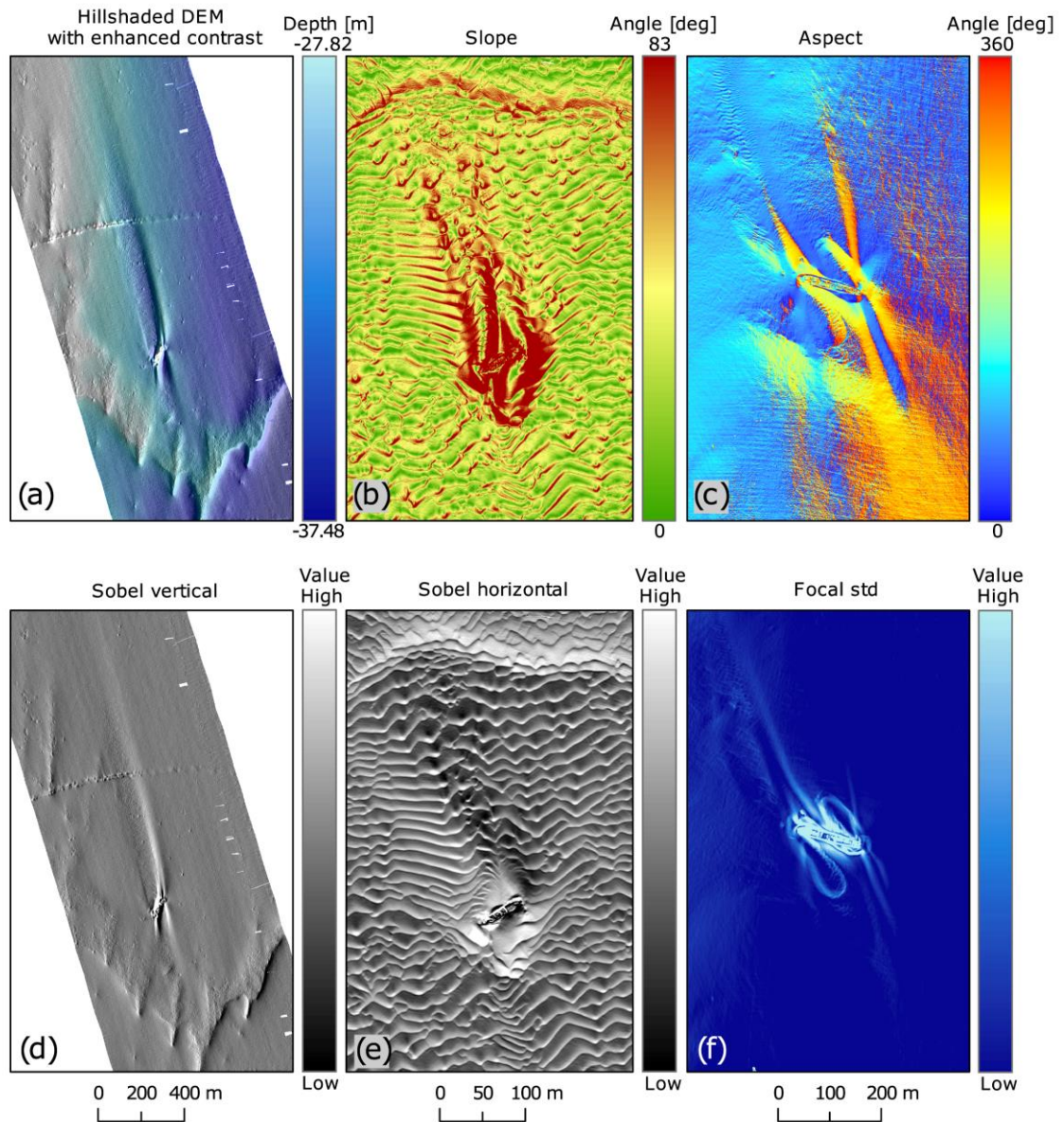
Figure 3.5. DEM visualisation techniques applied to the sites. (a) Increased contrast DEM with the multidirectional hillshade occlusion on SS *Polwell*, (b) slope on SS *Hare*, (c) aspect on SS *Tiberia*, (d) Sobel vertical on SS *Polwell*, (e) Sobel horizontal on SS *Hare*, (f) focal standard deviation on SS *Tiberia*.

3.3.3. Manual vectorisation of wreck marks as a validation method

The manual vectorisation supported by the 3D bathymetric profiles allowed for the separation of prevailing scour patterns (Fig. 3.7) and calculation of their areas; these in turn were compared with the areas of wreck marks separated by the RRM method (Table 3.1).

The greatest differences between the two methods occur where more subtle wreck marks, embedded in the regional bathymetry, are present. They were not straightforward to vectorise, even when supported with the 3D profiles. As an example, Fig. 3.6 represents the SS *Polwell* DEM with the 3D profiles used to support the manual vectorisation process. Whilst the wreck marks were clearly distinguishable on the near-field profile B-B′, the far-field profile C-C′ did not

provide enough information to ascertain the width of the scour. Similarly, the A-A′ profile drawn over the wreck showed two erosional lows, but the depositional mark which intersects the profile and extends to the south of the wreck (as seen on Fig. 3.7) was barely discernible from the featureless seabed. These uncertainties, which arose during the manual separation, caused differences compared with the RRM in the proximity of the shipwreck and to the south of it. With respect to the areal calculation, this resulted in the underestimation of erosional features using the manual method (Table 3.1).
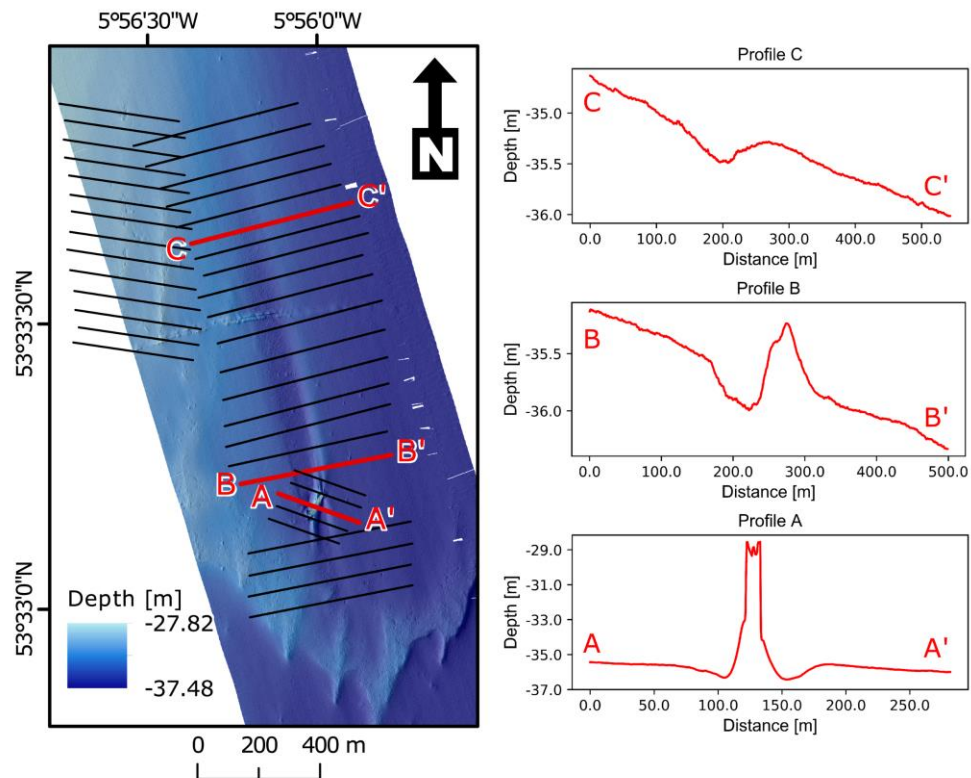
Figure 3.6. Depth profiles created for the manual vectorisation of wreck marks on the SS *Polwell* DEM. Profile graphs A, B and C are shown representatively.

On the SS *Tiberia* site, relief modelling also resulted in the detection of more extensive erosional and depositional features than the manual vectorisation approach (Table 3.1). The erosional pits proximal to the wreck (Fig. 3.7b) were recognised by both methods, but the relief modelling indicates the pits extending farther than when picked manually (Fig. 3.7b). In addition, a depositional mark southwest of the wreck, which was successfully separated by relief modelling, was missed in the manual vectorisation process. Differences between the techniques applied on the SS *Hare* site are negligible, with the scour pit defined by relief modelling reaching only slightly farther than that interpreted in the manual vectorisation process (Fig. 3.7c; Table 3.1).
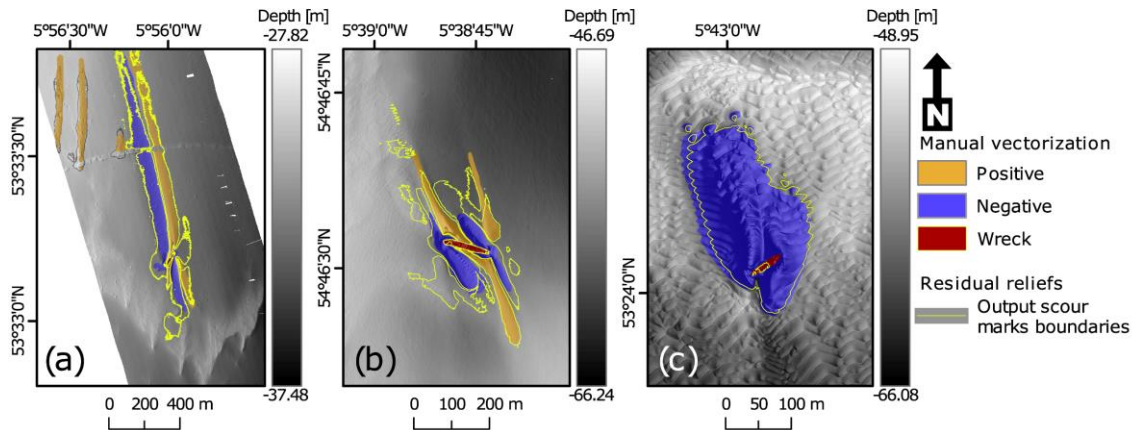
Figure 3.7. Results of the manual vectorisation for (a) SS *Polwell*, (b) SS *Tiberia* and (c) SS *Hare* with the scour areas separated by the RRM highlighted with a yellow line in the background for a comparison.

3.4. Discussion

3.4.1. Objective separation of erosional and depositional wreck marks

In this study, we aimed to develop a method for objective extraction and classification of erosional and depositional scour marks from high-definition bathymetric DEMs of shipwreck sites. We successfully used a combination of residual relief modelling and DEM visualisation techniques, building on previous work in several fields of study which required the separation of morphological features of various length-scales (Wessel 1998; Smith and Clark 2005; Walbridge *et al.* 2018).

Although separation of wreck marks can be performed by manual vectorisation in GIS, this naturally introduces user-bias due to the subjective nature of the process. In our study, the residual relief modelling method was compared with a manual separation supported by 3D profiles derived from the DEMs. Both methods were successful in identifying the main scour marks on all of the wreck sites. However, differences in the extents and shapes of the picked areas were observed (Fig. 3.7, Table 3.1). Relief modelling outperformed manual vectorisation with respect to the total defined erosion/deposition areas by 18% (Table 3.1). The greatest differences were noted in places with subtle scour marks, which are difficult to define visually and vectorise using the manual approach. The results indicate that manual vectorisation alone cannot be used as a benchmarking validation method, and that scour signature separation should always be accompanied by statistical analysis. The fact that the residual relief modelling method is semi-automated and based on statistical differences between elevation values (Wilson and Gallant 2000) makes it a more effective tool compared with manual vectorisation.

3.4.2. Methodological considerations for residual relief modelling

There are some important methodological points to consider when using residual relief modelling for wreck mark separation. For example, the residuals initially classified during the second step as erosional features extending from the pipeline at the SS *Polwell* site (Fig. 3.4b) are in fact the result of natural bathymetric variation rather than scour. So care must be taken when reviewing the outputs. High-pass filtering, the first step of the relief modelling method, can also create artificial positive and negative relief features. Mean values assigned to cells corresponding to a featureless seabed on the original DEM can be influenced by proximal positive and negative values. As a result, non-existing residuals may occur and later be classified. The morphology of the wreck structure and the presence of other additional high elevation differences inside a kernel are the significant factors that can introduce these types of errors during the first and second steps of the process.

Wessel (1998) demonstrated that the application of median filters for high-pass filtering avoids the bias of extreme observations and enables the effective separation of residual morphologies. However, empirical observations indicate that computation times to calculate focal medians as opposed to means is an order of magnitude higher, dependent on kernel size and raster size/resolution. Additionally, focal statistics window shape can be adjusted. For example, in the TPI (Weiss 2001) and BPI approaches (Walbridge *et al.* 2018), an annulus (donut)-shaped kernel is used when separating topographic features of various length-scales. Empirical testing indicated that a circular moving window is the most universal and time-effective solution, whereas pilot results obtained with an annulus kernel did not indicate significant improvement in the wreck mark separation for the test sites.

Another consideration is the choice of the moving mean's window size in the first step, which is determined by specific characteristics of the scour marks and other geomorphological features developed at each site. In general, the more complex the local geomorphology, the harder it becomes to estimate a filter radius. For example, a filtering window with a radius of 200 m was applied on the SS *Hare* site to separate the large and deep scour pits (Fig. 3.8). A smaller radius allowed separation of the wreck structure and the positive feature located inside the pit but did not fully separate the scour pit itself. As shown in Fig. 3.8, at point (S) which was picked near the side of the scour pit, a 50-m radius window would capture a similar amount of negative and positive cells, and thus, the calculated average would be close to the value of a central cell.

Therefore, this part of the scour pit would not be captured as an erosional wreck mark during the classification process. A 100-m radius window would potentially separate the wreck structure, the positive feature and the negative scour pit, but only partially (Fig. 3.8). Hence, when dealing with scour marks, wrecks and geomorphological features at various length-scales, multiple window sizes need to be applied iteratively.

Whilst the size of a kernel defines the accuracy of separation related to length-scales, the choice of breakpoints during the classification controls the tolerance of values inside the classes. For example, in this study, minus and plus 0.5 standard score were used as the main breakpoints for each of the sites. If they were to be moved closer to zero (e.g. plus and minus 0.2), anything in between these breakpoints would be classified as featureless, and more values would be classified as depositional and erosional scour marks (i.e. outside the plus and minus 0.2 range). However, this would also increase the number of irrelevant, natural morphological features inside the classes. Empirical refinement indicated that +/- 0.5 standard deviation breakpoints are the most robust.
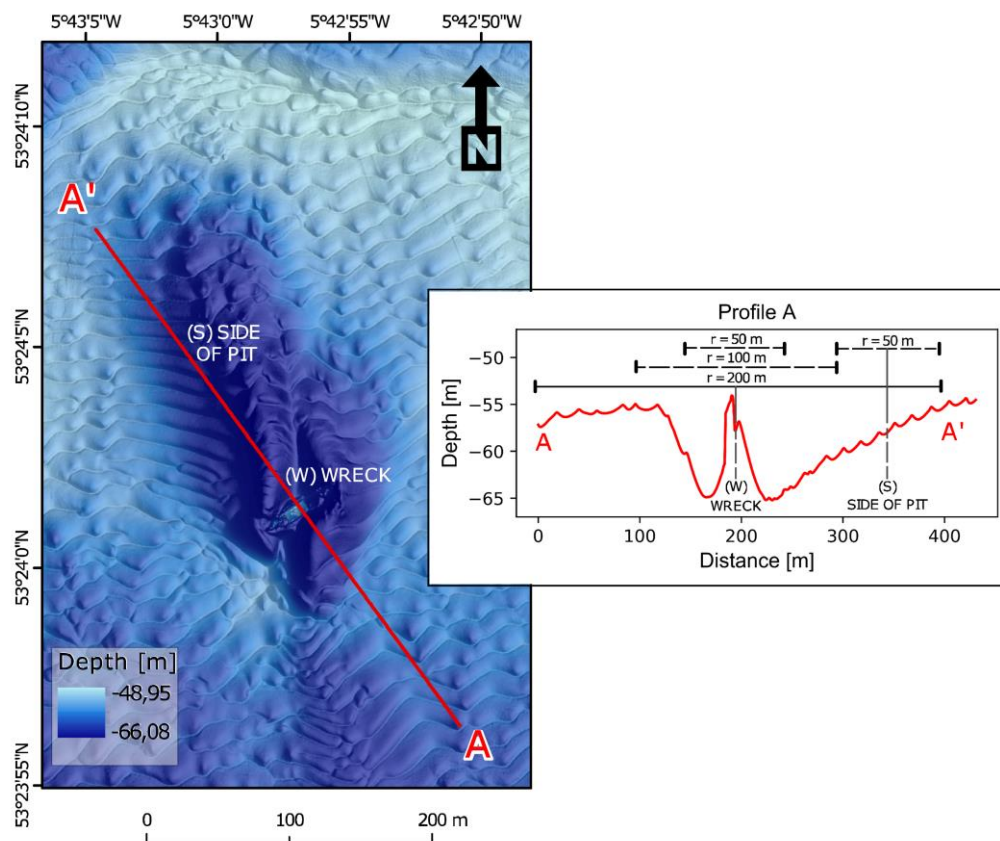
Figure 3.8. A-A′ depth profile drawn on SS *Hare* site to show the range of various filtering window sizes inside the scour pit. Filter ranges for circular window radiuses of 200 (used for the site in this study), 100 and 50 m are marked on profile graph A.

In the residual relief method developed in this study, the additional validating step supported by the DEM visualisation techniques was added in order to eliminate erroneous classifications and separate scour marks from other local geomorphological features. The techniques reveal some characteristics which are inherent to scour marks and difficult or impossible to spot solely by visual examination of the original DEM and bathymetric profiles. The enhanced visual techniques employed in this study not only serve for the separation of wreck marks but are also useful for the archaeological and geomorphological interpretation of wreck sites (e.g. for detection purposes or for drawing site plans).

3.4.3. Archaeological implications

Although the residual relief method was tested on three WW1 wreck sites, it is an important step towards the standardisation of the quantification of erosional and depositional zones on all underwater archaeological sites. As this method is semi-automated, it generates metrics for the delineation of local morphologies which are based on statistical comparisons, rather than on purely manual user interpretation. The method can be applied to any underwater site type, from individual artefacts to single wrecks, to submerged landscapes with varying characteristic length-scales. In this paper, we specifically tested it to separate scour signatures, as their quantification is fundamental to the understanding of wreck site formation processes.

Firstly, scour and associated sediment fluxes can trigger the burial of archaeological material within the sediments or can lead to the exposure of material into an oxygenated water column. This in turn influences processes like corrosion or biological encrustation (Ward *et al.* 1999). On the SS *Hare* site for example, scour processes cause the shipwreck to sink below the elevation of the regional seabed (Fig. 3.8). Similar scour mechanisms are described by Voropayev *et al.* (2003) and Jenkins *et al.* (2007) for small objects, where subsequent sinking of scour nuclei leads to their partial or complete burial. Similar processes happening on shipwreck sites influence the rate of their structural degradation (Ward *et al.* 1999).

Furthermore, changes in sediment budget caused by scouring in a dynamic marine environment may also influence the distribution of high- and low-pressure zones on a hull structure, potentially leading to the partial or complete collapse of the wreck (Quinn 2006). Erosional scour pits are also associated with increased local flow vorticity and turbulence (Quinn and Smyth 2018), and as a result, wreck elements in these areas are subject to increased fluid forcing. Thus, the objective separation of zones of erosion and accumulation helps to categorise a shipwreck site into regions characterised by different grades of preservation potential.

Zones undergoing erosional processes threaten the integrity of a submerged archaeological site, and therefore emphasis should be put on their monitoring. On the other hand, areas influenced by depositional processes generally represent the more stable component of the site, where the accumulated sediment aids preservation. Accurate characterisation and delineation of these zones can help site managers to target specific places to deploy monitoring equipment and undertake site protection measures involving, for example, the arrangement of sandbags and geotextiles. The residual relief modelling method provides an effective and objective method for the extraction of these features and therefore has great potential to enhance effective *in-situ* preservation planning, as encouraged by (UNESCO 2002).

From an oceanographic point of view, the distribution of scour marks provides information about directions and magnitudes of dominant bottom currents and the local net sediment transport (Caston 1979). The three shipwrecks chosen for this study are all located in similar bi-directional

flow regimes in the Irish Sea, on non-cohesive beds. However, the results of the RRM show that the complex patterns of wreck marks vary significantly across individual sites and between different shipwreck sites (Fig. 3.4). Although all three shipwreck sites are characterised by scour marks extending in opposite directions as a result of bi-directional tidal flow, only on the SS *Tiberia* site are the scour marks aligned symmetrically. Asymmetrical distribution of scour marks indicates two possibilities: either that ebb and flow current magnitudes are distributed unequally or that local variations in seabed morphology and/or composition can limit the extent of scour development. The RRM method successfully captured the zones of scour marks, which act as proxies allowing for the analysis of local sediment mobility.

The separation method reported here can also be applied to offshore engineering. For example, on the SS *Polwell* site, the wreck-related scour clearly extends beyond the pipeline located 600 m north of the wreck (Fig. 3.4c; Fig. 3.3a). The location of the wreck therefore influences the integrity of the seabed engineering, indicating that wreck marks should be mapped rigorously to estimate buffer zones, within which no offshore development should take place. Such an approach would potentially minimise detrimental effects caused by shipwreck-induced scour impacting offshore engineering, and vice versa. This factor is becoming increasingly important at a time when coastal and marine landscapes are being transformed as a result of coastal engineering initiatives to support developing urban centres.

3.5. Conclusions

In this study, we present a GIS-based residual relief modelling method for the semi-automated extraction of depositional and erosional features at wreck sites. We applied the method to three World War I shipwreck sites and evaluated it against traditional manual vectorisation techniques. The results suggest that the semi-automated modelling method is robust, time-effective and capable of quantifying the products of scour processes with increased objectivity. Our method holds great potential for the objective characterisation of erosional and depositional patterns and processes at wreck sites, which have important implications for site formation studies and *in-situ* preservation of underwater cultural heritage.

High-resolution multibeam echosounder surveys of wreck sites are now routinely used for archaeological prospection and assessment as they provide detailed, wide and time- effective coverage (Manders 2009; Plets *et al.* 2011; Astley *et al.* 2014). The increasing availability of high-definition multibeam-derived digital elevation models of historic wreck sites (Westley *et al.* 2019) allows for an entirely new level of detailed interrogation and analyses of the geomorphological features developed around them. Multibeam surveys are however still financially expensive and resource demanding. Therefore, their products should be used comprehensively to provide as much information as possible. The residual relief modelling coupled with the application of the DEM visualisation techniques adds another layer to the use of

the bathymetric surfaces. Accurately delineated zones of erosion and accumulation allow us to quantify seabed change by deriving areas, volumes and other metrics for the displaced sediments. The method presented in this paper helps to define the local geomorphology, which is a prerequisite for other established methods investigating the influence of fluid dynamics on the local seabed (Smyth and Quinn 2014; Fernández-Montblanc *et al.* 2018b) and assessing how it changes with time (Quinn and Boland 2010; Bates *et al.* 2011; Astley 2016).

4. Spatial and temporal variability in geomorphic change at tidally influenced shipwreck sites: The use of time-lapse multibeam data for the assessment of site formation processes

4.1. Introduction

Historic shipwrecks are of interest from many different perspectives (Firth 2018), as objects of cultural heritage and archaeological value (Delgado and Varmer 2015; Elkin *et al.* 2020), as hidden pollution sources (Landquist *et al.* 2013; Vanninen *et al.* 2020), as habitats for marine life (Balazy *et al.* 2019; Johnson *et al.* 2020), and as indicators of local oceanographic and seabed morphodynamic conditions (Caston 1979; Garlan *et al.* 2015; Geraga *et al.* 2020). Their preservation state is a result of site formation processes that comprise various natural and anthropogenic influences (Ward *et al.* 1999; O'Shea 2002). Understanding the temporal and spatial nature and scale of these processes is, therefore, critical to their long-term and sustainable management (Frost 1961; Muckelroy 1978; Pascoe 2012; Gregory *et al.* 2014).

In-situ preservation of shipwrecks is encouraged by the UNESCO Convention on the Protection of the Underwater Cultural Heritage, which states that assessments of environmental characteristics should be included in site investigations to examine long-term stability of the underwater cultural heritage (UNESCO 2002). According to the Convention, these assessments should be conducted without causing disruption to sites, thus promoting the use of non-destructive methods (UNESCO 2002).

Present-day seabed mapping technology and techniques allow for precise, nonintrusive mapping of underwater archaeological sites with centimetric precision (Plets *et al.* 2011; Westley *et al.* 2011, 2019; Ødegård *et al.* 2018; Ferentinos *et al.* 2020). It is now possible not only to detect and identify shipwrecks remotely, but also to analyze and quantify geomorphic change at underwater sites through repeat high-resolution multibeam echosounder (MBES) bathymetric surveys (Quinn and Boland 2010; Bates *et al.* 2011; Stieglitz and Waterson 2013; Astley 2016; Brennan *et al.* 2016). Moreover, buried parts of shipwrecks and sub-seabed records of site formation processes can be imaged using shallow seismic techniques (Quinn *et al.* 1997; Plets *et al.* 2009; Grøn *et al.* 2015; Cvikel *et al.* 2017). The use of a combination of these methods allows for a holistic characterization of sites and assessment of their evolution in a time-efficient, non-invasive way (Quinn *et al.* 2007; Astley 2016; Bethencourt *et al.* 2018; Geraga *et al.* 2020).

Shipwreck sites are often considered as systems in a state of equilibrium achieved sometime after an initial wrecking incident (Ward *et al.* 1999; Wheeler 2002; Quinn 2006; Quinn and Boland 2010; Astley 2016). This equilibrium state is dynamic, meaning that it can be perturbed by

external or internal forces. This perturbation in the system can result in either a new equilibrium state or maintenance of the current one, depending on the system's capacity to absorb external forces (Quinn 2006; Quinn and Boland 2010; Astley 2016). The dynamics of equilibrium varies across wreck sites, with some subject to disruptions by storms (McNinch *et al.* 2006; Fernández-Montblanc *et al.* 2016), varying tidal currents (Astley 2016; Quinn and Smyth 2018), or anthropogenic impacts (Gibbs 2006; Brennan *et al.* 2013), whereas others are nearly static, located in more stable physical environments (Eriksson and Rönnby 2012). What is common is that all wreck sites are characterized by a negative disequilibrium trend, as they undergo a gradual degradation due to chemical (i.e., corrosion) and biological (e.g., wood-boring organisms) formation processes (Foecke *et al.* 2010; Pournou 2017; Gregory 2020; Taormina *et al.* 2020). Nevertheless, sites in highly dynamic environments, leading to frequent changes in equilibrium states, are prone to accelerated disintegration (Quinn and Boland 2010). Therefore, the state of a shipwreck site as a system, and its susceptibility to disruption, should always be assessed before implementing any *in-situ* preservation measures (Astley 2016).

The dynamism of underwater sites is often controlled by their hydro-dynamic environment and sediment budget, defined as the rate of net supply or removal of different sediments to the wreck area (Ward *et al.* 1999). One of the key processes controlling the sediment budget and determining the integrity of underwater structures is seabed scour, which occurs as a result of magnified flow velocity around objects disrupting natural near-seabed currents (Sumer and Fredsøe 2002; Quinn 2006). In engineering applications, erosive scour processes are considered detrimental to the stability of underwater structures such as bridges and wind farm piles, which often require special mitigation measures. For example, in the Irish Sea, significant scour developed at the base of monopiles shortly after the construction of the Arklow Bank wind park, resulting in the need to use rock armour to mitigate further scouring (Whitehouse *et al.* 2011). Therefore, much attention has focused on geotechnical assessments of scour and related processes for offshore engineering purposes (Sumer 2007; Whitehouse *et al.* 2011; Matutano *et al.* 2013; Melling 2015).

Although scouring has been researched at shipwreck sites, studies have mostly focused on single surveys, investigating intricate depositional and erosional signatures, referred to as wreck marks (Caston 1979; Garlan *et al.* 2015). To fully understand the dynamics of scour development, however, high-resolution bathymetric surveys should be conducted at least two times. This approach, referred to as "time-lapse" or "repeat surveying," has not been used very often to date (Quinn and Boland 2010; Bates *et al.* 2011; Stieglitz and Waterson 2013; Astley 2016; Brennan *et al.* 2016), considering that 3 million shipwrecks are estimated worldwide (Croome 1999; UNESCO 2017).

As changes in sediment budget due to scour can ultimately lead to the exposure or burial of shipwrecks, it therefore, also controls oxygen availability, biological encrustation, corrosion rates,

and pressure gradients exerted on hulls (Ward *et al.* 1999; Quinn 2006), mechanisms significantly influencing site formation. The presence or absence of ongoing scour processes may also indicate whether a shipwreck site is in a stable or dynamic equilibrium. Considering all these points, it is critical that seabed change at shipwreck sites is understood at various time scales to fully assess their preservation potential.

The aim of this study is to expand the knowledge of formation processes at underwater shipwreck sites in the context of the sediment budget and the hydro-dynamic environment. We achieve this by comparing the spatial and temporal development of scour signatures and other bedforms around 10 metal-hulled shipwrecks lost between 1875 and 1918, located at moderate depths (26–84 m) in contrasting hydro-dynamic and sedimentary settings in the Irish Sea. Very high-resolution time-lapse bathymetric data were collected and integrated with seismics, sediment samples, and modeled near-seabed tidal currents. Bathymetric survey design was optimized to collect the highest resolution data possible, resulting in difference models and analysis of geomorphic change at a resolution previously unrealized in time-lapse assessments of underwater cultural heritage. The number of wrecks investigated, and the combination of methods provide new knowledge that allows for the development of more accurate underwater site formation models. In addition, we recognize this investigation as relevant for offshore engineering applications, as it focuses on localized morpho-dynamic change around submerged man-made structures.

4.2. Materials and methods

4.2.1. Study area

The study area encompasses the waters off the east and northeast coast of the island of Ireland from Rathlin Island in the north to Dublin Bay in the south (Fig. 4.1). Within this area, 10 wrecks were investigated: SS *Lugano*, SS *Santa Maria*, SS *Tiberia*, SS *Chirripo*, SS *Polwell*, FV *St. Michan*, SS *WM Barkley*, SS *Hare*, RMS *Leinster*, and HMS *Vanguard*. With the exception of HMS *Vanguard*, all shipwrecks investigated in this study were lost due to naval warfare during World War 1. HMS *Vanguard* sank in fog in 1875 due to a collision with its sister ship HMS Iron Duke. The 10 shipwreck sites were selected to represent a range of physical environments, characterized by different tidal conditions and varied geological substrates. These shipwrecks are just a few of more than 18,000 other wrecking incidents that are recorded off the island of Ireland (Forsythe *et al.* 2000; Brady *et al.* 2012).

The Irish Sea is a shelf sea dominated by tidal currents that are typically rectilinear along coasts and in straits (Ozer *et al.* 2015). Semidiurnal lunar (M2) and solar (S2) tides propagating from the Atlantic Ocean through the North Channel to the north and St. George's Channel to the south largely control the tidal current magnitudes (Neill *et al.* 2014; Ozer *et al.* 2015). The areas chosen for the study (Fig. 4.1) are characterized by depth-averaged peak spring tide magnitudes ranging

from 0.5 m/s around Belfast Lough (Atkins 1997), 1 m/s off Dublin Bay (Howarth 2001), to 3 m/s in Rathlin Sound. The latter is a candidate area for tidal turbine development (Lewis *et al.* 2015; Pérez-Ortiz *et al.* 2017), whereas offshore Dublin Bay is proposed for offshore wind development.

Flows in the Irish Sea are also influenced by surface waves, inertial currents, residual currents, and storm surges. Waves are generally characterized by a short period with a limited access of swell waves to the basin, as it is partly enclosed. In general, tidal current amplitudes are an order of magnitude greater than long-term averaged residual currents (Bowden 1980). Inertial currents, episodically generated in the thermally stratified waters of the western Irish Sea, are observed to reach 0.2 m/s in the surface layer (Sherwin 1987). The circulation in this part of the basin is also affected by a density-driven cyclonic gyre that forms during spring and summer, with modeled baroclinic currents reaching 0.14 m/s (Horsburgh and Hill 2003). The largest nontidal, depth-averaged current magnitude has been reported to reach 0.65 m/s in the North Channel (east from Belfast Lough; Fig. 4.1), which was attributed to a storm event (Knight and Howarth 1999). Externally generated storm surges propagating from south and north appear to interact with tides causing twice-daily intermittent oscillations (Howarth 2001). Nevertheless, the prevailing flows in the whole basin remain tidally generated.
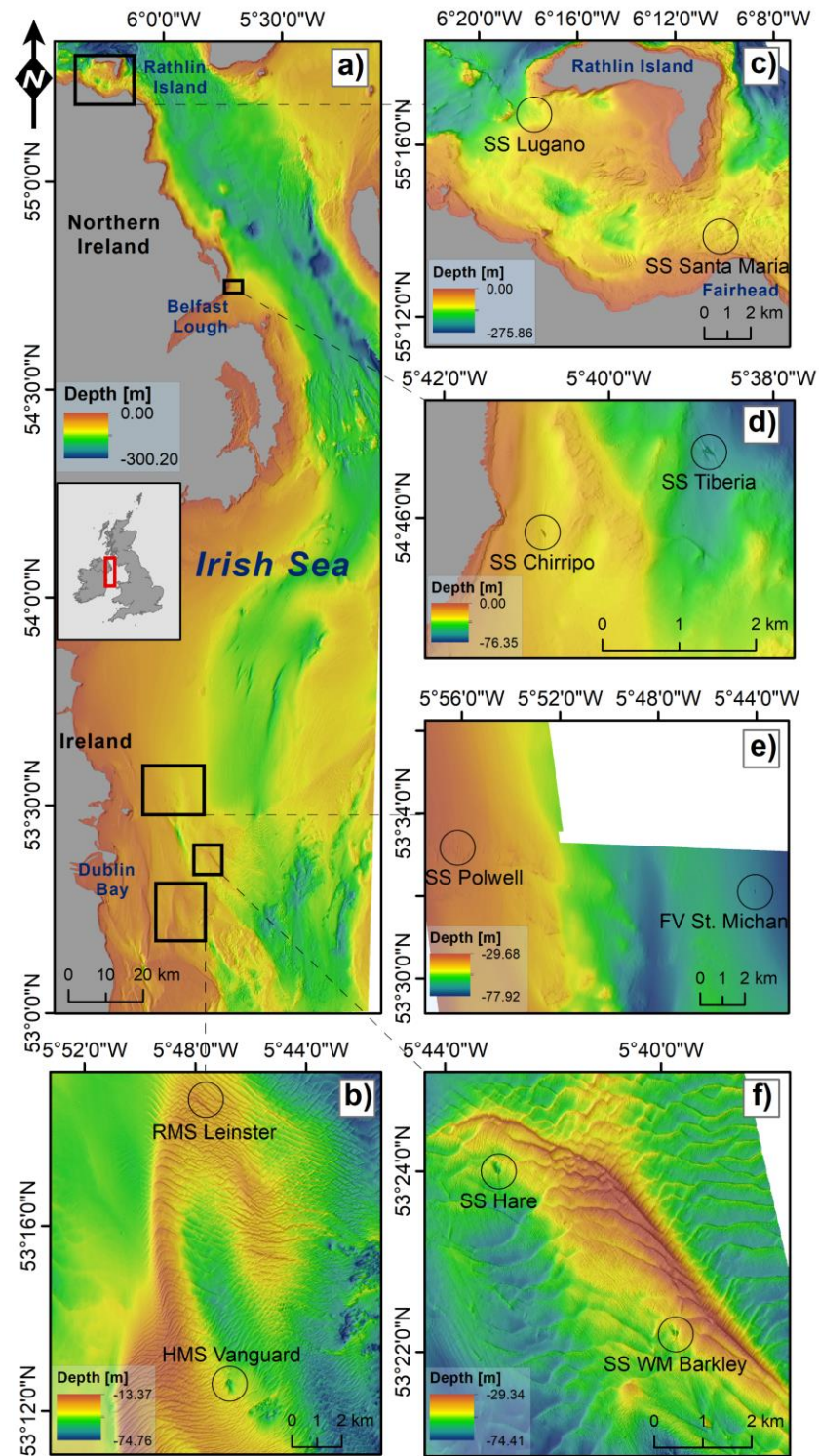
Figure 4.1. a) Location of the study area on the map of the United Kingdom and Ireland. (b) Locations of the study sites in the Irish Sea with inset maps representing sites (c) between Fairhead and Rathlin Island, (d) off Belfast Lough, (e) northeast of Dublin, (f) east of Dublin, (g) southeast of Dublin. Backdrop bathymetry presented in Figure 1 was obtained from (b) (EMODnet Bathymetry Consortium 2018), (c) Joint Irish Bathymetric Survey project (https://www.infomar.ie/partnerships/jibs-joint-irish-bathymetricsurvey), (d) Royal Navy (public sector information, licensed under the Open Government License v2.0), and (e–g) INFOMAR project.

4.2.2. Geological setting

The Irish Sea was glaciated during the Last Glacial Maximum (27 ka–18 ka BP; Scourse *et al.* 2019; Van Landeghem and Chiverrell 2020) when the Irish Sea Ice Stream advanced through the Irish Sea, eroding and reworking sediment, and depositing variable thicknesses of glacial diamict. This diamict was often deposited directly on the bedrock and is referred to as the upper till member (Jackson *et al.* 1995). The upper till member comprises sand to boulder-grade material and is often over-consolidated (Mellet *et al.* 2015; Coughlan *et al.* 2019). During the retreat phase of the Irish Sea Ice Stream during deglaciation, large amounts of meltwater were discharged along with outwash material in the form of a heterogeneous mix of sediments, predominately gravels, with mud, sand, and cobbles, referred to as the chaotic facies (Jackson *et al.* 1995; Coughlan *et al.* 2019).

The subsequent marine transgression and present-day hydro-dynamics reworked much of the glacial and postglacial sediment in the south Irish Sea into a mosaic of substrates (Ward *et al.* 2015). These processes created a series of dynamic bedforms, including migrating sediment waves, in an area dominated by coarse lag deposits. The sediment waves vary in size and morphology, with the magnitude of migration highest in the central Irish Sea, with average rates of up to 35 m/year, decreasing northward (Van Landeghem *et al.* 2009a, 2012; Coughlan *et al.* 2020). The northward transport of sediment eventually terminates in an area of low bed stress, referred to as the Western Irish Sea Mud Belt, where the fine-grained sediment has been accumulating since the end of the last glaciation (Belderson 1964; Woods *et al.* 2019). In this area, there are thick deposits (up to 40 m) of stratified gray-brown muddy sands with silts and clays referred to as the mud facies (Jackson *et al.* 1995). This mud facies is typically of low shear strength and so potentially prone to scour around obstacles (Coughlan *et al.* 2019).

4.2.3. Data acquisition and processing

4.2.3.1.   Time-lapse MBES data

Time-lapse surveys were designed to provide high-resolution MBES coverage for the selected shipwreck sites in 2015, 2016, and 2019 (Table 4.1). The 2015 and 2016 data comprise single surveys for selected wrecks, whereas in 2019, repeat surveys spaced 1 week apart were also conducted for three sites. The first survey took place before a spring tide (October 28, 2019) and stormy weather (October 29, 2019–November 3, 2019; Table 4.1, referred to as 2019a), after which the second, repeat survey was conducted (Table 4.1, referred to as 2019b). Additional lower resolution MBES legacy data from 2010 were included in the research to provide multiannual (2019–2010) change comparisons for the SS *Hare* and SS *WM Barkley* sites (Table 4.1). All the data were collected on the Marine Institute's RV *Celtic Voyager* during Integrated Mapping for the Sustainable Development of Ireland's Marine Resource (INFOMAR) project's survey CV10_01 and ship-time application surveys CV15021, CV16031, CV19027.

The 2015, 2016, and 2019 surveys were designed specifically to capture the shipwreck site and surrounding seabed including the full extent of observed wreck marks at a high spatial resolution. The same line plan was used through these surveys with slight *ad hoc* changes in line orientations due to weather constraints and to improve survey efficiency. Infill profiles were acquired in places where the vessel deviated from lines, to avoid creating holes in the data sets. Survey grids were planned to ensure 100% overlap, thus achieving 200% coverage. The vessel was moving between 3 and 5 knots during all surveys. This strategy ensured consistency between the acquired data sets and allowed imaging of the site's local geomorphology at the highest possible resolution.

The 2015 MBES data were acquired between 5 and 11 September using a hull-mounted single-head Kongsberg EM2040 operating at 400 kHz, a continuous wave (CW) pulse, and 110°–120° swath coverage. Integrated GNSS/L-Band receiver CNAV 3050 was used for primary position corrections with a Seatex Seapath 330+ acting as a secondary positioning system and providing motion referencing and timing. Sound velocity profiles for refraction corrections were acquired with a Valeport Midas SVP and real-time AML surface sensor. The October 4–10, 2016 and October 24–November 5, 2019 survey data were collected using the same survey setup, but with a dual-head Kongsberg EM2040 MBES.

Table 4.1. MBES time-lapse survey data availability for the candidate shipwrecks. 2019a and 2019b correspond to surveys before and after a storm/spring tide respectively.

Shipwreck	2010	2015	2016	2019a	2019b
SS *Lugano*			✓		
SS *Santa Maria*			✓		
SS *Chirripo*		✓	✓		
SS *Polwell*		✓	✓	✓	✓
SS *Tiberia*		✓	✓		
FV *St Michan*		✓		✓	
RMS *Leinster*		✓	✓	✓	
HMS *Vanguard*		✓			✓
SS *Hare*	✓	✓	✓	✓	✓
SS *WM Barkley*	✓	✓	✓	✓	✓

The legacy MBES data were collected in May 2010 using a hull-mounted single-head Simrad EM3002 operating at 300 kHz and a short CW pulse with a 100° swath angular coverage. Positional information was supplied by a combination of Seatex Seapath 200 DGPS and Fugro HP DGPS. Several onshore and offshore tide gauges were deployed to provide tidal corrections. The tidal data were later leveled to a chart datum using Vertical Offshore Reference Frames. The 2010 data were collected using a different survey design, which followed the Maritime and Coastguard Agency (MCA) guidelines for wreck surveys (MCA 2018), optimizing detailed wreck coverage over seabed contextualization. All MBES bathymetric data were cleaned with the Combined Uncertainty and Bathymetry Estimator algorithm (CUBE; Calder and Wells 2007) and

corrected for tides and refraction using CARIS Hips and Sips v. 9.1 software. The processed data were exported to rasterized digital elevation models (DEMs) in the UTM 30N projection. Quality control was performed using crosslines, which indicated at least 98% compliance with IHO Special Order standard (IHO 2020). The 2015, 2016, and 2019 bathymetric data sets were gridded to a common 30-cm spatial resolution for the time-lapse analysis. The 2010 data were gridded to the best achievable 50-cm resolution; thus, for the SS *Hare* and SS *WM Barkley* sites, the 2015 and 2019 data were additionally gridded to this resolution to ensure the same resolution for multiannual data comparisons (Table 4.1).

4.2.3.2.   Seismic data

Shallow seismic data were collected for the HMS *Vanguard* site during the 2015 MBES survey, using an SES probe 5000 sub-bottom profiler operating at 3.5 kHz. Raw data were exported from CODA Octopus v. 7.3.3 after applying a bandpass filter. Manual horizon picking was then performed in Adobe Illustrator 2020 to inform vertical constraints for scour development at the site.

4.2.3.3.   Sediment samples

Sediment samples were collected using a Shipek grab inside and outside the erosional and depositional signatures. The granulometric analysis of the sediments was performed using a MALVERN Mastersizer 3000 laser diffraction particle size analyzer for fractions with grain sizes <2.38 mm, with an exception for the samples collected at the FV *St. Michan* and HMS *Vanguard* sites, which were analyzed using a sieve stack. Sediment classification into Folk classes (Folk 1954) and median grain size (d_{50}) calculations including >2.38 mm particle sizes (i.e., gravel) were performed using Gradistat v. 8 software (Blott and Pye 2001). In cases where samples indicated gravelly components in the mixture or gravel as a main fraction, a nominal value of 4 mm was used to represent gravel in the median grain size calculations.

4.2.3.4.   Oceanographic data

Current velocity magnitudes and directions at 1 m above the seabed were obtained for the wreck sites from an operational model run by the Marine Institute of Ireland (Nagy *et al.* 2020). The model is an implementation of the Regional Oceanic Modeling System (ROMS; Shchepetkin and McWilliams 2005) for an area of the northeast Atlantic encompassing all Irish waters. The horizontal resolution of the model in the Irish Sea is between 1.1 and 1.7 km, and the temporal resolution of the model data is hourly. Models for SS *Santa Maria* and SS *Lugano* cover 1-year period (January 31, 2019–December 31, 2019), and those for all other sites cover two years (January 01, 2017–December 31, 2019).

Significant wave height and wave period data were obtained from an Ocean Data Acquisition Systems (ODAS) M2 buoy located around 20 nm east of Dublin (53°28′8″N 5°25′5″W, 95-m

water depth; Fig. 4.1b), which is a part of the Irish Marine Data Buoy Observation Network managed by the Marine Institute (Ireland) in collaboration with Met Éireann and the UK Met Office. The data cover a time period from May 03, 2001 to April 22, 2020, with some gaps.

4.2.4. Data analysis

The first step of the analysis procedure was to thoroughly characterize each site using the MBES and ROMS data. This entailed determining dimensions and depths of the shipwrecks and associated erosional/depositional signatures, their orientation relative to dominant tidal currents, and calculating the volume of eroded/deposited sediment. The second step was to determine sediment mobility from the collected sediment samples and ROMS data. This entailed calculating sediment mobility thresholds and the frequency of threshold exceedance for each site. The third step was to detect and quantify geomorphic change within the intervals covered by time-lapse bathymetric surveys. This included calculation of volumetric changes in sediment budget and maximum scour depths at each site. Effectively, this sequence enables us to characterize in detail the baseline oceanographic, bathymetric, and sedimentological conditions at each site (Steps 1 and 2) and, with this in hand, explore and advance secure explanations for the patterns of geomorphic change identified in Step 3. The procedure followed in each step is explained below.

4.2.4.1.   Site characterization

Data integration and analysis were conducted in ESRI ArcMap v. 10.6.1 GIS software. The DEMs were analyzed to measure the dimensions and orientations of the shipwrecks. Initial volumes of shipwreck-induced erosional and depositional signatures were calculated for the oldest time-step DEMs with extents covering the whole signatures. The 2015 DEMs were used for the calculation of initial volumes and maximum scour depths for every shipwreck, except for SS *Lugano* and SS *Santa Maria*, for which the 2016 DEMs were used. To perform the volume calculations, the extents of the wreck marks were delineated. As manual delineation through vectorization is highly subjective, the residual relief modelling approach of Majcher *et al.* (2020) was used to separate the wreck marks from the surrounding geomorphology. The methodology relies on a DEM high-pass filtering (Wessel 1998; Walbridge *et al.* 2018; Majcher *et al.* 2020), combined with a breakpoint classifier. Separate high-pass filtering moving mean kernels were chosen to delineate erosional and depositional signatures. High-pass filtered DEMs were then masked using the extents of the erosional scour features delineated by the breakpoint classifier. The 3D Analyst surface volume tool was used on these masked high-pass filtered DEMs to calculate volumes of all the pixels with values below (erosion) and above (deposition) zero. Shipwreck structures were removed for the volumetric calculations using clipping and masking tools.

4.2.4.2.   Sediment mobility

Current velocities derived from the ROMS model and sediment samples were used to estimate how often sediment may be mobilised at the candidate sites, according to the approach prescribed by Whitehouse (1998) and Soulsby (1997). In this method, the potential mobility of sediment can be assessed by comparing the values for current-related bed shear stress (τ_c) with the critical shear stress (τ_{cr}) and calculating exceedance levels ($\tau_{cr} < \tau_c$). The current-related bed shear stress is calculated using following equation:

$$\tau_c = \rho C_D \overline{U}^2 \tag{4.1}$$

where ρ is the water density, CD the drag coefficient and $\overline{U}$ the depth-averaged current speed. The critical shear stress is then defined by:

$$\tau_{cr} = \theta_{cr} \cdot g(\rho_s - \rho)d_{50} \tag{4.2}$$

where θ_{cr} is the critical Shields parameter, g is acceleration due to gravity (9.81 m s-2), ρ_s and ρ are densities of sediment and water respectively, and d_{50} is the median grain-size.

The presence of an obstacle to a flow causes its contraction and increase in speed, hence increasing shear stresses exerted on the bed downstream of the obstacle (Soulsby 1997; Whitehouse 1998). Therefore, in this study, exceedance levels were calculated separately assuming a fourfold shear stress amplification factor determined by Smyth and Quinn (2014) through computational fluid dynamic simulations, conducted using a 3D model of a shipwreck derived from high-resolution MBES data in the Irish Sea. The calculations of the exceedance levels presented in the results were averaged for each studied shipwreck site. Shear stress calculations for all the sediment samples are included as supporting information.

Furthermore, to assess the influence of waves at the sites, the 99th percentiles representing storm events (Wang and Swail 2001; Matulla *et al.* 2008) were calculated for 122222 buoy readings of significant wave heights. According to an approximation by (Soulsby 1997), oscillatory flows induced by waves can affect the seabed when relation (4.3) is satisfied:

$$h < 10 \, H_s \tag{4.3}$$

where H_s is significant wave height and h is water depth at the seabed. The calculated 99th percentile of the distribution of significant wave heights (H_{s99}) recorded at the M2 buoy were therefore used with equation (4.3) to assess the wave influence on the sediment mobility at the sites. The wave data were analyzed separately for the period of the 2019 survey (between 24.10 and 5.11.2019) to assess the wave regime for the weekly time-lapse bathymetric coverage.

4.2.4.3.   Bathymetric time-lapse analysis

The time-lapse analysis of the bathymetric datasets comprised multiple steps. Firstly, DEMs of Difference (DoD) were obtained by a subtraction of DEMs corresponding to subsequent surveys, using a raster minus tool. Shipwreck structures were masked in the DoDs as they introduce outliers in bathymetric time-lapse analyses (Astley 2016). Additionally, the study concentrates on geomorphic change at the sites and not on structural changes of the shipwrecks themselves. Recording the latter would require a different approach to survey design (Westley *et al.* 2019) and data analysis involving comparisons of dense point clouds rather than the digital elevation models.

Measured depth uncertainties were approximated for each bathymetric DEM using vertical total propagated uncertainty values (*vTPU*) calculated by the CUBE algorithm during the multibeam data processing. These *vTPU* values, corresponding to any two compared DEMs, were combined using equation (4.4) which provides a combined minimum level of detection threshold (LoD_{min}) (Brasington *et al.* 2003):

$$LoD_{min} = \sqrt{(vTPU_{survey1})^2 + (vTPU_{survey2})^2} \qquad (4.4)$$

All recorded geomorphic change contained within the minimum level of detection is considered unreliable. The *vTPU* values determined for the 2015, 2016 and 2019 surfaces equal to 20 cm and therefore the *LoD_{min}* value of the resulting DoDs is approximately ±30 cm. The *vTPU* values for the 2010 surfaces were not possible to estimate absolutely, but an examination of the acquired MBES data and analysis of equipment errors indicated that the same *LoD_{min}* values can be applied. Therefore, volumetric change calculations did not include pixel values within the *LoD_{min}* range (±30cm).

After obtaining the DoDs, volumetric changes were calculated within 50, 100, 200, 300, 400 and 500 m radii from the central positions of the shipwrecks, depending on the maximum extent of the DoD rasters. These radii were inspired by buffers which have been applied to UK historic shipwrecks in the eastern Irish Sea, designated under the Protection of Wrecks Act (1973) and which range between 100 and 500 m (Wessex Archaeology 2005). The smallest (50 m) radius was chosen to investigate changes in the immediate vicinity of the shipwrecks.

Lastly, the time-lapse analysis involved a comparison of maximum scour erosion depths for all the time steps in relation to the depth of the surrounding seabed. As the seabed outside of the scour impacted areas may be mobile, the surrounding seabed depths were picked in the oldest time-step DEMs and used for all subsequent time-steps.

4.3. Results

4.3.1. Site characterization

In this section, the results of the analysis of the bathymetric DEMs, modelled near-seabed current data and sediment samples are presented. Granulometric analysis of the sediment samples collected around the wrecks resulted in a classification of the sites into three categories: sand-dominated, multimodal and gravel-dominated.

4.3.1.1.   Sand-dominated sites

RMS *Leinster*, HMS *Vanguard*, SS *Hare* and SS *WM Barkley* rest on largely sandy substrates (Fig. 4.2, Table 4.2) and are surrounded by bifurcating sediment waves superimposed on larger sediment waves (Stow *et al.* 2009; Van Landeghem *et al.* 2009b). Modelled near-seabed current directional distributions vary slightly across these sites (Fig. 4.2), with maximum spring tide magnitudes oscillating around 0.5 m/s (Table 4.2).

RMS *Leinster* has an erosional depression with a maximum depth of 3.00 m on its SE side and a depositional tail extending south from the wreck (Fig. 4.2a). Both of these sedimentary signatures are aligned with the most frequent modelled near-seabed current, oriented N-S. The erosional signature merges with a natural depression, which may be a result of shipwreck- or sediment wave- induced scour and is aligned to the less frequent NNW-SSE currents. The wreck is bounded to the south and north by separate, large sediment waves characterized by a height of 5-8 m and a wavelength of 200 m. Ubiquitous bifurcating sediment waves, with heights and wavelengths typically not exceeding 0.5 m and 15 m respectively, are imaged around the wreck, including outside and inside the erosional and depositional zones. They are mostly perpendicular to the currents oriented NNW-SSE. On the other hand, the large sediment waves are not aligned with any component of the modelled currents, being oriented NNE-SSW. The total volumes of erosion and deposition are low at this site in comparison to other wreck sites located in the same sand substrate (Table 4.2).

SS *Hare* and SS *WM Barkley* are located within 5 km of one another in the same sediment wave field (see Fig. 4.1f). Both wreck sites are characterized by deep scour pits extending from their bow and stern (Fig. 4.2b and 2c). SS *Hare*'s pits have a maximum depth of 11.32 m in relation to the surrounding seabed and stretch up to 200 m from the wreck (NW direction) (Table 4.2). SS *WM Barkley's* pits have similar geometry, reaching a distance of 285 m from the shipwreck, with a maximum depth of 13.64 m. In both cases, the scour pits are separated by thin depositional ridges, parallel to the weaker, less frequent currents oriented N-S, while the scour pits correspond to the stronger NNW-SSE currents. Pervasive sediment waves, with typical wavelengths of 10 to 15 m and up to 0.5 m high are developed at both sites, aligned to modelled current directions, and are present inside the scour pits. Large sediment waves, 7 and 4 m high for SS *Hare* and SS *WM*

Barkley respectively, are present north of the sites. Their wavelengths are difficult to determine, as the large sediment wave field is highly irregular. Multiple grab samples collected at the SS *Hare* site indicate both the presence of sand and gravelly sand inside the pits (Table 4.2). High volumes of sediment are eroded at these sites, among the highest of all the candidate shipwrecks (Table 4.2).

At the HMS *Vanguard* site, an 11.69 m deep comet scour has developed, aligned with the bi-bidirectional current regime (Fig. 4.2d), reaching as far as 280 m south of the shipwreck. The shipwreck itself is entrenched between two depositional features, much smaller in size and volume (Table 4.2). Scour development is constrained by a large sediment wave to the NE of the site. The change in bathymetry from the base of the scour pit to the large sediment wave's crest reaches up to 13 m. Smaller sediment waves, typically 10-15 m long and 0.2 to 0.5 m high are present around the site, perpendicular to the currents; however, they are not developed in the central part of the scour pit. Three unsuccessful attempts to collect grabs from the scour pit indicate a coarser/hard substrate. Corroborating evidence comes from the seismic data acquired over the site, where laterally continuous, shallow medium amplitude horizontal reflectors at between 0-10 m below the seafloor (Fig. 4.3) are interpreted as hard layers, acting as a vertical constraint for scour development. The HMS *Vanguard* site is also characterized by the highest volume of erosion among all the recorded sites (Table 4.2).
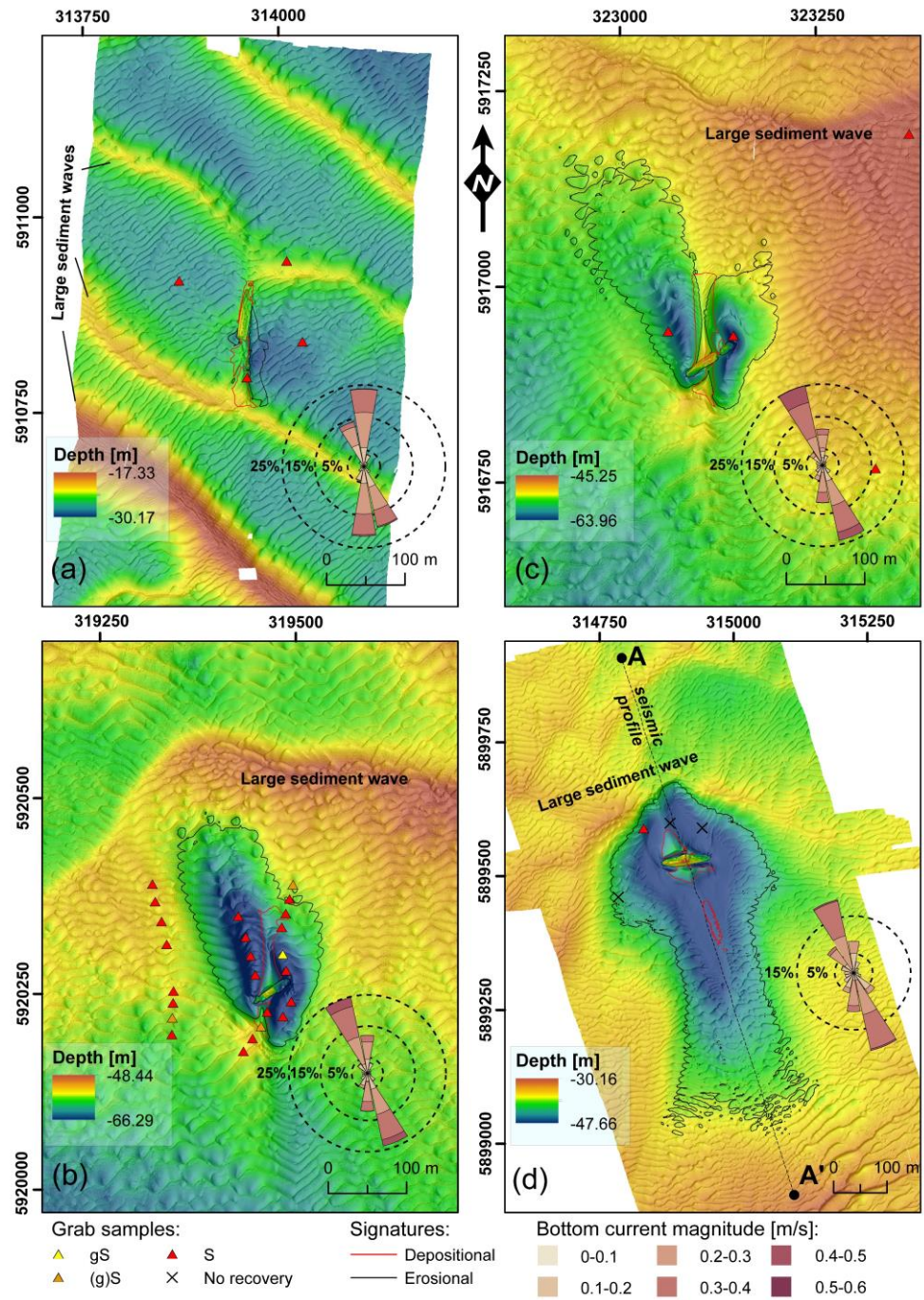
Fig. 4.2. Sand-dominated sites presented as digital elevation models with a multidirectional hillshade occlusion: (a) RMS *Leinster*, (b) SS *WM Barkley*, (c) SS *Hare*, (d) HMS *Vanguard* (the seismic profile is described in Figure 4.3). Rose charts represent the modeled near-seabed current data. Grab samples: gS, gravelly sand; (g)S, slightly gravelly sand; S, sand.

Table 4.2. Characterization of the shipwreck sites.

Category	Wreck	Length, width, height [m]	Seabed depth [m]	Year of loss	Orientation	Peak seabed current [m/s]	Maximum reach of signatures from a wreck		Sediment – Folk (1954) classification			Initial volumes [m³]		$T_{cr} < T_c$ (%) Threshold exceeded	$T_{cr} < T_c$ (%) Amplified
							Erosional [m]	Depositional [m]	Signatures – erosional	Signatures - depositional	Outside signatures	Erosion	Deposition		
Sand	**RMS** *Leinster*	110 x 13 x 5	28	1918	188°, aligned/oblique to currents	0.45	90	50	No data	Sand	Sand	1635	1213	43.9	79.0
	SS *Hare*	53 x 9 x 7	61	1917	55°, nearly perp. to currents	0.51	200	92	Sand/Gravelly sand	Sand/Gravelly sand	Sand	121235	3264	52.7	85.5
	SS WM *Barkley*	72 x 10 x 5	52	1917	54°, nearly perp. to currents	0.54	285	107	Sand	No data	Sand	108187	6211	56.1	87.6
	HMS *Vanguard*	90 x 20 x 12	40	1875	82°, perpendicular to currents	0.47	280	120	No recovery /Sand	No data	No data	345385	3897	56.6	91.2
Multimodal	**SS *Chirripo***	115 x 15 x 12	26	1917	146°, oblique to currents	0.28	-	700	No scour recorded	Gravelly muddy sand	More Gravel/muddy sandy gravel	-	415	2.3	52.5
	SS *Tiberia*	127 x 17 x 10	55	1918	285°, oblique to currents	0.53	110	500	Muddy sandy Gravel	Slightly gravelly muddy sand	Muddy sand	17631	18296	50.6	79.1
	SS *Polwell*	95 x 12 x 10	26	1918	208°, oblique to currents	0.38	1290	1190	Gravelly muddy sand	Muddy Sand	Muddy Sand	19286	14047	17.2	69.5
	FV *St. Michan*	30 x 6 x 5	72	1918	104°, perpendicular to currents	0.35	100	-	No recovery /Muddy Sandy Gravel	Muddy Sand/Grav. Mud/Grav. and Slightly Grav. Muddy Sand	Mud	8526	3038	32.5	70.8
Gravel	**SS *Lugano***	106 x 16 x 10	84	1917	97°, aligned with currents	0.82	-	120	No scour recorded	No data	Sandy Gravel/Gravel	-	114	4.9	58.5
	SS *Santa Maria*	100 x 16 x 16	67	1918	104° (hull), oblique to currents	0.97	140	-	Gravel/Boulders	No deposition recorded	Gravel/Boulders	21463	-	19.0	67.4
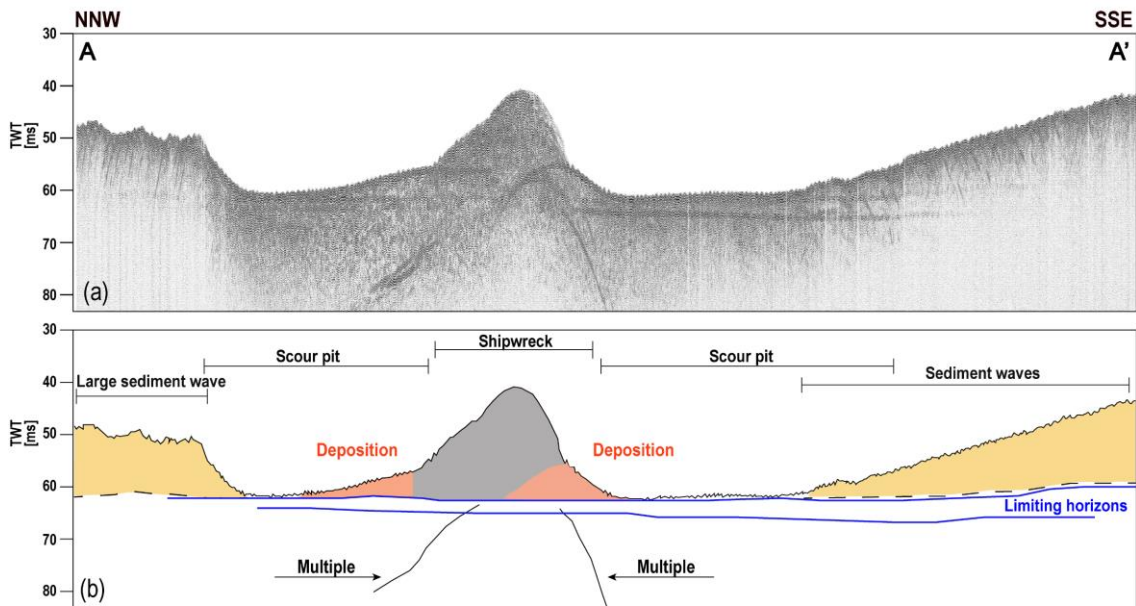
Figure 4.3. (a) Seismic line acquired over HMS *Vanguard* and (b) its interpretation, showing the digitized horizons vertically limiting further development of the scour pits. The profile's location is shown in Fig. 4.2d. Sediment waves and a large sediment wave are visible SSE and NNW of the wreck, correspondingly. Multiple reflections (seismic artifacts) are marked separately.

4.3.1.2.   Multimodal sites

SS *Chirripo*, SS *Tiberia*, SS *Polwell* and FV *St. Michan* rest on mixed substrates (Table 4.2), characterized by multimodal distribution of sediment fractions. The modelled current magnitudes vary across sites, with the weakest currents not exceeding 0.3 m/s at SS *Chirripo*, reaching 0.4 m/s for SS *Polwell* and FV *St. Michan,* and exceeding 0.5 m/s for SS *Tiberia* (Table 4.2).

At the SS *Chirripo* site*,* distinctive thin (10-15 m wide), typically 0.2-0.4 m high elongate depositional signatures extend symmetrically up to 700 m from the shipwreck (Fig. 4.4a). A slight offset between the directions of these features and the modelled current directions is noted. A group of pockmark-like holes are imaged W, NW and N of the shipwreck (Fig. 4.4a). They are circular, with approximate radii of 15 m and depths of 0.4 to 1 m. Granulometric analysis of the sediment samples indicates gravelly muddy sand on the depositional wreck marks, while gravel becomes more dominant away from these. No distinct scour zone is recorded at this site.

SS *Tiberia*, located 2.4 km NE of SS *Chirripo*, exhibits an intricate pattern of nearly symmetrical depositional and erosional signatures, aligned with the modelled currents (Fig. 4.4b) and reaching up to 500 m from the shipwreck (in NW direction). Two scour pits with maximum depths of 4.27 m are formed in immediate proximity to the wreck, extending from the bow and stern. The depositional ridges and erosional troughs extend far from the wreck (Fig. 4.4b), with variable lengths and widths. Sediment samples show muddy sandy gravel inside the scour pits and slightly gravelly muddy sand on the depositional signatures, while the seabed outside of the wreck marks

comprises muddy sand (Table 4.2). In terms of sediment volumes, the erosional and depositional zones are of similar magnitude (Table 4.2).
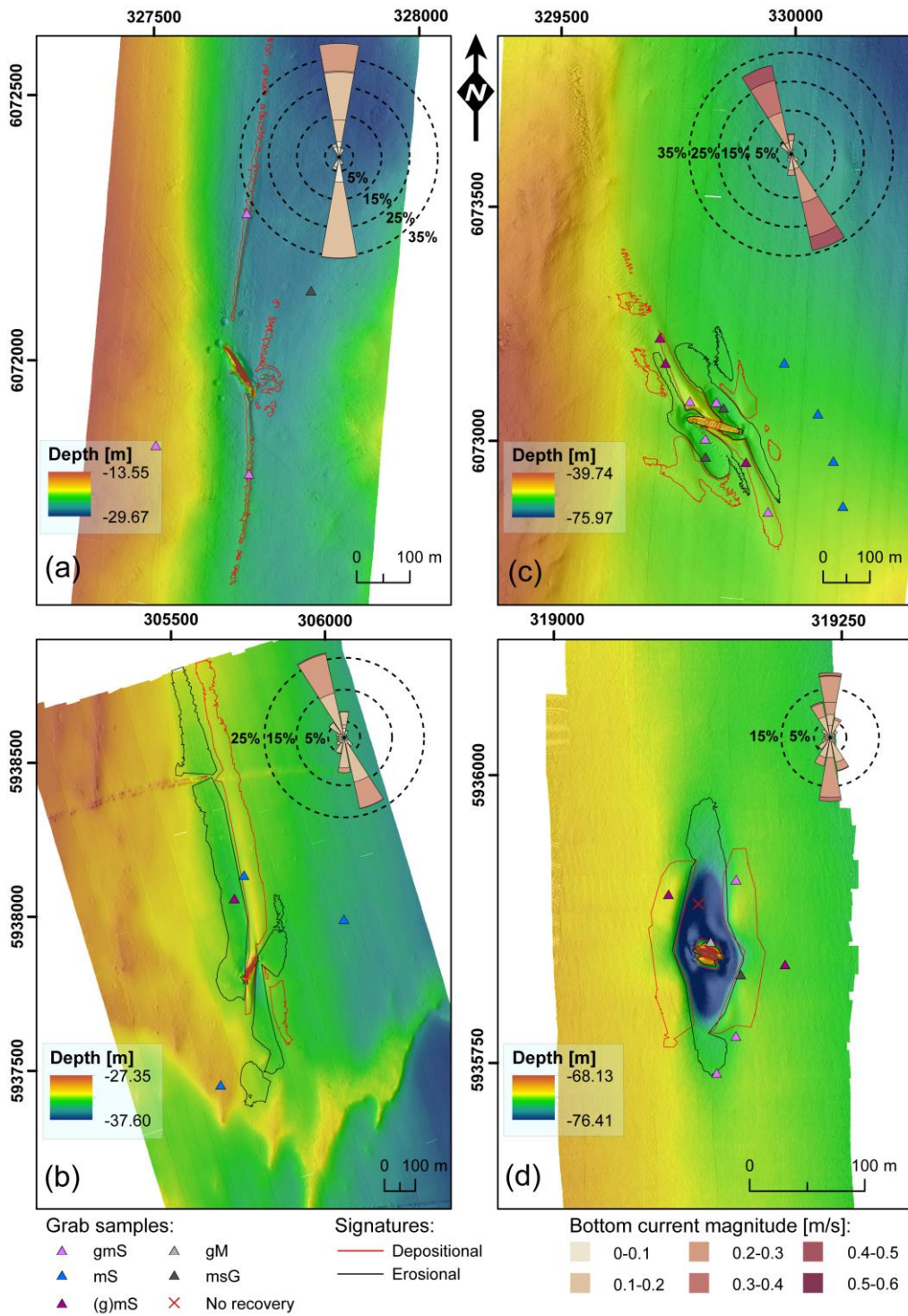
Figure 4.4. Multimodal sites presented as digital elevation models with a multidirectional hillshade occlusion: (a) SS *Chirripo*,(b) SS *Tiberia*, (c) SS *Polwell*,(d) FV *St. Michan*. Rose charts represent the modeled near-seabed current data. Grab samples: gM, gravelly mud; gmS, gravelly muddy sand; (g)mS, slightly gravelly muddy sand; mS, muddy sand; msG, muddy sandy gravel.

The longest flow-aligned depositional and erosional signatures are developed at the SS *Polwell* site, where ridges extend for 1190 m and scour features for 1290 m respectively, parallel to modelled NNW orientated peak tidal flow (Fig. 4.4c). The wreck marks, less developed in the SSE direction, are also up to 100 m wide, with the deepest depression and the highest elevation in relation to the ambient seabed being 1.48 m and 1.00 m respectively. Gravelly muddy sand is recorded in the erosional signature stretching to the NNW, while the rest of the samples indicate muddy sand (Fig. 4.4c). At this site, the volume of eroded material calculated from the relief modelling is slightly higher than for the deposited material (Table 4.2).

FV *St. Michan* rests on the boundary of the Western Irish Sea Mud Belt, an area that typically experiences lower bed stresses than the surrounding sand-dominated areas (Belderson 1964; Coughlan *et al.* 2020). Nevertheless, a deep scour pit has developed around the shipwreck with a maximum depth of 4.34 m (Fig. 4.4d). The shipwreck, which is much smaller in comparison to the other investigated vessels (Table 4.2) is elevated above the pit on a sediment mound (Fig. 4.4d). Some material has been redeposited around the pit and is therefore reflected in the calculated depositional volume (Table 4.2). Sediment samples were highly multimodal. Muddy sandy gravel is recorded close to the boundary of the scour pit. Attempted sampling was unsuccessful inside the pit, indicating a coarse sediment. Gravelly mud is recorded in the depositional mound proximal to the shipwreck and slightly gravelly and gravelly muddy sands are present in the depositional signatures outside the scour pit and in the surrounding seabed (Fig. 4.4d).

4.3.1.3.   Gravel-dominated sites

SS *Lugano* and SS *Santa Maria* are located on coarser substrates compared to the other sites, which is reflective of a much stronger tidal regime, with peak modelled flows of 1 m/s (Table 4.2). SS *Lugano* is situated on a sandy gravel and gravel bed, with a small depositional zone near the bow and lacking any erosional signature. A narrow (around 10 m wide) low-profile (0.1-0.2 m) depositional braid extends 120 m SSE from the shipwreck, probably comprising finer sediment (Fig. 4.5a). In contrast, at the SS *Santa Maria* site located 9.6 km SE of SS *Lugano*, significant flow-aligned erosional signatures (Table 4.2) with depths exceeding 5 m extend up to 140 m from the broken bow of SS *Santa Maria* (Fig. 4.5b). At this site, no clear depositional zone is imaged.
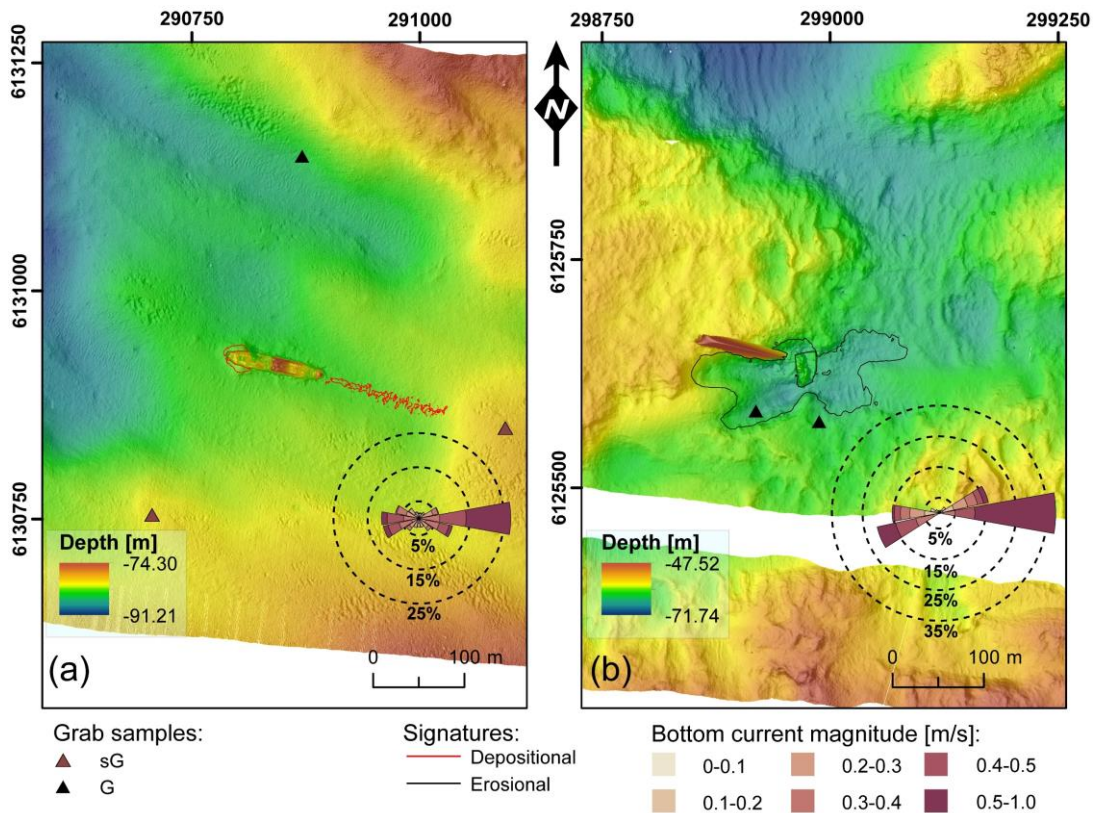
Figure 4.5. Gravel-dominated sites presented as digital elevation models with a multidirectional hillshade occlusion: (a) SS *Lugano*, (b) SS *Santa Maria*. Rose charts represent the modeled near-seabed current data. Grab samples: G, gravel; sG, sandy gravel.

4.3.2. Sediment mobility

4.3.2.1.   Current-induced sediment mobility

Bed shear stresses modelled from current values for each wreck site were compared against granulometric data from sediment samples to calculate how often sediment mobilization thresholds were exceeded as a measure of how dynamic these sites are. Sand-dominated wreck sites generally exhibit high levels of sediment threshold exceedance values, with averages of 43.9%, 52.7% and 56.1% for the RMS *Leinster*, SS *Hare* and SS *WM Barkley* respectively (Table 4.2). Sediment threshold exceedance values for the multimodal sites exhibit the broadest range, most likely due to the geographic and regional differences between these sites. However, despite their relative proximity, the exceedance levels calculated for samples from the SS *Chirripo* site (2.3%) were significantly lower than those for the samples from SS *Tiberia* (50.5%). Exceedance levels for sample data at the SS *Polwell* are relatively low at 17.2%. Wrecks in gravel-dominated settings exhibit low exceedance values, 4.9% for the SS *Lugano* site and limited exceedance of 19% at the SS *Santa Maria* site (Table 4.2). When the fourfold shear stress amplification factor established by Smyth and Quinn (2014) is applied to these sites, exceedance levels were exceeded at least 50% of the time for all sites. Greatest exceedances are modelled for the SS *WM Barkley* and HMS *Vanguard* sites, 87.6% and 91.2% of the time respectively.

4.3.2.2.   Wave influence

Analysis of the M2 wave buoy (Fig. 4.1b) data shows the calculated 99th percentile of significant wave height distribution is 3.5 m (18 years return period). According to equation (1), only wreck sites shallower than 35 m are directly affected by storms in the study area. The SS *Chirripo,* RMS *Leinster* and SS *Polwell* sites meet this criterion, but they are all located closer to the western shore of the Irish Sea than the M2 buoy and hence are assumed to be partly sheltered, with a very limited wave influence. During a storm event that disrupted the 2019 survey significant wave height did not exceed 3 m, hence none of the sites surveyed in the period were directly influenced by waves.

4.3.3. Time-lapse analysis

Results of the time-lapse analysis are divided into multiannual (9, 5 and 4 years), annual and weekly change. Table 4.3 contains measured maximum scour depths and their time-lapse changes, which are mostly within the detection threshold (30 cm) and are therefore deemed insignificant. SS *WM Barkley* is the exception*,* where the scour pit underwent significant (>30 cm) changes with respect to its maximum depth, however the net change (2010-2019) is only 33 cm (Table 4.3). Results of the time-lapse volumetric change calculations for shipwrecks on sandy beds are listed in Table 4.4. Analysis for the multimodal sites does not indicate any significant volumetric changes outside detection thresholds and no time-lapse data are available for the gravel-dominated substrate sites.

4.3.3.1.   Multi-annual change

Multiannual difference models were created using 2010, 2015 and 2019 DEMs. Sites with major and minor changes are shown in Fig. 4.6 and Fig. 4.7, respectively.

In general, the biggest changes occurred at the sand-dominated sites (Fig. 4.6, Table 4.4). At the SS *Hare* and SS *WM Barkley* sites, significant changes occurred outside and inside the dominant depositional and erosional signatures in all of the multiannual time steps. Changes at the SS *WM Barkley* site are the largest, with a maximum depth of erosion recorded at -4.9 m over a 4-year period (Fig. 4.6b) and maximum deposition of +3.3 m for the preceding 5-year period (Fig. 4.6a). These changes occurred in the immediate vicinity of the shipwreck, causing partial burial of its portside and partial exposure of the starboard side. A scour pit extending from the detached bow (NE part) was infilled with sediment between 2010 and 2015 (Fig. 4.6a) and eroded again to the initial condition between 2015 and 2019 (Fig. 4.6b). During the 9-year period, the seafloor immediately SE of the wreck structure eroded, and material was deposited further downstream (Fig. 4.6c), resulting in a build-up of a sand mound. In terms of volumetric changes, the overall net sediment budgets calculated for the SS *WM Barkley* and SS *Hare* wreck sites in the 100 m circular buffer are negative (Table 4.4). At SS *Hare,* major geomorphic changes occurred between

2010 and 2015 (Fig. 4.6d), but less-extensive change was recorded in the subsequent 4 years (Fig. 4.6e). This is also shown in the 9-year time-lapse (Fig. 4.6f), which mostly encompasses the
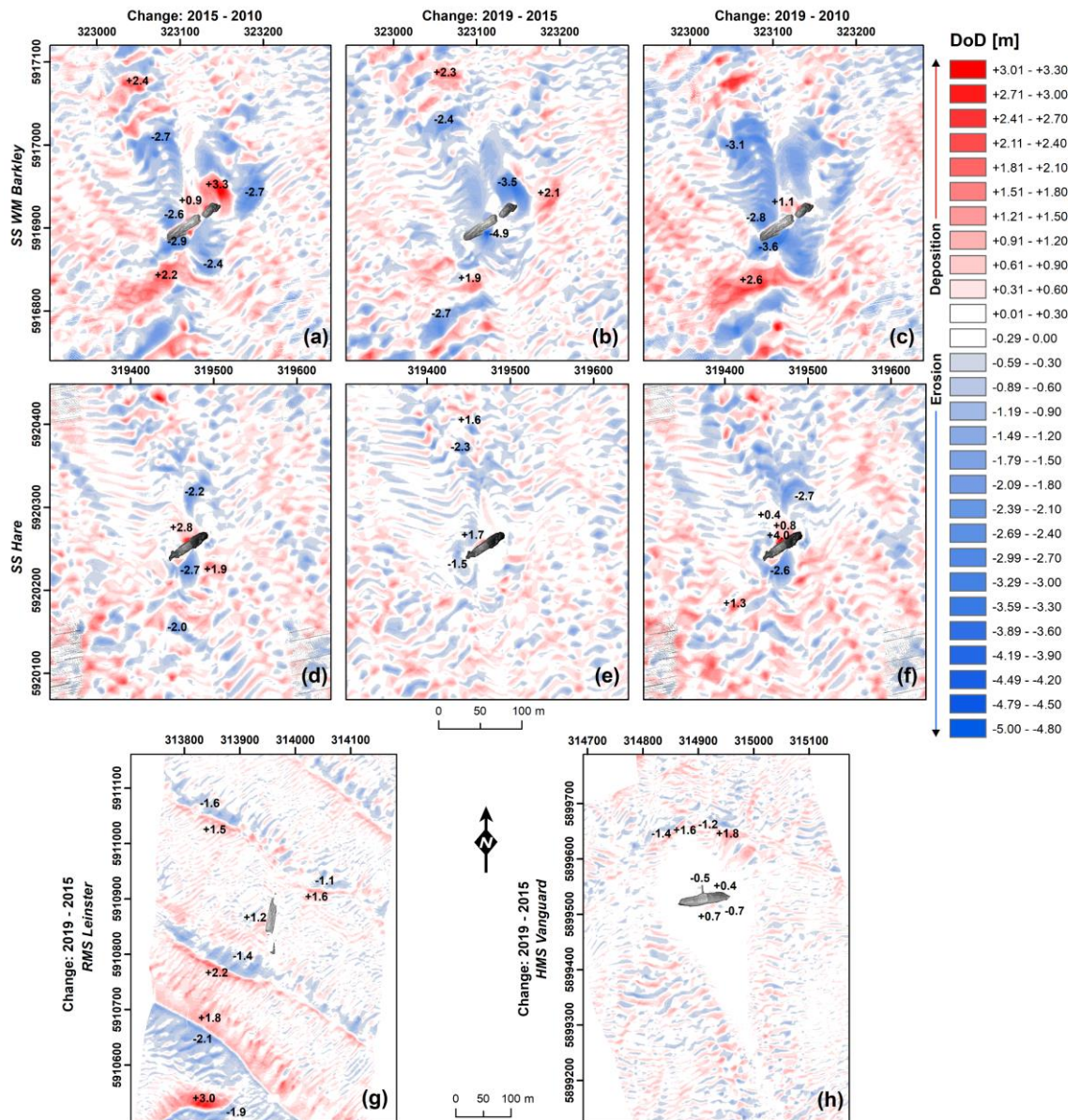
Figure 4.6. Multiannual digital elevation models of difference with major geomorphic changes for SS *WM Barkley* (a) 2015–2010, (b) 2019–2015, (c) 2019–2010; SS *Hare* (d) 2015–2010, (e) 2019–2015, (f) 2019–2010; RMS *Leinster* (g) 2019–2015; HMS *Vanguard* (h) 2019–2015. Pixels within the detection threshold (±30 cm) are in white.

changes which happened during its first 5 years (between 2010 and 2015). A very sharp increase is noted in volumetric change for the SS *Hare* site between the 200 m and 300 m buffers for the 2015-2019 time-step, which can be attributed to the build-up of a large sediment wave located north of the wreck (Table 4.4, Fig. 4.2b).

No significant change was detected in the immediate vicinity of the wreck for the RMS *Leinster* site (Fig. 4.6g). However, notable changes are present in the large sediment waves around the site

(Fig. 4.6g), emphasized by large volumetric changes for buffers exceeding 100 m radius (Table 4.4).

The 2019-2015 time-lapse analysis at the HMS *Vanguard* site (Fig. 4.6h) shows substantial changes associated with sediment wave migration largely outside the dominant comet-shaped scour pit, which remained relatively stable with its outline clearly visible in the DoD (Fig. 4.6h). In Table 4.4, this notable difference between processes inside and outside the scour pit is indicated by a significant increase in erosion/deposition values in a 200 m circular buffer around the wreck compared to a 100 m radius buffer.

Time-lapse analysis over a four-year period for the multimodal sites (SS *Polwell* and FV *St. Michan*) displayed little geomorphic change (Fig. 4.7). Almost all recorded changes at these sites are within the difference modelling's detection threshold, manifested as multiple striping artefacts in the DoDs (Fig. 4.7). Localized areas of ±0.3 m change are detected in the proximity of SS *Polwell* (Fig. 4.7a). FV *St. Michan*'s erosional signatures exhibit a negative change reaching up to -0.3 m and a slight, localized elevation (+0.2 m) of the seabed south of the shipwreck. Retaining some pixels within the detection threshold highlights trawl marks running across the site, including one trawl mark directly intersecting the shipwreck (Fig. 4.7b). As their linear appearance somewhat resembles striping artefacts normally occurring within the same DoD threshold, an additional examination of a multidirectional hillshade surface of the 2019 survey's DEM was performed (Majcher *et al.* 2020). The trawl marks are clearly manifested in the resultant hillshade raster (Fig. 4.7c). Further evidence that these linear features are trawl marks (and not survey artefacts) is their orientation relative to the N-S orientation of the survey lines.
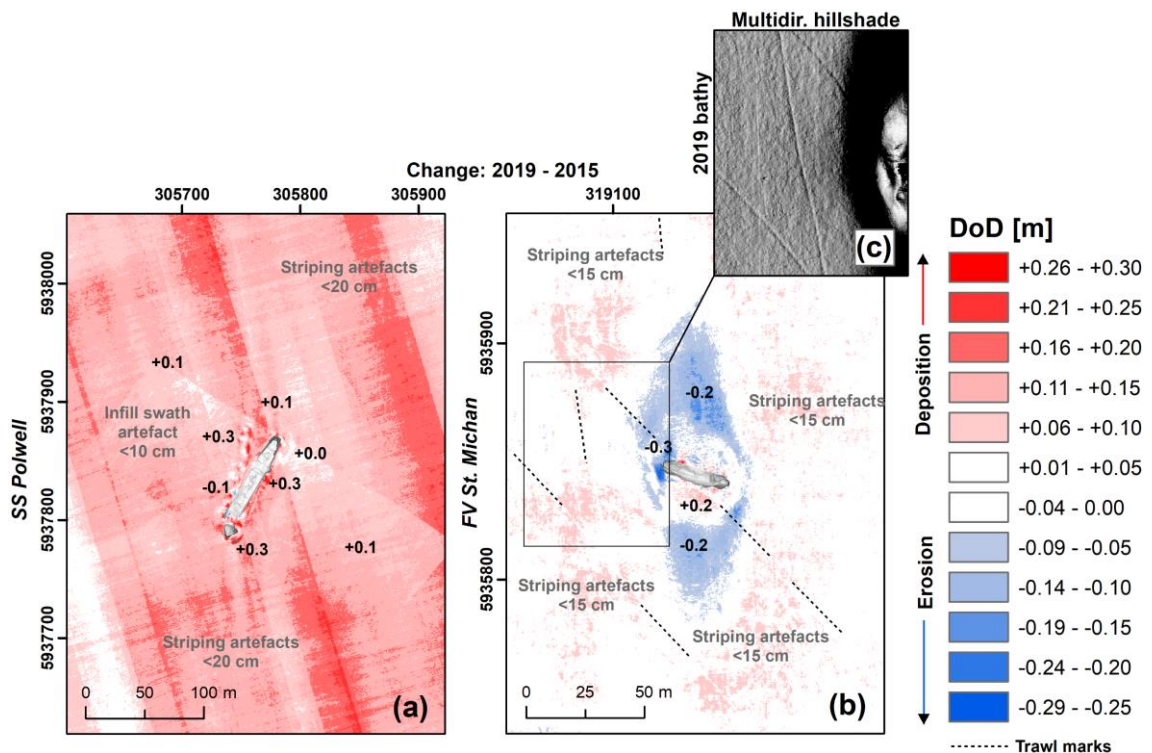
Figure 4.7. Multiannual digital elevation models (DEMs) of difference with minor geomorphic changes for (a) SS Polwell, 2019–2015, (b) FV St. Michan, 2019–2015, and (c) inset map showing a multidirectional hillshade raster created using the 2019 DEM with FV St. Michan. Pixels within the detection threshold (±30 cm) were retained to avoid information loss.

4.3.3.2.   Annual change

Annual DoDs were investigated with the 2015 and 2016 DEMs. Sites with major and minor changes are shown in Fig. 4.8 and Fig. 4.9, respectively.
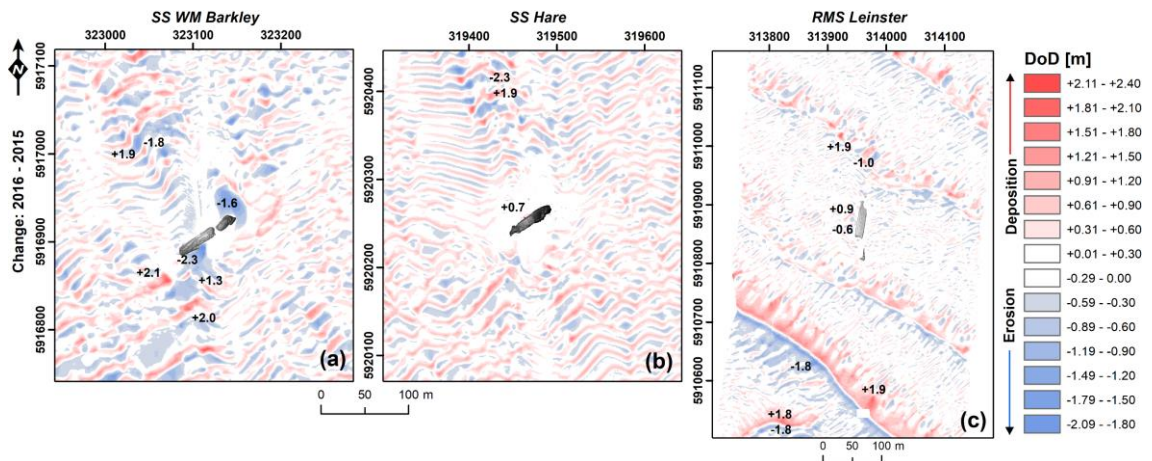
Figure 4.8. Annual digital elevation models of difference (2016–2015) with major geomorphic changes for (a) SS *WM Barkley*, (b) SS *Hare*, and (c) RMS *Leinster*. Pixels within the detection threshold (±30 cm) are in white.

Similar to the multiannual time-steps, the most substantial changes happened at the sand-dominated sites in terms of annual change (Fig. 4.8). The scour pit extending from SS *WM Barkley*'s detached bow is eroded further in this time-step (Fig. 4.8a), a process also manifested in the scour feature SW of the shipwreck. Data acquired over SS *WM Barkley* for this time-step allowed for wider areal perimeters for volumetric calculations (Table 4.4), which show a substantial increase in the volumes of displaced materials with buffers exceeding 200 m radii, especially considering deposition. A similar situation is recorded at the SS *Hare* site. This sharp increase in volumetric changes may be related to changes in the large sediment waves present north of the sites. Migration of the smaller sediment waves is visible across all the sites, although there are differences in magnitudes in the associated changes. Sediment wave migration inside SS *Hare*'s pit is minimal near the wreck and magnified farther from it (Fig. 4.8b), with the farther changes manifested by increasing volumetric changes with increased buffer sizes (Table 4.4). Time-lapse analysis of the zone near the shipwreck does not record significant changes, with the exception of a small depositional zone (reaching +0.7 m) developed in its immediate vicinity. Sediment movement is observed everywhere around RMS *Leinster*, with changes also recorded in the large sediment waves south and north of it. Volumetric changes at the site show a similar

pattern to its multiannual change, increasing significantly with buffers in excess of 100 m radius (Table 4.4).

All the annual changes recorded in the DoDs at the multimodal sites are within detection thresholds and are therefore deemed insignificant. The 2015-2016 difference model (Fig. 4.9a) for the SS *Chirripo* site shows virtually no change, with the positive/negative striping attributed to survey artefacts. Some areas of minor change are noted at the SS *Tiberia* shipwreck site (Fig. 4.9b), with similar localized change observed at the SS *Polwell* site for the same time-step. Although low-profile (±0.2m) sediment wave migration is modelled far from the SS *Tiberia* site (Fig. 4.9c), it is impossible to attribute this change directly to the presence of the shipwreck (Fig. 4.9c).
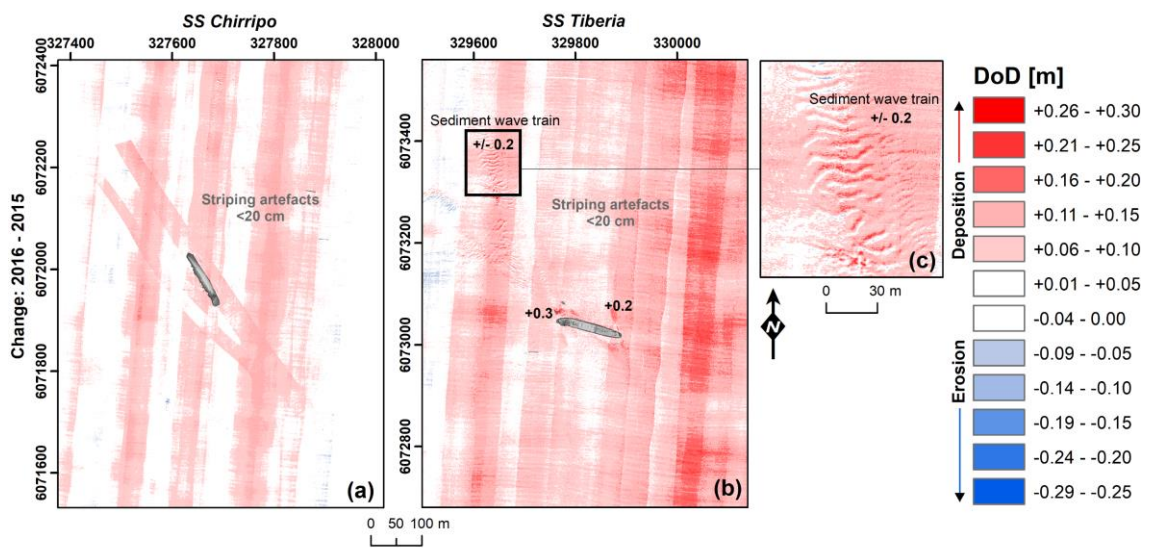
Figure 4.9. Annual digital elevation models of difference (2016–2015) with minor geomorphic changes for (a) SS *Chirripo*, (b) SS *Tiberia*, and (c) inset map showing a sediment wave train in SS *Tiberia*'s far field. Pixels within the detection threshold (±30 cm) were retained to avoid information loss.

4.3.3.3. Weekly change

Difference models for a one-week period before and after a spring tide and a coincident storm event at the SS *Polwell* site show no change. Difference models for the same period/event at the SS *WM Barkley and* SS *Hare* sites (Fig. 4.10) show migrating sediment wave trains around both shipwrecks. Sediment wave migration is amplified NNE and SSW of the shipwrecks, up to 200 m from the structures. Amplified change is also visible near the SE sides of the shipwrecks, reaching ±0.3 m in the case of SS *WM Barkley* and ±0.5 m for SS *Hare.* Survey artefacts are not aligned with the changes in the sediment waves, indicating the observations of migration are reliable, despite being largely within the detection thresholds. Volumetric changes for this time-step increase slightly with increasing buffer size (Table 4.4), due to the increasing number of sediment wave changes incorporated in consecutive perimeter radii.
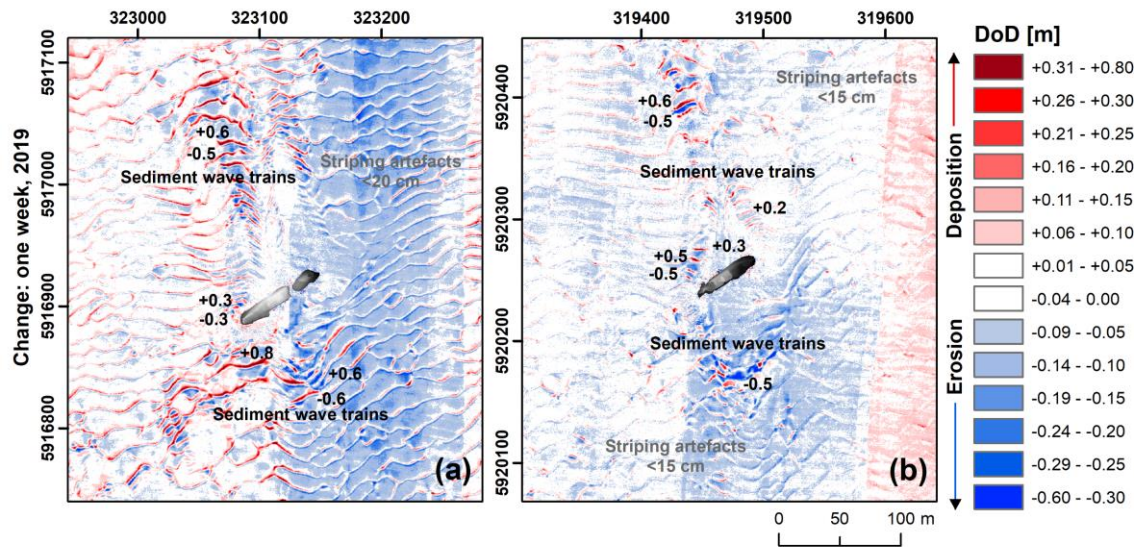
Figure 4.10. Weekly digital elevation models of difference (2019) for (a) SS *WM Barkley* and (b) SS *Hare*. Pixels within the detection threshold (30 cm) were retained to avoid information loss.

Table 4.3. Maximum depths and annual changes of bed erosion (relative to a preceding time-step) due to scour at the sites.

Category	Shipwreck	Year	Max. scour depth [m]	Change [m]
Sand	RMS *Leinster*	2015	-3.00	-
		2016	-2.99	+0.01
		2019	-3.00	-
	HMS *Vanguard*	2015	-11.69	-
		2019	-11.63	+0.06
	SS *Hare*	2010	-11.38	-
		2015	-11.32	+0.06
		2016	-11.13	+0.19
		2019	-11.15	-0.02
	SS *WM Barkley*	2010	-13.64	-
		2015	-12.96	+0.68
		2016	-13.50	-0.54
		2019	-13.97	-0.47
Multimodal	SS *Chirripo*	2015	No erosion recorded	-
		2016	No erosion recorded	-
	SS *Tiberia*	2015	-4.27	-
		2016	-4.18	+0.09
	SS *Polwell*	2015	-1.48	-
		2016	-1.52	-0.04
		2019	-1.54	-0.02
	FV *St. Michan*	2015	-4.34	-
		2019	-4.47	-0.13
Gravel	SS *Lugano*	2016	No erosion recorded	-
	SS *Santa Maria*	2016	-5.23	-

Table 4.4. Volumetric changes for different time steps, expressed in cubic meters within the 50- to 500-m radii buffer zones around the shipwrecks.

Wreck	Radius	1 week: 2019b-2019a			1 year: 2016-2015			4 years: 2019-2015			5 years: 2015-2010			9 years: 2019-2010		
		Erosion	Deposition	Net change	Erosion	Deposition	Net change	Erosion	Deposition	Net change	Erosion	Deposition	Net change	Erosion	Deposition	Net change
HMS Vanguard	50 m							-11.23	22.69	11.46						
	100 m							-47.09	174.12	127.03						
	200 m							-2575.28	4796.06	2220.78						
	300 m															
	400 m															
	500 m															
SS Hare	50 m	-0.23	0.49	0.26	-30.82	133.48	102.65	-505.20	221.82	-283.37	-1062.54	840.93	-221.61	-1523.81	918.72	-605.09
	100 m	-5.70	1.33	-4.37	-578.41	1764.14	1185.73	-1824.13	1375.70	-448.43	-2961.24	2818.04	-143.20	-3957.92	3463.40	-494.52
	200 m	-7.99	3.97	-4.03	-3444.22	9830.36	6386.14	-7604.72	8106.89	502.17	-9290.81	13211.29	3920.48	-10741.06	16810.23	6069.17
	300 m	-14.71	13.00	-1.71	-8088.05	24410.36	16322.31	-19561.66	20546.29	984.63						
	400 m				-10882.67	41934.36	31051.69	-28698.65	46692.15	17993.49						
	500 m				-13944.45	64839.67	50895.22	-43783.27	69741.71	25958.44						
SS WM Barkley	50 m	-0.68	0.47	-0.21	-935.32	81.39	-853.93	-3028.32	2.23	-3026.09	-2460.34	1330.30	-1130.04	-5042.73	185.70	-4857.02
	100 m	-2.63	12.10	9.48	-2234.40	1613.39	-621.00	-6699.85	2896.88	-3802.97	-7874.49	5242.73	-2631.76	-11866.02	4428.96	-7437.05
	200 m	-5.36	29.93	24.57	-7702.36	7984.55	282.19	-15797.30	10787.68	-5009.62						
	300 m				-16765.82	20671.64	3905.81									
	400 m				-27266.39	40097.33	12830.94									
	500 m															
RMS Leinster	50 m				-60.87	108.51	47.65	-95.84	301.77	205.93						
	100 m				-382.24	674.90	292.66	-784.22	1387.56	603.34						
	200 m				-2133.71	5006.53	2872.82	-4485.24	9396.18	4910.94						
	300 m															
	400 m															
	500 m															

4.4. Discussion

In this study, we aimed to expand our knowledge of shipwreck site formation processes, focusing on sediment budgets and hydrodynamic conditions. To accomplish this, we investigated the spatial and temporal scales of geomorphic change at metal-hulled historic shipwrecks in a tidally dominated environment. The sites, characterized by a mosaic of seabed substrates and varying tidal currents, are all more than 100 years old, thereby their protection is endorsed by UNESCO through the Convention on the Protection of Underwater Cultural Heritage (UNESCO 2002).

4.4.1. Variability of geomorphic change at sites in different seabed environments

At all wreck sites where erosional and depositional signatures were identified, a strong correlation between their directionality and the prevalent current direction is noted, suggesting that current-induced bed stress is the dominant control on scour processes. Geomorphic change verified by difference modelling primarily takes place either inside the scour signatures or is associated with the tidally controlled migration of sediment waves. Even during storm conditions, the influence of wave action on the sites is shown to be insignificant. However, in order to fully determine the influence of storm events, deployment of monitoring equipment at the sites would be necessary.

4.4.1.1.   Sand-dominated sites

Wreck sites located in sand-dominated settings are highly dynamic, with significant changes in seabed morphology recorded on a weekly, annual and interannual basis. Geomorphic change at sand-dominated sites includes the dynamic evolution of the scour pits and significant migration of sediment waves across individual wreck sites. Sediment wave trains provide a constant sediment supply, causing continued reorganization of both depositional and erosional signatures. Sediment is subsequently carried away from the sites with migrating sediment waves, which are magnified downstream of the shipwrecks. The sediment budget therefore fluctuates, which is reflected in the volumetric changes representing erosion and deposition at and around the sites.

Sand-dominated sites exhibit the highest, and most consistent levels of bed stress values exceeding sediment thresholds, enabling mobilization (Table 4.2). The stratigraphy at these sites is often complex, with Quaternary sediments overlain by migrating bedforms and sand sheets controlled by contemporary hydrodynamic processes. Sediment waves in this part of the Irish Sea are typically formed in an upper mobile layer that comprises reworked glacial and post-glacial sediments. Beneath this mobile layer lies a coarse gravel lag of glacial origin, either the Chaotic Facies or the Upper Till members described by Jackson *et al.* (1995). These Late-Pleistocene layers are more resistant to scour due to their coarse composition and/or over-consolidated nature (Coughlan *et al.* 2020). This is demonstrated at the HMS *Vanguard* site, where significant

geomorphic change is recorded (Fig. 4.6h), but further vertical erosion of the scour pit is limited by the presence of the underlying glacial deposits (Fig. 4.3). Given the similarities in regional geology, it is therefore possible that similar limiting layers occur at the RMS *Leinster*, SS *Hare* and SS *WM Barkley* sites. Seismic data collected at these sites is not of sufficient penetration to confirm this. Barriers limiting vertical geomorphic change at shipwrecks have previously been postulated, for example at the HMS *Scylla* site (investigated by Astley 2016) or *Queen Anne's Revenge* (McNinch *et al.* 2006). Here we demonstrate that such limits can be detected by shallow-seismic profiling, enabling accurate predictions of future scour progression at underwater sites. This technique therefore provides important information for site management, allowing for more accurate underwater site formation models.

In another possible scenario for the sand-dominated sites, a limit to further vertical erosion may appear when the scour pits develop to the level at which a shipwreck will be lowered below the ambient seabed, and cease to perturb the flow of tidal (McNinch *et al.* 2006; Trembanis *et al.* 2007). In this way, a low-lying shipwreck structure halts ongoing scour processes, so it becomes gradually buried under sediments supplied with the migrating bedforms or during quiescent periods (McNinch *et al.* 2006). However, the 2019 survey data indicate that all the investigated shipwrecks with deep scour pits still present significant obstructions to the tidal currents (Table 4.2) and do not appear to be sinking within the depressions. Hence this scenario has a low probability, unless the shipwrecks experience dramatic structural changes which would lower their height above the seabed (Astley 2016).

Notably, the maximum scour depths do not change significantly at any of the wreck sites investigated. The largest change in the total scour depth occurred at the SS *WM Barkley* site between the years 2010 and 2015, when one of the pits was infilled with sediment; however, the same pit was eroded again in the subsequent years (Table 4.3).

4.4.1.2.   Multimodal sites

Wrecks located in multimodal sedimentary settings are exposed to bidirectional tidal currents of similar magnitudes and exhibit an equally diverse range of geomorphic features as those located in sandy sediments. However, the multimodal sites display little or no volumetric or geomorphic change over time. This finding is important for future site predictions and reflects the advice from Ward *et al.* (1999), that although the sediment budget and hydrodynamic environment of a site are inextricably connected, they need to be examined collectively and independently to fully understand site formation processes. Although the presence of high magnitude currents at these sites increases the potential for bedform migration, it only occurs where substrates are prone to mobility. At the multimodal sites, bedform migration is very limited, hence the seabed around the shipwrecks is nearly stable, without significant loss or gain in sediment budgets.

Localized areas of low magnitude change not exceeding 30 cm at SS *Polwell* (Fig. 4.7a) *and* SS *Tiberia* (Fig. 4.9b) are attributed to fluctuating, turbulent components of flow around the shipwrecks, which locally magnify current-related shear stresses exerted on the seabed by introducing lee-wake vortices and vortex shedding (Quinn 2006; Smyth and Quinn 2014). The same mechanism was cited by Astley (2016) to explain localized, internal changes at the SS *Richard Montgomery* site.

At the SS *Chirripo site*, pockmark-like features are observed around the shipwreck. Their origin remains unknown, although they could be traces of salvage operations conducted at the site in the past. Another possibility is that the impact of the shipwreck on the seabed exerted excessive pressure on the sediments, causing gas emission from the interstitials, creating the pockmarks. This formation mechanism had been hypothesized by Geraga *et al.* (2020) for similar morphological features at wreck sites in the Ionian Sea.

The seabed around SS *Chirripo* is also characterized by elongate depositional ridges, with no significant erosional features (Fig. 4.4a). Despite its relative proximity (located 2.4 km to the north east), the SS *Tiberia* site (Fig. 4.4b) is characterized by more complex intricate patterns of erosional and depositional signatures. Differences in scour patterns at the two proximal sites are attributed to higher peak current values and subsequent higher levels of sediment threshold exceedance for mobilization at the SS *Tiberia* site. This influence is also reflected in the migration of low-profile sediment waves nearby the site (Fig. 4.9c). Additionally, SS *Chirripo* is orientated oblique (nearly parallel) to the dominant currents, hence perturbing flow to a far lesser extent than SS *Tiberia*, whose full length is oriented nearly perpendicular to peak flow (Quinn and Smyth 2018).

Local geological control on scour signature propagation is also observed at the multimodal SS *Polwell* site. Although extensive scour is recorded to the north of the wreck, scouring to the south of the structure is limited (Fig. 4.4c), despite a strong bidirectional current flow. A distinctive ridge feature located to the south acts as a horizontal (or spatial) impediment to scour propagation. Given its morphology and the regional geology, this ridge is likely to be a surface or near-surface expression of the Chaotic Facies or Upper Till member.

Difference modelling for the FV *St. Michan* site shows that the low-magnitude change is confined almost entirely to the scour pit (Fig. 4.7b), suggesting that the flows magnified by the shipwreck are still eroding the seafloor. Analysis of grab samples collected at the site indicate highly multimodal sediments, as the shipwreck rests on the rim of the Western Irish Sea Mud Belt. The sediments in this area, the Mud Facies of Jackson *et al.* (1995), are typically under-consolidated with low shear strength values and are prone to scour (Callaway *et al.* 2009; Coughlan *et al.* 2019). Furthermore, mobilization and removal of fine-grained sediments in this area of the Irish

Sea has been shown to be exacerbated by commercial trawling activity, which is clearly evidenced at the *St. Michan* site in Fig. 4.7c (Coughlan *et al.* 2015).

4.4.1.3.   Gravel-dominated sites

Although no time-lapse data of sufficient resolution are available for the gravel-dominated sites, MBES coverage and sediment samples, coupled with modelled near-seabed current information, allow for some observations. For example, at the SS *Santa Maria* site located off the north coast of Ireland, a significant volume of material has been eroded from around the bow of the wreck (Fig. 4.5b, Table 4.2), and it is the only site where no deposition of sediment is recorded. The complex bathymetry of the site makes it difficult to differentiate shipwreck-related geomorphological features from those developed naturally, even after applying a residual relief modelling approach to site characterisation (Majcher *et al.* 2020). In contrast, high-resolution MBES data from the nearby SS *Lugano* site displays no erosion, despite predictions from amplified shear stress calculations. This is attributed to the shipwreck's more streamlined orientation with respect to the dominant flow, analogous to the SS *Chirripo* case described above. The geometry of the depositional signatures recorded at the *Lugano* site matches the computational fluid dynamics-derived predictions of Quinn and Smyth (2018) for shipwrecks oriented parallel to peak flow.

4.4.2. Discrepancies between modelled and observed data

Discrepancies are noted between the predictions of the sediment transport models and direct, time-lapse observations at some of the wreck sites in the study. No significant geomorphic change is recorded at the multimodal sites, even though the sediment mobility thresholds are frequently exceeded (Table 4.2). These differences may be explained by the oversimplified nature of some sediment transport models which do not account for multimodality of sediments, leading to a substantial influence on calculating the critical shear stresses required to mobilize sediment. For example, at the SS *Polwell* site, a mud-sand-gravel mixture is observed inside the erosional signature. According to McCarron *et al.* (2019), the critical shear stress needed to mobilize sand-gravel sediments may be decreased by 64% and increased by 75% for gravel and sand respectively, when a hiding and exposure effect resulting from bimodality is introduced. Hence, it is possible that this effect resulted in finer sediments being removed from multimodal substrates at the SS *Tiberia,* FV *St. Michan* and SS *Polwell* sites, leaving behind a coarser lag which is resistant to scour. The calculated volumes of erosion and deposition at these sites are similar (Table 4.2), suggesting that the eroded material may have been redeposited further downstream from the shipwrecks. It is therefore proposed that no time-lapse change observed at the sites where the obstacle-amplified shear-stresses exceed mobility thresholds, can be also attributed to the effects caused by the multimodality of sediments.

4.4.3. Equilibrium states of shipwrecks and their implications for *in-situ* preservation

It is clear that sand-dominated sites are highly dynamic compared to the gravel-dominated and multimodal sites (Fig. 4.11a). This dynamism is manifested in all aspects of the sites' analyses, from the initial volumes calculated for the erosional and depositional signatures, through volumetric changes and changes detected in the DEMs of difference. The continual migration of sediment waves through the SS *WM Barkley,* SS *Hare* and RMS *Leinster* sites triggers a frequent reorganisation of material around the shipwrecks, which in turn causes them to shift from one equilibrium state to another. Such shifts may possibly be triggered on a weekly basis during spring tides, as significant wave migration is recorded even in the shortest time-step. These wrecks are not only affected by the constant external supply of sediment, but also by active scour processes, expressed by the negative net sediment budget in their 100 m circular buffers for multiannual surveys (Table 4.4). Similar to the *Burgzand Noord* shipwrecks in the North Sea described by Manders (2009) and Astley (2016), the sites in the Irish Sea undergo material loss. However, while the *Burgzand Noord* sites remain structurally unaffected by this change, the integrity of SS *Hare* and SS *WM Barkley* may be threatened longer term, as large volumes of sediments are constantly reorganised in their immediate surroundings.

The dynamism at these sites is more analogous to the HMS *Stirling Castle* wreck site, also located in the North Sea, where a constant sediment supply due to sandbank migration regularly causes significant geomorphic change, resulting in repeated burial and exposure of the shipwreck (Bates *et al.* 2011; Pascoe 2012). Significant changes (±2-3 m) on a multi-annual timescale were also noted at the more modern (World War 2) shipwreck site of SS *Richard Montgomery* (Astley 2016). The wreck is also situated on a sandy seabed (fine sand), with an external supply of sediments, and the reorganisation of the erosional/depositional signatures was observed around it (Astley 2016).

Such an open, high-energy system may have a profound impact on *in-situ* preservation of archaeological material. Tonnes of sediments are regularly eroded/deposited around the shipwrecks, acting as scrambling devices (Muckelroy 1978) and causing rapid shifts in pressures acting on their hulls. This mechanism probably affects the SS *WM Barkley* site. In the time-lapse data we collected, a build-up of sediment is initially recorded to the north of the shipwreck, partly covering its portside (years 2010-2015, Fig. 4.6a). Subsequently, substantial erosion of the site uncovered part of its starboard side (years 2015-2019, Fig. 4.6b). This erosion event also gave rise to the maximum bathymetric change (-4.9 m) recorded in any of the DEMs of difference. Such dramatic bed level change is likely to impact the structural stability of shipwrecks, resulting in mechanical damage and accelerated collapse (Quinn 2006). Therefore, such open sites, in highly dynamic equilibrium with their environment, should be a priority when it comes to

introducing *in-situ* preservation measures, planning regular monitoring or authorised emergency excavation.

An exception among the sand-dominated wrecks, is the HMS *Vanguard* site, where scouring appears to have reached its maximum depth. A non-erodible coarser sediment layer exposed in the scour pit limits the vertical scour extent and sediment wave migration occurs only outside of it. As sediment supply to the site has ended, the site appears to have reached a static equilibrium phase (Fig. 4.11a). This stability has possibly aided the remarkable preservation of the shipwreck, despite it being older than the other sites investigated. HMS *Vanguard* is nearly fully intact on the seabed in comparison to the other sand-dominated sites (Table 4.2), which are partly buried and scattered. Although the site appears stable, change may be triggered in the future by events like severe storms, anthropogenic activities or parts of the wreck itself collapsing (Fig. 4.11a). HMS *Vanguard* is still in a negative disequilibrium trend like any other underwater site and will undergo a gradual degradation due to corrosion and other formation processes, as she is almost entirely exposed to the seawater (Ward *et al.* 1999) (Fig. 4.11c).
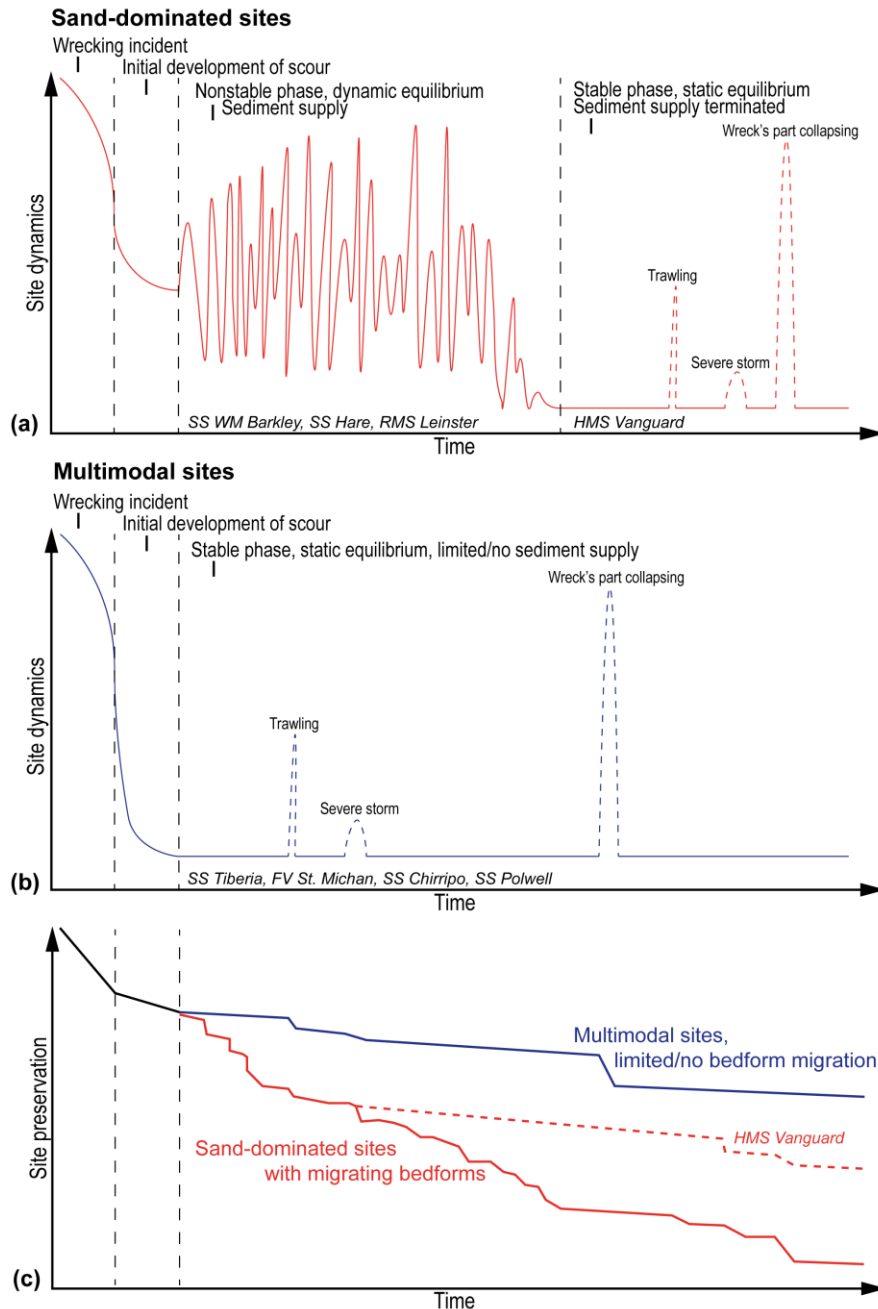
Figure 4.11. Conceptual site dynamics models for the investigated sand-dominated (a) and multimodal sites (b) with a corresponding site preservation estimation for the two categories (c). Rapid changes in the site dynamics due to continuous sediment supply and/or single events cause accelerated degradation and lower site preservation. In contrast, stable periods favor preservation, which is, however, always decreasing due to chemical and biological deterioration.

The sites dominated by multimodal sediments expressed virtually no significant geomorphic change throughout all the time-lapse periods and may therefore be described as static, closed systems, which have achieved a stable equilibrium (Fig. 4.11b). These shipwrecks are only slightly buried in the seabed, and the scour processes have settled analogous to artificial reef structures on a mixed seafloor described by Raineault *et al.* (2013). At the SS *Tiberia*, FV *St. Michan* and SS *Polwell* sites, scour processes caused the removal of fine-grained sediments,

leaving only coarser, non-erodible substrates in the pits. SS *Chirripo* must have reached the equilibrium state soon after the wrecking incident, as no scour is recorded around her. As a result, these shipwrecks are generally largely intact and have a higher preservation potential, akin to HMS *Vanguard*.

Even though no time-lapse data are available for the SS *Lugano* site, it is also assumed to be in a static equilibrium with the environment. No erosion is recorded in the DEM (Fig. 4.5a) and no sediment waves are present, thus the geomorphological context is assumed static. On the other hand, SS *Santa Maria*'s broken bow caused the advance of significant erosional signatures (Fig. 4.5b), despite resting on a coarse seabed dominated by gravel and boulders. The tidal currents at the location are among the strongest in the Irish Sea (Pérez-Ortiz *et al.* 2017), hence some geomorphic change and the associated system's instability is probable.

Nevertheless, it is important to understand that stability of underwater sites is not solely controlled by their geomorphological and hydrodynamic settings. A disruption of any equilibrium state can be triggered by external anthropologic influences like digging (Manders 2009), trawling (Brennan *et al.* 2016) or dredging operations (Quinn and Boland 2010). In this study, a direct indication that anthropogenic activity impacts the sites is evidenced by the trawl marks at FV *St. Michan*. Although, no obvious significant reorganisation of material has occurred at that site, it is possible that continuation of the trawling may damage the shipwreck, and trigger further changes as new nuclei for scour may be introduced, increasing site dynamics (Fig. 4.11b) (Quinn 2006).

In summary, we suggest that knowledge about sediment types, bathymetry and hydrodynamic processes at underwater sites can provide invaluable information for cultural resource managers. Importantly, such high quality hydrographic, oceanographic and geological data are becoming increasingly publicly available through various studies, initiatives and projects like INFOMAR in Ireland (Guinan *et al.* 2020; O'Toole *et al.* 2020). Such open-sourced datasets can be used for pilot studies, assessing preservation potential of individual sites and targeting the shipwrecks which need more detailed investigation, for example involving high-resolution time-lapse surveys.

Further research is needed in understanding vertical propagation of scour at shipwreck sites, for example using shallow-seismic profiling, which is proven to be an effective method for detecting limiting horizons. Studies of internal reorganization of scour pits and depositional signatures caused by the external supply of sediments through migrating bedforms, need to be investigated in greater detail, in order to understand how these two processes are related. Future sediment budget investigations should also include multimodality effects on sediment mobility at sites (McCarron *et al.* 2019).

Although we successfully investigated geomorphic change at shipwreck sites at weekly, annual and multi-annual time-steps, these time series should be extended at both ends, allowing the

capture of very short term (daily tidal oscillations and storms) and longer-term (10+ years) changes at sites. Additionally, we recognize the need to evaluate the direct influence of dynamic geomorphic change on the structural integrity of shipwrecks. Although such geomorphic changes are known to have detrimental effects on frequently monitored offshore engineering structures (Whitehouse *et al.* 2011; Melling 2015), the scale of potential damage to historic shipwrecks remains unclear. Filling these knowledge gaps would result in further refinements of shipwreck site formation models.

4.5. Conclusions

This work offers new knowledge about site formation processes and long-term stability of metal-hulled shipwrecks. These remain largely unresearched (Keith 2016), despite their rising archaeological value. The management of such shipwrecks is at the crossroads of diverse interests and factors, arising from cultural heritage management, environmental risks, sport diving accessibility and others (Tomalin *et al.* 2000; Firth 2018). As geomorphic change at the sites is demonstrated to have a direct link to their *in-situ* preservation, we recognize this investigation as highly pertinent to support site-management decisions. In the end, it is also applicable for informing future offshore developments and marine spatial planning, as shipwreck sites can be inversely used as proxies of local geomorphological and hydrodynamic conditions (Caston 1979; Geraga *et al.* 2020).

5. Using difference modelling and computational fluid dynamics to investigate the evolution of complex, tidally influenced shipwreck sites

5.1. Introduction

The wrecks of historic, metal-hulled ships are an integral part of the underwater landscape and new discoveries are made every year with increasingly sophisticated sensors and methodologies (Plets *et al.* 2011; McCartney 2017, 2018; Geraga *et al.* 2020; Grządziel 2020a, b; O'Toole *et al.* 2020). Many wrecks are archaeologically and historically significant, acting as time-capsules capturing contemporary technological advancements, life on-board and other information relevant for heritage science (Firth 2018; Elkin *et al.* 2020). The UNESCO Convention on the Protection of the Underwater Cultural Heritage, adopted in 2001 (UNESCO 2002) puts strong emphasis on *in-situ* preservation of underwater cultural heritage (defined as more than 100 years old). This is partly due to the vast extent of the submerged archaeological resource - currently estimated to number around 3 million wrecks worldwide (Croome 1999; UNESCO 2017) - which hinders costly active investigation and conservation measures. The occurrence of shipwrecks on the seabed also has important ocean engineering implications. Upstanding wreck structures present complex obstacles to the water flow, locally modifying its magnitude and turbulence (Quinn 2006). The seabed adjusts to these modifications and undergoes geomorphic changes, frequently forming intricate erosional and depositional signatures, referred to as scour or wreck marks (Caston 1979; Majcher *et al.* 2020). The alignment of wreck marks along the dominant local current flow makes them proxies for magnitudes and directions of local hydro-dynamic settings and net sediment transport (Caston 1979). Wrecks of metal-hulled vessels lost up to the end of World War I have resided on the seabed for more than 100 years. Therefore examining the combined fluid-sediment dynamic response at such sites provides insights into potential issues with the stability of other large and complex man-made structures after their long-term emplacement on the seabed.

Shipwrecks are often treated as impediments to offshore developments, leading to re-routing of undersea pipelines and cables and reconsideration of the placement of offshore infrastructure (Evans and Firth 2016; Majcher *et al.* 2020). Therefore, using wrecks as indicators of the locally operating hydro-dynamic and physical processes may be beneficial for ocean engineering, influencing marine spatial planners and stakeholders to recognise shipwreck sites as valuable elements of our maritime landscape. This is especially important in times of the rapid expansion of the offshore renewable energy sector and development of the seabed.

Geomorphic change at shipwreck sites is complex and depends on a range of local environmental factors and processes (Astley 2016; Quinn and Smyth 2018; Majcher *et al.* 2021). Precise hydrographic surveys using multibeam echosounders (MBES) combined with geophysical and geological sampling provides data essential to understand these variables (Bates *et al.* 2011; Plets *et al.* 2011; Westley *et al.* 2019). Such datasets are becoming increasingly available due to national and international seabed mapping programmes (EMODnet Bathymetry Consortium 2018; Guinan *et al.* 2020; O'Toole *et al.* 2020). Furthermore, validated shelf-scale oceanographic models provide another layer of information, allowing insights into hydro-dynamic triggers for geomorphic change (Shchepetkin and McWilliams 2005; King *et al.* 2019; Nagy *et al.* 2020).

However, in order to understand the rates and magnitude of geomorphic change at shipwreck sites, at least two high-resolution hydrographic surveys, separated in time, are needed; an approach commonly referred to as repeat or time-lapse bathymetric surveying (Quinn and Boland 2010; Bates *et al.* 2011; Astley 2016; Fernández-Montblanc *et al.* 2016; Couldrey *et al.* 2020; Majcher *et al.* 2021). This strategy allows a comparison of the differences in bathymetric surfaces corresponding to consecutive surveys i.e., to conduct difference modelling. To date, investigations using difference modelling have confirmed a wide spectrum of geomorphic change affecting individual underwater sites (Quinn and Boland 2010; Astley 2016; Fernández-Montblanc *et al.* 2016), even for wrecks located at similar depths within a single, tidally dominated shelf-sea (Majcher *et al.* 2021). This variability in seabed dynamism indicates further research on possible factors controlling geomorphic change at wreck sites is required.

Numerical modelling is increasingly used in conjunction with hydrographic data to investigate detailed patterns of water flow and turbulence around manmade structures and to analyse factors driving geomorphic change and site evolution. For example, Couldrey *et al.* (2020) investigated how a barchan dune migrated past an offshore wind turbine monopile foundation using multi-annual repeat MBES surveys and a coupled sediment- and hydro-dynamic model. In another example, hydro-dynamic modelling validated by *in-situ* observations and combined with repeat singlebeam bathymetric data was used to characterize sediment erosion and seasonal geomorphic changes at a scattered, partly buried and shallow, wave-dominated shipwreck site (Fernández-Montblanc *et al.* 2016). The investigation was later extended to 2D Computational Fluid Dynamic (CFD) simulations, using two different bathymetric profiles corresponding to high- (winter) and low- (summer) wave energy periods, providing insight into the effecy of seasonality on local geomorphic change (Fernández-Montblanc *et al.* 2018b). Extending these approaches to combining CFD with high-resolution MBES bathymetric data has the potential to further improve our understanding of the physical factors influencing stability of complex

underwater structures like wrecks. This in turn can extend our knowledge of physical site formation processes (Ward *et al.* 1999). Even though successful CFD simulations have been carried out for wave-dominated (Fernández-Montblanc *et al.* 2018b) and current-dominated (De Hauteclocque *et al.* 2007; Smyth and Quinn 2014; Quinn and Smyth 2018) wreck sites, none have been compared against high-resolution difference modelling from time-lapse MBES surveys.

Moreover, no comparisons of fluid dynamics and geomorphic change between individual wreck sites have been performed, either for sites located within similar or contrasting environmental settings. Finally, all CFD investigations published to date for shipwreck sites (Smyth and Quinn 2014; Fernández-Montblanc *et al.* 2018b; Quinn and Smyth 2018) focus on older, pre-industrial wooden wrecks, and scattered (Fernández-Montblanc *et al.* 2018b) or low-relief sites (Smyth and Quinn 2014). Therefore, hydro-dynamic simulations around complex, upstanding, metal-hulled wrecks presenting significant obstacles to flow are unrealised.

This knowledge gap is highly relevant and important to address considering that there are 3 million shipwrecks estimated worldwide (Croome 1999; UNESCO 2017), with a significant portion originating from World War I and II. At least 8500 of these may contain oil and are classified as potentially polluting shipwrecks (Landquist *et al.* 2013; Carter *et al.* 2021). Understanding long-term stability, seabed geomorphic change and its drivers at metal-hulled shipwreck sites may enhance decision making processes in cultural heritage and pollution risk management, supporting marine spatial planning (Papageorgiou 2018).

In this study we set out to extend the knowledge about the relations between hydro- and sediment-dynamics and the stability of complex, tidally influenced underwater structures. To do so, we analyse differences in geomorphic change and patterns of flow at two historic, metal-hulled shipwreck sites located within similar environmental contexts. The wrecks of HMS *Vanguard* and SS *W.M. Barkley* are both more than 100 years old (lost in 1875 and 1918 respectively), located in sand wave fields at depths of 40 and 52 m in the Irish Sea and with their hulls aligned oblique to tidal flows. Difference modelling of very high-resolution time-lapse bathymetric data allows us to quantify multi-annual and weekly geomorphic change at the sites and compare the registered seabed changes to the CFD simulations. CFD is used to understand patterns of flow and turbulence at the sites. A shelf-scale oceanographic model provides tidal current velocity profiles for the inlets of the CFD domains. Finally, very dense MBES-derived point clouds enable evaluation of structural damage sustained by the wrecks. This unique combination of very high-resolution repeat bathymetric and modelled oceanographic data, together with seabed sampling and CFD simulations provides new insights into formation processes of underwater wreck structures.

We believe that this study points to obvious analogies to offshore engineering and presents a new set of applications for high-resolution hydrographic and oceanographic data.

5.2. Theoretical background

Geomorphic change at shipwreck sites is largely driven by seabed scour. Scour occurs when sediment is eroded due to forcing by waves and/or currents (Whitehouse 1998). It can be initiated by a change in morphology and/or migration of bedforms (Soulsby 1997; Hay and Speller 2005; Ginsberg and Aliotta 2019) or by the intentional (e.g. seabed engineering; Whitehouse *et al.* 2011, unexploded ordnance, mines; Jenkins *et al.* 2007) or accidental (e.g. a shipwreck; Quinn 2006) introduction of an object to the seabed.

When an object is introduced to the seabed it causes changes in the ambient flow regime, resulting in some combination of the following phenomena: streamline compression and acceleration of flow; formation of vorticial structures: a horseshoe vortex enveloping the structure and lee wake vortices downstream of the structure, occasionally accompanied by vortex shedding; increased flow turbulence and velocity; sediment liquefaction enhancing material loss (Sumer *et al.* 2001; Quinn 2006). The seabed responds to this flow alteration and undergoes scour until a new equilibrium state with a maximum scour depth is reached (Soulsby 1997; Whitehouse 1998).

The horseshoe vortex is formed by the rotation of the seabed boundary layer. An adverse pressure gradient is formed by the structure, separating the flow, which consequently rolls up to form a swirling vortex wrapped around it (Sumer *et al.* 1997; Whitehouse 1998). The morphology of the horseshoe vortex can be variable, forming intricate flow patterns (like vortex shedding; Testik *et al.* 2005), especially at complex wreck structures (Quinn and Smyth 2018). The lee wake vortices are created by the rotation of the boundary layer flow over the surface of the obstacle and brought together at some distance from it due to flow convergence (Testik *et al.* 2005). Two counter-rotating vortices may also form near the downstream side of the obstacle, depending on its morphology and orientation (Testik *et al.* 2005; Quinn and Smyth 2018).

Two scour regimes are frequently distinguished in engineering (Whitehouse 1998) and also recognized in shipwreck site characterization (Astley 2016): live-bed and clear-water scour. These are defined in terms of the critical shear stress (τ_{cr}) required for incipient motion of sediments, and the bed shear stress (τ_c) exerted by the flow, both measured in Nm^{-2} or Pa in SI units. Live-bed conditions occur when τ_c exceeds τ_{cr} everywhere across the site, both inside and outside the scour signatures. On the other hand, the clear-water criterion is satisfied when τ_{cr} is exceeded only in the vicinity of the structure, where τ_c is amplified due to flow modification and not at the surrounding seabed. Both scenarios result in an equilibrium scour depth. However, while the clear-water scenario implies stability

after the initial development of scour, the live-bed condition suggests continuous seabed dynamism. This is important in terms of the stability and preservation of underwater structures, especially for fragile objects like shipwrecks, which reside on the seabed over long time periods without any maintenance (Majcher *et al.* 2021).

Adverse effects due to the scour-induced geomorphic changes are well-known for underwater structures like bridges (Sumer 2007), wind and tidal turbines (Whitehouse *et al.* 2011; Matutano *et al.* 2013; Melling 2015; Sun *et al.* 2019) and jackup rigs (Sweeney *et al.* 1988). Sediment budget changes due to scour may also compromise the stability of shipwrecks, ultimately leading to partial or complete collapse and/or cause either burial or exposure of their corrosion-prone structures to the oxygenated water-column, enabling the development of biological encrustation (Ward *et al.* 1999; Quinn 2006). Therefore, the importance of the scour phenomenon have been also recognized and extensively researched at shipwreck sites in the context of their *in-situ* preservation (McNinch *et al.* 2006; Quinn 2006; Bates *et al.* 2011; Plets *et al.* 2011; Astley 2016; Fernández-Montblanc *et al.* 2016, 2018b; Quinn and Smyth 2018; Majcher *et al.* 2020, 2021).

As upstanding, high-relief metal shipwreck structures frequently present substantial obstacles to flow, the scour signatures around them can be extensive (up to a few kilometres long; Garlan *et al.* 2015) and deep (up to several meters; Caston 1979). The mechanisms guiding the temporal and spatial scales at which scour functions at shipwreck sites, are not yet fully understood and vary significantly between sites depending on local geological, geomorphological, geotechnical and oceanographic conditions and morphometric characteristics of the wreck itself (Astley 2016; Quinn and Smyth 2018; Majcher *et al.* 2021).

5.3. Materials and methods

5.3.1. Study sites

Two wrecks were investigated in the study: SS *W.M. Barkley* and HMS *Vanguard*. Both are located in the Irish Sea, a shelf basin characterized by dominating semidiurnal lunar (M2) and solar (S2) tides (Neill *et al.* 2014; Ozer *et al.* 2015). Surficial sediments in the Irish Sea mostly comprise reworked glacial and post-glacial substrates creating a complex mosaic of sediment types (Jackson *et al.* 1995; Ward *et al.* 2015; Coughlan *et al.* 2020). Continuous sheets of sand up to 40 m thick are present, frequently associated with migrating bedforms (i.e., sand waves) of various shapes, heights and spacings (Van Landeghem *et al.* 2009b, 2012). Where sand supply is limited, a gravel lag deposit is exposed (Jackson *et al.* 1995). SS *W.M. Barkley* and HMS *Vanguard* are located in sand wave fields approximately 35 and 31 km east and south-east of Dublin respectively, approximately 19 km apart (Fig. 5.1). Depth-averaged, spring tide current velocities reach

1 m/s (Howarth, 2001) and previous studies have determined that the seabed is highly mobile in the area (Coughlan *et al.*, 2021; Majcher *et al.*, 2021), based on the data from the validated regional ocean modelling system (ROMS; Nagy *et al.*, 2020). Sediments can be mobilised by tidal currents for 56% of the year around SS W.M. Barkley and 57% around HMS Vanguard, with waves having a limited influence on the sites due to their depth (52 and 40 m, respectively) (Coughlan *et al.*, 2021; Majcher *et al.*, 2021).
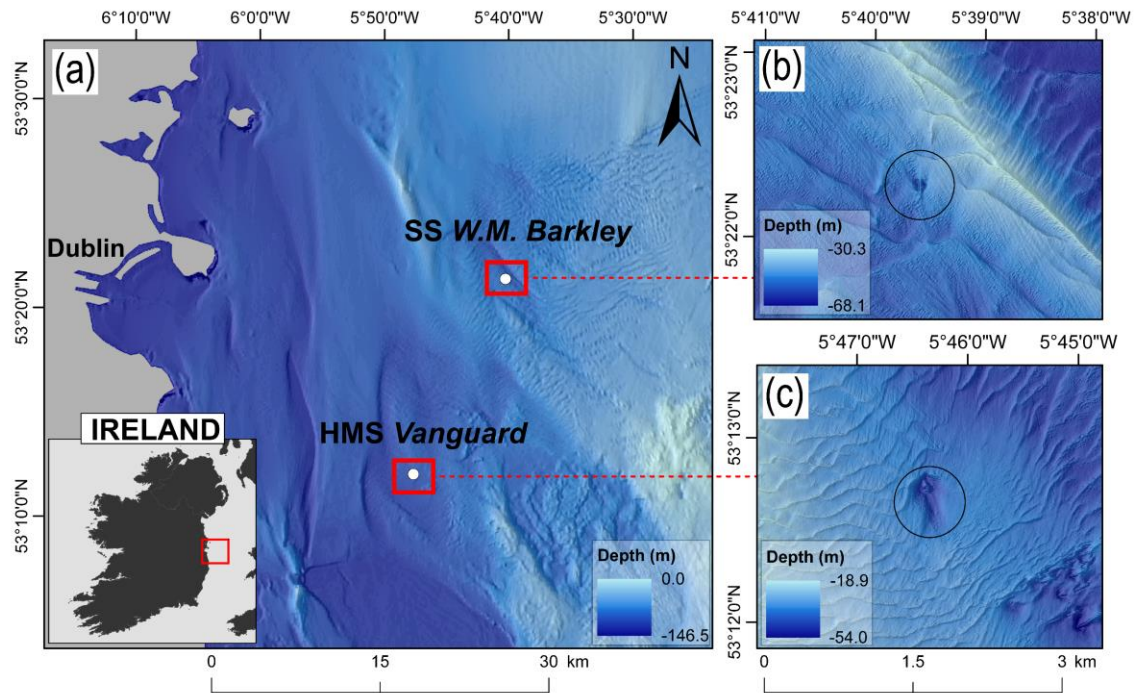
Figure 5.1. (a) Location of the study area and the (b) SS W.M. Barkley and (c) HMS Vanguard sites. Backdrop bathymetry was obtained from (a): EMODnet (EMODnet Bathymetry Consortium 2018); (b) and (c): INFOMAR project (Guinan *et al.* 2020).

SS *W.M. Barkley* was the first steamship employed by Arthur Guinness and Sons Ltd., producers of Guinness stout. She sank on 12.10.1917 after a torpedo strike by the German U-boat *UC-75* while sailing from Dublin to Liverpool and resulted in the loss of four lives (Brady *et al.* 2012). HMS *Vanguard* was an *Audacious*-class ironclad battleship. On 1.09.1875 HMS *Vanguard* was sailing from Dublin to Queenstown (Cobh) with six other battleships, when the formation encountered fog and *Vanguard* was accidentally rammed by her sistership HMS *Iron Duke*, resulting in sinking with no loss of life (Brady *et al.* 2012). Both wrecks are more than 100 years old and protected in Ireland by the National Monuments Act (National Monuments Service 1987).

5.3.2. Oceanographic data

Depth-averaged current velocity magnitudes and directions were obtained for the area covering the wreck sites from an operational model run by the Marine Institute of Ireland (Nagy *et al.* 2020). The model is an implementation of the Regional Oceanic Modelling

System (ROMS; Shchepetkin and McWilliams 2005) for an area of the NE Atlantic encompassing Irish waters. The temporal resolution of the model data is hourly and the horizontal resolution in the Irish Sea ranges from 1.1 to 1.7 km. Model data used in this study cover a 1-year period (January 31, 2019–December 31, 2019) and were used for site characterization to provide current roses and to establish inlet current velocity profiles for the CFD simulations.

5.3.3. Repeat hydrographic surveys

High-resolution repeat hydrographic surveys were conducted in September 2015 and October/November 2019 to provide data for site characterization and detection of geomorphic and structural changes over a 4-year interval. Additionally, in 2019, two hydrographic surveys spaced 1 week apart were conducted at the SS *W.M. Barkley* site. The first survey (26 October) took place before a spring tide (28 October) and a storm (29 October – 3 November) after which the second, repeat survey was conducted (3 November). Westley *et al.* (2019) and Majcher *et al.* (2021) provide comprehensive descriptions of the survey methods and strategies used to collect the high-density, detailed shipwreck-focused and repeat regional MBES data used for assessing structural and geomorphic changes respectively. Only the key parts of these methods are described here, for brevity and more details are included in the supplementary material.

Bathymetric and backscatter data were collected onboard RV *Celtic Voyager* using a hull-mounted MBES. The bathymetric data were processed in CARIS Hips and Sips v. 9.1 software, including point cloud cleaning and tidal and refraction corrections. Quality control using crosslines showed >98% compliance with the IHO Special Order standard (IHO 2020). The processed datasets were exported to rasterized digital elevation models (DEMs) in the UTM 30N projection with a common 0.3 m pixel size (i.e., spatial resolution) and clipped to the extents of CFD domains. The backscatter data were imported to QPS Fledermaus Geocoder Toolbox (FMGT v.7.8.9) and corrected for angular varying gains with 25% of the nadir zone blended between lines to reduce artefacts (Lurton and Lamarche 2015). Backscatter intensity mosaics were then generated at 0.3 m spatial resolution.

The regional acquisition strategy for site characterization and geomorphic change detection was designed specifically to capture the shipwreck sites and the surrounding seabed including the full extent of observed scour signatures at high resolution, using the same, consistent equipment setup between the consecutive surveys (Majcher *et al.* 2021). On the other hand, the high-density, detailed acquisition strategy was used to assess structural changes at shipwrecks and involved multiple slow passes over the wrecks to capture dense point clouds (MCA 2018; Westley *et al.* 2019). Rapidly changing weather conditions and

time constraints did not allow us to apply the detailed strategy to the SS *W.M. Barkley* during the 2019 survey. Hence, the assessment of structural changes for this site compares the 2015 detailed survey data with the 2019 regional survey data plus a cross line running over the wreck.

5.3.4. Site characterization

The regional bathymetric and backscatter datasets collected in 2015 were used for site characterization. The DEMs of HMS *Vanguard* and SS *W.M. Barkley* were imported into ESRI ArcMap 10.7.1 GIS software, where erosional and depositional signatures were delineated following Majcher *et al.* (2020). The shipwrecks' dimensions, morphometry of sand waves and scour dimensions and depths were obtained using GIS measuring tools. Migration directions of sand waves were determined from their asymmetric profiles (Van Landeghem *et al.* 2009b, 2012). Slope layers were derived from the DEMs to enhance morphometric description of the scour signatures.

5.3.5. Structural change

CloudCompare v. 2.11.3 software was used to assess structural changes on the wrecks between 2015 and 2019, by comparing dense point clouds. The point clouds were initially imported and cropped to the same extents encompassing a box around the wrecks. Their volumetric densities were calculated using the Compute Geometric Features tool. Signed differences between the 2015 and 2019 point clouds were obtained using the M3C2 plugin (James *et al.* 2017), taking into account the +/- 0.3 m vertical positioning uncertainty. The resulting difference scalar fields were projected onto the point clouds of SS *W.M. Barkley* and HMS *Vanguard* obtained in 2015.

Cleaning multibeam echosounder-derived point clouds collected over shipwrecks is not straightforward, as parts of their complex structures may be confused with noise. Therefore, the data from the M3C2 analysis were carefully examined for false indicators. Discrepancies were checked by superimposing the two consecutive point clouds for each wreck and visually assessing whether a difference could be attributed to a real event or to acquisition artefacts. The ambient occlusion ShadeVis plugin and the EyeDome Lighting OpenGL shader were applied together to enhance the comparisons and visualization of the point cloud data.

5.3.6. Geomorphic change

To perform difference modelling, the 2015 and 2019 regional DEMs of HMS *Vanguard* and SS *W.M. Barkley* were imported into ArcMap 10.7.1 software and used with the Geomorphic Change Detection (GCD) Addin for ArcGIS (Wheaton *et al.* 2010). The resulting 0.3 m resolution difference models represent geomorphic change between 2015

and 2019 for both wrecks, and additionally over a one-week interval in 2019 for SS *W.M. Barkley*. Percentages of erosional and depositional change were calculated based on pixel values in the difference models. Pixels within the +/- 0.3 m vertical range were excluded from the analysis, as they were within the vertical uncertainty calculated by the CUBE algorithm (Majcher *et al.* 2021), except for the visualization of the short-term difference model for the SS *W.M. Barkley* site, where majority of the change was of low magnitude.

5.3.7. Sediment samples

Sediment samples were collected using a Shipek grab inside and outside the erosional and depositional signatures. Granulometric analysis of the sediments was performed using a MALVERN Mastersizer 3000 laser diffraction particle size analyzer for samples collected at the SS *W.M. Barkley* site and using a sieve stack for the HMS *Vanguard* samples. Sediment classification into Folk classes (Folk 1954) and median grain size (d_{50}) calculations were performed using Gradistat v. 8 software (Blott and Pye 2001).

5.3.8. Flows at the sites - computational fluid dynamic simulations

5.3.8.1. Stereolithography geometry

CFD simulations were conducted using triangular meshes constructed using DEMs and dense point clouds from the 2015 MBES surveys. The Poisson Surface Reconstruction plugin (Kazhdan *et al.* 2006) in CloudCompare was used to triangulate the MBES data and export the obtained meshes as stereolithography (.stl) files. The files were then imported to the Autodesk Meshmixer v. 3.5.474 software for quality checks and smoothing of mesh artefacts. The meshes covered a stretch of the seabed approximately 900 m long and 200 m wide, with the shipwrecks in the middle (Fig. 5.2). The direction of the longer sides of the rectangular domains was the same as the direction of the inlet tidal current for each mesh.
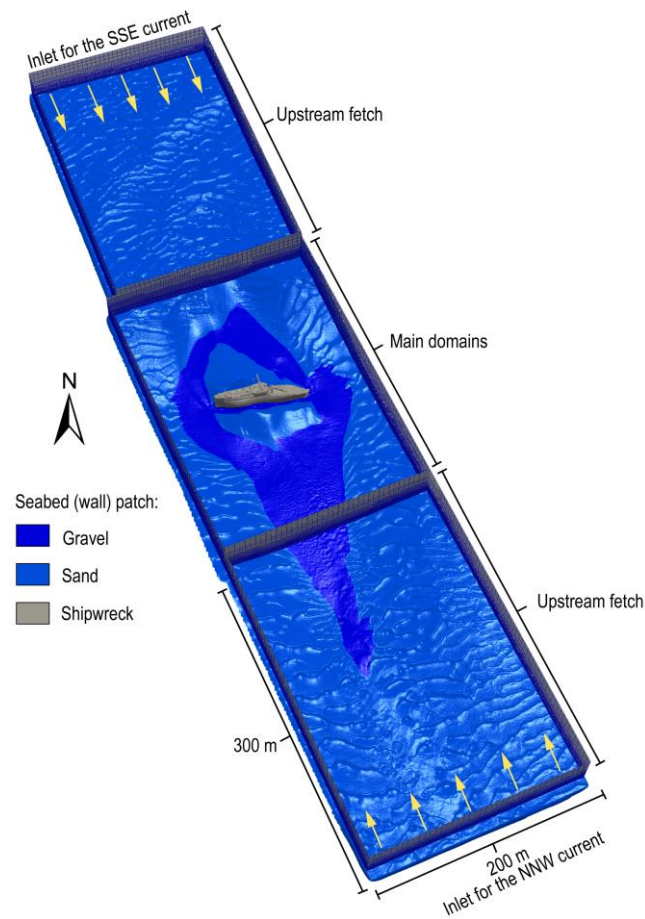
Figure 5.2. CFD mesh setup for the HMS Vanguard site including the upstream fetch domains for both simulated current directions and the main domains with the shipwreck site. SS *W.M. Barkley* site's mesh setup is analogous, except the sand-grain roughness height parameter was set as uniform.

For SS *W.M. Barkley*, a DEM with a spatial resolution of 0.3 m (from the regional survey) was used to represent the seabed around the wreck, which was merged with a finer DEM of 0.1 m resolution (from the detailed survey) encompassing the wreck. The resulting point cloud was then triangulated. The hull of HMS *Vanguard* is better preserved than that of SS *W.M. Barkley*, with most of its structure standing proud of the seabed. This complex structure, which includes well-preserved discrete structural elements (e.g. a collapsed mainmast), necessitates fully 3-dimensional rendering of the site (rather than 2.5-dimensional provided by DEM representation). Therefore, additional points were added to the DEM points from the non-gridded, dense point cloud obtained during the detailed survey to represent parts of the hull and the collapsed mast, which would otherwise be obscured using only the regularly gridded DEM data. Using these detailed point clouds to represent the entire wrecks was deemed unfeasible, due to their high irregularity causing triangulation problems.

5.3.8.2. Simulation setup and initial conditions

OpenFOAM v.6 (Weller *et al.* 1998) was used for creating computational domains (or CFD meshes) and simulating flows. ParaView v. 5.9.0 was used for processing and visualization of the CFD results. The OpenFOAM code solves Reynolds-averaged Navier–Stokes (RANS) equations using the finite volume method. Three-dimensional CFD RANS simulations of water flows over complex terrain using the OpenFOAM code have been previously validated against and have shown good agreement with experiment data (for example for riverine flows over dunes: Unsworth *et al.*, 2020). Additional remarks on the validation of simulations with experiment data are included in the supplementary material. Main simulations were run in parallel on 80 processors on the high-performance computer facility at Ulster University. Second-order accuracy schemes were used to translate governing partial differential equations into algebraic equations, solved within the computational domains. OpenFOAM's Geometric-Algebraic Multi-Grid solver (GAMG) was used for the Poisson equation for pressure and the Stabilised Preconditioned (Bi-) Conjugate Gradient (PBiCGStab) (Van Der Vorst 1992) for all other equations.

Details about the RANS equations can be found in Versteeg and Malalasekera (2007). Flow fields were calculated using the shear-stress transport (SST) k-ω turbulence closure (Menter *et al.* 2003), previously used for flow simulations at shipwreck sites (De Hauteclocque *et al.* 2007; Fernández-Montblanc *et al.* 2018b) and for analogue problems like solving turbulent flows around tidal turbines (Shives and Crawford 2014; Sun *et al.* 2019) and sand dunes (Liu *et al.* 2021). The inlet turbulence kinetic energy, k, and specific dissipation rate, ω, were estimated according to the equations included in the supplementary material (Simpson *et al.* 1996; OpenCFD Ltd. 2019).

Directions and magnitudes of the inlet tidal currents were obtained using the ROMS model outputs (see section 5.3.2). Specifically, the 90th percentiles of the current magnitudes for two main directional lobes of the current roses (tidal currents are strongly bi-directional at the sites) were extracted from the data and used at the inlets, as they were determined to represent spring tide current speeds accurately. Mean directions of the currents exceeding the 90th percentiles of current magnitudes (speeds) within these two directional lobes were calculated and used as the inlet current directions

Current velocity profiles were then calculated using the depth-averaged velocity magnitudes according to the empirical formula provided by Soulsby (1997) (see supplementary material).

As the flow becomes unsteady around underwater obstacles (e.g., Roulund *et al.* 2005), simulations of such flows at shipwreck sites usually use transient solvers (De Hauteclocque *et al.* 2007; Smyth and Quinn 2014; Quinn and Smyth 2018). In this paper, the Pressure

Implicit with Splitting of Operators (PISO) algorithm (Issa 1986), which maintains unsteady components of the flow, was used. Time-steps were assigned in such a way that the maximum Courant number never exceeded 0.3. Simulations were considered converged when the calculated initial residuals, measuring the local imbalances of conserved variables in control volumes, dropped below 1e-05 or levelled-off.

The 3D computational domains were created using the OpenFOAM's native mesh generator, SnappyHexMesh, which is capable of incorporating stereolithography files into CFD meshes. The meshing strategy generally followed the previously established workflows for 3D CFD simulations at shipwreck sites (Smyth and Quinn 2014; Quinn and Smyth 2018), with a gradual increase in refinement with a decreasing distance to the seabed (i.e., cells are the finest close to the seabed) and with the same boundary conditions applied. Additional refinement boxes were added to provide greater refinement of the mesh cells corresponding to shipwreck structures and the water mass up to approximately 5 m above them. Three layers were extruded adjacent to the shipwreck/seabed geometries to provide further refinement of the near-wall region.

In order to model realistic inlet conditions and develop flows for the main simulations (Wakes 2013; Blocken *et al.* 2015), the flows were initially simulated at a coarse resolution (approximately 2.7 million cells) at extended domains over the seabed, captured using the regional hydrographic survey strategy (referred to as upstream fetch domains). The stereolithography files were subdivided into three parts in such a way that the first part corresponded to the upstream fetch of one tidal current direction, the second part to the main domain containing the shipwrecks and the third part to the upstream fetch of the opposite tidal current direction (Fig. 5.2). Hence, four simulations were conducted for each site: two for each current direction. The first simulation of each current direction regime was simulated at the upstream fetch domain corresponding to that direction, and all the flow fields were then mapped from its outlet to the inlet of the second, main domain. The main domains were designed in such a way that their widths and the lengths of the downstream zones exceeded 15 and 5 mean heights of the shipwrecks, accordingly, to exclude the influence of CFD domain size on the simulations (Blocken 2015). Additionally, grid independence tests were carried out by performing simulations using grids with increasing numbers of cells: 2.1, 5.0 and 13.4 million cells and 4.5, 7.3 and 12.1 million cells for the SS *W.M. Barkley* and HMS *Vanguard* sites, respectively. Comparison of flow characteristics for the simulations demonstrated that differences related to grid resolution were irrelevant for the purpose of the investigation (see details in the supplementary material).

The results of the granulometric analysis of sediment samples (presented in sections 5.4.1.1. and 5.4.2.1.) guided the choice of the sand-grain roughness height parameter, k_s for the seabed wall patch. This parameter is defined as $k_s = 2.5d_{50}$, where d_{50} is the median grain parameter (Soulsby 1997). As sediments are uniform at the SS *W.M. Barkley* site, a uniform k_s was imposed at the seabed wall patch. At the HMS *Vanguard* site, the seabed wall patch was segmented into regions of different k_s based on the sediment grab information and manual classification of the backscatter data (section 5.4.2.1).

5.3.8.3. Flow patterns

Flow streamlines were extracted near the seabed using velocity components, time-averaged over 100 s windows, to visualize flow patterns over the wreck sites. Additionally, in order to define vortices objectively, iso-surfaces of the Q values were rendered for the sites. The Q-criterion, expressed in s^{-2}, defines vortices as areas where the Euclidean norm of the vorticity tensor, Ω, dominates that of the rate of strain S (Hunt *et al.* 1988): $Q = (|\Omega|^2 - |S|^2) > 0$.

5.3.8.4. Sediment mobility and wall shear stress

Mobility of sediments can be evaluated by comparing two variables: wall (or bed) shear-stress (τ_c) exerted by the flow and the critical shear stress which is specific to the sediment type (τ_{cr}). In OpenFOAM, the flow-related wall shear stress (τ_c) can be calculated using a built-in function, and is retrieved from the Reynolds stress tensor, resolved in the direction normal to each face of the wall patch (OpenCFD Ltd. 2019). In our modelling, the simulated τ_c values were time-averaged using a 100 s window after the convergence criteria were met, to represent determinative flow conditions. The calculation procedure (Whitehouse 1998) for the critical shear stress, τ_{cr} is provided in the supplementary material.

Whenever $\tau_c > \tau_{cr}$, the sediment mobility criterion is met (Whitehouse 1998). Therefore, in order to determine the areas prone to sediment mobility, the simulated and time-averaged wall shear stress values were exported as .csv files from ParaView for both sites, gridded as mosaics at the 0.3 m spatial resolution, compared against the critical shear stresses and represented on maps in GIS. The simulated τ_c distributions were also used to discuss the influence of flows on structural changes sustained by the wrecks.

5.4. Results

5.4.1. SS *W.M. Barkley*

5.4.1.1.   Site characterization

SS *W.M. Barkley* is broken into two pieces and lists to starboard, with her bow detached from the torpedo strike (Brady *et al.* 2012). The main hull section measures 49 x 10 x 8 m, and the detached bow section 23 x 10 x 5 m. The shipwreck is surrounded by a scour pit, extending 285 m to the NNW and reaching a maximum depth of 13.96 m (in 2015, relative to the surrounding seabed) at approximately 4 m distance from the detached hull (Fig. 5.3a). This erosional signature is asymmetric, more developed in the NNW direction than SSE and divided by a depositional ridge, which intersects the wreck midships, causing partial burial. Similar signatures are not clearly defined in the backscatter data, suggesting sediments are nearly uniform across the site (Fig. 5.3b). Variations in the backscatter intensity are attributed to the variable slopes and acoustic shadows associated with pervasive sand waves. The seabed slopes steeply within the scour signatures, with gradients exceeding 30° (Fig. 5.3c).

Granulometric analysis of the grab samples confirms that the sediments are uniform across the site, comprising medium sand (average $d_{50} = 0.302$ mm). The bathymetry around the wreck is variable, with sand waves dominant. Bedforms, with typical wavelengths of 10-15 m and heights of 0.5-1.0 m, are aligned to the dominant depth-averaged current directions (NNW-SSE) derived from the regional ocean model, with maximum currents of 0.94 m/s. Sand waves' asymmetry indicates that the majority propagate with the stronger NNW-directed tidal current. Notably, the propagation is reversed in the scour pit SSE of the wreck (5.3a). A large, presumably relict sand wave (not aligned with the currents) is present to the north of the wreck, with an approximate height of 4 m.
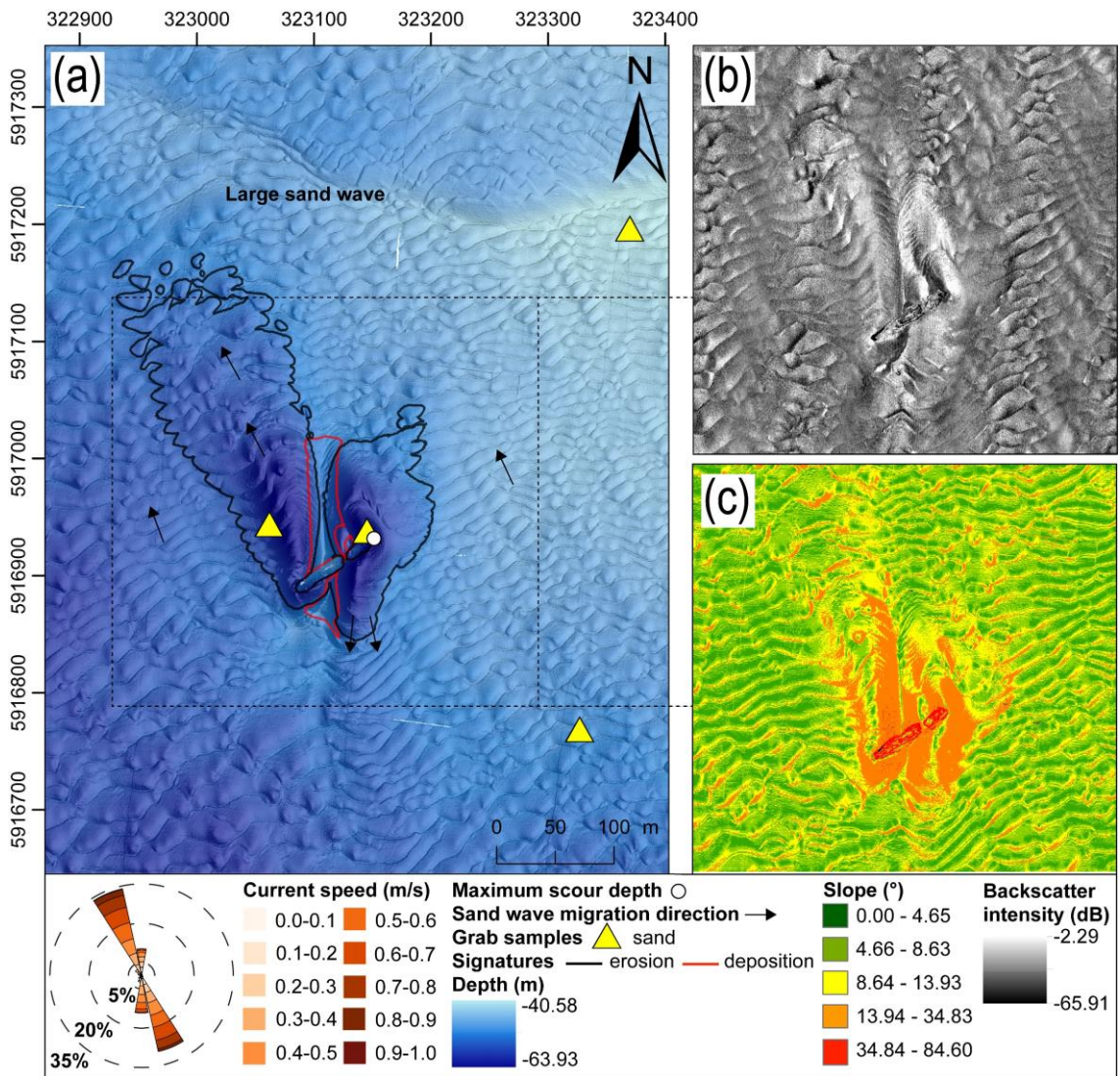
Figure 5.3. Site characterization of the SS W.M. Barkley site. (a) Bathymetric DEM with the current rose obtained from the regional oceanographic model, (b) backscatter intensity mosaic, (c) slope map segregated using Jenks natural breaks optimization.

5.4.1.2.   Geomorphic change

The high-resolution bathymetric surveys conducted at the SS *W.M. Barkley* site allowed for evaluation of both long-term (2015-2019: Fig. 5.4a,b) and short-term (one week: Fig. 5.4c,d) differences in bathymetry.

High-magnitude differences reaching up to -4.9 m and +3.0 m are observed around the site in the long-term difference model (Fig. 5.4a) and are associated not only with sand wave migration, but also reorganization of sediments within the erosional and depositional signatures. Notably, the location of the maximum scour depth moved farther north from the wreck, by approximately 4 m and was 1.01 m deeper. The largest changes occurred in the pits located in immediate proximity to the wreck. In terms of areal coverage, negative change (38.5% of the area) is more extensive than positive change (21.6% of the area),

suggesting that the site is in a state of net erosion (Fig. 5.4b). The calculated mean bathymetric change (-0.17 m) also suggests net erosion.
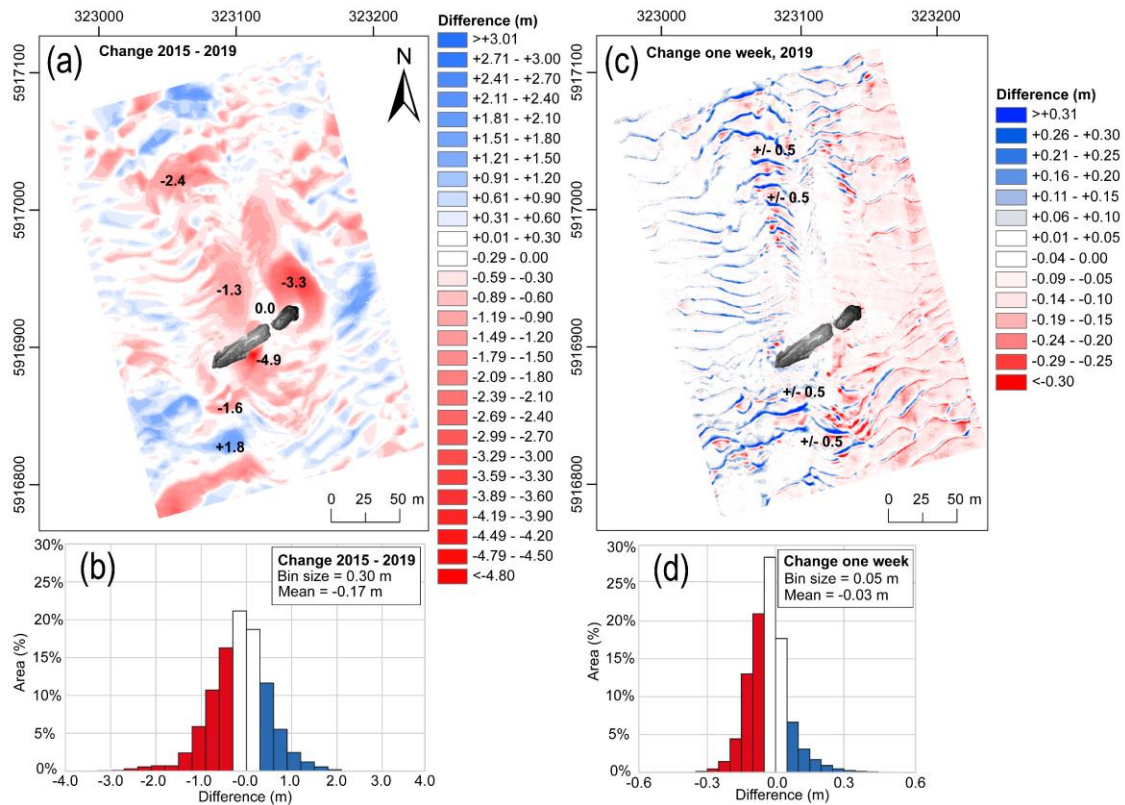
Figure 5.4. Difference models for the SS W.M. Barkley site. (a) long-term model (2015-2019), (b) areal percentage histogram for the long-term model, (c) short-term model (one week, 2019), (d) areal percentage histogram for the short-term model. Numbers on the difference models represent localised changes. Note that the bin sizes for the histograms are different.

Significant bathymetric changes are observed at the site even in the short-term (one week) difference model (Fig. 5.4c). Retaining pixels within the vertical measurment uncertainty (+/- 0.3 m) highlights sand wave migration everywhere across the site. The migration is clearly enhanced to the NNW and SSE of the wreck, corresponding to downstream regions of the tidal currents, where changes of the highest magnitude for this interval were recorded, exceeding the measurement uncertainty (up to +/- 0.5 m). The mean bathymetric change for this interval is also negative, however, as shown in Fig. 5.4d, most of the change (99.2%) fits between +/- 0.3 m. Hence, any statistical quantification (including areal percentage calculations) for these short-term changes is deemed unreliable.

5.4.1.3.   Structural change

Structural change was assessed through point cloud comparisons. The mean number of points within 1 m radius spheres (volumetric density) of the point clouds obtained for SS *W.M. Barkley* in 2015 and 2019 was 1037 and 46, respectively. Point cloud density from

2019 is significantly lower as weather conditions did not allow a high-density survey. Nevertheless, both point clouds successfully capture all the main structural elements of the wreck (Fig. 5.5a, b), including a counter stern, funnel hole, gunwales and other intricate details.
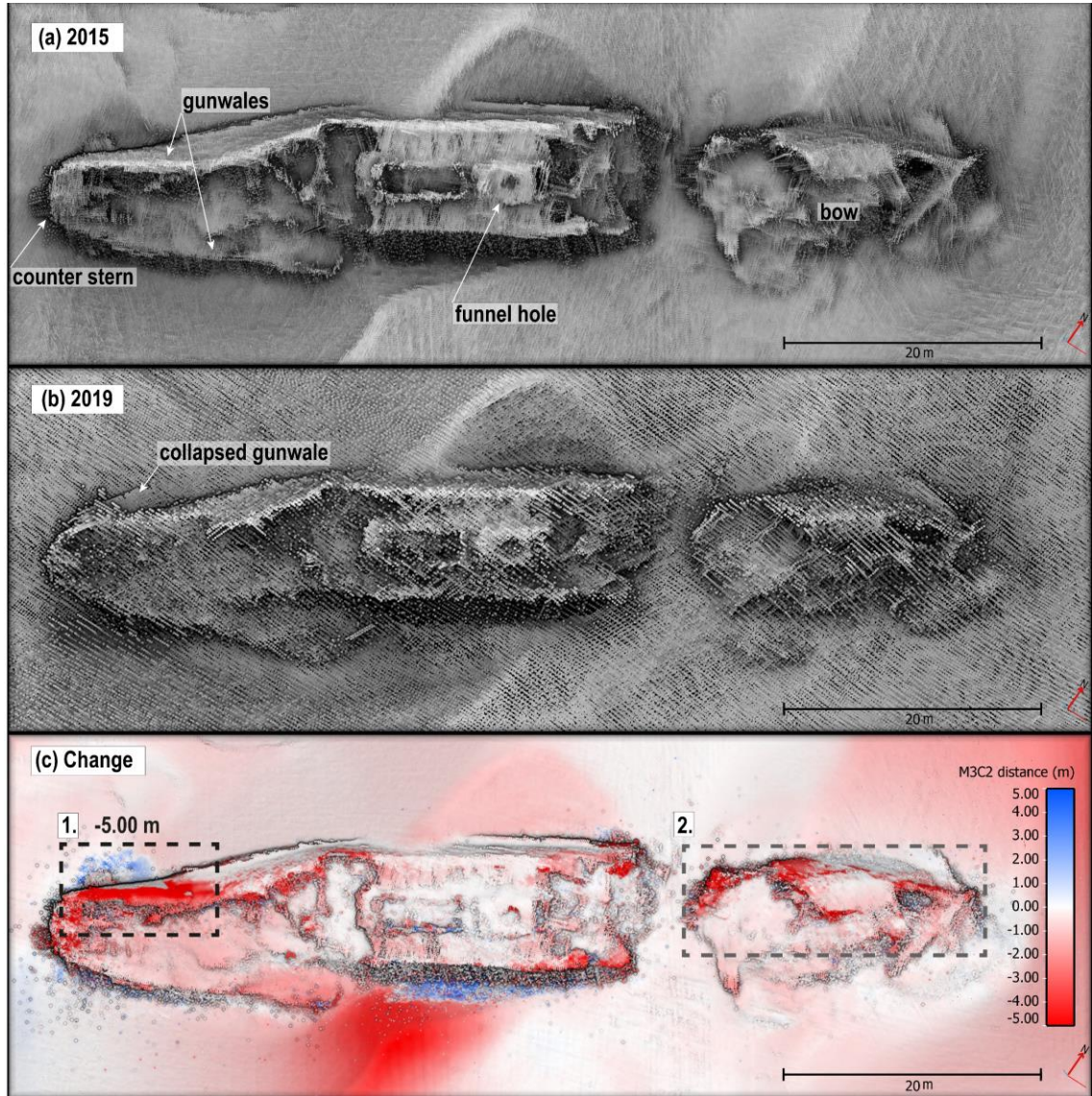
Figure 5.5. Structural change model for the SS W.M. Barkley site. (a) point cloud corresponding to the 2015 survey , (b) point cloud corresponding to the 2019 survey, (c) difference model for the interval 2015-2019. Black and grey dashed lines represent certain and uncertain changes respectively.

The M3C2 difference model highlights two regions of major structural change: the detached bow section and the portside gunwale of the counter stern (Fig. 5.5c). Examination of the difference model (Fig. 5.5c, box 1) indicates that a significant portion of the gunwale collapsed and is now hanging from the portside, leaning against the seabed (Fig. 5.5b). Differences noted at the bow (Fig. 5.5c, box 2) (and elsewhere) may be associated with disparities in point cloud densities and subjective cleaning of the point

cloud during data processing. The bow structure is highly complex with multiple protruding elements, making point cloud cleaning difficult.

5.4.1.4.   Sediment mobility and wall shear stress

Analysis of sediment samples indicate uniform sand (mean d_{50} = 0.302 mm) at the SS *W.M. Barkley* site, and an equivalent uniform k_s was imposed at the seabed wall patch for the simulations. The extracted 90th percentiles of depth-averaged current speeds are 0.77 m/s and 0.74 m/s for the NNW and SSE directions and were imposed at the inlets to the computational domains.

The resulting wall shear stress maps for both current directions are presented in Fig. 5.6. Three τ_c groups were empirically distinguished, based on the areal frequency distributions of the values and the critical shear stress value, τ_{cr} (0.19 Pa): low, which comprises values below the τ_{cr}; moderate, comprising values between the τ_{cr} and three times larger (0.19 – 0.58 Pa); and high containing all the values above 0.58 Pa.
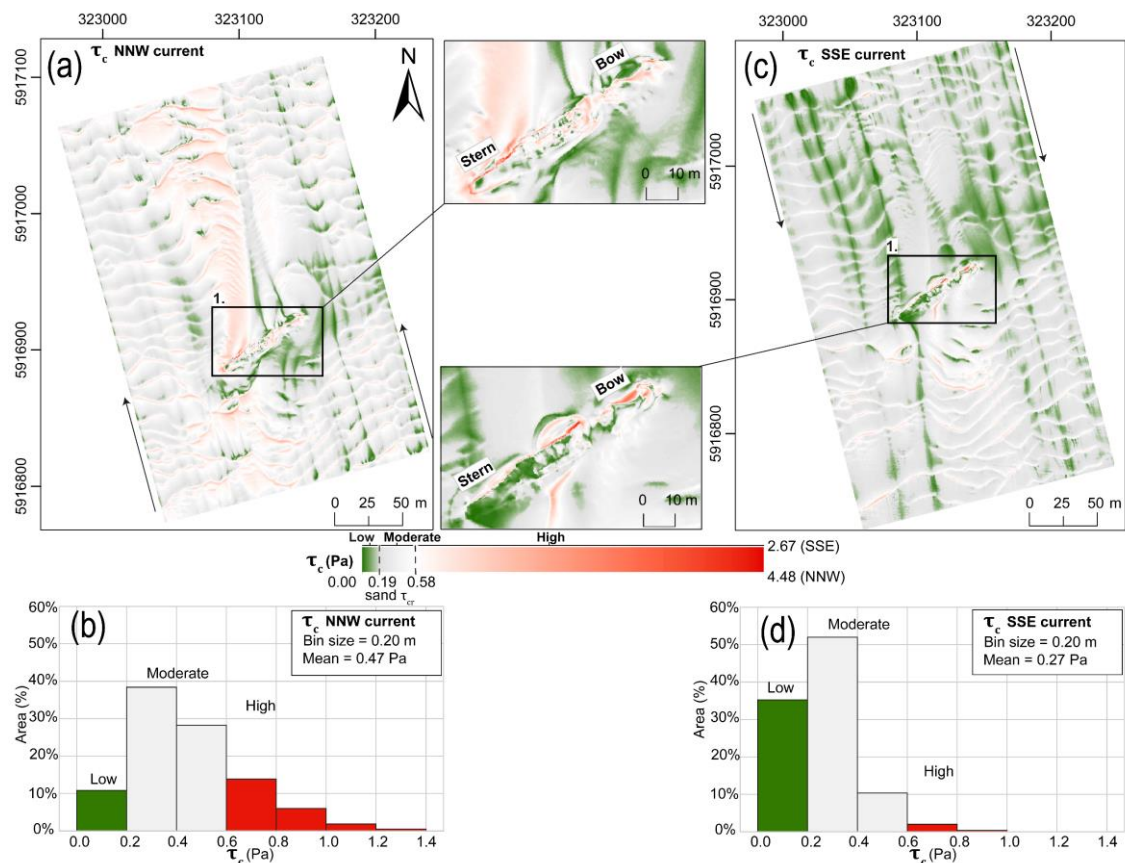
Figure 5.6. Simulated wall shear stress maps for the SS W.M. Barkley site. (a) Wall shear stress under the NNW current with (1) close-up on the wreck, (b) areal percentage histogram for the wall shear stress values under the NNW current, (c) wall shear stress under the SSE current with (1) close-up on the wreck, (d) areal percentage histogram for the wall shear stress values under the SSE current.

The sediment mobility criterion is met ($\tau_c > \tau_{cr}$) across the site, indicating sediment is mobilised under the simulated current regimes (Fig. 5.6a,c) with 90.1% of the area experiencing the critical shear exceedance under the NNW regime (Fig. 5.6b) and 68.0% under the SSE current (Fig. 5.6d).

For the NNW current, τ_c is heavily modified at the lee side of the wreck, with an elongated high magnitude zone stretching from the stern toward the NNW and a low magnitude shadow zone extending from midships and from the detached bow (Fig. 5.6a). Additionally, τ_c is substantially elevated on the crests of the sand waves everywhere across the site, in particular SE of the wreck (Fig. 5.6a). τ_c is also amplified on the lee side of the wreck under the SSE current, with the highest level of magnitude adjacent to the midship section. Mean τ_c values calculated for both current directions (0.47 Pa for the NNW current and 0.27 Pa for the SSE current), together with distribution of values (Fig. 5.6 c,d), suggest that overall the NNW current regime is associated with significantly higher bed shear stresses than the SSE current regime.

With respect to the distribution of τ_c at the shipwreck itself, the parts of the wreck structure standing high above the seabed are exposed to the highest shear stresses under both current regimes (Fig. 5.6a, 1 and Fig. 5.6c, 1). Under the NNW current, the highest τ_c is modelled at the ship's portside gunwale near the counter stern (Fig. 5.6a, 1). The detached bow also experiences elevated wall shear stress. Under the SSE current, τ_c is increased midships and at the detached bow (Fig. 5.6c, 1).

5.4.1.5. Flow patterns

The simulated NNW and SSE currents are orientated at 69° and 68° to the SS *W.M. Barkley*'s broken hull. Fig. 5.7 shows fully developed, averaged flow patterns at the site represented with flow streamlines and *Q* value iso-surfaces at Q=0.0001 s^{-2}. Intricate flow patterns are developed around the complex structure of the wreckage. An irregular horseshoe vortex is developed around the main body of the wreck, but not around its bow under the NNW current (Fig. 5.7a,b). The right leg of the vortex passes through the gap between the broken midship part of the wreck and the detached bow, and the left leg terminates at the counter stern (Fig. 5.7b). Both legs appear to merge with complex vorticial patterns developed in the wake of the shipwreck (Fig. 5.7b). The wake vortices are generally characterized by a strong asymmetry; the stern-orignating (inflow) vortices are more developed than the bow-originating ones. At least two wake vortices extend from the wreck's main structure; one closer to the stern and one closer to midships. They merge downstream in proximity to the wreck to form a single wake vortex stretching along the side of the depositional ridge (Fig. 5.7b, Fig. 5.3a). Another, less pronounced wake vortex

is developed at the bow part, getting closer to the larger in-flow wake vortex with increasing downstream distance over the opposite slope of the depositional signature (Fig. 5.7a,b).

Under the SSE current, a horseshoe vortex is formed only at midships (Fig. 5.7d), on one side climbing the depositional ridge, which partially covers the wreck, and passing through the bow-midship gap on the other side. Similar to the patterns developed under the NNW current regime, the incoming SSE current causes the development of separate wake vortices over the bow and the main part of the wreck. Here, the inflow, bow-orginating vortex seems to be less developed than the larger midship-stern originating vortex.
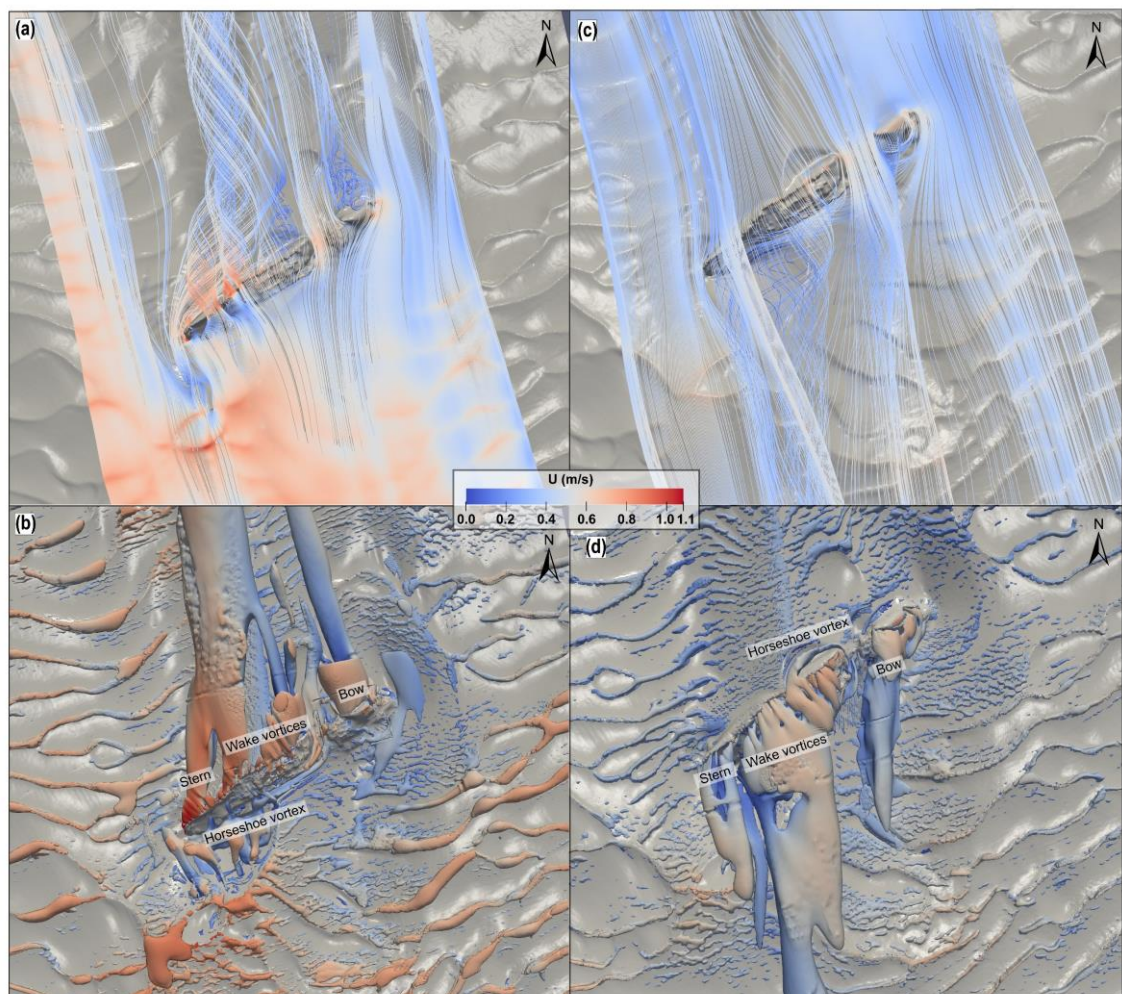
Figure 5.7. Simulated flow patterns for the SS W.M. Barkley site. (a) Flow streamlines and (b) Q iso-surface (Q=0.0001) under the NNW current, (c) flow streamlines and (d) Q iso-surface under the SSE current.

5.4.2. HMS *Vanguard*

5.4.2.1.   Site characterization

HMS *Vanguard* lists to starboard, measures 90 x 20 x 12 m in length, width and height, respectively. An extensive, comet-shaped scour pit is developed at the site, with its main body stretching up to 280 m SSE of the wreck (Fig. 5.8a). The erosional influence of the shipwreck on the seabed, however, can be observed at a larger distance, exceeding 400 m (Fig. 5.8a). The scour pit is asymmetric, developed more towards the SSE, with a maximum depth of -11.69 m at the stern section, and a depth of -11.60 m at the bow section (white dots on Fig. 5.8a). A streamlined depositional zone is delineated proximal to the wreck, extending in both directions along the main axis of the pit.
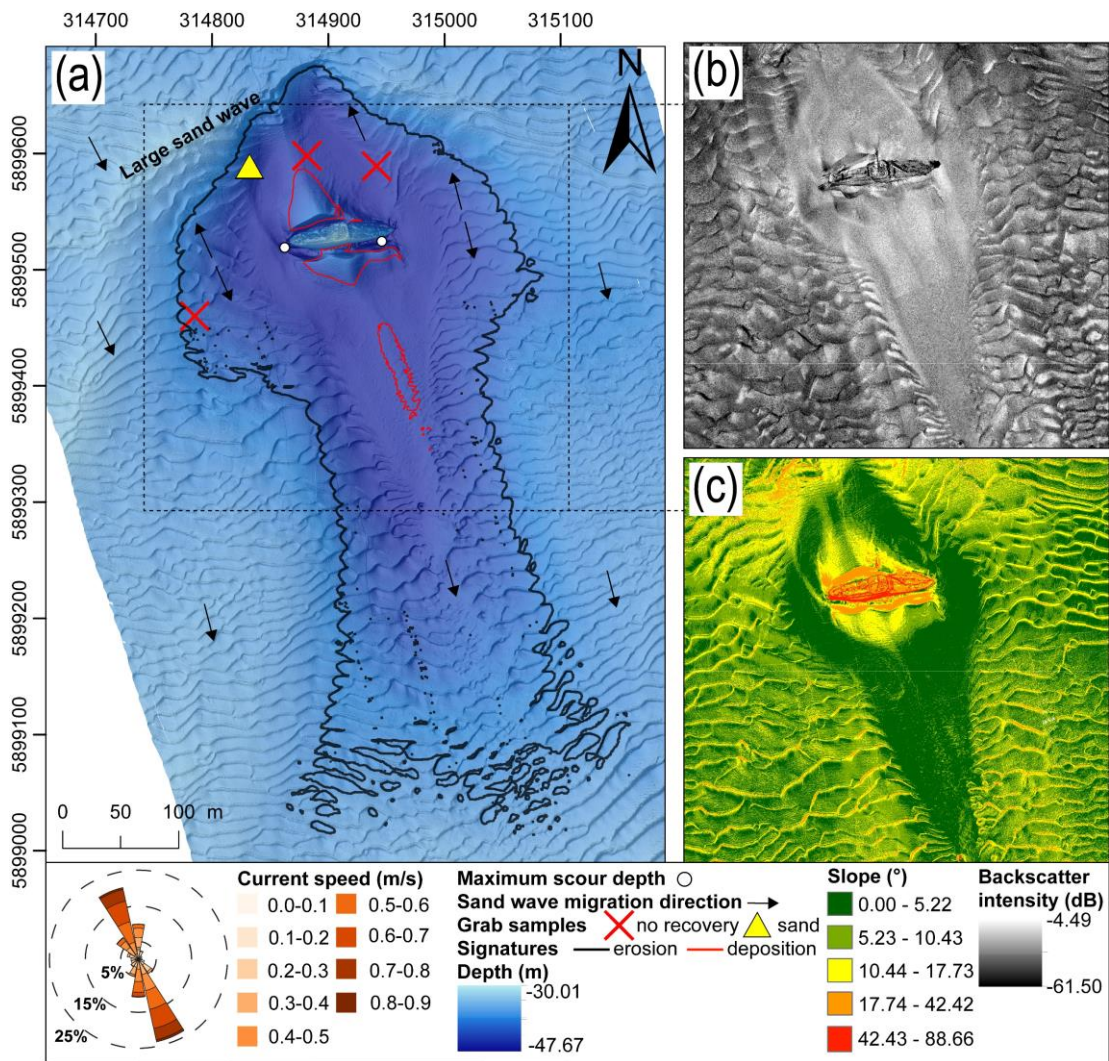
Figure 5.8. Site characterization of the HMS Vanguard site. (a) Bathymetric DEM with the current rose obtained from the regional oceanographic model, (b) backscatter intensity mosaic, (c) slope map segregated using Jenks natural breaks optimization.

The main part of the scour pit stands out in the slope map as it is nearly flat compared to the highly variable surrounding bed (Fig. 5.8c). No sediment grabs were retrieved from the

erosional zone despite three sampling attempts, suggesting coarse sediment is exposed here by erosional processes. This interpretation is supported by seismic profiles (Majcher *et al.* 2021) and the higher backscatter intensity signature observed in the pit (Fig. 5.8b).

A sediment sample retrieved from the sand waves adjacent to the scour pit contained fine sand (d_{50} = 0.104 mm) (Fig. 5.8a). As depositional signatures extending from wrecks usually consist of fine, redeposited sediments (Quinn 2006; Raineault *et al.* 2013), here we assume that the depositional zone developed around the wreck consists of the same fine sand as the sand waves outside of the signatures (Fig. 5.8a).

The sand waves typically measure 10–15 m in length and 0.2–0.5 m in height and are pervasive around the wreck, but not developed within the main scour pit. Their dominant propagation direction is aligned with the stronger SSE current modelled for the site (reaching a maximum speed of 0.90 m/s). However, this is reversed NNW of the main axis of the wreck, at the rim of the scour pit, similar to the pattern observed at the SS *W.M. Barkley* site (Fig. 5.8a). A large relict sand wave envelops the northern part of the scour pit, with a crest 13 m higher than the scour pit surface.

5.4.2.2.   Geomorphic change

The high-resolution bathymetric surveys conducted at the HMS *Vanguard* site enabled evaluation of long-term bathymetric differences between 2015 and 2019 (Fig. 5.9). The vast, comet-shaped scour pit remained largely unaltered over the four years, with no detectable change over 81.1% of the area (Fig. 5.9a,b) and no change in the maximum scour depth. Some submetre changes are evidenced by the difference model in the area immediately surrounding the wreck, extending from its mast (-0.5 m) and near the portside (+/- 0.7 m). Nevertheless, the majority of detectable geomorphic change was recorded outside of the pit and is associated with the migrating sand waves. In terms of areal coverage, erosion and deposition covered 5.7% and 13.2% of the area, respectively.
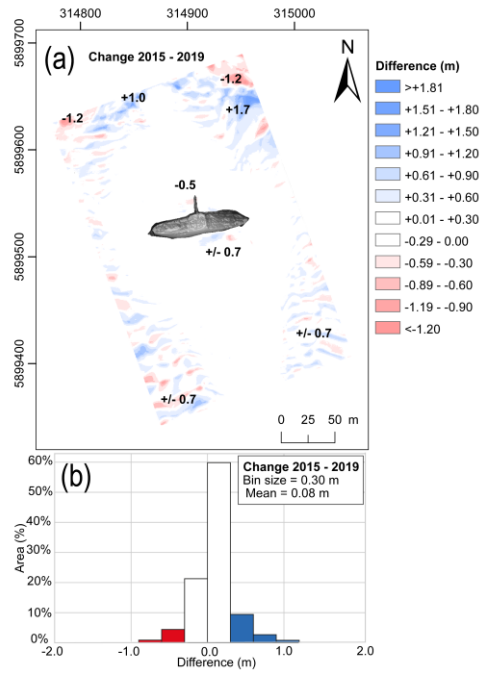
Figure 5.9. Difference models for the HMS Vanguard site. (a) long-term model (2015-2019), (b) areal percentage histogram for the long-term model. Numbers on the difference model represent localised changes.

5.4.2.3. Structural change

The mean volumetric density within 1 m radius spheres of the point clouds obtained for HMS *Vanguard* in 2015 and 2019 was 483 and 515, respectively. The very high density of the points allowed for the visualization of the wreck's structure, containing a high level of detail, not only preserving major structural features, but also details like a hole created as a result of the impact of HMS *Iron Duke* and many deck elements including an anchor, funnel hole and gunwales (Fig. 5.10a).
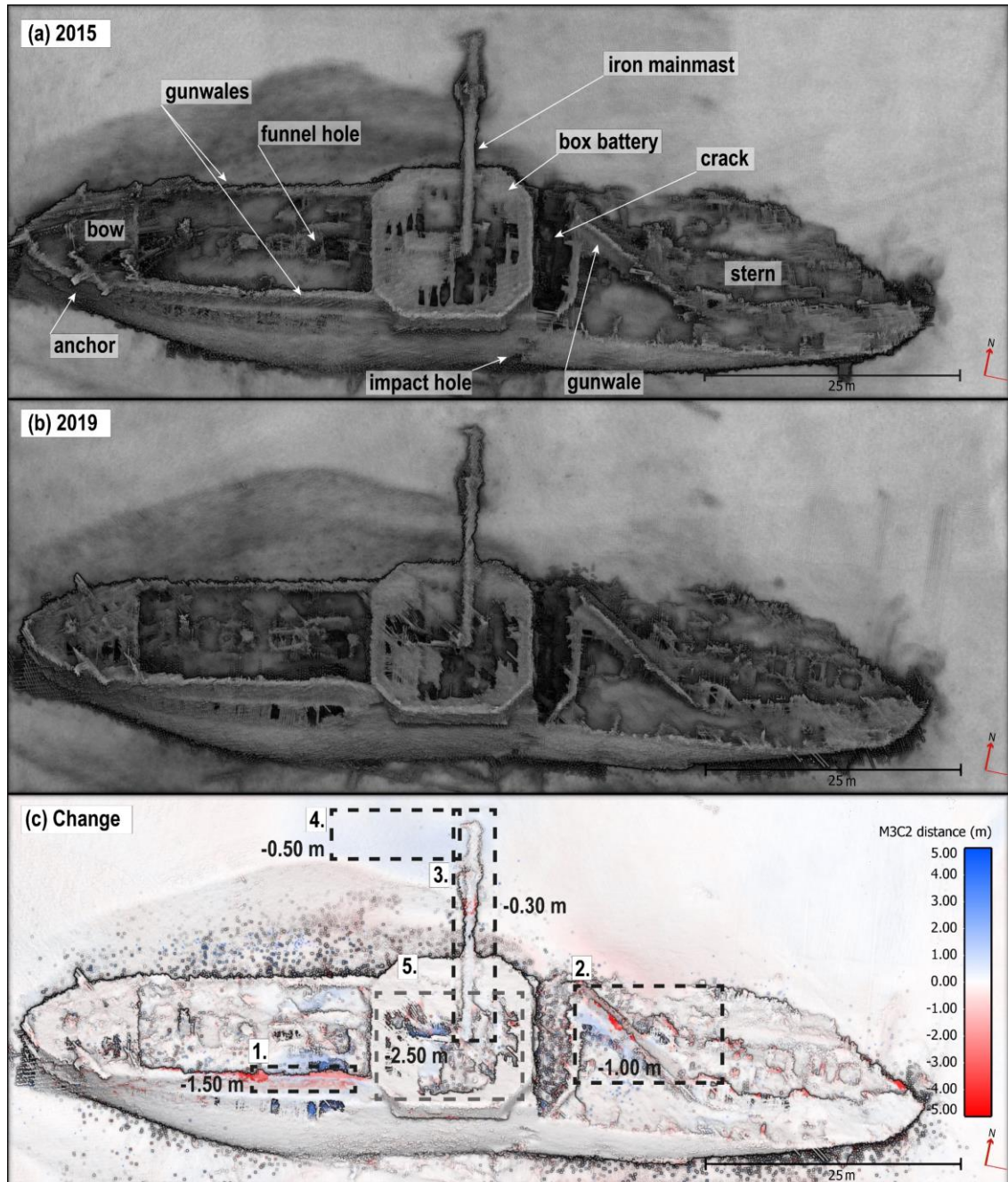
Figure 5.10. Structural change model for the HMS Vanguard site. (a) point cloud corresponding to the 2015 survey, (b) point cloud corresponding to the 2019 survey , (c) difference model for the interval 2015-2019. Black and grey dashed lines represent certain and uncertain changes respectively.

Five regions of structural change are captured in the M3C2 difference model. The first region comprises a bending portside gunwale, which was displaced downwards by approximately 1.5 m (Fig. 5.10c, box 1). The second region is associated with one of the stern gunwales sliding down 1 m towards the seabed (Fig. 5.10c, box 2). The third and fourth regions are related to the iron mainmast lowering slightly (by approximately 0.3 m). This change in the mainmast's position is associated with erosion of the seabed around its tip (Fig. 5.10c, boxes 3,4 and Fig. 5.9a). Finally, highly localized, but potentially high

magnitude (-2.5m) changes are registered on the upper surface of the box battery (Fig. 5.10c, box 5), which could be caused by plating falling into the hull, or like at the SS *W.M. Barkley*'s bow, uncertainties given the structural complexity.

5.4.2.4.   Sediment mobility and wall shear stress

Grab sample and backscatter data indicate sandy sediment (mean d_{50} = 0.104 mm) dominates outside of the scour pit at the HMS *Vanguard* site, and gravel dominates within it. Different k_s values were therefore prescribed for the regions outside (corresponding to d_{50} = 0.104 mm) and inside of the pit (d_{50} = 4 mm) and for the exposed wreck itself (smooth). The 90th percentiles of depth-averaged current speeds are 0.74 m/s and 0.73 m/s for the NNW and SSE directions, and equivalent velocity profiles were imposed at the inlets to the computational domains.
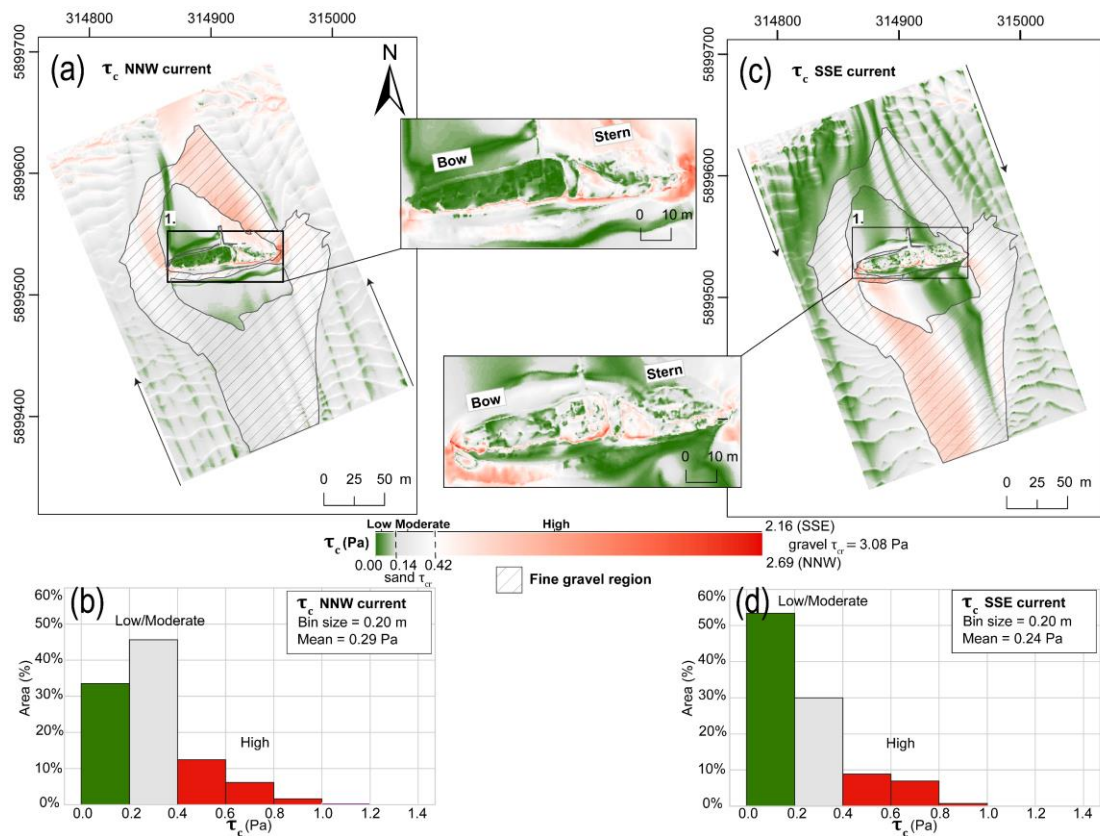
Figure 5.11. Simulated wall shear stress maps for the *HMS Vanguard* site. (a) Wall shear stress under the NNW current with (1) close-up on the wreck, (b) areal percentage histogram for the wall shear stress values under the NNW current, (c) wall shear stress under the SSE current with (1) close-up on the wreck, (d) areal percentage histogram for the wall shear stress values under the SSE current.

τ_c maps and frequency distributions for the HMS *Vanguard* site are presented in Fig. 5.11. As for the SS *W.M. Barkley* site, three wall shear stress groups were distinguished: low (below the τ_{cr} of fine sand; 0.14 Pa), moderate (between 0.14 Pa and 0.42 Pa) and high (all other values).

τ_{cr} for gravel (3.08 Pa) is not exceeded anywhere across the sites, including the area of the gravel bed (highlighted with the grey hatched area in Fig. 5.11 a,c) under NNW and SSE currents. This means that 42.0% and 64.2% of the total area is under no-exceedance conditions for the NNW and SSE current regimes, respectively. The remaining 58.0% and 35.8% of the areas, where the τ_{cr} exceedance was modelled, constitute the sand wave field outside of the scour pit (Fig. 5.11a) and some parts of the depositional zone (comprising fine sand), where the bed shear stress is amplified downstream of the wreck.

Simulations show the NNW current results in the development of a strong gradient of wall shear stress near the bow and stern (Fig. 5.11a). The elevated τ_c zone sourced at the bow reaches the end of the gravel bed and terminates nearby the stoss slope of the large sand wave NE of the wreck (Fig. 5.11a), while the ship's stern causes shear stress amplification reaching the NNW outlet of the computational domain. A mirrored distribution of shear stresses is observed under the SSE current regime. However, as there is no natural barrier SE (i.e. no large sand wave) of the wreck, τ_c amplification zones sourced at both tips of the wreck reach the outlet of the domain (Fig. 5.11c). τ_c is also amplified at the crests of the sand waves outside of the scour zone under both current regimes.

Concerning the shear stresses exerted at the shipwreck structure, high τ_c values are observed at the gunwales on the higher side of the wreck (portside) (Fig. 5.11a, 1 and Fig. 5.11c, 1). The SSE current also exerts increased shear stresses midships, at the box battery section (Fig. 5.11c, 1), while the NNW current has a strong influence on the collapsed gunwale intersecting the stern section diagonally (Fig. 5.11a, 1).

5.4.2.5.   Flow patterns

The simulated NNW and SSE currents are orientated at 75° and 78° to the wreck of HMS *Vanguard*. Fig. 5.12 shows fully developed, averaged flow patterns at the site represented with flows streamlines and Q iso-surface at Q=0.0001 s^{-2}. The remarkable preservation of this nineteenth century shipwreck, retaining much of its original integrity on the seabed, causes substantial disruption to the tidal flows at the site.
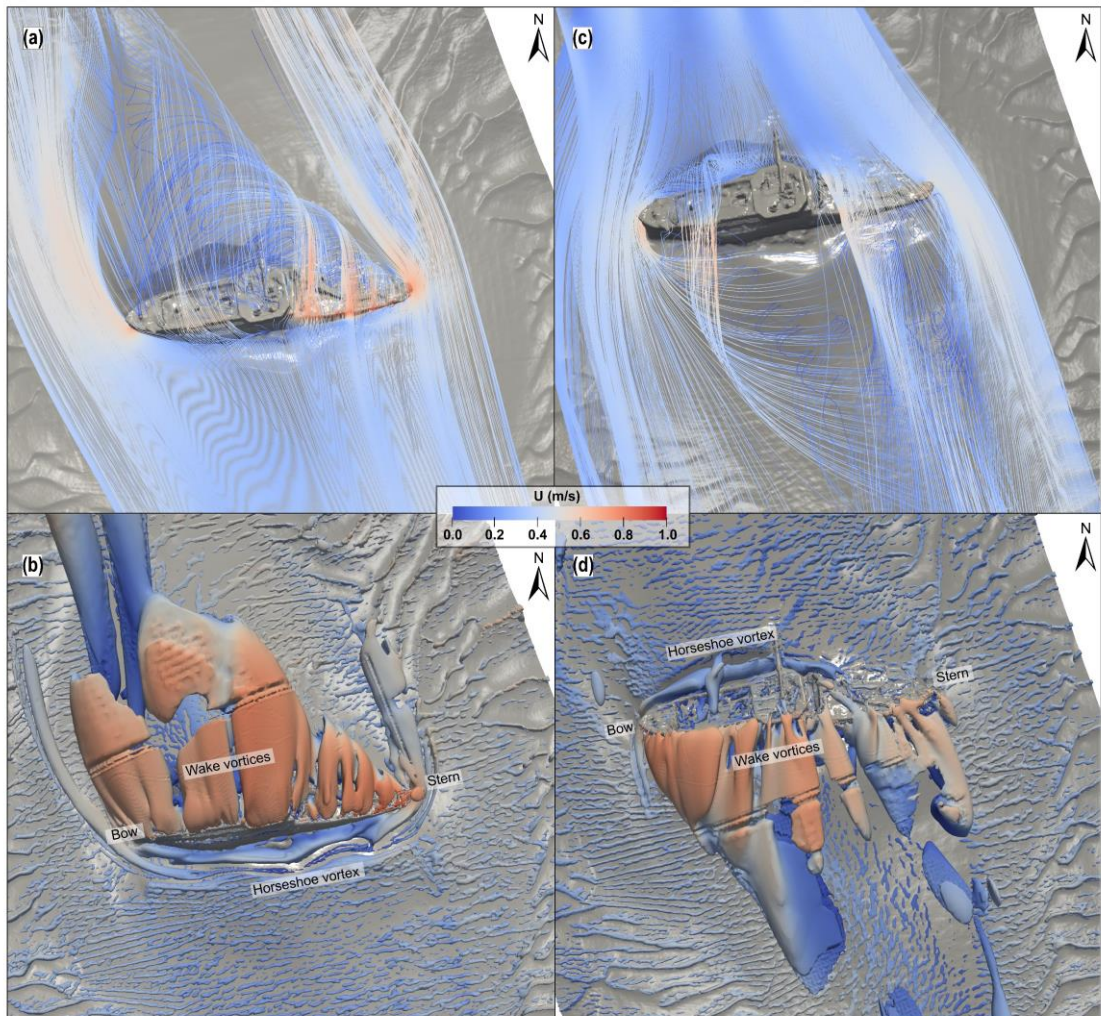
Figure 5.12. Simulated flow patterns for the HMS Vanguard site. (a) Flow streamlines and (b) Q iso-surface (Q=0.0001) under the NNW current, (c) flow streamlines and (d) Q iso-surface under the SSE current.

Under the NNW current, a horseshoe vortex is clearly discernible in the Q iso-surface (Fig.5.12b). It extends from the erosional trench, developed between the wreck and the depositional zone around it, and envelopes its structure, passing over the bow and stern with an overall asymmetric geometry, resulting from the wreck's oblique orientation towards the incoming flow. The vortex's diameter is larger at the inflow, stern side, and extends a shorter distance than at the bow. The wreck's structure poses a higher obstacle to the flow at the bow than at the partly collapsed stern section. The highest part of the wreck is at the armored box battery located midships. These irregularities in height, together with the shipwreck's list towards the starboard and the oblique incidence angle of flow, lead to an elaborate pattern of vortices developed over the wreck and in its wake (Fig. 5.12ab). Separate vortices originate at the bow and stern sections of the wreck (Fig. 5.12a). Flow streamlines have a lower obstacle to overcome when passing through the collapsed stern and curl towards midships near the box battery (Fig. 5.12a). The stern- and bow- originating

vortices merge downstream of the wreck to form a large assymetric wake vortex. The complexity of the vortices is visible in the Q iso-surface, which captures their large, irregular and highly three-dimensional geometry (Fig. 5.12b).

The horseshoe vortex developed under the SSE current does not envelop the entire hull, unlike under the NNW current regime (Fig. 5.12 c,d). The collapsed stern section lists towards the oncoming SSE flow, presenting a surface with a shallower gradient (Fig. 5.12c,d) than the near vertical face presented to the flow in the opposite direction (Fig. 5.12a,b). This causes the inflow arm of the horseshoe vortex to pass over the wreck above the stern, rather than at the seabed around it. On the other hand, at the bow side, the vortex passes under the bow's tip and extends further downstream, similar to that under the NNW flow regime. The SSE flow causes similar, complex and asymmetric distribution of wake vortices. Under the NNW current, the wake vortices form on the portside of the hull and cover the deck along the full length of the vessel (Fig. 5.12b). When the current approaches from the opposite direction, vortices are formed at the far side of the wreck, leaving the deck area unimpacted (Fig. 5.12d). Again, this is related to the fact that the wreck presents a less substantial, smoother obstacle for the SSE flow due to its starboard list, resulting in delayed flow separation.

5.5. Discussion

We now discuss in more detail the contribution of CFD to understanding the processes driving observed geomorphic and structural changes, additional methodological considerations and, finally, the wider implications of this work for ocean engineering and heritage/environmental management.

5.5.1. CFD simulations and geomorphic change

Previous research has investigated the role of wreck orientation relative to incoming steady flows using CFD (De Hauteclocque *et al.* 2007; Quinn and Smyth 2018) and compared geomorphic changes with modelled flows at shipwreck sites using lower resolution bathymetric data (Smyth and Quinn 2014; Fernández-Montblanc *et al.* 2018b). However, the diverse geomorphology, structural complexity of the shipwreck sites, and the very high-resolution nature of the input DEMs investigated here result in the development of intricate flow and geomorphic change patterns, which have not been realised in previous studies. The novel combination of very high-resolution spatial and temporal datasets with CFD and sediment data allowed for a holistic investigation of these patterns.

Notably, wall shear stress is amplified by a factor of 4 to 5 due to the interaction of flow with both shipwrecks, which is in close agreement with previous studies of flows at shipwreck sites (Smyth and Quinn 2014) and other underwater structures (Sumer *et al.*

1997; Whitehouse 1998). Vortex shedding and the formation of a pair of counter-rotating, low-velocity vortices simulated downstream of wrecks at incidence angles of 75° observed in previous models by Quinn and Smyth (2018) are absent at our sites despite their orientations (*Barkley*: 75°- 78° , *Vanguard:* 69°-68°). Flow and the associated vorticial patterns simulated for HMS *Vanguard* are more similar to those simulated by Quinn and Smyth (2018) for a 60° incidence angle. This discrepancy may be due to the fact that, while Quinn and Smyth (2018) used an upright hull structure in their simulations, the hull of HMS *Vanguard* lists to starboard, and is located in a topographic low (i.e. the scour depression), influencing flow separation. The flow separation is stronger for the upright hull of Quinn and Smyth (2018), and results in the development of the pair of counter-rotating vortices. Similarly, the list of SS W.M. Barkley, its irregular morphology (the wreck is broken into two), and emplacement within a deep scour pit causes the development of more complex flow and vortex patterns, but counter-rotating vortices are not observed, despite the wreck's orientation. Flow and wall shear stress patterns are discussed below for both sites in the context of geomorphic change recorded in the difference models.

5.5.1.1.   SS *W.M. Barkley*

High-magnitude geomorphic change is recorded nearly everywhere in both the 4-year and one-week difference models. This corresponds well to the modelled τ_{cr} exceedance at the site (90.1% and 68.0% of the total area under the NNW and SSE currents). Therefore, it is evident that SS *W.M. Barkley* is in a live-bed scour regime (Whitehouse 1998), under the simulated spring tide currents. This process is also reflected in sand wave migration everywhere across the site, including within the scour pits.

The most substantial changes are in the area immediately surrounding the shipwreck, causing reorganisation of the scour pits and an increase of the maximum scour depth by 1.01 m. This may be explained by several factors, some possibly inter-related. Firstly, it could be that the maximum scour depth has not yet been reached, despite the wreck resting on the seabed for 102 years. Secondly, occasional high-intensity storm surges could cause increased erosion. Thirdly, the changing morphology of the disintegrating wreck structure may directly affect scour processes and patterns. Fourthly, the migrating sand dunes, which move sediment through the system, may cause dynamic reorganisation of the pits. Finally, unsteady behaviour and flow turbulence could lead to temporary fluctuations in seabed levels.

Most probably, the recorded changes and the observed distribution of the scour and depositional signatures results from some combination of these factors. However, the first possibility is unlikely, as the time of the scour development would greatly exceed previously reported timescales of scour reaching equilibrium depths at underwater

structures (Whitehouse 1998; Whitehouse *et al.* 2011; Raineault *et al.* 2013; Yao *et al.* 2021). According to Whitehouse (1998) the equilibrium scour depth, S_e, at a single vertical pile with a diameter D can be described using the relation $S_e/D = 1.3$, under the live-bed scour condition. SS *W.M. Barkley* is approximately 10 m wide and the average maximum scour depth (for the years 2015 and 2019) is 13.47 m. Despite the complexity of the shipwreck's structure compared to a monopile, these values compliment the relation of Whitehouse (1998), suggesting that the 1.01 m increase in scour pit depth may be a temporary fluctuation, rather than ongoing deepening. The simulated τ_c values are also low to moderate in the part of the pit where the maximum scour depth is recorded (Fig. 5.6a,c; Fig. 5.3a). Majcher *et al.* (2021) analysed longer time-lapse intervals and observed that between 2010 and 2015, the scour pit extending from the wreck's bow (Fig. 5.3) was infilled by sediments, rather than eroded further as shown in Fig. 5.4a. However, in terms of volumetric (Majcher *et al.* 2021) and areal changes (Fig. 5.4b), the site seems to have a negative sediment budget, hence, whilst unlikely, the possibility that scour has not reached its maximum depth cannot be completely discarded.

The influence of combined tidal and storm surge currents on bed shear stresses exacerbating erosion or deposition of sediments (the second possibility) at the sites should be also considered. The short-term difference model created for the SS *W.M. Barkley* site (Fig. 5.4c) represents changes, which happened in the one-week period, when a storm happened (29.10-03.11.2019). While sand wave migration is visible all over the site, the scour pits remain either unchanged or the changes are within the measurement errors (centimetric). Majcher *et al.* (2021) determined that wave influence has been limited at both investigated sites based on calculations involving mean wave lengths and significant wave heights recorded by a buoy located in the study area. The analysis included the storm event, which happened between the surveys in 2019. The same study (Majcher *et al.* 2021) and the investigation of Coughlan *et al.* (2021) determined that tidal currents enable the live-bed condition more than 50% of time of the year at the seabed around the SS *W.M. Barkley* site, based on the ROMS model data (Nagy *et al.* 2020) used to establish initial conditions for the simulations presented in this study. The simulations presented herein confirm that live-bed conditions exist during spring tides. Nevertheless, although the site's geomorphic change seems to be controlled by tidal currents most of the time, non-linear tide-surge interactions are known to affect the Irish Sea (Jones and Davies 2003; Olbert and Hartnett 2010) and should be considered as a factor occasionally intensifying scour processes.

The third possibility, involving feedback loops between the changing morphology of the disintegrating wreck structure and geomorphic changes is highly probable, considering the structural changes experienced by the wreck during the investigation timeframe (Fig. 5.5).

Every change in the obstacle's morphology results in some modification of flow patterns and the associated horseshoe and wake vortices. The seabed around the obstacle, in turn, responds to flow modification and more material is either deposited or eroded.

Even though the influence of migrating bedforms on the morphology of scour signatures has been deemed insignificant in a case study at a wind farm site (Couldrey *et al.* 2020), the fourth possibility seems probable, as sand dune migration across the site and inside the scour pits is recorded even in the one-week time-lapse (Fig. 5.4c). Migration is strongly exacerbated downstream of the wreck under the NNW current regime (Fig. 5.4c), in the same area where the τ_c values are highly elevated (Fig. 5.6a). As shown in Fig. 5.3, south of the wreck, the sand waves migrate in the opposite direction to the other sand waves in the area. This occurs due to the presence of the wreck and the local τ_c amplification south of the wreck under the SSE current regime, which has a weaker overall influence at the site (hence the global sand wave migration is oriented towards NNW). Nevertheless, the elaborate pathways of the sand wave migration within the pits may have caused their shifts.

Alternatively, shifts in the seabed might have been caused by unsteady flow behaviour, specifically fluctuating velocity due to turbulence and vortices developed around the shipwreck. Under the NNW regime, the horseshoe vortex is developed inside a trench between the depositional signature and the wreck (Fig. 5.3a) and essentially prevents the wreck from being covered with sediments on its starboard side (Fig. 5.7b). Under the SSE regime, the horseshoe vortex is developed only midships, and this corresponds to the high wall shear stress exerted on the depositional zone near its portside (Fig. 5.6c, 1) and subsequent erosion of sediments (Fig. 5.4a). High τ_c is also exerted downstream of the wreck on the depositional mound adjacent to the wreck's starboard, where the wake vortices are formed (Fig. 5.6c). In the same place, the highest bathymetric change (-4.9 m) is recorded between the years 2015 and 2019 (Fig. 5.4a). Altogether, the formation of vortices clearly influences the τ_c values around the wreck, which causes further reorganisation of sediments.

5.5.1.2.   HMS *Vanguard*

In contrast to the *Barkley* site, at the HMS *Vanguard* site, the seabed is only highly mobile outside the main scour pit (Fig. 5.9a). According to the CFD simulations, τ_{cr} is not exceeded at the gravel bed, encompassing a significant portion of the computational domain. We propose that the site was initially characterised by live-bed scour conditions, which waned as the gravel lag was exposed by erosion. This resulted in the site reaching a somewhat combined clear-water and live-bed scour condition under strong spring tide currents, where no bedform migration is observed within the erosional signature but is observed elsewhere around the site.

However, τ_{cr} is exceeded at some parts of the depositional zone extending from both sides of the wreck (Fig. 5.8a, Fig. 5.11), where no geomorphic change is recorded (Fig. 5.9a). Although we assumed that the depositional zone consists of redeposited fine sand, it is possible that the sandy sediment is mixed with fine gravel from the main scour pit or contains a shell fraction (or a combination of both). McCarron *et al.* (2019) estimated that τ_{cr} of sand in sand-gravel mixtures can be increased by up to 75% due to the hiding-exposure effect, which modifies the critical shear stress of individual grain classes in sediment mixtures depending on the grain size distribution. Additionally, Whitehouse (1998) noted the influence of slope on the critical shear stress required to mobilise sediments, which can be described using the relation: $\tau_{\beta cr}/\tau_{cr} = sin\,(\Phi_i + \beta)/sin\,(\Phi_i)$, where $\tau_{\beta cr}$ is the corrected critical shear stress, β is the is the local bedslope in the along flow direction (in degrees) and Φ_i is the angle of repose (32° by default; Soulsby 1997). The average slope within the depositional zones here (Fig. 5.8a, Fig. 5.8c) is 12.6°. Therefore, the relation suggests that the corrected critical shear stress required to mobilise sediments at the depositional zone, can be up to 32.5% higher. These factors combined may explain why the depositional zone remains largely unchanged over the survey period, despite the modelled critical shear stress exceedance.

Nevertheless, some localised geomorphic changes are visible around the wreck extending from its collapsed mainmast (-0.5 m) and at the portside (+/- 0.7 m) (Fig. 5.9a). Both are most probably related to the development of vortices around the wreck, and in particular, horseshoe vortices (Fig. 5.12b,d). They envelop the wreck causing its entrenchment between the depositional zones, which would otherwise (with less developed horseshoe vortices) most probably partially bury its structure. The erosional change extending from the tip of the collapsed mainmast may have happened due to the lowering of the mainmast itself (Fig. 5.10c). Another possibility is that erosion of the sediment caused the displacement of the mast. Certainly, a feedback loop exists between these two processes and flow patterns, discussed in more detail below.

5.5.2. CFD simulations and structural change

To the authors' knowledge this is the first published investigation that attempts to correlate outputs from CFD simulations with recorded structural changes (deterioration) of historic shipwrecks. Here we discuss how the modelled flow patterns and distribution of wall shear stresses may have affected the wrecks. Simulated pressure distributions on the shipwreck structures are included to support this discussion. Of note, the complexity of the physical processes affecting the sites, which may involve storm surges, varying tidal currents, and destructive anthropogenic impacts (e.g., bottom trawling) cannot be neglected when discussing damage sustained by the wreck structures. The simulated spring tide currents

cannot be considered as representative of this wide range of processes. Therefore, the CFD outputs are discussed here to identify simulated flow characteristics which may have contributed to the collapse of parts of the shipwrecks, rather than having directly caused the damage.

5.5.2.1.   SS *W.M. Barkley*

The most substantial damage experienced by SS *W.M. Barkley* between 2015 and 2019 happened at the portside of the counter stern, where a significant portion of the gunwale collapsed and now leans against the seabed (Fig. 5.5b, Fig. 5.5c, box 1). This coincides with the area of the highest modelled mean wall shear stresses (Fig. 5.6a, 1) under the NNW current regime. Additionally, strong flow separation and formation of wake vortices occurs over the gunwale (Fig. 5.7a, b) and the whole counter stern is exposed to the highest pressures of all the structural elements of the wreck (Fig. 5.13a, box 1). Clearly, flows had exerted increased friction (induced by wall shear stresses) and pressure drags on the gunwale during energetic tidal periods (i.e. spring tides). This may have gradually weakened it with the aid of corrosion, resulting in its failure, possibly during a storm event. Longer-term, the wreck's counter stern may be prone to further damage, ultimately leading to its complete collapse.

Although the damage sustained by the wreck's bow section (Fig. 5.5c, box 2) is deemed uncertain due to the subjectivity introduced during point cloud cleaning, increased wall shear stresses are modelled here under the SSE current regime (Fig. 5.6c, 1). This part of the wreck is also highly exposed and therefore, these structural changes remain probable.

5.5.2.2.   HMS *Vanguard*

During the 2015-2019 interval, HMS *Vanguard* sustained damage to three, possibly four, parts of its structure (Fig. 5.10c). The displacement of the portside gunwale near the box battery (Fig. 5.10c, box 1) can be correlated with the increased wall shear stresses exerted on elevated sections under both current regimes (Fig. 5.11a, 1; Fig. 5.11c, 1). The change in the collapsed gunwale at the stern section (Fig. 5.10c, box 2) coincides with increased shear stresses under both current directions (Fig. 5.11a, 1; Fig. 5.11c, 1) and with an elevated pressure zone (Fig. 5.13b, box 1). Similar to SS *W.M. Barkley*, the combination of these may have created a drag force causing gradual wear of the gunwale, contributing to its eventual displacement.
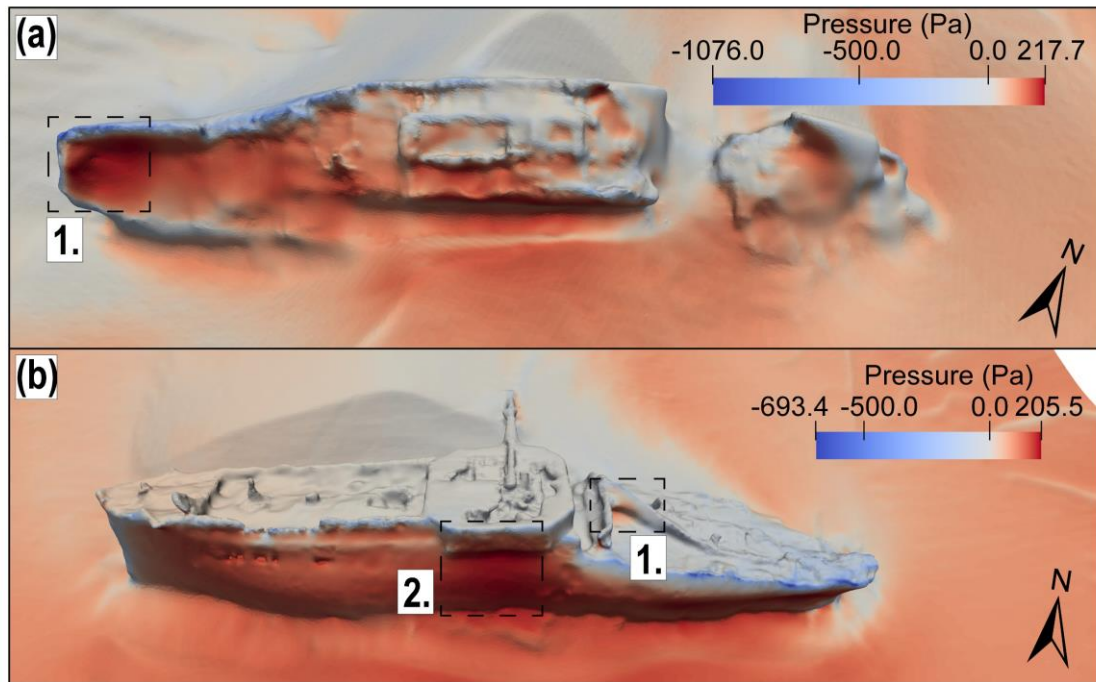
Figure 5.13. Simulated pressure distributions under the NNW current regimes for the (a) SS *W.M. Barkley* site and (b) HMS *Vanguard* site. Hydrostatic pressure contribution is omitted.

The wreck's mainmast, leaning on the seabed, has been lowered by approximately 0.30 m (Fig. 5.10c, box 3). Two mechanisms are possible here: either the mast was lowered before erosion of the seabed or seabed scour caused the lowering of the mast (Fig. 5.10c, boxes 3 and 4). As some seabed fluctuations are also recorded on the opposite side of the wreck (Fig. 5.9a), the scouring mechanism is probable. The complex arrangement of wake and horseshoe vortices (Fig. 5.12) (Sumer *et al.* 1997; Dixen *et al.* 2013; Lee and Hong 2019), changing tidal currents (neap and spring) together with the possible influence of combined tidal and storm surge currents may have caused the changes in scour equilibrium, promoting further erosion at the mast's tip and its subsequent lowering.

Although the box battery changes could result from the point cloud cleaning (Fig. 5.10c, box 5), they are probably real considering the fragile state of its upper part. The upstanding, bluff body of the box battery is the highest part of the wreck and increased wall shear stresses are simulated at this structure under the SSE current (Fig. 5.11c, 1). Even though this part of the shipwreck is very well preserved, the highest pressure is exerted on the portside of the hull under the box battery by the oncoming NNW current (Fig. 5.13b, box 2). The flow-exerted pressure together with the weight of the heavily armoured box battery and the existing hull damage (impact hole, crack across the stern; Fig. 5.10a) could contribute to an eventual collapse of the hull structure underneath, for example during a severe storm event.

5.5.3. Methodological considerations

Numerical modelling of fluid flows over any complex terrain involves multiple considerations (Wakes *et al.* 2010; Blocken *et al.* 2015; Smyth 2016; Blocken 2018; Grau-Bové *et al.* 2019). Our study has partially explored some of them, particularly in relation to obtaining current speed and direction in tidally-influenced moderate depth shelf-sea and mesh resolution for complex wreck structures. Additional remarks are made on structural change detection using high-resolution MBES data to supplement methodological considerations previously discussed in (Quinn and Boland 2010; Bates *et al.* 2011; Plets *et al.* 2011; Astley 2016; Westley *et al.* 2019; Majcher *et al.* 2020).

5.5.3.1. CFD simulations

The choice of initial conditions (i.e. input current velocity profiles, turbulence kinetic energy and dissipation rate and roughness length parameter) can inevitably influence the results of the simulations. Here we attempted to mimic real ocean conditions using all available information (i.e. regional ocean current data of Nagy *et al.* (2020), sediment data, high-resolution bathymetry). However, some simplifications and assumptions were necessary to make the modelling feasible. The choice of the 90th percentile current speed coming from two dominant directions obtained at one grid node of a regional scale oceanographic model is a simplification considering the tidal harmonics in the region (Lewis *et al.* 2015, 2017). Nevertheless, the results show good agreement between the observed geomorphological features (sand waves and scour marks), geomorphic changes and the modelled currents, suggesting that the chosen flow directions were suitable. The inlet velocity profiles and turbulence, which influence simulated wall shear stresses (used to assess sediment mobility) were also in agreement with presence or absence of geomorphic changes observed in the difference models. Another measure to improve the quality and accuracy of the simulations was to use the extended upstream fetch domains meshed over the regional bathymetry (Fig. 5.2) to develop the flows, before imposing the initial conditions at the inlets to the main computational domains.

Additionally, it is noted that the results of the grid independence study show some considerable (>1%) differences between flow variables modelled at the fine and medium resolution meshes (see supplementary material) . Although these differences were deemed insignificant for the purpose of this research, guidelines and norms for achieving grid independence for this type of CFD simulation (i.e. involving highly complex topography derived from remote sensing data) should be established for standardization. Further refinement of CFD domains here was deemed unfeasible, as the computational costs of multiple simulations performed in this study would become prohibitive.

Nevertheless, more research should be conducted into the influence of the choice of the turbulence closure, initial conditions and domain resolution on the results of site-scale underwater CFD simulations. Ideally, such investigations could not only be compared against observed geomorphic changes and geomorphology, but also validated with physical modelling (e.g. Yiannoukos *et al.*, 2020) or with *in-situ* data (e.g. Unsworth *et al.*, 2020), capturing speeds and directions of currents and flow turbulence at several strategic locations at a site.

5.5.3.2.   Structural change

In this paper, dense, MBES-derived point clouds corresponding to repeat bathymetric surveys were used to assess changes in shipwreck structures. Although major structural changes were straightforward to validate in the difference models, some detected changes may be associated with the subjective point cloud cleaning process. Ideally, structural changes registered in such difference models should be further validated with either visual inspection by a diver or a remotely operated vehicle using video recording, photogrammetry or laser-line scanning techniques (Johnson *et al.* 2020). However such operations remain costly and difficult, especially at nearly intact metal-hulled wreck sites (e.g. Nornes *et al.* 2015) with low water visibility (e.g. Pacheco-Ruiz *et al.* 2018), and strong currents like the ones investigated here.

5.5.4. Implications

This investigation has clearly demonstrated the links which exist between the sediment- and hydro-dynamic environment and stability of complex underwater structures like shipwrecks. This was made possible through the multi-disciplinary methodology involving repeat, high-resolution hydrographic surveys designed to capture shipwreck sites at their full extent, CFD simulations with MBES data-derived stereolithography representations of the sites, regional ocean current data and sediment information obtained from grab samples.

Given that shipwrecks are of interest to multiple stakeholders in the marine environment, our methods and observation have applications in the following:

1. Distribution of simulated wall shear stresses and pressures at shipwreck structures gives hints about areas potentially prone to structural damage. Thus, CFD outputs in conjunction with bathymetry-derived models could inform more sophisticated engineering models involving finite element analysis (Foecke *et al.* 2010) to predict long-term deterioration.

2. The approach developed here could be used in heritage condition assessments to capture the physical state of historically significant sites, identify threats and assess the viability of long-term, *in-situ* preservation (Gregory and Manders 2015a;

Gregory 2020). Importantly, by incorporating high to very high-resolution data, it enables an empirical assessment of intra-site vulnerability (e.g. identification of damage to specific wreck elements), a level of detail which goes beyond many existing condition assessments. This in turn enables more precise assignation of responsive management actions, such as targeted recording of vulnerable structures.

3. Similarly, these observations can aid environmental risk assessments of potentially polluting wrecks, which should involve investigation of geohazards i.e. seabed stability, the influence of currents and waves (Ventikos *et al.* 2016; Goodsir *et al.* 2019; Hac and Sarna 2021; Szafrańska *et al.* 2021) as well as ideally considering the stability of the wreck structure itself, and thus the likelihood of deterioration-induced pollution release.

4. Gathering information about the geotechnical parameters of the seabed is important for the developments of offshore infrastructure. Together with natural bedforms (Stow *et al.* 2009; Van Landeghem *et al.* 2009b, 2012), shipwrecks act as proxies indicating dominant current directions (Caston 1979; Garlan *et al.* 2015) and susceptibility of the seabed to scour when complex man-made objects are introduced. Detailed investigations as performed here can provide valuable information for planning new developments.

5. Taking into consideration all the points outlined above, the combined methodology can inform marine spatial planning, which should include shipwrecks as they are an inherent component of the underwater landscape (Papageorgiou 2018).

5.6. Conclusions

In this study, we combined very high resolution repeat bathymetric surfaces and point clouds with modelled oceanographic current and sediment substrate data, to provide inputs for CFD simulations and assess how sediment- and hydro-dynamic settings affect wreck site stability. We demonstrated that this integrated methodology can be used to predict live-bed or clear-water scour conditions, which control geomorphic change at submerged wreck sites, and explain patterns of sediment erosion and deposition. Additionally, some interrelations between flow patterns, exerted wall shear stresses, pressures and structural changes (i.e. deterioration) in shipwrecks were observed, suggesting that the combination of methods can help to identify wreck parts prone for accelerated wear. We propose that the methods presented and resulting observations can not only aid archaeological assessments and management of potentially polluting shipwrecks, but also inform ocean engineering.

.

6. Discussion

6.1. Outline

This PhD project aimed to extend the knowledge of shipwreck site formation processes, focusing on physical processes, comprising coupled hydro- and sediment-dynamic factors. In order to do that, very high-resolution bathymetric, seismic, geological and oceanographic data were collected and analysed over ten metal-hulled shipwreck sites, located in different parts of the Irish Sea, and characterized by contrasting seabed environments.

6.2. Key findings and implications

6.2.1. Objective 1: To objectively map geomorphological and scour features at shipwreck sites

The importance of understanding geological and other environmental factors affecting submerged sites has been recognized since the early development of underwater archaeology and shipwreck science (Frost 1961; Muckelroy 1978). Sediment erosion and deposition can cause either burial of sites or their exposure to the oxygenated water column. Therefore these sediment-dynamic processes control the rate of corrosion and can either enable or disable/limit biological processes such as the development of encrustation (Ward *et al.* 1999). The distribution and alignment of depositional and erosional features around shipwrecks not only provide key indicators of sediment-dynamics, but as their form and occurrence are inherently dependant on waves and currents, they act as proxies of local hydro-dynamic settings (Caston 1979; Stow *et al.* 2009).

In order to be understood, these features first need to be demarcated and classified, i.e. separated from other features present at a site. This can be performed manually through digitisation, which relies on visual tracing of features in a digital elevation model. However, this process is laborious and highly subjective. Therefore, the first objective of this thesis was to delineate these geomorphological features objectively and efficiently, separating erosional and depositional signatures around wrecks in DEMs derived from the high-resolution MBES data.

To delineate features objectively, unique attributes common to the target features, but absent from other geomorphological signatures, were identified in the DEMs. One such attribute is the spatial scale at which these features develop. For instance, objective separation of fine-scale (tens of metres wide) features from broad-scale (hundreds of metres wide) features creates classes containing potentially related geomorphologies of similar size, effectively narrowing down the possibilities in further separation. This idea of segregating geomorphological features based on their spatial scales is not new and has been used extensively with DEMs to map terrestrial (Guisan *et al.* 1999; Weiss 2001) and underwater (Walbridge *et al.* 2018) habitats, to separate drumlins (Hiller and Smith 2008), seamounts and islands (Wessel 1998, 2016), and map small-scale

features for efficient archaeological prospection (Hesse 2010). Essentially, all these case studies utilised the technique called DEM high-pass filtering or Residual Relief Separation.

In this thesis (see chapter 3), the high-pass filtering technique was adjusted and applied to separate wreck marks from the regional geomorphology (Fig. 3.4). An additional validating step was also proposed. Although this step is based on manual inspection of the high-pass filtering results, it uses a set of visualization techniques derived from the original DEM (focal standard deviations, slope, aspect, multidirectional hillshade, Sobel; Fig. 3.5), increasing the objectivity of the validation. The methodology is proven to be time-efficient, and is semi-automatic and objective, as it relies on statistical comparisons (high-pass filtering relies on computing focal statistics; eq. 3.1). Notably, all steps in the methodology can be performed using widely available GIS software, including open-source packages like QGIS.

Although this method was tested to separate wreck marks from the regional geomorphology, it can be applied to delineate any seabed features in high-resolution DEMs. Fig. 6.1 shows how various high-pass filtering kernel sizes delineate different morphologies. Fig. 6.1a and 6.1b represent DEMs of the seabed off Belfast Lough in proximity to the SS *Tiberia* site and off Dublin, around the SS *W.M. Barkley* site; both characterized by diverse geomorphological features. The coarser spatial resolution (2 m) and geometric similarity of all the geomorphological features in the Belfast Lough DEM (Fig. 6.1a) enabled simultaneous delineation of sediment waves of various sizes and wavelengths (however, all of them have similarly steep crests) and wreck marks extending from the SS *Tiberia* site (Fig. 6.1c). On the other hand, the vast scour pit developed around SS *W.M. Barkley* could not be delineated with the same filter from the sediment waves at the site, as their spatial scales are different (hundreds of metres versus a few metres) (Fig. 6.1d). This demonstrates both the versatility and limitation of the Residual Relief Modelling methodology.

Highly diverse geomorphologies of various length-scales can be easily delineated using various filter kernel sizes, like at the SS *W.M. Barkley* site (Fig. 6.1d). However, if non-related features have similar length-scales (like in Belfast Lough; Fig. 6.1a), the Residual Relief Modelling can only serve to separate them from the features of other length-scales, but not from each other. Features of similar length-scales can be classified further with the third, non-automated step of the methodology, involving validation of the Residual Relief Modelling results guided by DEM visualization techniques.
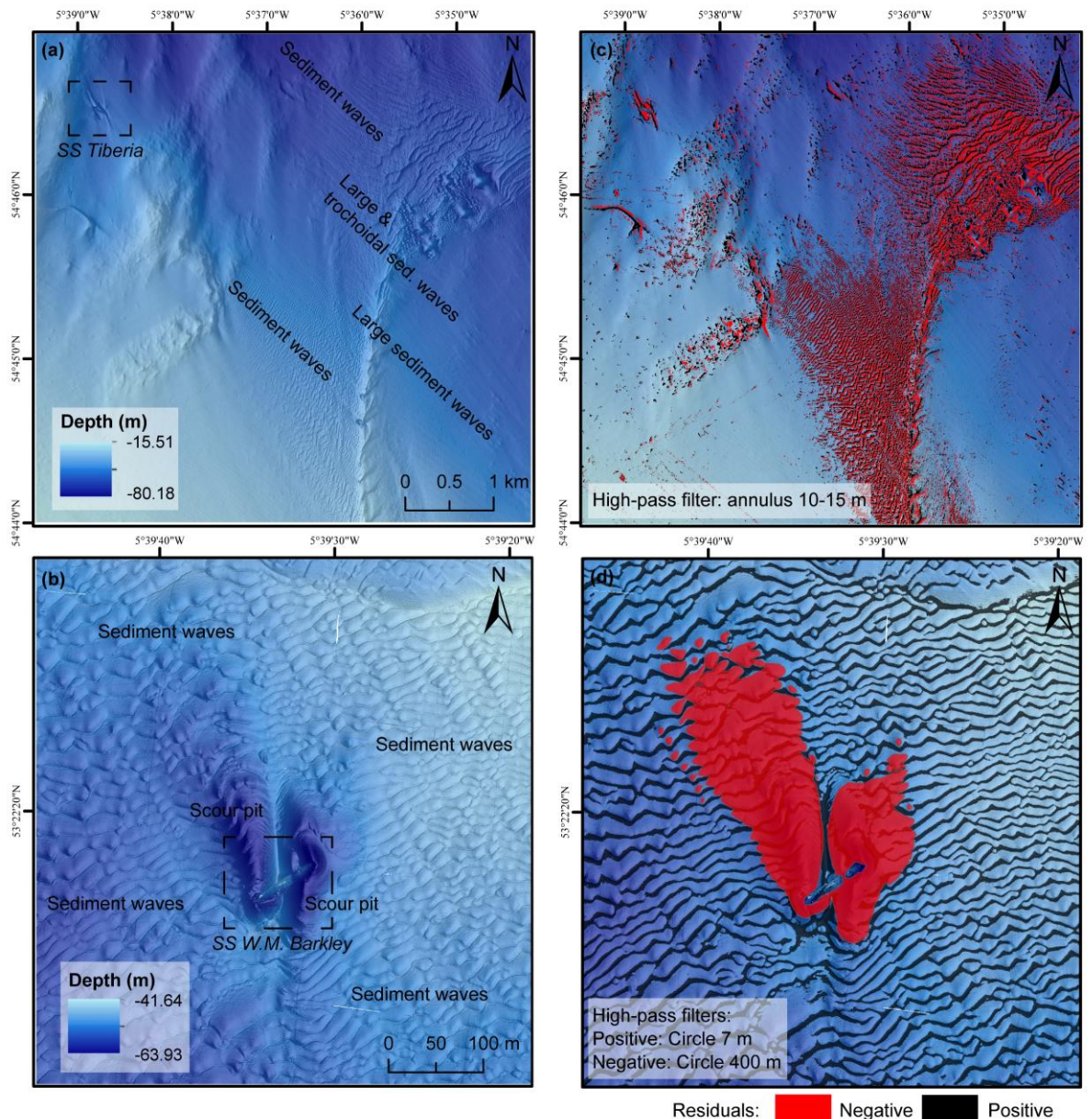
Figure 6.1. The Residual Relief Modelling workflow applied to two different datasets: (a) the seabed off Belfast Lough near the SS *Tiberia* site (spatial resolution of 2 m); data courtesy of Royal Navy (public sector information, licensed under the Open Government License v2.0), (b) regional dataset for the SS *W.M. Barkley* site (spatial resolution of 0.5 m). An annulus filter with the inner radius of 10 m and the outer radius of 15 m was applied to the dataset off Belfast Lough (c) and circular filters with radii of 7 and 400 m were applied to the SS *W.M. Barkley* regional dataset (d).

Importantly, in order to assure reproducibility of results, the applied filter type (annulus, circle etc.) and size (radii) together with breakpoints for the preliminary classification (see sections 3.2.3.1 and 3.2.3.2) should always be reported. The capability of the method to delineate features of various spatial scales is associated with one fundamental flaw: using even a slightly different filtering window alters the delineated features (i.e. their total areas, extents). Therefore, the method is only objective when all the key parameters used when applying the workflow, are reported. It is also important to consider the resolution of the original DEM: delineating fine-scale

features in low-resolution data may be difficult as their true relief is not retained. All these considerations imply that the results must be carefully reviewed and that the validation process using the DEM visualization techniques is inherent to the workflow.

6.2.2. Objective 2: To characterise the evolution of shipwreck sites through observations of geomorphic change and assessing environmental parameters

After developing and applying the residual relief modelling method for characterization of the shipwreck sites, their dynamism was investigated. Dynamism is controlled by the hydro- and sediment-dynamic environment and has important implications for *in-situ* preservation of underwater sites. As highlighted previously, continuous or instantaneous shifts in sediments can cause either burial or exposure of sites, thus they impart control on biological and chemical formation processes (Ward *et al.* 1999). Such shifts are also associated with changing forces exerted on the shipwreck's hull. Sediment partially or fully covering a shipwreck can be considered as a static (or dead) load. A sudden or continuous seabed change due to a build-up of a depositional mound, progression of sediment waves or seabed scour can not only endanger the wreck's stability, but also crush its unmaintained, corroded and consequently brittle structure, which is not able to withstand large dead loads.

Shipwreck sites may therefore be considered as process-response systems, at some state of equilibrium with their surrounding environment. The seabed movement (also referred to as geomorphic change) and the associated sediment budget change (Ward *et al.* 1999) may affect this equilibrium and either cause the whole site to reach a new equilibrium state or retain the current one, depending on the system's capacity to absorb the disruption (Quinn and Boland 2010). Geomorphic change can operate at various temporal- and spatial-scales, depending on the current and wave regime in the area, geological settings, underlying substrates and other environmental and morphometric characteristics of the site. These complexities led the development of the second objective of the thesis, which focused on characterising the evolution of the shipwreck sites through the investigation of local geological and oceanographic settings and recording and investigating geomorphic change at local and regional spatial scales and four temporal scales: 1 week, annual, inter-annual (4-5 years) and decadal.

Difference modelling using high-resolution DEMs from MBES surveys performed in 2010, 2015, 2016 and 2019 was at the core of the investigation (see chapter 4). Similar workflows involving difference modelling using time-lapse MBES data have been previously applied to historic wreck sites (Quinn and Boland 2010; Bates *et al.* 2011; Stieglitz and Waterson 2013; Astley *et al.* 2014; Astley 2016; Brennan *et al.* 2016; Fernández-Montblanc *et al.* 2016). However, in this thesis the number of shipwrecks investigated, their location within the same shelf-sea, at similar, moderate depths and times of residence at the seabed, together with the uniform high quality of the DEMs

accompanied by sediment, seismic and oceanographic data, all collected with the same strategy, allowed investigation of the physical processes acting *in-situ,* with near laboratory conditions.

The key finding of this part of the thesis is that although the wrecks are all located within the same geographic region, they are affected by very different rates of geomorphic change and therefore the dynamism at the sites also varies substantially (Table 6.1). This potentially has critical implications for the *in-situ* preservation of the shipwrecks and should be taken into consideration when managing sites.

Table 6.1. Key outcomes of the time-lapse analysis for the investigated shipwreck sites.

Shipwreck	Dominant substrate	Scour marks	Geomorphic change	Scour regime	State	Other influences	Equilibrium
RMS Leinster	Sand	Yes	High magnitude	Live-bed	Almost completely buried	-	Dynamic
SS *Hare*	Sand	Yes	High magnitude	Live-bed	Partly buried	-	Dynamic
SS *W.M. Barkley*	Sand	Yes	High magnitude	Live-bed	Partly buried	-	Dynamic
HMS *Vanguard*	Sand and Gravel	Yes	High magnitude only outside of scour	Live-bed/clear-water	Exposed	-	Nearly static
SS *Chirripo*	Multimodal	Only deposition	No change	Clear-water	Exposed	Pockmark-like features	Static
SS *Tiberia*	Multimodal	Yes	Low magnitude	Clear-water	Exposed	-	Nearly static
SS *Polwell*	Multimodal	Yes	Low magnitude	Clear-water	Exposed	Pipeline within scour marks	Nearly static
FV *St. Michan*	Multimodal	Yes	Low magnitude	Clear-water	Exposed	Bottom trawling	Nearly static
SS *Lugano*	Gravel	Only deposition	No data	No data/ clear-water?	Exposed	-	No data
SS *Santa Maria*	Gravel	Yes	No data	No data/ clear-water?	Exposed	-	No data

Furthermore, it was observed that sandy sites are generally the most dynamic among those investigated. This is due to frequent exceedance of critical shear stress required to mobilise sediments. The sites investigated in the Irish Sea are clearly characterized by live-bed scour conditions (Whitehouse 1998). The high seabed mobility is expressed in sediment wave migration at all these sites, recorded in both short-term, weekly and long-term, annual, multi-annual and

decadal difference models. The sediment wave trains may contribute to the reorganization of scour pits, especially at sites like SS *Hare* and SS *W.M. Barkley*, where changes in scour pits are the most pronounced. This suggests that the state of these shipwrecks as a system changes frequently, reaching new equilibria as sediment material is delivered to and transported from the sites. HMS *Vanguard* is an exception among the sandy sites, as the base of its comet-shaped scour pit comprises an erosion-resistant, exposed gravel lag. Therefore, the dynamism at this site is significantly lower than at the other sandy sites. This state of equilibrium has probably been achieved some time after the wreck's residence on the seabed (a few years e.g. Raineault *et al.* (2013)).

On the other hand, multimodal sites are all nearly completely static, and characterized by clear-water scour conditions (Whitehouse 1998). High dynamism affected these sites only in the initial phase of their site formation, when the scour pits were being developed. At the site of SS *Chirripo*, almost no erosion has happened at all, and the seabed stability has ensured that the wreck is nearly intact (most of the damage sustained by the wreck happened due to salvage operations; Cotswold Archaeology 2015). However, it is demonstrated that such sites can still be affected by anthropogenic impacts (salvage at SS *Chirripo*; pipeline laying at SS *Polwell*, and commercial fishing at FV *St. Michan*), as they lie exposed on the seabed.

Additionally, although the full exposure of wrecks with nearly stable conditions on the seabed is associated with some factors favouring preservation (i.e. no change in dead loads, no periodic burial/exposure, structural stability), the physical (abrasive hydro-dynamic action), chemical and biological processes cannot be neglected. In Fig. 4.11. it is speculated that wrecks characterised by nearly static conditions have a higher *in-situ* preservation potential than those located in dynamic settings. These sites, however, are also characterised by negative disequilibrium, as they are left exposed with virtually no protection against hydro-dynamic action or corrosion. In one of the pioneering site formation classifications, Muckelroy (1977) distinguished class 1 sites, which become buried within static sediments a short time after their deposition, with no further disturbance. According to the author, such sites are characterized by the best preservation potential. However, Muckelroy (1977) also highlights that stability of sediments is essential to retain the class 1 categorization, as drastic sediment shifts can harm a site as effectively as forces encountered by any exposed site on rocky beds. This supports the predictions presented in Fig. 4.11; although the sandy sites are semi-buried, seabed movement causes their rapid deterioration and loss of structure. Destructive forces generated by geomorphic change seem to affect these sites more than the hydro-dynamic, chemical and biological processes affecting exposed multimodal sites. This is expressed in their appearance and condition; while the multimodal and gravel sites stand proud on the seabed, the sand-dominated sites are somewhat scattered and do not retain their original integrity.

6.2.3. Objective 3: To model and characterize flow regimes around complex shipwreck structures

The remains of metal-hulled vessels, like those investigated in this thesis, are not only important from a historical perspective but are also associated with environmental risks, as they may contain unexploded ordnance, fuels, oils, lubricants and other chemicals detrimental to the natural environment (Michel *et al.* 2005; Landquist *et al.* 2013; Ndungu *et al.* 2017; Goodsir *et al.* 2019; Carter *et al.* 2021). These shipwrecks are relatively young and, as they were constructed using metals, they often remain nearly intact on the seabed. Their substantial size causes significant disruption to local hydrodynamics, resulting in pronounced seabed scouring. In turn, scour jeopardises the stability of wrecks. This feedback loop exists not only at shipwrecks sites, but also at other objects emplaced on the seabed. The current rapid energy transition from fossil fuels to efficient, sustainable sources puts offshore renewables in the spotlight. So far, offshore wind farm developments have assumed a central role in the marine renewable energy sector; however, there are still challenges to be resolved (Kallehave *et al.* 2015). Among them are environmental factors which affect the lifespan of individual turbines (Harris *et al.* 2011), as they are often exposed to far more extreme conditions at sea compared to any terrestrial development. These environmental factors comprise the hydro- and sediment-dynamic settings, similar to those acting at shipwreck sites. As shipwrecks have been deposited at the seabed and unmaintained for many years, examining their state of preservation and forces affecting them can potentially provide information for such offshore developments, aiding turbine siting and design optimisation. This possibility is especially worth investigating and should not be neglected, taking into account the sheer number of shipwrecks worldwide and their presence in every sea where renewable developments are considered.

All these points, spanning across disciplines related to ocean engineering, underwater archaeology, and environmental science led to the development of the third objective of this thesis, aiming to model and understand flow patterns at shipwreck sites in detail. Two sites were chosen: HMS *Vanguard* and SS *W.M. Barkley*, representing similar environmental settings, but characterized by different site dynamism, as determined by the preceding investigation of geomorphic change using difference modelling. Both sites are situated in sand wave fields dominated by sandy sediments and characterized by bi-directional tidal currents of similar magnitudes. However, while the seabed around HMS *Vanguard* has remained relatively static between 2015 and 2019, the sediments around SS *W.M. Barkley* underwent significant mobilisation, erosion and deposition. In order to understand these differences, CFD modelling was implemented.

Numerical modelling has been increasingly used in conjunction with hydrographic data to investigate detailed patterns of water flow and turbulence around wrecks and other manmade

structures and to analyse factors driving geomorphic change and site evolution (Dix *et al.* 2009a; Smyth and Quinn 2014; Fernández-Montblanc *et al.* 2018b; Couldrey *et al.* 2020). In this investigation, high-resolution digital elevation model and point cloud data were used to construct 3D representations of the shipwreck sites. The CFD simulations were conducted at computational domains constructed on the 3D geometries of the sites with an unprecedented resolution (centimetric cell height close to the seabed). Additionally, the initial conditions were informed using data from a broad-scale oceanographic model (Nagy *et al.* 2020) and sediment information obtained through the analysis of grab samples. Finally, the dense point clouds derived from the time-lapse MBES surveys allowed for difference modelling of structural changes experienced by the wrecks between 2015 and 2019.

The main outcome of this part of the thesis is that the simulations were capable of predicting scour regimes at the sites, namely live-bed and clear-water scour conditions. As evidenced by the weekly, annual, multi-annual and decadal difference models, the SS *W.M. Barkley* site undergoes continuous, high-magnitude geomorphic changes associated with sand wave migration and deepening/infilling of scour pits and depositional ridges. Some of these changes happen very close (<1 m distance) to the shipwreck. This corresponds well to the critical shear stress exceedance modelled nearly everywhere across the site. On the other hand, at the HMS *Vanguard* site, the critical shear stress is exceeded only outside the main scour pit, which itself consists of an erosion-resistant gravel layer. Although the bed shear stresses in this region of the site cannot mobilise gravel, they are too high to permit entrainment of the sand waves migrating across the surrounding seabed (Fig. 5.9 and Fig. 5.11a,c). Therefore, there is no supply of sediments to the area immediately surrounding the wreck, ensuring quasi-stability of the site (only minor, submetre geomorphic changes occur due to the flow turbulence).

These differences in flow patterns and geomorphic change between sites result in the different distribution of wrecks on the seabed and may influence *in-situ* preservation. The shipwreck of SS *W.M. Barkley* is broken up, less coherent than that of HMS *Vanguard* and partly buried on its portside. According to sport divers' reports, sediments are also present on the portside in the wreck's interior (S. Andrews, personal communication, February 12, 2021). On the other hand, the wreck of HMS *Vanguard* is nearly intact, largely exposed to the water column and retaining much of its original integrity, despite residing on the seabed for 42 years longer. Noteworthy, these two wrecks differ significantly with regards to primary construction materials (steel; SS *W.M. Barkley*, iron and wood; HMS *Vanguard*), their purpose (merchant ship/naval warship) and cause of sinking (torpedo strike/collision). Although their current state of preservation results from some combination of these factors and characteristics, the local hydro- and sediment-dynamic settings have inevitably influenced the wrecks.

Both wrecks also experienced substantial structural changes over the investigated period (2015-2019). SS *W.M. Barkley* lost a portion of her portside gunwale near the counter stern (Fig. 5.5c, box 1) and possibly parts of her bow (Fig. 5.5c, box 2). HMS *Vanguard* underwent less severe damage, albeit at four distinct regions (Fig. 5.10c, boxes 1-5). These regions of damage correspond well to the zones of elevated wall shear stress (Fig. 5.6 and Fig. 5.11) and pressure (Fig. 5.13) simulated in CFD models. Therefore, it is possible that hydrodynamic wear also contributes significantly to the observed state of the sites.

Nevertheless, the study demonstrates that knowledge of the underlying hydro- and sediment-dynamic regime at an underwater site is paramount for understanding its preservation. It is clear that while HMS *Vanguard* will gradually deteriorate due to corrosion and hydro-dynamic processes, the influence of geomorphic change at the site is limited. On the other hand, the situation at the SS *W.M. Barkley* site is much more dynamic and seabed instabilities may lead to abrupt structural changes in the future. These conclusions were realised due to the integration of remote sensing and modelling datasets with CFD simulations, which inevitably enhance site formation assessments.

CFD simulations presented in this study identify areas at underwater sites where sediment mobility and structural wear are enhanced. Therefore, this technique can not only aid archaeological investigation, but also environmental risk assessments. Currently, 8569 shipwrecks worldwide are identified as potentially polluting (Michel *et al.* 2005; Carter *et al.* 2021), with the majority dating from World War 2. Many of these sites will require systematic monitoring and the establishment of management strategies to mitigate against pollution. One example of a relatively inexpensive *in-situ* solution for preventing oil leaks from shipwrecks is capping (Fig. 6.2a) (Alcaro *et al.* 2007; Hac and Sarna 2021). Capping aims to completely cover a potentially polluting shipwreck to avoid leakage of pollutants into the marine environment. Capping material consists of a specially prepared mixture of sediments and other materials, ensuring low permeability of the mound and providing conditions which facilitate the eventual hydrolysis of the pollutants (Alcaro *et al.* 2007). It is paramount to ensure that the capping material deposited on the wreck will remain erosion-resistant. CFD simulations involving 3D meshes of shipwrecks constructed with high-resolution MBES data can inevitably support such endeavours, by predicting the patterns of flow, turbulence, and regions of elevated bed shear stress and pressure. One of the advantages of CFD is that the triangulated meshes representing shipwreck sites in simulations can be easily modified to incorporate planned pollutant spill prevention or *in-situ* preservation developments. For example, if the wreck of the oil tanker SS *Santa Maria* investigated in this thesis was to be capped, the stereolithography mesh representing the site, constructed using the MBES data (Fig. 6.2b) could be modified to include the material deposited during the capping operation (Fig. 6.2c). CFD could then be used with both meshes to simulate changes in flow patterns and identify areas susceptible to erosion. Similarly, examining

how the introduction of *in-situ* scour-prevention measures like polypropylene nets and geotextiles to the site (Gregory *et al.* 2014; Gregory and Manders 2015a; Pournou 2017) changes flow patterns and exerted forces could be conducted using CFD. This approach is widely utilised in design optimisation for offshore, inland water and terrestrial developments (Sumer 2007; Shives and Crawford 2014; Sun *et al.* 2019).
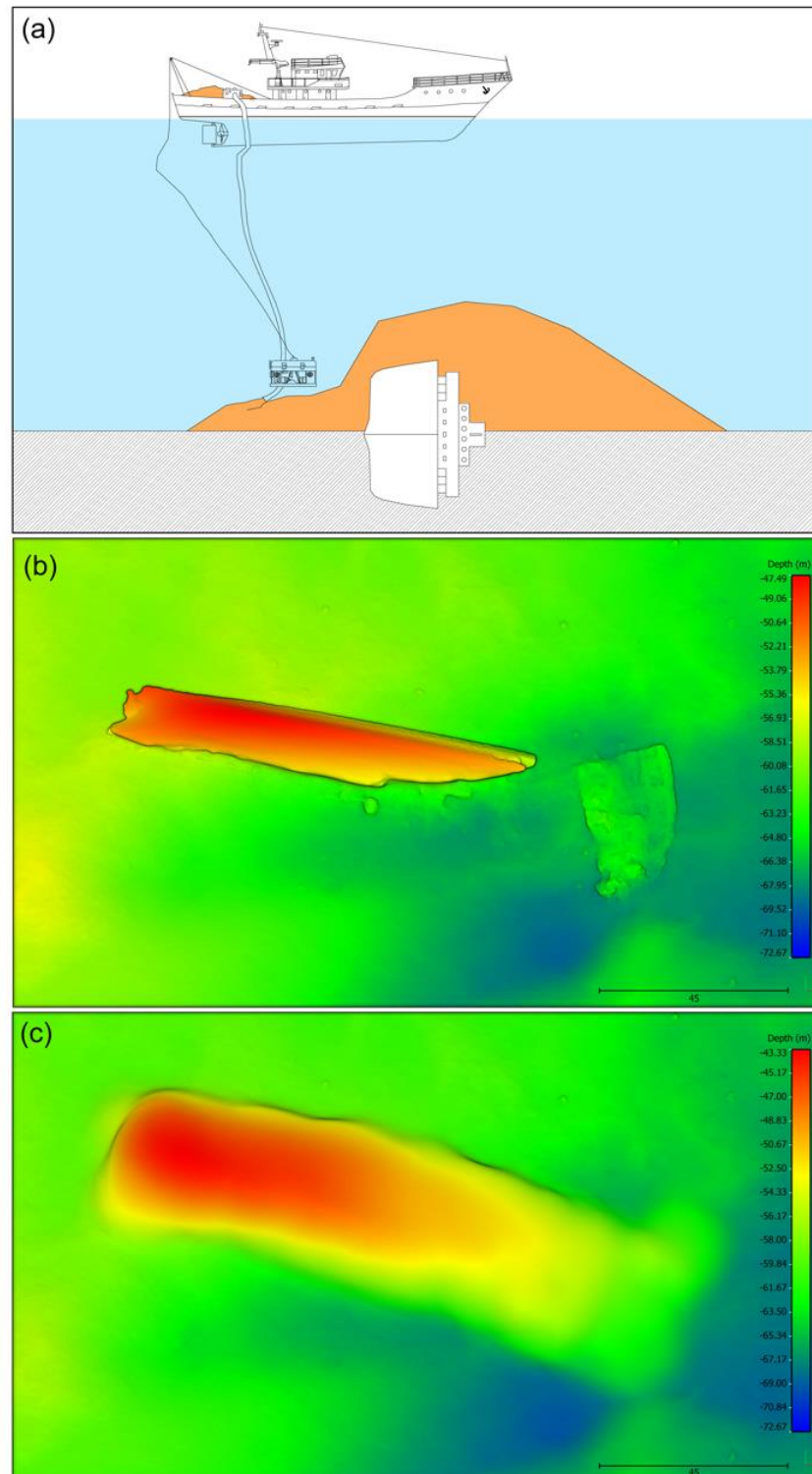
Figure 6.2. (a) Conceptual diagram showing shipwreck capping (adapted from: Alcaro *et al.* 2007), (b) 3D mesh of the SS *Santa Maria* site constructed with the survey data, (c) modelled 3D mesh of the SS *Santa Maria* site after capping.

However, it should be emphasised there are some prerequisites and limitations related to the use of CFD, which apply both to terrestrial and underwater heritage science (Grau-Bové *et al.* 2019) (also described in section 2.4.4). For example, it became apparent through the CFD modelling that the choice of initial conditions and mesh refinement for shipwreck site simulations is of paramount importance to realistic simulations of the natural environment (see section 5.5.3). It is also important to highlight that although open-source software was used to prepare and conduct the CFD simulations, this kind of investigation is resource-demanding. High-performance computing is essential to conduct site-scale simulations with suitable mesh resolution (controlled by $y+$, see section 5.3.8.2). Additionally, the preliminary trials conducted in this research project to establish robust methodological procedures for CFD modelling of shipwreck sites demonstrated the complexity of such simulations. This complexity requires knowledge and a skillset capable of handling and processing MBES data using specialist hydrographic and GIS software, triangulating point cloud data to obtain stereolithography representations of sites, preparing and conducting simulations (i.e. creating computational meshes with embedded stereolithography of complex seabed-shipwreck bathymetries, establishing initial conditions, which are both accurate and permit the solver's convergence, choosing appropriate solvers, discretization schemes etc.) and finally, post-processing the outputs of the simulations. All these tasks require multi-disciplinary expertise and therefore establishing the workflow should involve cooperation between qualified parties involving, for example, heritage managers or archaeologists, ocean modellers, and hydrographers/geophysicists.

Similarly, the studies conducted under the first two objectives, which were prerequisites for the CFD study, also required collaboration between trained specialists and used expensive field-survey assets (i.e. fully equipped research vessel costing €20,000 per day) and software to conceptualize and plan surveys, deliver, and process high-resolution marine remote sensing and ground-truthing datasets. As this project intended to push physical site formation science forward by exploring hydro- and sediment-dynamics in the greatest possible detail, full control of the data acquisition strategies and parameters was desired. However, it is important to note that residual relief and difference modelling workflows can be conducted with previously acquired and processed datasets, using open-source software. The methods are also straightforward to implement using basic GIS tools, do not require vast computational resources, and therefore, are highly accessible. Although CFD could also utilise existing shipwreck models, the complexity of the method should always be considered when planning investigations.

6.3. Summary

The research questions developed in the introduction and gaps in knowledge identified in the literature review chapters informed the investigations conducted in the experimental chapters, which correspond to the research objectives. The realisation of these research objectives resulted in the development of a new workflow (Fig. 6.3) aimed at assessing the combined sediment- and hydro-dynamic environment and structural deterioration at shipwreck sites, or in other words, physical site formation processes.

Firstly, a method for objective delineation of erosional and depositional signatures and local geomorphology at shipwreck sites was developed. This was a pre-requisite for the ensuing research, exploring the spatial and temporal evolution of these delineated and quantified features, allowing detailed characterization of the sites.

In order to characterize evolution of the sites, high-resolution repeat bathymetric, seismic, sediment and hydrodynamic data were used. The repeat bathymetric data collected over a wide area around the wrecks with a consistent survey strategy allowed the detection of change at the seabed with a centimetric accuracy at weekly, annual, multiannual and decadal time scales. Sediment data from the grab samples and hydrodynamic data from the regional ocean modelling allowed for assessment of the potential for seabed movement at the sites, while the seismic datasets provided insights into geological control on erosion.

The sites which exhibited very different patterns in geomorphic change, despite their proximity and similar seabed environments (HMS *Vanguard* and SS *W.M. Barkley*) were investigated further using CFD modelling, with simulations informed by the preceding steps (Fig. 6.3). CFD model outputs successfully explained geomorphic change around the sites, and also provided insights into why some parts of the shipwrecks underwent structural change. This multi-method characterization of shipwreck sites ultimately allows us to make data-informed predictions of their future evolution (Fig. 6.3).

Figure 6.3. The comprehensive, multi-method approach aiming at evaluating physical site formation processes developed through realisation of the research objectives. Arrows indicate dependencies between the tiles representing methods, datasets and products.
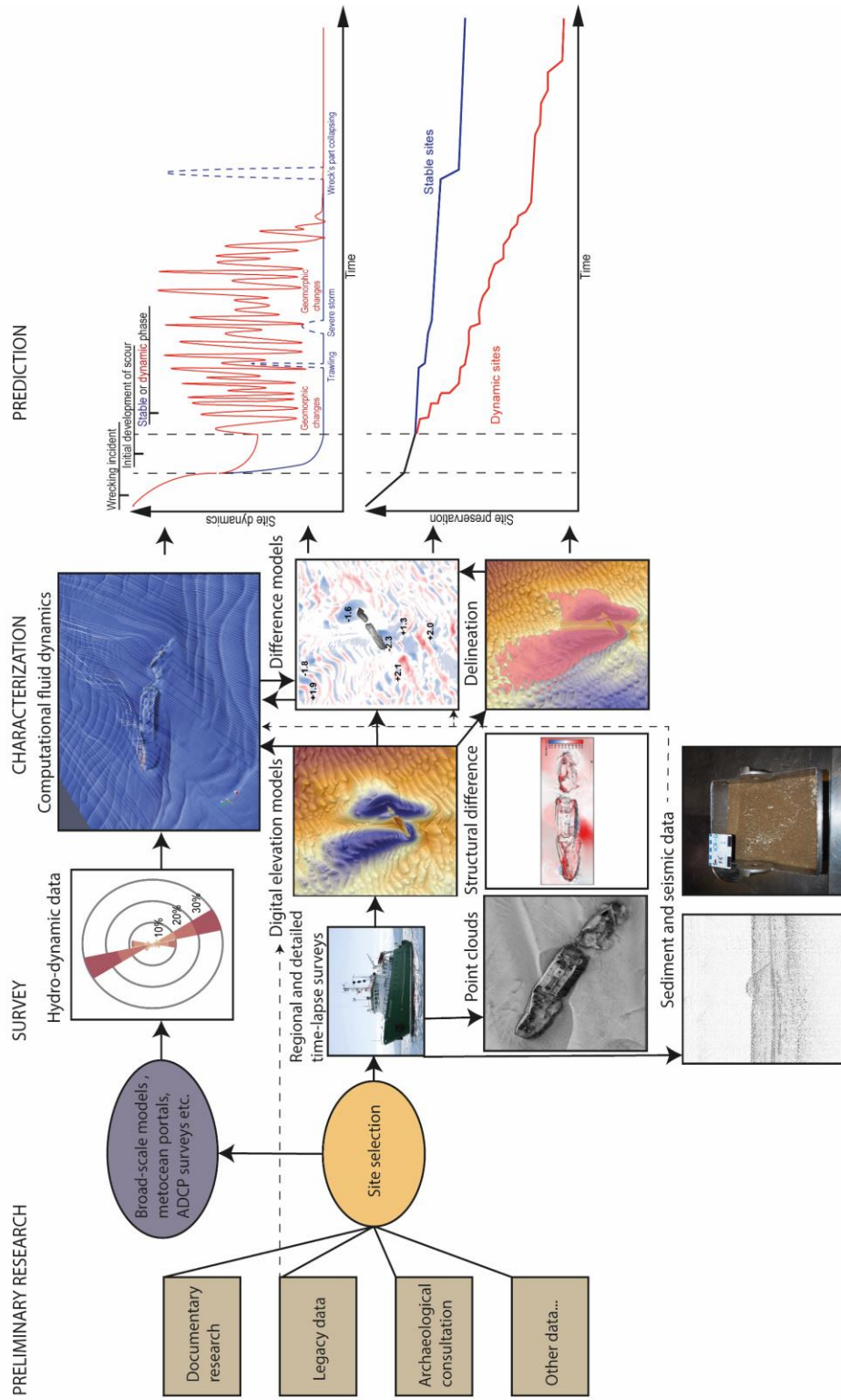
6.4. Recommendations for future research

The combination of non-invasive methods used here complies with the UNESCO-2001 Convention on the Protection of the Underwater Cultural Heritage (UNESCO, 2002), which also states that submerged sites which are over 100 years old should be classified as underwater cultural heritage. Therefore, according to the convention, the metal-hulled shipwrecks of World War 1 (and older), like those investigated in this thesis, should be somehow protected and monitored. Considering the amount of such sites (around 1800 alone offshore Ireland; Brady *et al.* 2012) and other shipwrecks, which should be investigated soon (e.g., 8500 potentially polluting shipwrecks around the world; Landquist *et al.* 2013), the findings presented here are potentially important for the long-term management of this submerged resource.

This study also identified some important knowledge gaps and opened up possibilities for further research regarding physical site formation processes at shipwreck sites. Based on the literature review in the first two chapters, and the empirical knowledge gained through the completion of the subsequent chapters, the following recommendations for future research are suggested:

- There is a vast potential for future research regarding the automatic and objective characterization of shipwreck sites. Novel methods used in automatic classification of remotely sensed data are already being applied for detection of underwater (e.g. using commercial software for object based image analysis; Janowski *et al.* 2021; Summers *et al.* 2021) and terrestrial (e.g. open-source Google Earth Engine-based machine learning; Orengo and Garcia-Molsosa, 2019) geomorphology, archaeological artefacts and sites. Such workflows, although often characterized by higher complexity, could be potentially compared against, used with or completely independent of the Residual Relief Modelling method to provide objective site characterization for shipwreck sites.

- Although the number of shipwrecks investigated in this study is the largest reported in the scientific literature for this type of research, ten shipwrecks are not enough to make unequivocal, conclusive remarks about which seabed environment is the most favourable for *in-situ* preservation. This study demonstrates that the spectrum of possibilities regarding site formation of shipwrecks is wide, even for sites located within the same shelf sea. This highlights the need to perform more case studies in varied geographic locations, at multiple temporal scales, in order to carry out quantitative research and comparisons.

- Furthermore, the investigation conducted in this thesis in terms of Objective 2 shows that such research can be enhanced with or conducted entirely using extant data collected by national or international seabed mapping programmes (like INFOMAR and EMODnet), naval and public hydrographic offices, port authorities and by the commercial sector (e.g., Quinn and Boland 2010), while hydrodynamic and geological information can be

obtained from regional operational oceanographic models, and national geological surveys etc.. For example, the decadal difference modelling conducted for the SS *W.M. Barkley* and SS *Hare* sites was possible owing to legacy MBES data collected by the INFOMAR project (Guinan *et al.* 2020) in 2010. Investigating the hydrodynamic regime at the sites was in turn possible due to the freely available data produced by the regional oceanographic modelling system run by the Marine Institute in Ireland (Nagy *et al.* 2020).

- Precise physical site formation assessments, involving multi-temporal-scale difference modelling like the one presented here, could be extended to include chemical and biological processes (e.g. Bethencourt *et al.* 2018). Feedback loops between sediment-dynamics, hydro-dynamics, encrustation, corrosion and structural deterioration of wrecks should be investigated further. As highlighted multiple times in this thesis, more site formation-oriented case studies conducted for shipwrecks would be beneficial for many sectors, improving heritage management (Gregory and Manders 2015a; Firth 2018) and marine pollution prevention (Landquist *et al.* 2013).

- Regarding CFD simulations for shipwreck site formation assessments, it is recognized that more research on the choice of initial conditions and their influence on solver convergence and results should be conducted. In the CFD investigation presented here, the velocity profile was obtained from a shelf-scale oceanographic model, and the turbulence variables were estimated using relations proposed in the software documentation (OpenCFD 2021). Additionally, a simple, depth-dependant mixing length formulation (Simpson *et al.* 1996) was implemented. This combination turned out to be computationally stable and produced accurate, indirectly validated (i.e. through comparisons with the observed geomorphic change) results, which provide invaluable information for the assessment of physical site formation processes. Nevertheless, using CFD in conjunction with physical modelling and validating high-resolution simulations with *in-situ* measurements of flow characteristics could help to determine how the choice of initial conditions affects the results and which setup provides the best approximation of the real flows.

- Moreover, more research should be conducted on the meshing process (i.e. creating the computational mesh) for CFD modelling at shipwreck sites. Complex seabed topographies and shipwreck morphologies required in such simulations create meshing problems and to model the full extents of sites, large areas need to be covered by the mesh. Additionally, CFD solvers and turbulence closures require very well refined meshes close to the wall (i.e. seabed/shipwreck) patch in order to produce accurate results (Versteeg and Malalasekera 2007). Such refined meshes ($y+<30$) are prohibitively computationally expensive over large domains. However, they could be used to model flow at discrete sections/elements of sites, where additional knowledge on processes is critical. In this thesis, these high computational costs motivated the implementation of

wall functions and although the simulations accurately predict and explain geomorphic change, grid independence (<1% difference in monitored variables between meshes) could not be achieved. Therefore, future investigations should explore and determine optimal refinement strategies and meshing parameters for CFD investigations at shipwreck sites.

- CFD could be tested and used to support design optimisation for *in-situ* preservation and pollutant leakage prevention measures from wrecks.

References

Al-Hamdani Z, Appelqvist C, Gjelstrup Björdal C, et al (2011) Guidelines for Protection of Submerged Wooden Cultural Heritage 2011. WreckProtect

Alcaro L, Amato E, Cabioch F, et al (2007) DEEPP PROJECT DEvelopment of European guidelines for Potentially Polluting shipwrecks

Andrady AL (2011) Microplastics in the marine environment. Mar Pollut Bull 62:1596–1605. https://doi.org/10.1016/j.marpolbul.2011.05.030

Ansys (2021) Ansys Fluent: Fluid Simulation Software . https://www.ansys.com/products/fluids/ansys-fluent. Accessed 18 Jan 2021

Astley AJ (2016) The Taphonomy of Historic Shipwreck Sites. University of Southampton

Astley AJ, Dix JK, Thompson C, Sturt F (2014) A seventeen year, near- annual, bathymetric time-series of a marine structure (SS Richard Montgomery). In: Cheng L, Draper S, An H (eds) Scour and erosion: Proceedings ofthe 7th International Conference on Scour and Erosion. Taylor & Francis, Perth, pp 715–724

Atkins WS (1997) Chapter 2.3 Wind and water. In: Doody JP, Davidson NC, Barne JH, *et al.* (eds) Coasts and Seas of the United Kingdom. Region 17, Northern Ireland. Joint Nature Conservation Committee, Peterborough, pp 28–32

Baeye M, Quinn R, Deleu S, Fettweis M (2016) Detection of shipwrecks in ocean colour satellite imagery. J Archaeol Sci 66:1–6. https://doi.org/10.1016/j.jas.2015.11.006

Balazy P, Copeland U, Sokołowski A (2019) Shipwrecks and underwater objects of the southern Baltic – Hard substrata islands in the brackish, soft bottom marine environment. Estuar Coast Shelf Sci 225:. https://doi.org/10.1016/j.ecss.2019.05.022

Ballard B, Cornwell K, Opait A (2018) Deep-water archaeological discoveries on Eratosthenes Seamount. Deep Res Part II Top Stud Oceanogr 150:4–21. https://doi.org/10.1016/j.dsr2.2017.10.014

Ballard RD (2007) Archaeological Oceanography. In: Wiseman J, El-Baz F (eds) Remote Sensing in Archaeology. Springer New York, New York, NY, pp 479–497

Ballard RD, Hiebert FT, Coleman DF, et al (2001) Deepwater Archaeology of the Black Sea : The 2000 Season at Sinop , Turkey. Archaeol Inst Am 105:607–623

Basta DJ, Symons L, Wagner J, et al (2013) Risk Assessment for Potentially Polluting Wrecks in U.S. Waters. National Oceanic and Atmospheric Administration

Bates CR, Lawrence M, Dean M, Robertson P (2011) Geophysical Methods for Wreck-Site

Monitoring: The Rapid Archaeological Site Surveying and Evaluation (RASSE) programme. Int J Naut Archaeol 40:404–416. https://doi.org/10.1111/j.1095-9270.2010.00298.x

Belderson RH (1964) Holocene sedimentation in the western half of the Irish Sea. Mar Geol 2:147–163. https://doi.org/10.1016/0025-3227(64)90032-5

Bełdowski J, Brenner M, Lehtonen KK (2020) Contaminated by war: A brief history of sea-dumping of munitions. Mar Environ Res 162:2020–2021. https://doi.org/10.1016/j.marenvres.2020.105189

Bethencourt M, Fernández-Montblanc T, Izquierdo A, et al (2018) Study of the influence of physical, chemical and biological conditions that influence the deterioration and protection of Underwater Cultural Heritage. Sci Total Environ 613–614:98–114. https://doi.org/10.1016/j.scitotenv.2017.09.007

Blocken B (2015) Computational Fluid Dynamics for urban physics: Importance, scales, possibilities, limitations and ten tips and tricks towards accurate and reliable simulations. Build Environ 91:219–245. https://doi.org/10.1016/j.buildenv.2015.02.015

Blocken B (2018) LES over RANS in building simulation for outdoor and indoor applications: A foregone conclusion? Build Simul 11:821–870. https://doi.org/10.1007/s12273-018-0459-3

Blocken B, van der Hout A, Dekker J, Weiler O (2015) CFD simulation of wind flow over natural complex terrain: Case study with validation by field measurements for Ria de Ferrol, Galicia, Spain. J Wind Eng Ind Aerodyn 147:43–57. https://doi.org/10.1016/j.jweia.2015.09.007

Blott SJ, Pye K (2001) Gradistat: A grain size distribution and statistics package for the analysis of unconsolidated sediments. Earth Surf Process Landforms 26:1237–1248. https://doi.org/10.1002/esp.261

Boldreel LO, Grøn O, Cvikel D (2021) Synthetic 3D Recording of a Shipwreck Embedded in Seafloor Sediments : Distinguishing Internal Details. heritage 4:541–553. https://doi.org/10.3390/heritage4020032

Bond J (2014) Exploring the relationships between scour , backscatter and sediment grain size at the Tiberia wreck site , Belfast Lough. Ulster University

Bos J, Frederiks B (2019) Shipwreck Monitoring in the North Sea. In: Hydro Int. https://www.hydro-international.com/content/article/shipwreck-monitoring-in-the-north-sea. Accessed 15 Apr 2021

References

Bowden KF (1980) Chapter 12 Physical and Dynamical Oceanography of the Irish Sea. In: Banner FT, Collins MB, Massie KS (eds) Elsevier Oceanography Series. pp 391–413

Brady K, McKeon C, Lyttleton J, Lawler I (2012) Warships, U-Boats & Liners - A guide to shipwrecks mapped in Irish waters. The Stationery Office, Dublin

Brasington J, Langham J, Rumsby B (2003) Methodological sensitivity of morphometric estimates of coarse fluvial sediment transport. Geomorphology 53:299–316. https://doi.org/10.1016/S0169-555X(02)00320-3

Brennan ML, Davis D, Ballard RD, et al (2016) Quantification of bottom trawl fishing damage to ancient shipwreck sites. Mar Geol 371:82–88. https://doi.org/10.1016/j.margeo.2015.11.001

Brennan ML, Davis D, Roman C, et al (2013) Ocean dynamics and anthropogenic impacts along the southern Black Sea shelf examined through the preservation of pre-modern shipwrecks. Cont Shelf Res 53:89–101. https://doi.org/10.1016/j.csr.2012.12.010

Brown CJ, Smith SJ, Lawton P, Anderson JT (2011) Benthic habitat mapping: A review of progress towards improved understanding of the spatial ecology of the seafloor using acoustic techniques. Estuar Coast Shelf Sci 92:502–520. https://doi.org/10.1016/j.ecss.2011.02.007

Calder B, Wells DE (2007) CUBE User Manual. University of New Hampshire, Durham

Callaway A, Smyth J, Brown CJ, et al (2009) The impact of scour processes on a smothered reef system in the Irish Sea. Estuar Coast Shelf Sci 84:409–418. https://doi.org/10.1016/j.ecss.2009.07.011

Calvert J, Strong JA, Service M, et al (2015) An evaluation of supervised and unsupervised classification techniques for marine benthic habitat mapping using multibeam echosounder data. ICES J Mar Sci 72:1498–1513. https://doi.org/10.1093/icesjms/fsu223 Original

Carter M, Goodsir F, Cundall P, et al (2021) Ticking ecological time bombs: Risk characterisation and management of oil polluting World War II shipwrecks in the Pacific Ocean. Mar Pollut Bull 164:112087. https://doi.org/10.1016/j.marpolbul.2021.112087

Caston GF (1979) Wreck marks: Indicators of net sand transport. Mar Geol 33:193–204. https://doi.org/10.1016/0025-3227(79)90080-X

Castro-García M, Rojas-Sola JI, De La Morena-de La Fuente E (2015) Technical and functional analysis of Albolafia waterwheel (Cordoba, Spain): 3D modeling, computational-fluid dynamics simulation and finite-element analysis. Energy Convers Manag 92:207–214. https://doi.org/10.1016/j.enconman.2014.12.047

References

Cederlund CO (2006) Vasa I: The Archaeology of a Swedish Warship of 1628. National Maritime Museum of Sweden

Church RA (2014) Deep-Water Shipwreck Initial Site Formation: The Equation of Site Distribution. J Marit Archaeol 9:27–40. https://doi.org/10.1007/s11457-014-9128-6

Colbo K, Ross T, Brown C, Weber T (2014) A review of oceanographic applications of water column data from multibeam echosounders. Estuar Coast Shelf Sci 145:41–56. https://doi.org/10.1016/j.ecss.2014.04.002

Collier JS, Brown CJ (2005) Correlation of sidescan backscatter with grain size distribution of surficial seabed sediments. Mar Geol 214:431–449. https://doi.org/10.1016/j.margeo.2004.11.011

Cotswold Archaeology (2015) An Archival Assessment of World War I Wrecks in Northern Irish Waters

Coughlan M, Guerrini M, Creane S, et al (2021) A new seabed mobility index for the Irish Sea: Modelling seabed shear stress and classifying sediment mobilisation to help predict erosion, deposition, and sediment distribution. Cont Shelf Res 229:104574. https://doi.org/10.1016/j.csr.2021.104574

Coughlan M, Long M, Doherty P, Coughlan M (2020) Geological and geotechnical constraints in the Irish Sea for offshore renewable energy energy. J Maps 16:420–431. https://doi.org/10.1080/17445647.2020.1758811

Coughlan M, Wheeler AJ, Dorschel B, et al (2015) Record of anthropogenic impact on the Western Irish Sea mud belt. Anthropocene 9:56–69. https://doi.org/10.1016/j.ancene.2015.06.001

Coughlan M, Wheeler AJ, Dorschel B, et al (2019) Stratigraphic model of the Quaternary sediments of the Western Irish Sea Mud Belt from core, geotechnical and acoustic data. Geo-Marine Lett. https://doi.org/10.1007/s00367-019-00569-z

Couldrey AJ, Benson T, Knaapen MAF, et al (2020) Morphological evolution of a barchan dune migrating past an offshore wind farm foundation. Earth Surf Process Landforms 45:2884–2896. https://doi.org/10.1002/esp.4937

Council of Europe (1992) European Convention on the Protection of the Archaeological Heritage

Croome A (1999) Sinking Fast. In: Rhind D (ed) Marine Industrial Technology, 1st&2nd edn. United Nations Industrial Development Organization (UNIDO), Vienna

Cullimore DR, Johnston LA (2008) Microbiology of concretions, sediments and mechanisms

influencing the preservation of submerged archaeological artifacts. Int J Hist Archaeol 12:120–132. https://doi.org/10.1007/s10761-008-0045-y

Cvikel D, Grøn O, Boldreel LO (2017) Detecting the Ma'agan Mikhael B shipwreck. Underw Technol 34:93–98. https://doi.org/10.3723/ut.34.093

D'Agostino D, Congedo PM (2014) CFD modeling and moisture dynamics implications of ventilation scenarios in historical buildings. Build Environ 79:181–193. https://doi.org/10.1016/j.buildenv.2014.05.007

Davies L (2011) Atlantic wreck set to yield £150m haul

Davis DS, Buffa DC, Wrobleski AC (2020) Assessing the Utility of Open-Access Bathymetric Data for Shipwreck Detection in the United States. Heritage 3:364–383. https://doi.org/10.3390/heritage3020022

De Hauteclocque G, Dix JK, Lambkin D, Turnock S (2007) Flow and likely scour around three-dimensional seabed structures evaluated using RANS CFD (Ship Science Report, 144). Southampton

Delgado J, Varmer O (2015) The Public Importance of World War I Shipwrecks : Why a State Should Care and the Challenges of Protection. In: Underwater Cultural Heritage from World War I, Proceedings of the Scientific Conference on the Occasion of the Centenary of World War I Bruges, Belgium, 26 & 27 June 2014. pp 105–116

Demesticha S, Skarlatos D, Neophyto A (2014) The 4th-century B.C. Shipwreck at Mazotos, Cyprus: New techniques and methodologies in the 3D mapping of shipwreck excavations. J F Archaeol 39:134–150. https://doi.org/10.1179/0093469014Z.00000000077

DHI (2021) MIKE 21/3. https://www.mikepoweredbydhi.com/products/mike-21-3. Accessed 18 Jan 2021

Discamps E, Muth X, Gravina B, et al (2016) Photogrammetry as a tool for integrating archival data in archaeological fieldwork: Examples from the Middle Palaeolithic sites of Combe-Grenal, Le Moustier, and Regourdou. J Archaeol Sci Reports 8:268–276. https://doi.org/10.1016/j.jasrep.2016.06.004

Dix JK, Cazenave P, Lambkin D, et al (2009a) Sedimentation-Erosion Modelling as a tool for Underwater Cultural Heritage Management. In: MACHU Final Report NR. 3 - Managing Cultural Heritage Underwater. pp 48–53

Dix JK, Rangecroft T, Lambkin D, et al (2009b) Physical Modelling as a tool for Underwater Cultural Heritage Management. In: MACHU Final Report NR. 3 - Managing Cultural Heritage Underwater. pp 54–55

References

Dixen M, Sumer BM, Fredsøe J (2013) Numerical and experimental investigation of flow and scour around a half-buried sphere. Coast Eng 73:84–105. https://doi.org/10.1016/j.coastaleng.2012.10.006

Elkin D, Gutiérrez G, Underwood CJ (2020) Metal shipwrecks in Patagonia, Argentina: contributions to their research and management. Int J Naut Archaeol 49:303–317. https://doi.org/10.1111/1095-9270.12441

EMODnet Bathymetry Consortium (2018) EMODnet Digital Bathymetry (DTM 2018)

Eriksen AM, Gregory D (2016) Degradation of Archaeological Remains by Shipworm. Conserv Manag Archaeol Sites 18:30–39. https://doi.org/10.1080/13505033.2016.1181931

Eriksson N, Rönnby J (2017) Mars (1564): the initial archaeological investigations of a great 16th-century Swedish warship. Int J Naut Archaeol 46:92–107. https://doi.org/10.1111/1095-9270.12210

Eriksson N, Rönnby J (2012) ' The Ghost Ship '. An Intact Fluyt from c . 1650 in the Middle of the Baltic Sea. Int J Naut Archaeol 43:350–361. https://doi.org/10.1111/j.1095-9270.2012.00342.x

Evans AM, Firth A (2016) Anthropogenic Impacts of Development-Led Archaeology in an Offshore Context. In: Keith M (ed) Site Formation Processes of Submerged Shipwrecks. University Press of Florida, Gainesville, pp 133–156

Ferentinos G, Fakiris E, Christodoulou D, et al (2020) Optimal sidescan sonar and subbottom profiler surveying of ancient wrecks: The 'Fiskardo' wreck, Kefallinia Island, Ionian Sea. J Archaeol Sci 113:105032. https://doi.org/10.1016/j.jas.2019.105032

Fernández-Montblanc T, Izquierdo A, Bethencourt M (2018a) Scattered shipwreck site prospection: the combined use of numerical modeling and documentary research (Fougueux, 1805). Archaeol Anthropol Sci 10:141–156. https://doi.org/10.1007/s12520-016-0348-6

Fernández-Montblanc T, Izquierdo A, Quinn R, Bethencourt M (2018b) Waves and wrecks: A computational fluid dynamic study in an underwater archaeological site. Ocean Eng 163:232–250. https://doi.org/10.1016/j.oceaneng.2018.05.062

Fernández-Montblanc T, Quinn R, Izquierdo A, Bethencourt M (2016) Evolution of a Shallow Water Wave-Dominated Shipwreck Site: Fougueux (1805), Gulf of Cadiz. Geoarchaeology 31:487–505. https://doi.org/10.1002/gea.21565

Firth A (2018) Managing Shipwrecks. Fjord Limited for Honor Frost Foundation

Foecke T, Ma L, Russell MA, et al (2010) Investigating archaeological site formation processes

on the battleship USS Arizona using finite element analysis. J Archaeol Sci 37:1090–1101. https://doi.org/10.1016/j.jas.2009.12.009

Folk RL (1954) The Distinction between Grain Size and Mineral Composition in Sedimentary-Rock. J Geol 62:344–359

Forsythe W, Breen C, Callaghan C, McConkey R (2000) Historic storms and shipwrecks in Ireland: A preliminary survey of severe synoptic conditions as a causal factor in underwater archaeology. Int J Naut Archaeol 29:247–259. https://doi.org/10.1006/ijna.2000.0313

Frost H (1961) THE ANNUAL LECTURE 1961. Mar Mirror 48:82–89. https://doi.org/https://doi.org/10.1080/00253359.1962.10657686

Garlan T, Marches E, Brenon E (2015) A classification of scouring marks in macrotidal environments from analysis of long term wreck marks. In: Wang P, Rosati JD, Cheng J (eds) The Proceedings of the Coastal Sediments 2015. World Scientific, Singapore, p 14

Geraga M, Christodoulou D, Eleftherakis D, et al (2020) Atlas of Shipwrecks in Inner Ionian Sea (Greece): A Remote Sensing Approach. Heritage 3:1210–1236. https://doi.org/10.3390/heritage3040067

Gibbs M (2006) Cultural site formation processes in maritime archaeology: Disaster response, salvage and Muckelroy 30 years on. Int J Naut Archaeol 35:4–19. https://doi.org/10.1111/j.1095-9270.2006.00088.x

Ginsberg SS, Aliotta S (2019) Impact of a rocky outcrop on hydrodynamics and geomorphology in a mesotidal channel. Estuar Coast Shelf Sci 225:106250. https://doi.org/10.1016/j.ecss.2019.106250

González-Duarte MM, Fernández-Montblanc T, Bethencourt M, Izquierdo A (2018) Effects of substrata and environmental conditions on ecological succession on historic shipwrecks. Estuar Coast Shelf Sci 200:301–310. https://doi.org/10.1016/j.ecss.2017.11.014

Goodsir F, Lonsdale JA, Mitchell PJ, et al (2019) A standardised approach to the environmental risk assessment of potentially polluting wrecks. Mar Pollut Bull 142:290–302. https://doi.org/10.1016/j.marpolbul.2019.03.038

Grau-Bové J, Mazzei L, Strlic M, Cassar M (2019) Fluid simulations in heritage science. Herit Sci 7:1–12. https://doi.org/10.1186/s40494-019-0259-9

Gregory D (2016) Degradation of Wood. In: Keith M (ed) Site Formation Processes of Submerged Shipwrecks. University Press of Florida, Gainesville, pp 114–129

Gregory D (2020) Characterizing the Preservation Potential of Buried Marine Archaeological

Sites. Heritage 3:838–857. https://doi.org/10.3390/heritage3030046

Gregory D, Eriksen AM, Pedersen R, et al (2014) Development of tools and techniques to survey, assess, stabilise, monitor and preserve underwater archaeological sites: SASMAP, a European research project. In: Bridgland J (ed) ICOM-CC 17th Triennal Conference Preprints. International Council of Museums, Paris, p 7

Gregory D, Manders M (2015a) Guidelines to the process of underwater archaeological research, SASMAP Guideline Manual 1. SASMAP

Gregory D, Manders M (2015b) Best practices for locating, surveying, assessing, monitoring and preserving archaeological sites, SASMAP Guideline Manual 2. SASMAP

Grøn O, Boldreel LO, Cvikel D, et al (2015) Detection and mapping of shipwrecks embedded in sea-floor sediments. J Archaeol Sci Reports 4:242–251. https://doi.org/10.1016/j.jasrep.2015.09.005

Grządziel A (2020a) Using Remote Sensing Techniques to Document and Identify the Largest Underwater Object of the Baltic Sea: Case Study of the Only German Aircraft Carrier, Graf Zeppelin. Remote Sens 12:4076. https://doi.org/10.3390/rs12244076

Grządziel A (2020b) Using remote sensing data to identify large bottom objects: The case of world war II shipwreck of general von Steuben. Geosciences 10:1–15. https://doi.org/10.3390/geosciences10060240

Guinan J, McKeon C, O'Keeffe E, et al (2020) INFOMAR data in the EMODnet Geology data portal supports marine spatial planning and offshore energy development in the Irish offshore. Q J Eng Geol Hydrogeol 54:. https://doi.org/10.1144/qjegh2020-033

Guisan A, Weiss SB, Weiss AD (1999) GLM versus CCA spatial modeling of plant species distribution. Plant Ecol 143:107–122

Hac B, Sarna O (2021) General Methodology Of Oil Removal Operations On Baltic Shipwrecks. The MARE Foundation

Harris JM, Whitehouse RJS, Sutherland J (2011) Marine scour and offshore wind - Lessons learnt and future challenges. Proc Int Conf Offshore Mech Arct Eng - OMAE 5:849–858. https://doi.org/10.1115/OMAE2011-50117

Hay AE, Speller R (2005) Naturally occurring scour pits in nearshore sands. J Geophys Res Earth Surf 110:1–15. https://doi.org/10.1029/2004JF000199

Helgason G Motor fishing vessel St. Michan . https://uboat.net/wwi/ships_hit/5731.html. Accessed 30 Apr 2021

Hensley RT (1996) A preliminary survey of benthos from the Nephrops norvegicus mud grounds in the North-western Irish Sea. Estuar Coast Shelf Sci 42:457–465. https://doi.org/10.1006/ecss.1996.0029

Hesse R (2010) LiDAR-derived Local Relief Models - a new tool for archaeological prospection. Archaeol Prospect 17:67–72. https://doi.org/10.1002/arp.374

Hiller JK, Smith M (2008) Residual relief separation: Digital elevation model enhancement for geomorphological mapping. Earth Surf Process Landforms 33:2266–2276. https://doi.org/10.1002/esp.1659

Horsburgh KJ, Hill AE (2003) A three-dimensional model of density-driven circulation in the Irish Sea. J Phys Oceanogr 33:343–365. https://doi.org/10.1175/1520-0485(2003)033<0343:ATDMOD>2.0.CO;2

Howarth MJ (2001) Hydrography of the Irish Sea

Hunt JCR, Wray AA, Moin P (1988) Eddies, streams, and convergence zones in turbulent flows. In: Studying Turbulence Using Numerical Simulation Databases, 2. Proceedings of the 1988 Summer Program. Center for Turbulence Research, pp 193–208

Hussein AS, El-Shishiny H (2009) Influences of wind flow over heritage sites: A case study of the wind environment over the Giza Plateau in Egypt. Environ Model Softw 24:389–410. https://doi.org/10.1016/j.envsoft.2008.08.002

ICOMOS (2007) HERITAGE at risk

IHO (2020) IHO Standards for Hydrographic Surveys. International Hydrographic Organization

Issa RI (1986) Solution of the Implicitly Discretised Fluid Flow Equations by Operator-Splitting. J Comput Phys 62:40–65. https://doi.org/10.1016/0021-9991(86)90099-9

Jackson DI, Jackson AA, Evans D, et al (1995) United Kingdom offshore regional report: the geology of the Irish Sea. British Geological Survey, London

James MR, Robson S, Smith MW (2017) 3-D uncertainty-based topographic change detection with structure-from-motion photogrammetry : precision maps for ground control and directly georeferenced surveys. Earth Surf Process Landforms 42:1769–1788. https://doi.org/10.1002/esp.4125

Janowski L, Kubacka M, Pydyn A, et al (2021) From acoustics to underwater archaeology: deep investigation of a shallow lake using high-resolution hydroacoustics - the case of lake Lednica, Poland. Archaeometry. https://doi.org/10.1111/arcm.12663

Jenkins SA, Inman DL, Richardson MD, et al (2007) Scour and burial mechanics of objects in

the nearshore. IEEE J Ocean Eng 32:78–90. https://doi.org/10.1109/JOE.2007.890946

Johnson KH, Paxton AB, Taylor JC, et al (2020) Extracting ecological metrics from archeological surveys of shipwrecks using submersible video and laser-line scanning. Emerg Technol 11:. https://doi.org/10.1002/ecs2.3210

Jones JE, Davies AM (2003) Processes influencing storm-induced currents in the Irish Sea. J Phys Oceanogr 33:88–104. https://doi.org/10.1175/1520-0485(2003)033<0088:PISICI>2.0.CO;2

Kallehave D, Byrne BW, LeBlanc Thilsted C, Mikkelsen KK (2015) Optimization of monopiles for offshore wind turbines. Philos Trans R Soc A Math Phys Eng Sci 373:. https://doi.org/10.1098/rsta.2014.0100

Kazhdan M, Bolitho M, Hoppe H (2006) Poisson surface reconstruction. Eurographics Symp Geom Process 44:61–70

Keith ME (2016) Conclusion. In: Keith ME (ed) Site Formation Processes of Submerged Shipwrecks. University Press of Florida, Gainesville, pp 259–262

King E V., Conley DC, Masselink G, et al (2019) The Impact of Waves and Tides on Residual Sand Transport on a Sediment-Poor, Energetic, and Macrotidal Continental Shelf. J Geophys Res Ocean 124:4974–5002. https://doi.org/10.1029/2018JC014861

Kirwan S (2010) Ireland and the UNESCO Convention on the Protection of the Underwater Cultural Heritage. J Marit Archaeol 5:105–115. https://doi.org/10.1007/s11457-010-9067-9

Knight PJ, Howarth MJ (1999) The flow through the North Channel of the Irish Sea. Elsevier Oceanogr Ser 19:693–716. https://doi.org/10.1016/S0278-4343(98)00110-1

Lamarche G, Lurton X (2018) Recommendations for improved and coherent acquisition and processing of backscatter data from seafloor-mapping sonars. Mar Geophys Res 39:5–22. https://doi.org/10.1007/s11001-017-9315-6

Landquist H, Hassellöv IM, Rosén L, et al (2013) Evaluating the needs of risk assessment methods of potentially polluting shipwrecks. J Environ Manage 119:85–92. https://doi.org/10.1016/j.jenvman.2012.12.036

Lee SO, Hong SH (2019) Turbulence characteristics before and after scour upstream of a scaled-down bridge pier model. Water (Switzerland) 11:1–14. https://doi.org/10.3390/w11091900

Lesser GR, Roelvink JA, van Kester JATM, Stelling GS (2004) Development and validation of a three-dimensional morphological model. Coast Eng 51:883–915.

https://doi.org/10.1016/j.coastaleng.2004.07.014

Lewis M, Neill SP, Robins P, et al (2017) Characteristics of the velocity profile at tidal-stream energy sites. Renew Energy 114:258–272. https://doi.org/10.1016/j.renene.2017.03.096

Lewis M, Neill SP, Robins PE, Hashemi MR (2015) Resource assessment for future generations of tidal-stream energy arrays. Energy 83:403–415. https://doi.org/10.1016/j.energy.2015.02.038

Liu B, Qu J, Niu Q, et al (2021) Impact of anthropogenic activities on airflow field variation over a star dune. Catena 196:. https://doi.org/10.1016/j.catena.2020.104877

Lurton X, Lamarche G (2015) Backscatter Measurements by Seafloor-mapping Sonars: Guidelines and Recommendations

MacLeod ID (2016) Corrosion Products and Site Formation Processes. In: Keith ME (ed) Site Formation Processes of Submerged Shipwrecks. University Press of Florida, Gainesville, pp 90–113

Majcher J, Plets R, Quinn R (2020) Residual relief modelling: digital elevation enhancement for shipwreck site characterisation. Archaeol Anthropol Sci 12:. https://doi.org/10.1007/s12520-020-01082-6

Majcher J, Quinn R, Plets R, et al (2021) Spatial and temporal variability in geomorphic change at tidally influenced shipwreck sites: The use of time-lapse multibeam data for the assessment of site formation processes. Geoarchaeology 36:429–454. https://doi.org/10.1002/gea.21840

Manders M (2009) Multibeam recording as a way to monitor shipwreck sties. MACHU Final Rep NR 3 - Manag Cult Herit Underw 59–66

Manders M, Oosting R, Brouwers W (2009) MACHU Final Report. MACHU, Rotterdam

Masetti G, Calder B (2012) Remote identification of a shipwreck site from MBES backscatter. J Environ Manage 111:44–52. https://doi.org/10.1016/j.jenvman.2012.06.037

Matulla C, Schöner W, Alexandersson H, et al (2008) European storminess: Late nineteenth century to present. Clim Dyn 31:125–130. https://doi.org/10.1007/s00382-007-0333-y

Matutano C, Negro V, López-Gutiérrez JS, Esteban MD (2013) Scour prediction and scour protections in offshore wind farms. Renew Energy 57:358–365. https://doi.org/10.1016/j.renene.2013.01.048

MCA (2018) UK Hydrography Programme. Survey Specification. Southampton

McCarron CJ, Van Landeghem KJJ, Baas JH, et al (2019) The hiding-exposure effect revisited:

A method to calculate the mobility of bimodal sediment mixtures. Mar Geol 410:22–31. https://doi.org/10.1016/j.margeo.2018.12.001

McCarthy JK, Jonathan B, Trevor W, Wendy van D (2019) 3D Recording and Interpretation for Maritime Archaeology

McCartney I (2018) Scuttled in the Morning: the discoveries and surveys of HMS Warrior and HMS Sparrowhawk, the Battle of Jutland's last missing shipwrecks. Int J Naut Archaeol 47:253–266. https://doi.org/10.1111/1095-9270.12302

McCartney I (2017) The Battle of Jutland's Heritage Under Threat: Commercial salvage on the shipwrecks as observed 2000 to 2016. Mar Mirror 103:196–204. https://doi.org/10.1080/00253359.2017.1304701

McGonigle C, Collier JS (2014) Interlinking backscatter, grain size and benthic community structure. Estuar Coast Shelf Sci 147:123–136. https://doi.org/10.1016/j.ecss.2014.05.025

McLarty MJ, Gonzalez-Socoloske D, Alvarez-Alemán A, Angulo-Valdés J (2020) Manatee habitat characterization using side-scan sonar. J Mar Biol Assoc United Kingdom 100:173–179. https://doi.org/10.1017/S0025315419000973

McNinch JE, Wells JT, Trembanis AC (2006) Predicting the fate of artefacts in energetic, shallow marine environments: An approach to site management. Int J Naut Archaeol 35:290–309. https://doi.org/10.1111/j.1095-9270.2006.00105.x

Mellet CL, Long D, Carter G (2015) Geology of the seabed and shallow subsurface: the Irish Sea. Edinburgh

Melling G (2015) Hydrodynamic and geotechnical control of scour around offshore monopiles. University of Southampton, Ocean and Earth Science

Menter FR (1992) Improved two-equation k-omega turbulence models for aerodynamic flows. NASA Tech Memo 1–31

Menter FR, Kuntz M, Langtry R (2003) Ten Years of Industrial Experience with the SST Turbulence Model. In: Hanjalic K, Nagano Y, Tummers M (eds) Turbulence, Heat and Mass Transfer 4. Begell House, Inc., pp 625–632

Michel J, Gilbert T, Etkin DS, et al (2005) Potentially Polluting Wrecks in Marine Waters. In: International Oil Spill Conference Proceedings. pp 1–40

Mikayama A, Hokoi S, Ogura D, et al (2015) Effects of drifting sand particles on deterioration of mural paintings on the east wall of cave 285 in Mogao caves, Dunhuang. Energy Procedia 78:1311–1316. https://doi.org/10.1016/j.egypro.2015.11.146

Moore D (1997) Blackbeard the Pirate: Historical Background and the Beaufort Inlet Shipwrecks. Tributaries 30–39

Muckelroy K (1976) The integration of historical and archaeological data concerning an historic wreck site: The 'Kennemerland.' World Archaeol 7:280–290. https://doi.org/10.1080/00438243.1976.9979641

Muckelroy K (1978) Maritime Archaeology. Cambridge University Press, Cambridge

Muckelroy K (1977) Historic wreck sites in Britain and their environments. Int J Naut Archaeol 6:47–57. https://doi.org/10.1111/j.1095-9270.1977.tb00987.x

Nagy H, Lyons K, Nolan G, et al (2020) A Regional Operational Model for the North East Atlantic: Model Configuration and Validation. J Mar Sci Eng 8:673. https://doi.org/10.3390/jmse8090673

National Monuments Service (1987) National Monuments (Amendment) Act, 1987. Republic of Ireland

Ndungu K, Beylich BA, Staalstrøm A, et al (2017) Petroleum oil and mercury pollution from shipwrecks in Norwegian coastal waters. Sci Total Environ 593–594:624–633. https://doi.org/10.1016/j.scitotenv.2017.03.213

Neill SP, Hashemi MR, Lewis MJ (2014) Optimal phasing of the European tidal stream resource using the greedy algorithm with penalty function. Energy 73:997–1006. https://doi.org/10.1016/j.energy.2014.07.002

Nornes SM, Ludvigsen M, Ødegård Ø, Sørensen AJ (2015) Underwater photogrammetric mapping of an intact standing steel wreck with ROV. IFAC-PapersOnLine 48:206–211. https://doi.org/10.1016/j.ifacol.2015.06.034

O'Shea J (2002) The archaeology of scattered wreck-sites: formation processes and shallow water archaeology in western Lake Huron. Int J Naut Archaeol 31:211–227. https://doi.org/10.1006/ijna.2002.1044

O'Toole R, Judge M, Sachetti F, et al (2020) Mapping Ireland's coastal, shelf and deep water environments using illustrative case studies to highlight the impact of seabed mapping on the generation of blue knowledge. Geol Soc London, Spec Publ SP505-2019–207. https://doi.org/10.1144/sp505-2019-207

Ødegård Ø, Hansen RE, Singh H, Maarleveld TJ (2018) Archaeological use of Synthetic Aperture Sonar on deepwater wreck sites in Skagerrak. J Archaeol Sci 89:1–13. https://doi.org/10.1016/j.jas.2017.10.005

Olbert AI, Hartnett M (2010) Storms and surges in Irish coastal waters. Ocean Model 34:50–62.

https://doi.org/10.1016/j.ocemod.2010.04.004

OpenCFD (2021) OpenFOAM® - Official home of The Open Source Computational Fluid Dynamics (CFD) Toolbox. https://www.openfoam.com/. Accessed 18 Jan 2021

OpenCFD Ltd. (2019) OpenFOAM: User Guide v2012. https://www.openfoam.com/documentation/guides/latest/doc/index.html. Accessed 23 Jun 2021

Orengo HA, Garcia-Molsosa A (2019) A brave new world for archaeological survey : Automated machine learning- based potsherd detection using high-resolution drone imagery. J Archaeol Sci 105013. https://doi.org/10.1016/j.jas.2019.105013

Oxley I, Keith ME (2016) Site Formation Processes of Submerged Shipwrecks. In: Keith ME (ed) Site Formation Processes of Submerged Shipwrecks. University Press of Florida, Gainesville, p 276

Ozer J, Legrand S, Od R, Mumm N (2015) BEAWARE II: Review of the physical oceanography in the area of the Bonn Agreement

Pacheco-Ruiz R, Adams J, Pedrotti F (2018) 4D modelling of low visibility Underwater Archaeological excavations using multi-source photogrammetry in the Bulgarian Black Sea. J Archaeol Sci 100:120–129. https://doi.org/10.1016/j.jas.2018.10.005

Papageorgiou M (2018) Underwater cultural heritage facing maritime spatial planning: Legislative and technical issues. Ocean Coast Manag 165:195–202. https://doi.org/10.1016/j.ocecoaman.2018.08.032

Pascoe D (2012) Samuel pepys's navy preserved in situ? Conserv Manag Archaeol Sites 14:182–192. https://doi.org/10.1179/1350503312Z.00000000015

Pérez-Ortiz A, Borthwick AGL, McNaughton J, Avdis A (2017) Characterization of the tidal resource in Rathlin Sound. Renew Energy 114:229–243. https://doi.org/10.1016/j.renene.2017.04.026

Perkol-Finkel S, Shashar N, Benayahu Y (2006) Can artificial reefs mimic natural reef communities? The roles of structural features and age. Mar Environ Res 61:121–135. https://doi.org/10.1016/j.marenvres.2005.08.001

Peters JL, Butschek F, O'Connell R, et al (2020) Geological seabed stability model for informing Irish offshore renewable energy opportunities. Adv Geosci 54:55–65. https://doi.org/10.5194/adgeo-54-55-2020

Plets R, Dix JK, Adams JR, et al (2009) The use of a high-resolution 3D Chirp sub-bottom profiler for the reconstruction of the shallow water archaeological site of the Grace Dieu

(1439), River Hamble, UK. J Archaeol Sci 36:408–418.
https://doi.org/10.1016/j.jas.2008.09.026

Plets R, Dix JK, Adams JR, Best AI (2008) 3D reconstruction of a shallow archaeological site
from high-resolution acoustic imagery: The Grace Dieu. Appl Acoust 69:399–411.
https://doi.org/10.1016/j.apacoust.2007.04.004

Plets R, Quinn R, Forsythe W, et al (2011) Using Multibeam Echo-Sounder Data to Identify
Shipwreck Sites: Archaeological assessment of the Joint Irish Bathymetric Survey data. Int
J Naut Archaeol 40:87–98. https://doi.org/10.1111/j.1095-9270.2010.00271.x

Pournou A (2013) The MERMAID project: Saving wooden shipwrecks in the Mediterranean
marine ecosystem- research , development and application of innovative The MERMAID
project : Saving wooden shipwrecks in the Mediterranean marine ecosystem- research ,
development and app. In: 12th ICOM-CC Group on Wet Organic Archaeological
Materials Conference. Istanbul

Pournou A (2017) Assessing the Long-Term Efficacy of Geotextiles in Preserving
Archaeological Wooden Shipwrecks in the Marine Environment. J Marit Archaeol 13:1–
14. https://doi.org/10.1007/s11457-017-9176-9

Pringle H (2013) Troubled waters for ancient shipwrecks. Science (80-) 340:802–807.
https://doi.org/10.1126/science.340.6134.802

Quinn R (2006) The role of scour in shipwreck site formation processes and the preservation of
wreck-associated scour signatures in the sedimentary record - evidence from seabed and
sub-surface data. J Archaeol Sci 33:1419–1432. https://doi.org/10.1016/j.jas.2006.01.011

Quinn R, Boland D (2010) The role of time-lapse bathymetric surveys in assessing
morphological change at shipwreck sites. J Archaeol Sci 37:2938–2946.
https://doi.org/10.1016/j.jas.2010.07.005

Quinn R, Bull JM, Dix JK, Adams JR (1997) The Mary Rose site-geophysical evidence for
palaeo-scour marks. Int J Naut Archaeol 26:3–16

Quinn R, Dean M, Lawrence M, et al (2005) Backscatter responses and resolution
considerations in archaeological side-scan sonar surveys: A control experiment. J Archaeol
Sci 32:1252–1264. https://doi.org/10.1016/j.jas.2005.03.010

Quinn R, Forsythe W, Breen C, et al (2007) Process-based models for port evolution and wreck
site formation at Mombasa, Kenya. J Archaeol Sci 34:1449–1460.
https://doi.org/10.1016/j.jas.2006.11.003

Quinn R, Smyth TAG (2018) Processes and patterns of flow, erosion, and deposition at

shipwreck sites: a computational fluid dynamic simulation. Archaeol Anthropol Sci 10:1429–1442. https://doi.org/10.1007/s12520-017-0468-7

Raineault NA, Trembanis AC, Miller DC, Capone V (2013) Interannual changes in seafloor surficial geology at an artificial reef site on the inner continental shelf. Cont Shelf Res 58:67–78. https://doi.org/10.1016/j.csr.2013.03.008

Ramos PX, Pego JP, Maia R (2014) Numerical Simulation of the Flow Around a PIER USING OPENFOAM. In: 3rd IAHR Europe Congress. Porto, pp 1–12

Robakiewicz M (2009) Hydrodynamics in the Gulf of Gdansk. In: MACHU Final Report NR. 3 - Managing Cultural Heritage Underwater. pp 75–79

Roberts H (2018) The British Ratification of the Underwater Heritage Convention: Problems and Prospects. Int Comp Law Q 67:833–865. https://doi.org/10.1017/S0020589318000210

Roulund A, Sumer BM, Fredsøe J, Michelsen J (2005) Numerical and experimental investigation of flow and scour around a circular pile. J Fluid Mech 534:351–401. https://doi.org/10.1017/S0022112005004507

Ruuskanen AT, Kraufvelin P, Alvik R, et al (2015) Benthic conditions around a historic shipwreck: Vrouw Maria (1771) in the northern Baltic proper. Cont Shelf Res 98:1–12. https://doi.org/10.1016/j.csr.2015.02.006

Salazar M, Little B (2017) Review : Rusticle Formation on the RMS Titanic and the Potential Influence of Oceanography. J Marit Archaeol 12:25–32. https://doi.org/10.1007/s11457-016-9168-1

Schiffer MB (1996) Formation Processes of the Archaeological Record. University of Utah Press, Salt Lake City

Scourse J, Saher M, Van Landeghem KJJ, et al (2019) Advance and retreat of the marine-terminating Irish Sea Ice Stream into the Celtic Sea during the Last Glacial: Timing and maximum extent. Mar Geol 412:53–68. https://doi.org/10.1016/j.margeo.2019.03.003

Secci M, Demesticha S, Jimenez C, et al (2021) A LIVING SHIPWRECK : An integrated three-dimensional analysis for the understanding of site formation processes in archaeological shipwreck sites. J Archaeol Sci Reports 35:102731. https://doi.org/10.1016/j.jasrep.2020.102731

Shchepetkin AF, McWilliams JC (2005) The regional oceanic modeling system (ROMS): A split-explicit, free-surface, topography-following-coordinate oceanic model. Ocean Model 9:347–404. https://doi.org/10.1016/j.ocemod.2004.08.002

Sherwin TJ (1987) Inertial oscillations in the Irish Sea. Cont Shelf Res 7:191–211.

https://doi.org/10.1016/0278-4343(87)90079-3

Shih PT-Y, Chen Y-H, Chen J-C (2014) Historic Shipwreck Study in Dongsha Atoll with Bathymetric LiDAR. Archaeol Prospect 21:139–146. https://doi.org/10.1002/arp.1466

Shives M, Crawford C (2014) Turbulence Modelling for Accurate Wake Prediction in Tidal Turbine Arrays. In: 5th International Conference on Ocean Energy. Halifax

Simpson JH, Crawford WR, Rippeth TP, et al (1996) The Vertical Structure of Turbulent Dissipation in Shelf Seas. J Phys Oceanogr 26:1579–1590. https://doi.org/10.1175/1520-0485(1996)026<1579:TVSOTD>2.0.CO;2

Smith MJ, Clark CD (2005) Methods for the visualization of digital elevation models for landform mapping. Earth Surf Process Landforms 30:885–900. https://doi.org/10.1002/esp.1210

Smyth TAG (2016) A review of Computational Fluid Dynamics (CFD) airflow modelling over aeolian landforms. Aeolian Res 22:153–164. https://doi.org/10.1016/j.aeolia.2016.07.003

Smyth TAG, Hesp PA, Walker IJ, et al (2019) Topographic change and numerically modelled near surface wind flow in a bowl blowout. Earth Surf Process Landforms 44:1988–1999. https://doi.org/10.1002/esp.4625

Smyth TAG, Quinn R (2014) The role of computational fluid dynamics in understanding shipwreck site formation processes. J Archaeol Sci 45:220–225. https://doi.org/10.1016/j.jas.2014.02.025

Soulsby R (1997) Dynamics of marine sands A manual for practical applications. Thomas Telford

Sténuit R (1973) Treasures of the Armada. Macdonald & Co

Stewart DJ (1999) Formation processes affecting submerged archaeological sites:An overview. Geoarchaeology 14:565–587. https://doi.org/https://doi.org/10.1002/(SICI)1520-6548(199908)14:6<565::AID-GEA5>3.0.CO;2-F

Stieglitz TC, Waterson P (2013) Impact of Cyclone Yasi on the wreck of the SS Yongala documented by comparative multibeam bathymetry analysis. Queensl Archaeol Res 16:33. https://doi.org/10.25120/qar.16.2013.222

Stow DAV, Hernández-Molina FJ, Llave E, et al (2009) Bedform-velocity matrix: The estimation of bottom current velocity from bedform observations. Geology 37:327–330. https://doi.org/10.1130/G25259A.1

Sumer BM (2007) Mathematical modelling of scour: A review. J Hydraul Res 45:723–735.

https://doi.org/10.1080/00221686.2007.9521811

Sumer BM, Christiansen N, Fredsøe J (1997) The horseshoe vortex and vortex shedding around a vertical wall-mounted cylinder exposed to waves. J Fluid Mech 332:41–70. https://doi.org/10.1017/s0022112096003898

Sumer BM, Fredsøe J (2002) The mechanics of scour in the marine environment. World Scientific, Singapore

Sumer BM, Whitehouse RJS, Tørum A (2001) Scour around coastal structures: A summary of recent research. Coast Eng 44:153–190. https://doi.org/10.1016/S0378-3839(01)00024-2

Summers G, Lim A, Wheeler AJ (2021) A scalable , supervised classification of seabed sediment waves using an object-based image analysis approach. Remote Sens Environ 1–43

Sun C, Lam WH, Dai M, Hamill G (2019) Prediction of seabed scour induced by full-scale darrieus-type tidal current turbine. J Mar Sci Eng 7:. https://doi.org/10.3390/jmse7100342

Sweeney M, Webb RM, Wilkinson RH (1988) Scour Around Jackup Rig Footings. In: Offshore Technology Conference. Houston

Szafrańska M, Gil M, Nowak J (2021) Toward monitoring and estimating the size of the HFO-contaminated seabed around a shipwreck using MBES backscatter data. Mar Pollut Bull 171:. https://doi.org/10.1016/j.marpolbul.2021.112747

Taormina B, Percheron A, Marzloff MP, et al (2020) Succession in epibenthic communities on artificial reefs associated with marine renewable energy facilities within a tide-swept environment. ICES J Mar Sci. https://doi.org/10.1093/icesjms/fsaa129

Testik FY, Voropayev SI, Fernando HS (2005) Flow around a short horizontal bottom cylinder under steady and oscillatory flows. Phys Fluids 17:. https://doi.org/10.1063/1.1868012

Tomalin DJ, Simpson P, Bingeman JM (2000) Excavation versus sustainability in situ: A conclusion on 25 years of archaeological investigations at Goose Rock, a Designated historic wreck-site at the Needles, Isle of Wight, England. Int J Naut Archaeol 29:3–42. https://doi.org/10.1006/ijna.2000.0285

Trembanis AC, Friedrichs CT, Richardson MD, et al (2007) Predicting seabed burial of cylinders by wave-induced scour: Application to the sandy inner shelf off Florida and Massachusetts. IEEE J Ocean Eng 32:167–183. https://doi.org/10.1109/JOE.2007.890958

UNESCO (2017) The underwater heritage: Wrecks. http://www.unesco.org/new/en/culture/themes/underwater-cultural-heritage/underwater-cultural-heritage/wrecks/. Accessed 13 Apr 2021

References

UNESCO (2002) Records of the General Conference, 31st session. In: October. UNESCO, Paris, pp 50–61

Unsworth CA, Nicholas AP, Ashworth PJ, et al (2020) Influence of Dunes on Channel-Scale Flow and Sediment Transport in a Sand Bed Braided River. J Geophys Res Earth Surf 125:. https://doi.org/10.1029/2020JF005571

Van Damme T (2015) Computer Vision Photogrammetry for underwater archaeological site recording in a low-visibility environment. Int Arch Photogramm Remote Sens Spat Inf Sci - ISPRS Arch 40:231–238. https://doi.org/10.5194/isprsarchives-XL-5-W5-231-2015

Van Der Vorst HA (1992) Bi-CGSTAB: A Fast and Smoothly Converging Variant of Bi-CG for the Solution of Nonsymmetric Linear Systems. SIAM J Sci Stat Comput 13:631–644

van der Werf A (2010) Mast Tracking Capability of EM3002D Using Water Column Imaging. New Brunswick

Van Landeghem KJJ, Baas JH, Mitchell NC, et al (2012) Reversed sediment wave migration in the Irish Sea , NW Europe : A reappraisal of the validity of geometry-based predictive modelling and assumptions. Mar Geol 295–298:95–112. https://doi.org/10.1016/j.margeo.2011.12.004

Van Landeghem KJJ, Chiverrell RC (2020) Bed erosion during fast ice streaming regulated the retreat dynamics of the Irish Sea Ice Stream. Quat Sci Rev 245:106526. https://doi.org/10.1016/j.quascirev.2020.106526

Van Landeghem KJJ, Uehara K, Wheeler AJ, et al (2009a) Post-glacial sediment dynamics in the Irish Sea and sediment wave morphology: Data-model comparisons. Cont Shelf Res 29:1723–1736. https://doi.org/10.1016/j.csr.2009.05.014

Van Landeghem KJJ, Wheeler AJ, Mitchell NC, Sutton G (2009b) Variations in sediment wave dimensions across the tidally dominated Irish Sea, NW Europe. Mar Geol 263:108–119. https://doi.org/10.1016/j.margeo.2009.04.003

Vanninen P, Östin A, Bełdowski J, et al (2020) Exposure status of sea-dumped chemical warfare agents in the Baltic Sea. Mar Environ Res 161:105112. https://doi.org/10.1016/j.marenvres.2020.105112

Ventikos NP, Louzis K, Koimtzoglou A, Delikanidis P (2016) Enhanced decision making through probabilistic shipwreck risk assessment: Focusing on the situation in Greece. Front Mar Sci 3:1–13. https://doi.org/10.3389/fmars.2016.00097

Versteeg HK, Malalasekera W (2007) Conservation laws of fluid motion and boundary conditions

References

Voropayev SI, Testik FY, Fernando HJS, Boyer DL (2003) Burial and scour around short cylinder under progressive shoaling waves. Ocean Eng 30:1647–1667. https://doi.org/10.1016/S0029-8018(02)00146-4

Wakes S (2013) Three-dimensional Computational Fluid Dynamic experiments over a complex dune topography. J Coast Res 165:1337–1342. https://doi.org/10.2112/si65-226.1

Wakes SJ, Maegli T, Dickinson KJ, Hilton MJ (2010) Numerical modelling of wind flow over a complex topography. Environ Model Softw 25:237–247. https://doi.org/10.1016/j.envsoft.2009.08.003

Walbridge S, Slocum N, Pobuda M, Wright DJ (2018) Unified Geomorphological Analysis Workflows with Benthic Terrain Modeler. Geosciences 8:94. https://doi.org/10.3390/geosciences8030094

Walker SJ, Schlacher TA, Schlacher-Hoenlinger MA (2007) Spatial heterogeneity of epibenthos on artificial reefs: Fouling communities in the early stages of colonization on an East Australian shipwreck. Mar Ecol 28:435–445. https://doi.org/10.1111/j.1439-0485.2007.00193.x

Wang XL, Swail VR (2001) Changes of extreme Wave Heights in northern Hemisphere Oceans and related atmospheric circulation regimes. J Clim 14:2204–2221. https://doi.org/10.1175/1520-0442(2001)014<2204:COEWHI>2.0.CO;2

Ward IAK, Larcombe P, Veth P (1999) A new process-based model for wreck site formation. J Archaeol Sci 26:561–570. https://doi.org/10.1006/jasc.1998.0331

Ward SL, Neill SP, Van Landeghem KJJ, Scourse JD (2015) Classifying seabed sediment type using simulated tidal-induced bed shear stress. Mar Geol 367:94–104. https://doi.org/10.1016/j.margeo.2015.05.010

Weinberg GD, Grace VR, Edwards GR, et al (1965) The Antikythera Shipwreck Reconsidered. Trans Am Philos Soc 55:3–48. https://doi.org/10.2307/1005929

Weiss AD (2001) Topographic Position and Landforms Analysis. In: ESRI user conference. San Diego, CA, p 200

Weller HG, Tabor G, Jasak H, Fureby C (1998) A tensorial approach to computational continuum mechanics using object-oriented techniques. Comput Phys 12:620. https://doi.org/10.1063/1.168744

Wessel P (1998) An Empirical Method for Optimal Robust Regional-Residual Separation of Geophysical Data. Math Geol 30:391–408. https://doi.org/https://doi.org/10.1023/A:1021744224009

Wessel P (2016) Regional-residual separation of bathymetry and revised estimates of Hawaii plume flux. Geophys J Int 204:932–947. https://doi.org/10.1093/gji/ggv472

Wessex Archaeology (2011) Assessing Boats and Ships 1914-1938

Wessex Archaeology (2005) Strategic Enviromental Assessment Sea 6: Irish Sea. Maritime Archaeology

Westley K, Plets R, Quinn R, et al (2019) Optimising protocols for high-definition imaging of historic shipwrecks using multibeam echosounder. Archaeol Anthropol Sci 11:3629–3645. https://doi.org/10.1007/s12520-019-00831-6

Westley K, Quinn R, Forsythe W, et al (2011) Mapping Submerged Landscapes Using Multibeam Bathymetric Data: A case study from the north coast of Ireland. Int J Naut Archaeol 40:99–112. https://doi.org/10.1111/j.1095-9270.2010.00272.x

Wheaton JM, Brasington J, Darby SE, Sear DA (2010) Accounting for uncertainty in DEMs from repeat topographic surveys: Improved sediment budgets. Earth Surf Process Landforms 35:136–156. https://doi.org/10.1002/esp.1886

Wheeler AJ (2002) Environmental controls on shipwreck preservation: The Irish context. J Archaeol Sci 29:1149–1159. https://doi.org/10.1006/jasc.2001.0762

Whitehouse RJS (1998) Scour at marine structures: a manual for practical applications. Thomas Telford, London

Whitehouse RJS, Harris JM, Sutherland J, Rees J (2011) The nature of scour development and scour protection at offshore windfarm foundations. Mar Pollut Bull 62:73–88. https://doi.org/10.1016/j.marpolbul.2010.09.007

Wilson I (1979) Shipwrecks of the Ulster Coast. Impact-Amergin, Coleraine

Wilson JP, Gallant JC (2000) Elevation residual analysis. In: Wilson JP, Gallant JC (eds) Terrain analysis: principles and applications. John Wiley & Sons, New York, pp 73–76

Winton T (2019) Quantifying Depth of Burial and Composition of Shallow Buried Archaeological Material: Integrated Sub-bottom Profiling and 3D Survey Approaches. In: McCarthy J, Benjamin J, Winton T, van Duivenvoorde W (eds) 3D Recording and Interpretation for Maritime Archaeology, vol. 31. Coastal Research Library, Springer, Cham

Woods MA, Wilkinson IP, Leng MJ, et al (2019) Tracking Holocene palaeostratification and productivity changes in the Western Irish Sea: A multi-proxy record. Palaeogeogr Palaeoclimatol Palaeoecol 532:109231. https://doi.org/10.1016/j.palaeo.2019.06.004

References

Yakhot V, Orszag SA, Thangam S, et al (1992) Development of turbulence models for shear flows by a double expansion technique. Phys Fluids A Fluid Dyn 4:1510–1520. https://doi.org/10.1063/1.858424

Yao W, Draper S, An H, et al (2021) Experimental study of local scour around submerged compound piles in steady current. Coast Eng 165:103831. https://doi.org/10.1016/j.coastaleng.2020.103831

Yiannoukos I, Benson T, Van Landeghem K, et al (2020) Modelling scour around submerged objects with TELEMAC3D - GAIA. In: Breugem WA, Frederickx L, Koutrouveli T, *et al.* (eds) Online proceedings of the papers submitted to the 2020 TELEMAC- MASCARET User Conference. International Marine & Dredging Consultants, pp 68–73

Zaid M, Yazdanfar Z, Chowdhury H, Alam F (2019) Numerical modeling of flow around a pier mounted in a flat and fixed bed. Energy Procedia 160:51–59. https://doi.org/10.1016/j.egypro.2019.02.118

Zintzen V, Norro A, Massin C, Mallefet J (2008) Spatial variability of epifaunal communities from artificial habitat: Shipwrecks in the Southern Bight of the North Sea. Estuar Coast Shelf Sci 76:327–344. https://doi.org/10.1016/j.ecss.2007.07.012

Supplementary material for *Residual relief modelling: digital elevation enhancement for shipwreck site characterisation*

Step-by-step residual relief modelling GIS workflow for geomorphological characterization of shipwreck sites

1. **In ESRI ArcMap v. 10.6.1**

Step 1: High-pass filtering

Open ArcMap

Add digital elevation model (DEM) data to *Table of Contents*

Locate *Focal Statistics* tool. Open *ArcToolbox/Spatial Analyst Tools/Neighborhood/Focal Statistics* or use ArcMap search engine (Windows/Search in Menu Bar) and type *Focal Statistics.*

Make sure you have *Spatial Analyst* extension active (Customize/Extensions… in Menu Bar)

Focal Statistics parameter set-up is described in subsection 2.3.1 of the paper and discussed in subsection 4.2. The general rule is that the moving kernel needs to be wide enough to capture more cells from the outside of a scour mark than from the inside. High-pass filtering can be performed using moving mean or median (see section 4.2). When working with floating-point DEM in ArcMap, *statistics type* can be set to mean only. Moving median can be calculated in QGIS with GRASS (see section 2 of this appendix).

Calculate the low-pass filter by executing *Focal Statistics* tool.

Locate *Raster Calculator* tool. Open *ArcToolbox/Spatial Analyst Tools/Map Algebra/Raster Calculator* or use ArcMap search engine. Set-up *Map Algebra expression*: subtract the low-pass layer (result of *Focal Statistics*) from the original DEM; "DEM" – "low_pass_result"

Calculate the high-pass filter by executing *Raster Calculator* tool.

Normalise the high-passed DEM to standard scores for further classification. Open *Raster Calculator*, set-up *Map Algebra expression:* (("high_pass_result")-mean_raster_value))/standard_deviation

mean_raster_value and standard_deviation values can be found by opening the resultant high-pass filtered DEM's (high_pass_result) *properties* and then *source/Statistics/Mean* and *Std dev*.

Calculate the normalised standard score layer by executing *Raster Calculator* tool.

Step 2: Preliminary classification

Open *Raster Calculator* tool. Breakpoint classification is conducted using Con() statements:

$Con("HPstdd"<-0.5,2, Con("HPstdd">5,3, Con("HPstdd">0.5,1,0)))$

Where: $HPstdd$ is the normalised high-passed filtered DEM

Values: below -0.5 are assigned to Class 2 (negative residuals), above 0.5 to Class 1 (positive residuals), between -0.5 and 0.5 to Class 0 and above 5 to Class 3 (wreck separation). Breakpoint values can be adjusted to capture features, accordingly to a target of the classification (see subsection 4.2 of the paper).

Step 3: Wreck marks separation with support of DEM visualization techniques

For the preliminarily classified layer, Class 0 fill color should be set to *No Color* in the layer's *Symbology* tab in *Properties*. In the *Display* tab, *Transparency* should be set to 50%. The layer should be moved up to the top in the *Table Of Contents.*

In Menu Bar, open Windows/Image Analysis. Choose the original, unfiltered DEM raster. In *Processing* tab, choose *Add Function* button, then right click on *Identify Function* and choose *Insert Function/Hillshade function*. Choose *Multidirectional* in *Hillshade Type* dropdown menu. Execute the multidirectional *hillshade* function by clicking Ok. In *Symbology* tab in the new layer's *Properties* choose *Stretch Type: Standard Deviations* and compute statistics for the layer. *Stretch Type* needs to be set to *standard deviations* for each layer derived from *Image Analysis* to improve visualization.

Apply other functions (see subsection 2.3.3 of the paper) and examine the geomorphological setting of the site.

Final separation is supported by clipping out unwanted residuals, using *Extract by Mask* tool from *Spatial Analyst Tools/Extraction* toolbox.

Create a new polygon shapefile – mask for extraction. Set the layer's transparency to 100%. In Menu Bar, open Customize/Toolbars and add *Editor* toolbar. *Start Editing* the mask for extraction. Based on the detailed examination of the residual geomorphological features on the site, delineate a polygon around residuals corresponding to scour features. In the *Editor* toolbar, *Save Edits* and *Stop Editing* the mask layer.

Use *Extract by Mask* tool. *Input raster* is the preliminarily classified layer, *Input raster or feature mask data* is the mask polygon layer created in the Step 3 of the workflow. Execute the tool and examine the resulting layer.

2. In QGIS 3.10.0 with GRASS 7.8.0*

*GRASS plugin is necessary to calculate kernel statistics for the high-pass filtering step 1. QGIS 3.10.0 cannot calculate Sobel edge detection filters used in the paper in the Step 3. Instead, open-sourced ORFEO standalone toolbox can be used to apply Sobel function to a DEM.

Step 1: High-pass filtering

Add DEM data to *Layers*.

In *Processing Toolbox* available in Menu Bar/Processing/Toolbox search for *r.neighbors* tool. Parameter set-up is described in subsection 2.3.1 of the paper and discussed in subsection 4.2. The general rule is that the moving kernel needs to be wide enough to capture more cells from the outside of a scour mark than from the inside. High-pass filtering can be performed using moving mean or median (see section 4.2). Note that in GRASS, neighborhood size unit corresponds to pixels, not to distance units and the input value must be an **<u>odd</u>** number. Execute *r.neighbors* – low-pass filter is calculated. The process may take from several minutes to several hours depending on kernel size, raster resolution and statistics type.

Open *Raster Calculator* tool from *Processing Toolbox*. Subtract the result of *r.neighbors* from the original DEM to calculate high-pass filter.

Normalise the high-passed DEM to standard scores for further classification. In *Layer Properties* check raster's *STATISTICS_MEAN and STATISTICS_STDDEV* values. Expression in *Raster Calculator* should be written accordingly: (("high_pass_result")-*STATISTICS_MEAN* value))/*STATISTICS_STDDEV* value. Execute the *Raster Calculator*.

Step 2: Preliminary classification

For breakpoint classification, *Reclassify by table* tool can be used. See Step 2 of the ArcMap workflow (section 1 of this appendix) and subsection 4.2 of the paper for the details regarding breakpoints choice for the classification. After executing the classification, adjust the symbology of the resultant layer (*Render type Paletted/Unique values* and then *Add values manually*), set opacity of the Class 0 to 0%.

Step 3: Wreck marks separation with support of DEM visualization techniques

Duplicate the original DEM, by right clicking on it in *Layers* window and choosing *Duplicate.* In layer's properties change *Render type* to *Hillshade* and tick *Multidirectional* box. For better visualization, decrease the raster's *Brightness* and increase its *Contrast*.

Slope/*Aspect* functions are available in Raster/Analysis tab in Menu Bar.

Examine the geomorphological setting of the site (see subsection 2.3.3 of the paper) with support of the DEM derivatives and visualization techniques.

Create a new polygon shapefile and delineate area comprising scour marks. Save edits and clip-out unwanted residuals using *Clip Raster by Mask Layer* tool.

Supplementary material for *Using difference modelling and computational fluid dynamics to investigate the evolution of complex, tidally influenced shipwreck sites*

1. Grid independence study

A grid independence study was conducted for the main simulation domains to check the influence of mesh resolution on the modelling. The refinement levels were progressively increased, yielding higher numbers of cells: 2.1, 5.0 and 13.4 million cells and 4.5, 7.3 and 12.1 million cells for the coarse, medium and fine resolution meshes of the SS *W.M. Barkley* and HMS *Vanguard* sites, respectively. Firstly, flow velocities were compared at approximately 10000 randomly sampled, nearly uniformly distributed points within the first 5 m of the seabed, by evaluating the mean absolute percentage error (MAPE) (Table 1).

Table 1. Mean absolute percentage differences between averaged simulated flow velocity magnitudes for grids with different cell numbers at common grid points.

	MAPE (%)	
Site	Coarse and medium	Medium and fine
SS *W.M. Barkley*	3.6	3.9
HMS *Vanguard*	8.7	6.6

Although there are significant differences (MAPE>1%) between the fine and medium resolution meshes, the average dimensionless wall distance $y+$, calculated for the finest meshes reached well below 500 (305 for the SS *W.M. Barkley* and 243 for the HMS *Vanguard* simulations), hence, the cells adjacent to the wall patch (seabed) were within the log-law layer (Versteeg and Malalasekera 2007), allowing implementation of wall functions. Wall functions are a set of empirical equations, applied to satisfy the physics of the flow in the near wall region. If the first cell centre is placed within the log-law region, they can be used to model the boundary layer, instead of resolving it using a very fine mesh (Versteeg and Malalasekera 2007), significantly reducing computational costs.

Furthermore, as the evaluation of critical shear exceedance at the sites was important to the investigation, a comparison of mean magnitudes and distribution of simulated mean wall shear stresses between the coarse, medium and fine meshes for both sites was performed. Surface points containing wall shear stress magnitudes were firstly exported to .csv files and then imported to ArcMap 10.7.1. As the density of the surface points is variable within an individual CFD mesh (more surface points located in refinement boxes defined around wreck structures), the point data were then interpolated (moving mean) to raster images with uniform pixel sizes. These raster images were gridded at 1.35, 0.65 and 0.30 m spatial resolution for the coarse, medium and fine domains, respectively. In the end, global means of the rasters were compared (Table 2).

Table 2. Absolute differences between mean wall shear stress calculated for rasters gridded with point data extracted from CFD domains with different cell numbers.

	Difference (%)	
Site	Coarse and medium	Medium and fine
SS *W.M. Barkley*	4.01	4.67
HMS *Vanguard*	0.34	1.66

Similar to the comparison of mean velocities in Table 1, Table 2 shows significant differences in the mean wall shear stress between the coarse, medium, and fine domains at the SS *W.M. Barkley* site (4.01% and 4.67%). These differences are also registered between the medium and fine meshes for HMS *Vanguard* (1.66%), and arise from the sheer complexity of both the object (i.e. wreck) and seabed surfaces implemented in the simulations.

However, these differences do not invalidate the investigation. The focus of the study was to qualitatively determine zones of relatively high and low modelled wall shear stresses and examine critical shear stress exceedance to determine whether the sites are in live-bed or clear-water scour regime under the simulated spring tide currents. As shown in Fig. S1 and Fig. S2 (subplots a, b, and c), representing modelled wall shear stresses for both sites, differences in patterns of τ_c and τ_{cr} exceedance zones for sand (silver to red colours) remain virtually unaltered with the increasing resolution of the surfaces. The grid independence with regards to the results discussed in the paper is also evidenced in the profile data extracted from

the low, medium and fine surfaces for both sites (Fig. S1,d and Fig. S2,d). The yellow line, representing the critical shear stress required to mobilise sand is below the simulated wall shear stresses at points along the profiles for the medium and fine resolution meshes, represented by grey and blue lines, respectively. Therefore, the main conclusion with regards to the scour regime remains the same, regardless of the mesh refinement. As for the HMS *Vanguard* site (Fig. S2), the critical shear stress required to mobilise the gravel fraction (3.08 Pa) dominating the scour pit, is never exceeded at the investigated grids (low, medium and fine), even in the downstream zone in the wreck's wake, where the wall shear stresses are elevated by a factor of 4 to 5 (this factors also remains the same at all the mesh resolutions).
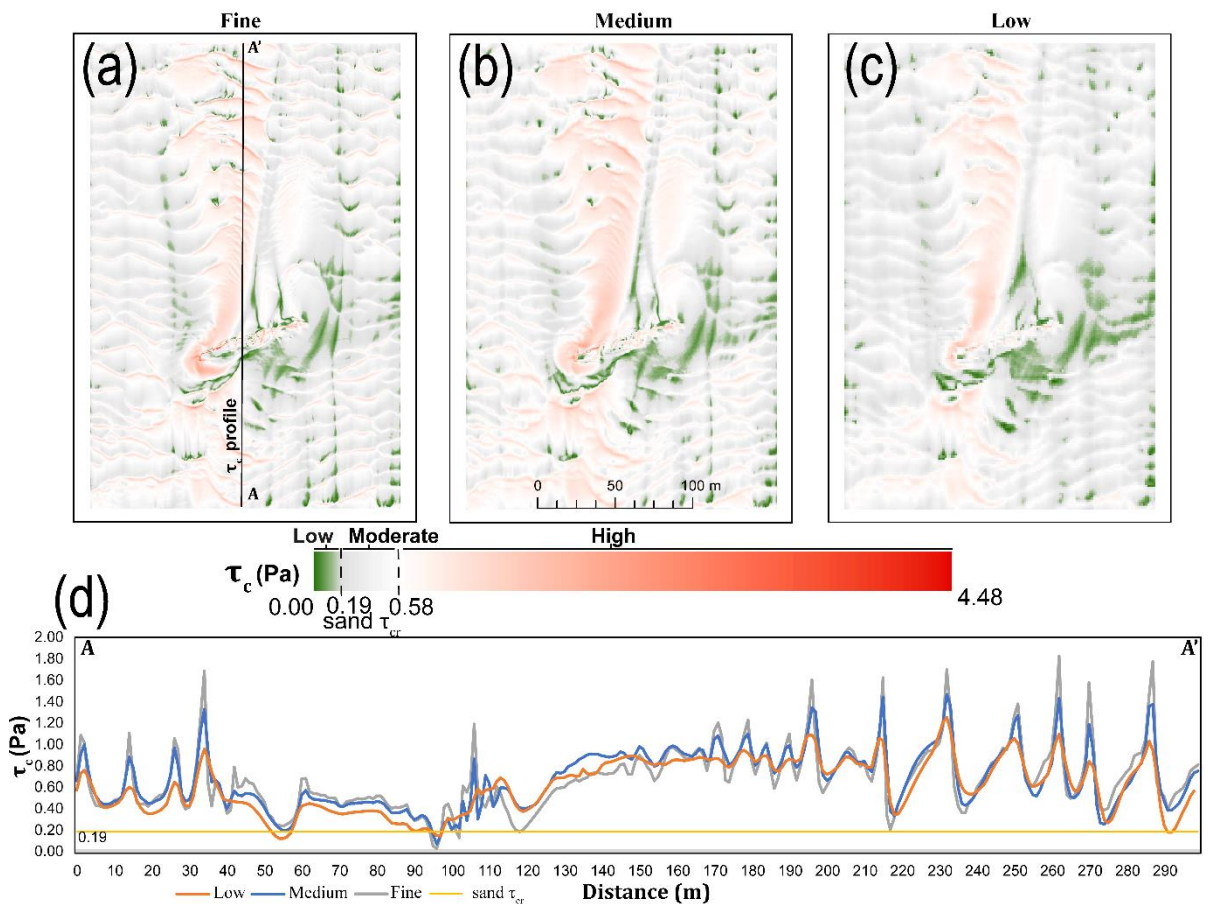
Figure S1. Simulated, averaged wall shear stress surface maps for the SS *W.M. Barkley* site for the (a) fine, (b) medium, and (c) low resolution meshes and (d) wall shear stress profiles A-A' extracted from the surfaces (location of the profiles is marked in subplot (a)).
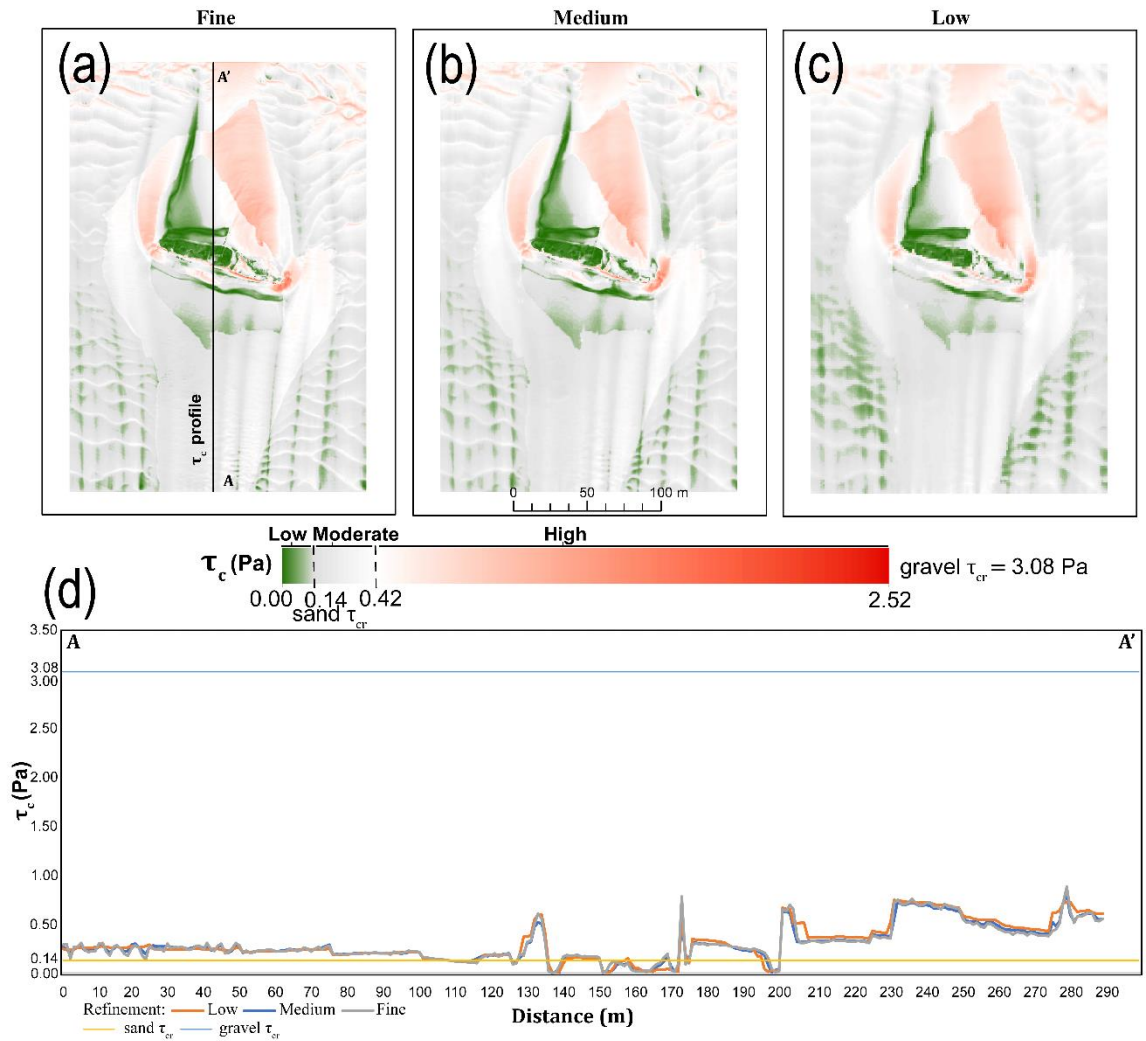
Figure S2. Simulated, averaged wall shear stress surface maps for the HMS *Vanguard* site for the (a) fine, (b) medium, and (c) low resolution meshes and (d) wall shear stress profiles A-A' extracted from the surfaces (location of the profiles is marked in subplot (a)).

Further refinement was therefore deemed unnecessary. Furthermore, the computational costs of additional simulations and model data post-processing and visualization would become prohibitive.

2. Model validation with field and experiment data

2.1. Field data

3D CFD simulations are sometimes validated using *in-situ* measurements of flow field, using for example an ADCP sensor. Such measurements also provide input velocities and inform initial conditions. In this study, the CFD simulations are fed with input velocities from the validated regional ocean modelling system (ROMS) (Nagy *et al.* 2020) established for the Irish waters, and therefore the modelling can be viewed as a nested model of the wider shelf-scale operational model, which is validated by *in-situ*

measurements. This approach was chosen, considering the complexity of the hydrodynamic regime at the sites (bi-directional tidal currents operating in neap-spring cycles), which would otherwise require long-term deployment and maintenance of ADCP devices at both sites. While MBES and ROMS datasets are becoming widely available due to platforms and projects like EMODNet (EMODnet Bathymetry Consortium 2018) and INFOMAR (Guinan *et al.* 2020), *in-situ* measurement data for local flows remain scarce. In fact, this was one of the motivations for this investigation. The study shows that desk-based ROMS-informed CFD modelling combined with difference modelling of MBES data provides a touchstone quantification of physical forces influencing the stability of underwater shipwreck sites. It can be considered as the first step towards delivering quantitative site-focused information, which can greatly improve decision making in marine spatial planning and archaeological site management.

The CFD results reveal prevailing wall shear stress patterns and determine the occurrence of critical shear stress exceedance (live-bed and clear-water scour regimes), which agree with differences registered by the repeat MBES data. Therefore, the simulations are supported by difference modelling data captured *in-situ*.

2.2.Experiment data

Although performing physical modelling was beyond the scope of this paper, the choice of the turbulent closure scheme - shear-stress transport (SST) k-ω – was guided by the previous research conducted by De Hauteclocque *et al.* (2007). This study was divided into four phases. In the first phase, flow was modelled around a surface mounted cube and results of steady-state, unsteady RANS (URANS) and LES simulations were compared; this included various turbulence models for the RANS simulations, including k-ω SST, k-ω and k-ε. Secondly, simulations were performed around a cuboid, oriented at various angles in relation to the upstream flow's direction using k-ω SST and k-ε models and compared against physical modelling results. In the third phase, flow around a modelled shipwreck was simulated and again validated with a physical modelling study. In the fourth phase, flow was modelled on a DEM of an unknown shipwreck site located off the south coast of England and the results were compared against acoustic Doppler current profiler (ADCP) data and observed scour signatures. One of the objectives of the last two phases was to estimate scour and deposition patterns around the shipwreck geometries, by examining wall shear stress and turbulent kinetic energy exerted by the flow.

The results of the first phase indicated that although LES provides the most accurate results compared to physical modelling (predicting reattachment length with the highest accuracy), the simulations require very fine meshes, for which computation times are prohibitive. RANS k-ω SST was deemed an optimal model, yielding good accuracy in reproducing flow patterns, while retaining reasonable computation times (De Hauteclocque *et al.* 2007). The second phase of the modelling indicated that unsteadiness of simulation generally decreases, when a cuboid is at an oblique angle in relation to the upstream flow. Both the k-ε and k-ω SST models provided acceptable results when compared to the results of physical modelling. The last two phases involved modelling of flow around shipwreck geometries. With regards to the modelled wreck, the simulated wall shear stress was used to evaluate critical shear stress exceedance, and this provided good estimation of the extent of scour for a tilted hull (25°) orientated 45° towards the flow. The authors did not, however, specify the method for calculation of the wall shear stress. Additionally, wall shear stress and turbulent kinetic energy patterns showed good spatial correlation in simulations conducted for shipwrecks, which were also compared against observed scour in DEM data (Smyth and Quinn 2014; Quinn and Smyth 2018), similar to the investigation presented here. Smyth and Quinn (2014) and Quinn and Smyth (2018) also used the same method for the calculation of wall shear stress as the one used in this study.

One recent physical modelling experiment which may act as an analogy for our simulations was conducted for a half-buried cylindrical object located in a substrate with d_{50} of 0.259 mm, at an oblique angle to a steady 0.26 m/s flow and compared against a coupled model (CFD coupled with sediment transport equations) (Yiannoukos *et al.* 2020). The setting (Yiannoukos *et al.* 2020) is somewhat similar to the environment of the SS *W.M. Barkley* site, where the wreck has a similar aspect ratio as the half-buried cylinder, the substrate has a d_{50} of 0.302 mm and the near-seabed current (<1 m above the seabed) velocities reach approximately 0.30 – 0.50 m/s during spring tides. Qualitatively, there are similarities in the observed scour and depositional patterns developed around the two objects: near-field erosion developed upstream of the wreck, and two scour pits developed at both ends of the wreck, separated by a depositional mound. The object's inflow side-originated scour feature is also longer than the scour feature originating from the opposite side of both the wreck and the cylindrical object. Additionally, migrating bedforms are present in both models. The big difference between the modelled and real-world data is that scour pits at the *Barkley* site extend

asymmetrically in opposite directions, due to the bi-directional tidal regime. The authors (Yiannoukos *et al.* 2020) do not analyse flow structures and wall shear stress patterns, but compare the outcomes of the physical modelling to the simulated surface of the coupled model. Nevertheless, the CFD modelling presented here predicts wall shear stresses of higher magnitudes at the wake of the inflow, stern side of the wreck, which explains the longer extent of the scour at this side. Upstream near-field scour is explained by the presence of a horseshoe vortex and high wall shear stresses are modelled at the crests of sand waves, explaining their development and movement. In summary, this <u>qualitative</u> comparison between the main article's difference modelling, CFD outputs and the physical modelling of Yiannoukos *et al.* (2020) results in observations of similar patterns of flow and scour.

On the other hand, it is difficult to compare outputs from our CFD study with the physical modelling of Yiannoukos *et al.* (2020) <u>quantitatively</u>, as the investigations had different aims. While this study aimed at examining interrelations between CFD modelled flow patterns and recorded geomorphic change at an actual shipwreck site, the other one compared results from a coupled model and a flume tank experiment, both involving a scaled cylindrical object (Yiannoukos *et al.* 2020). Therefore, the authors did not examine the intermediate products of the simulations (i.e. hydrodynamic patterns and wall shear stress distribution) but focused on the final output of the coupled modelling.

With regards to the quantitative description of the observed scour signatures, there are significant differences between the SS *W.M. Barkley* site and the flume tank experiment of Yiannoukos *et al.* (2020). The mean depth of scour around the cylindrical object in the flume tank experiment was determined to be 0.09 m, while at the mean depth of scour at the *Barkley* site is 2.92 m. Therefore, the mean scour depth to the object's diameter ratio is significantly larger for the flume tank experiment (0.090/0.022=4.091) than the wreck site (2.92/10=0.292). Yiannoukos *et al.* (2020) do not mention information on the equilibrium scour depth reached at the experiment. With regards to the extent of scour, SS *W.M. Barkley's* erosional signatures seem to be relatively more extensive than those developed in the flume tank experiment. The former's length to the object's width ratio (285/10 m) is 28.50, while the same calculation (0.300/0.022) for the latter gives the value of 13.63. The SS *W.M. Barkley* site's bathymetry is complex, with a sloping seabed (associated with a sand bank topography) and is not bounded at the sides, like in the idealised laboratory experiment. Naturally, the bi-directional neap-spring tide cycle flow regime at the shipwreck site is also significantly more complex than in the experimental

setup (steady, unidirectional flow). Therefore, these discrepancies may result from the inherent differences between the laboratory-based, scaled experiment and the natural seabed environment.

Nevertheless, as described above, scour patterns express some qualitative similarities between the experiment (Yiannoukos *et al.* 2020) and the SS *W.M. Barkley* wreck site. Therefore, the prevailing flow patterns, discussed in the main paper, must have been similar (regions of increased and decreased wall shear stresses, appearance of wake and horseshoe vortices) to the flow patterns developed in the controlled experiment.

3. Methods

3.1. Details of the repeat hydrographic survey

The Kongsberg EM2040 MBES operated at 400 kHz with a short continuous wave pulse. The MBES was in a dual-head configuration during the 2019 survey. An integrated GNSS/L-Band receiver CNAV 3050 was used for primary positioning and a Seatex Seapath 330+ acted as a back-up positioning system and provided motion referencing and accurate timing. Survey speed did not exceed 5 kn. Sound velocity profiles for refraction corrections were conducted using a Valeport Midas SVP and a real-time AML surface sensor.

During the regional surveys, survey lines were aligned parallel to each other, with 110°–120° swath coverage and the same acquisition parameters were maintained during the two subsequent surveys (2015, 2019) to ensure consistency. The Combined Uncertainty and Bathymetry Estimator (CUBE; Calder and Wells, 2007) algorithm was used to automatically clean the point clouds for geomorphic change detection. Quality control using crosslines showed >98% compliance with the IHO Special Order standard (IHO 2020).

During the detailed surveys, survey lines were oriented parallel and perpendicular to the major axes of the wrecks following the guidelines for wreck investigation of the Maritime and Coastguard Agency UK (MCA 2018) with a narrow swath coverage ranging 40°–80° (Westley *et al.* 2019). The point clouds acquired for the structural change detection were cleaned manually and exported as text files with point coordinates.

3.2. Details of the simulation setup

The inlet turbulence kinetic energy, k, and specific dissipation rate, ω, were estimated according to the following equations (OpenCFD Ltd. 2019):

$$k = 3/2\left(I|u_{ref}|\right)^2; \tag{1}$$

$$\omega = \frac{k^{0.5}}{C_\mu^{0.25}L}; \tag{2}$$

where the turbulence intensity $I = 0.16Re^{-\frac{1}{8}}$, depends on the Reynolds number, Re. The depth-averaged current speed was used as the reference velocity, u_{ref}. C_μ is an empirical constant equal to 0.09 and the mixing length, L, was calculated as: $L = \kappa z(1 - z/h)^{0.5}$, where κ is the Von Kármán constant and equals to 0.4. The water depth is represented by h and z is the height above the seabed (Simpson _et al._ 1996).

Inlet current velocity profiles were calculated using the depth-averaged velocity magnitudes according to the empirical formula provided by Soulsby (1997), starting from the deepest point of an inlet and with a 0.1 m increment:

for 0<z<0.5h,

$$U(z) = \left(\frac{z}{0.32h}\right)^{1/7} \bar{U}; \tag{3}$$

for 0.5h <z<h,

$$U(z) = 1.07\bar{U}; \tag{4}$$

where $\bar{U}$ is the depth-averaged current speed.

3.3. Critical shear stress calculation

In order to define and calculate the critical shear stress, τ$_{cr}$, the critical Shields parameter (θ_{cr}) must be introduced first (Whitehouse 1998):

for fine grained sediments (D_*<10),

$$\theta_{cr} = \frac{0.3}{1+1.2D_*} + 0.055[1 - \exp(-0.02D_*)]; \tag{6}$$

for coarse sediments (D_*>10),

$$\theta_{cr} = \frac{0.24}{D_*} + 0.055[1 - \exp(-0.02D_*)]; \tag{7}$$

where D_* is the dimensionless grain size parameter,

$$D_* = \left[\frac{g(s-1)}{v^2}\right]^{1/3};$$ (8)

where v is the kinematic viscosity of water, g is the acceleration due to gravity and s is the ratio of the sediment density (ρ_s) to the water density (ρ), $s = \rho_s/\rho$. Finally, the critical shear stress (τ_{cr}) is defined as follows:

$$\tau_{cr} = \theta_{cr}(\rho_s - \rho)d_{50}.$$ (9)